03339-1-T

NASA CR-117047

A Study of the Thermal Structure of the Mesosphere and Lower Thermosphere

JOHN JOSEPH OLIVERO, JR.

September 1970

National Aeronautics and Space Administration
Grant NGR 23-005-360
Washington, D.C.

and

National Science Foundation
Grant GA-1025
Washington, D.C.

High Altitude Engineering Laboratory
Departments of Aerospace Engineering
Meteorology and Oceanography

This report was also a dissertation submitted in partial fulfillment of the requirements for the degree of Doctor of Philosophy in the University of Michigan, 1970.

THE UNIVERSITY OF MICHIGAN

COLLEGE OF ENGINEERING

AERONOMY PROGRAM

Aeronomy Program Report No. 5

A STUDY OF THE THERMAL STRUCTURE OF THE MESOSPHERE AND LOWER THERMOSPHERE

John Joseph Olivero, Jr.

ORA Projects 03015 and 03339

under contract with:

NATIONAL AERONAUTICS AND SPACE ADMINISTRATION

Grant No. NGR 23-005-360
Washington, D. C.

NATIONAL SCIENCE FOUNDATION

Grant No. GA 1025
Washington, D. C.

administered through:

OFFICE OF RESEARCH ADMINISTRATION ANN ARBOR

September 1970

ACKNOWLEDGEMENTS

I wish to thank my doctoral committee, Professors Paul B. Hays, S. Roland Drayson, William R. Kuhn, Andrew F. Nagy, and Aksel C. Wiin-Nielsen, for their help and support. Most of the inspiration and critical guidance came from Dr. Hays, the committee chairman. The considerable time and extra effort contributed to the work by Drs. Drayson and Kuhn is greatly appreciated. The calculations performed for the CO_2 (15μ bands) linearized flux divergence by Dr. Drayson is an especially significant contribution. I would also like to thank Dr. R. S. Stolarski for many helpful discussions.

Most of this study was performed while I was on leave from NASA-Langley Research Center, Hampton, Va. I wish to thank the center for financial support and encouragement. A special note of thanks is due Mr. G. B. Graves, Chief, Flight Instrumentation Division, for his efforts on my behalf.

I am grateful for the use of the facilities of the High Altitude Engineering Laboratory of the University of Michigan, and for the help received from its staff.

I wish to thank the Aeronomy Program Committee for its personal interest and help in obtaining financial support in the form of IST (Institute of Science and Technology - U. of Michigan) Pre-Doctoral Fellowships. The financial support received over the past two years from the National Aeronautics and Space Administration under NASA Contract NASr 54(05) and NASA Grant NGR 23-005-360 is gratefully acknowledged.

The use of the Control Data 6600 computer of the National Center for Atmospheric Research, sponsored by the National Science Foundation, is appreciated. I also appreciate the use of the computing center facilities and grants of computing time made available for thesis research by the University of Michigan.

A personal note of thanks is extended to Mrs. M. Boissonneault and Mrs. L. Deakin for their considerable efforts in typing and preparing several drafts and the final manuscript. I also thank Mr. R. Wilkins for his review and helpful comments.

Lastly, I thank my wife, Kathy, and children, Lisa, Mary, and Michael, for their patience and understanding.

TABLE OF CONTENTS

TABLE OF CONTENTS (continued)

TABLE OF CONTENTS (continued)

LIST OF TABLES

LIST OF FIGURES

LIST OF FIGURES (continued)

LIST OF FIGURES (continued)

LIST OF FIGURES (conclusion)

LIST OF SYMBOLS

a_{ij}	element of matrix $\mathbf{A}$
$a(L,I)$	(Appendix F) matrix element
$\mathbf{A}$	matrix of the temperature coefficients
A	coefficient of energy equation, Equation (2.2.23)
A_n^m	coefficient of energy equation for the m^{th} level, n^{th} time step
$b(L)$	parameter, Equation (F.2)
B	Planck black body function
B	coefficient of energy equation, Equation (2.2.23)
B_n^m	coefficient of energy equation for the m^{th} level, n^{th} time step
$B(K)$	Planck black body function at the K^{th} level
c	speed of light in a vacuum
$c(I,K)$	matrix element, Equation (F.4)
C	coefficient of energy equation, Equation (2.2.23)
C_n^m	coefficient of energy equation for the m^{th} level, n^{th} time step
C_{max}	perturbation parameter
C_p	specific heat at constant pressure
C_p^*	reduced quantity, C_p plus potential energy term, Equation (2.2.8)
C_R	constant, Equation (2.6.7)
C_v	specific heat at constant volume
$C_v(^3P)$	additional specific heat, at constant volume, from fine structure of $O(^3P)$
C_λ	constant, used in approximating the thermal conductivity
$d(K)$	coefficient, linear approximation of Planck black body function
D	coefficient of energy equation, Equation (2.2.23)

D_n^m	coefficient of energy equation for the m^{th} level, n^{th} time step
D_1	effective molecular diffusion coefficient for CO
D_2	effective molecular diffusion coefficient for CO_2
$DH(L,K)$	(Green's function) matrix element, linearized flux divergence of CO_2 (15μ bands)
$e(K)$	coefficient, linear approximation of Planck black body function
e_ν	emission coefficient
E_o	energy of lower vibrational state
E^ℓ	average photon energy, ℓ^{th} wavelength interval
E^λ	photon energy, at wavelength λ
E_n^m	coefficient used in numerical approximation to the energy equation, Equation (A. 11)
$f(T)$	degrees of freedom
f_j	element of column vector $\overline{F}$
f_{rot}	rotational degrees of freedom
f_{trans}	translational degrees of freedom
$f_{vib}^i(T)$	vibrational degrees of freedom of the i^{th} constituent
$f_{^3P}^o(T)$	additional degrees of freedom from fine structure of $O(^3P)$
F	IR energy flux
$\overline{F}$	column vector of the coefficients F(m)
$\vec{F}$	frictional force
$F(m)$	coefficient used in numerical approximation to the energy equation, Equations (A. 13) and (A. 14)
F_x	x component of frictional force
F_y	y component of frictional force
F_z	z component of frictional force

g	gravity
g_o	gravity at the Earth's surface
h	enthalpy per unit mass
h	Planck's constant
h	(Appendix B) scale length for ozone distribution
H	atmospheric scale height
$H_i(z)$	specific scale height of the i^{th} constituent at height z
H_1	(Appendix E) specific scale height for CO
H_2	(Appendix E) specific scale height for CO_2
HZERO(L)	linearized flux divergence parameter for CO_2(15μ bands)
$\hat{\imath}$	unit vector in the x-direction
$I(\nu,\tau,\mu)$	specific intensity
$\hat{\jmath}$	unit vector in the y-direction
$J(I)$	source function at the I^{th} level
$J(\nu,\tau)$	source function
J_{dis}	photodissociation rate per molecule
J_{ion}	photoionization rate per molecule
k	Boltzmann's constant
$\hat{k}$	unit vector in the z-direction
K_a	rate coefficient
K_b	rate coefficient
K_E	kinetic energy per unit mass
K_{ij}	rate coefficient for recombination of O_i and O_j
K_Q	quenching rate coefficient
K_T	eddy diffusion coefficient
$\tilde{K}_T$	eddy thermal conductivity

K_ν	absorption coefficient
K.E.	kinetic energy
$K_{T(equil)}$	equilibrium (earth average) eddy diffusion coefficient
$\bar{K}_{T(equil)}$	equilibrium (earth average) eddy thermal conductivity
ℓ	(Chapter 2) mixing length
ℓ_{ij}	element of matrix $\mathbf{L}$
$\mathbf{L}$	auxiliary matrix
m_i	molecular mass of the i^{th} constituent
M	unspecified constituent with approximately same concentration as total gas (usually N_2, O_2)
$\bar{M}$	mean molecular weight
M^*	unspecified constituent in vibrationally or electronically excited state
n_i	concentration of the i^{th} constituent
N	total number density
N_J	population (concentration) of the J^{th} level of $O(^3P)$
$N_i(z,\theta)$	column density of the i^{th} constituent along the atmospheric path through height z, for zenith angle θ
p	pressure
P_E	potential energy per unit mass
P_J	partition function of the J^{th} level of $O(^3P)$
P_Q	probability of de-excitation through quenching
P_R	probability of de-excitation through radiation
q	heat per unit mass
Q_n	solar heating rate at n^{th} time step, Equation (D. 7)
Q_{BATES}	maximum O(63μ line) cooling rate (Bates, 1951) Equation (2. 5. 5)
Q_{CHEM}	chemical recombinational heating rate

Q_{TOTAL}	total heating rate
$Q_{9.6\mu}$	cooling rate for O_3(9.6μ bands)
$Q_{15\mu}$	cooling rate for CO_2(15μ bands)
$Q_{63\mu}$	cooling rate for O(63μ line)
$\overline{Q_{SOLAR}(z)}$	earth average solar heating rate at height z
$Q_{SOLAR}(z,\theta)$	solar heating rate at height z, for zenith angle θ
r	perpendicular distance from sun-Earth line
R	gas constant
R	height above the center of the earth
R_E	radius of the earth
$s(z,\theta)$	distance along line through height z in direction of zenith angle θ , Figure C-1
$s_0(z,\theta)$	value of s(z, θ) at height z, Figure C-1
S	band strength
a	parameter in temperature expression, Equation (B.2)
t	time
t_j	element of column vector $\overline{T}$
t_n	(Appendix A) elapsed time at n^{th} time step
t_n	(Appendix D) number of hours after meridional passage for n^{th} time step
T	temperature
$\overline{T}$	column vector of the unknown temperatures
$T(equil)$	equilibrium (earth average) temperature
$T(K)$	(Appendix F) temperature at the K^{th} level
$T_0(K)$	(Appendix F) standard temperature at the K^{th} level
$T_0(z')$	(Chapter 2) standard temperature at height z'
T_{120}	temperature at 120 Km

T_∞	exospheric temperature
T_n^m	temperature at the m^{th} level, n^{th} time step
$T_{lower\ boundary}$	temperature at lower boundary
(TPF)	temperature perturbation factor
u	x-component of general velocity
u	optical mass of absorbing gas
u_{ij}	element of matrix $\mathbf{U}$
$\mathbf{U}$	auxiliary matrix
u_x	horizontal wind speed
v	y-component of general velocity
v	vibrational quantum number
$\vec{V}$	general velocity
V_z	vertical phase speed
w	z-component of general velocity
w_E	eddy velocity
w_{120}	vertical velocity at 120 Km
y_j	element of column vector $\overline{Y}$
$\overline{Y}$	auxiliary column vector
z	height above sea level
z_j	height of j^{th} level
z_m	height of ozone maximum
z_{max}	(Appendix C) upper limit of numerical integration (column density)
z_{max}	upper boundary of the atmosphere ($\sim \infty$)
z_{min}	lower boundary of the atmosphere (~ 0)
z_p	natural logarithm of pressure used as vertical coordinate

$z_p(m)$	natural logarithm of pressure (used as vertical coordinate) at the m^{th} level
z_p^s	natural logarithm of pressure (used as vertical coordinate) at the lower boundary
z_o	(Appendix G) perturbation level
z_o	(Chapter 3) apparent scale length
z_{pj}	natural logarithm of pressure (used as a vertical coordinate) at the j^{th} level
α	temperature ratio parameter
α	specific volume
$\alpha(m)$	coefficient used in numerical approximation to the energy equation, Equations (A. 13) and (A. 14)
$\beta(m)$	coefficient used in numerical approximation to the energy equation, Equations (A. 13) and (A. 14)
$\gamma(m)$	coefficient used in numerical approximation to the energy equation, Equations (A. 13) and (A. 14)
γ_i	volume mixing ratio of the i^{th} constituent
γ_i	(Appendix B) concentration expression parameter
γ_1	(Appendix E) CO volume mixing ratio
γ_2	(Appendix E) CO_2 volume mixing ratio
$\tilde{\gamma}_2$	CO_2 volume mixing ratio, zero flux case
δ	coefficient used in upper boundary condition, Equation (A. 22)
δA	element of area
δQ	local heating imbalance
$\delta T(z')$	temperature difference (from standard profile) at height z
Δ_{max}	perturbation amplitude
Δt_s	one half the number of daylight hours (for local conditions)
$\Delta F(L)$	flux difference between the boundaries of the th interval
ΔQ	integral (column) heating imbalance

ΔT_n^m	temperature difference between the n^{th} and $(n+1)^{th}$ time steps at level m
Δs_j	increment of $s(z, \theta)$
Δz_p	increment of natural logarithm of pressure, used as a vertical coordinate
ϵ	internal energy per unit mass
ϵ	(Appendix A) coefficient used in upper boundary condition, Equation (A. 22)
ϵ_J	energy of the J^{th} level of $O(^3P)$
$\epsilon_i^{\ell}(z)$	effective heating efficiency of the i^{th} constituent for the ℓ^{th} wavelength interval at height z
$\epsilon_i^{\lambda}(z)$	heating efficiency of the i^{th} constituent at wavelength λ, at height z
$\overline{\epsilon_2(z)}$	heating efficiency for O_2 averaged over wavelength
$\overline{\epsilon_4(z)}$	wavelength independent heating efficiency for O_3
$\langle\epsilon\rangle$	ensemble average energy of $O(^3P)$
$\langle\epsilon^2\rangle$	ensemble average of the square of the $O(^3P)$ energy
φ	(Appendix A) arbitrary variable
φ	(Appendix B) geopotential height
φ	(Appendix E) volume mixing ratio parameter
η	entropy per unit mass
η	dummy integration variable
θ	zenith angle
θ	radiative lifetime; used only in Equation (2. 5. 3)
θ	(Appendix A) arbitrary variable
λ	molecular thermal conductivity
λ	wavelength
λ	vibrational relaxation time

λ_O	molecular thermal conductivity for pure O
λ°	sea level value of vibrational relaxation time
λ_{air}	empirical expression for molecular thermal conductivity at sea level conditions
$\lambda_1(\ell)$	lower limit of ℓ^{th} wavelength interval
$\lambda_2(\ell)$	upper limit of ℓ^{th} wavelength interval
μ	cosine of the zenith angle
ν	frequency
ν_0	mid-band frequency
π	mathematical constant (=3.14159.....)
ρ	(mass) density
ρ_{120}	(mass) density at 120 Km
σ	parameter in temperature expression, Equation (B.4)
σ_i^ℓ	effective absorption cross section of the i^{th} constituent for the ℓ^{th} wavelength interval
σ_i^λ	absorption cross section for the i^{th} constituent at wavelength λ
$\bar{\sigma}_{ij}$	viscosity cross section for the i^{th} constituent interacting with the j^{th}
τ	lifetime (with respect to a given process)
τ_ν	optical depth at frequency ν
τ_z^λ	optical depth at wavelength λ , at height z
φ_{dis}	photodissociation (induced) flux
φ_{ion}	photoionization (induced) flux
Φ_{EDDY}	eddy heat flux
Φ_{MOL}	molecular heat flux
Φ_{TIDE}	tidal energy flux
Φ_{TOTAL}	total heat flux, molecular plus eddy
$\Phi_{\substack{upper \\ boundary}}$	specified heat flux at upper boundary

LIST OF SYMBOLS (conclusion)

$\Phi^{\lambda}(z)$	solar photon flux at wavelength λ reaching height z
$\Phi_E^{\lambda}(z)$	solar energy flux at wavelength λ reaching height z
Φ_{∞}^{ℓ}	integrated solar photon flux above the atmosphere for the ℓ^{th} wavelength interval
Φ_{∞}^{λ}	solar photon flux above the atmosphere at wavelength λ
Φ_E^{λ}	solar energy flux above the atmosphere at wavelength λ
$\Phi_{TOTAL}^{(120\,equil)}$	specified heat flux at 120 Km (upper boundary) for the equilibrium (earth average) thermal model
$\overline{\Phi_{TIDE}}$	hemisphere averaged tidal energy flux
$\overline{\Phi_E^{\lambda}(z)}$	earth average solar energy flux at wavelength λ reaching height z
ψ_n	temperature derivative parameter, Equation (A.19)
$\Psi(z,z')$	Green's function, influence of temperature at height z' on the IR flux divergnece at height z
ω_J	multiplicity of the J^{th} level of $O(^3P)$

ABSTRACT

This study considers a number of mechanisms by which the energy balance of the mesosphere and lower thermosphere (50 Km to 120 Km) is maintained. The following physical processes are investigated: absorption of solar radiation at wavelengths below 3000 Å; IR radiative transfer of CO_2(15μ bands), O_3(9.6μ bands), and O(63μ line); chemical recombination of O and O_3; dissipation of atmospheric tidal oscillations and gravity waves; and molecular and eddy thermal transport.

A major consideration of the study is the role of vertical eddy transport in the overall energy budget of the mesosphere and lower thermosphere. Eddy transport coefficients are estimated from the heat flux necessary to achieve an equilibrium thermal state. This is based on the quantitatively similar eddy transport estimates used in many recent compositional studies.

A global scale model is derived as a geographical and seasonal average of the thermal structure and processes at these levels. The influence of uncertainties in several of the physical processes considered on the required thermal transport are examined. Below the mesopause the ozone concentration has a major effect, however, the empirical expression adopted leads to reasonable eddy transport values. Above the mesopause the chief uncertainty is the upward flux of tidal energy estimated by Lindzen (1967). The tidal energy is assumed to be dissipated above 120 Km, redistributed latitudinally, and to appear as a hemisphere average downward heat flux at 120 Km. The resulting eddy transport is too large; this leads to the conclusion that the bulk of the

tidal energy flux must be either reflected or dissipated at heights below about 100 Km.

Thermal models are also presented for individual latitude cases for solstice and equinox conditions. Hemisphere contours of net radiative and chemical heating rates are presented for each season, along with vertical eddy transport required to achieve energy balance. As anticipated, the effects of meridional circulation are apparent in these results, especially at high latitudes. The integral (column) heating imbalance attributable to circulation, and other large scale dynamic processes not included, is estimated from the integral radiative and chemical heating and the thermal flux based on the eddy transport coefficients from the global scale model.

CHAPTER 1

INTRODUCTION

1.1 GENERAL INTRODUCTION

This study examines a number of physical processes which contribute to the thermal structure of the mesosphere and lower thermosphere[1]. The role of eddy transport in the overall energy balance of this region is quantitatively evaluated through a simple vertical transport model. Estimates are made of the heat transported by large scale horizontal and vertical motions not specifically included in the present study. These are shown to be important especially at high latitudes, in accord with earlier studies.

1.2 HISTORICAL BACKGROUND

The structure of the mesosphere and lower thermosphere was only rather tentatively known before instruments could be taken to these heights. Early observational evidence of the gross structure of the mesosphere came from density determinations of Lindeman and Dobson (1923) obtained from photographing visible meteors. A second early indication was the consistent observation of noctilucent clouds at heights of 80-85 Km, strongly suggesting a correlation with atmospheric structure. Humphreys (1933) ice crystal hypothesis qualitatively identified the deep temperature minimum at these heights especially at high latitudes in summer.

---

[1] In this study this region is assumed to be bounded by 50 Km and 120 Km.

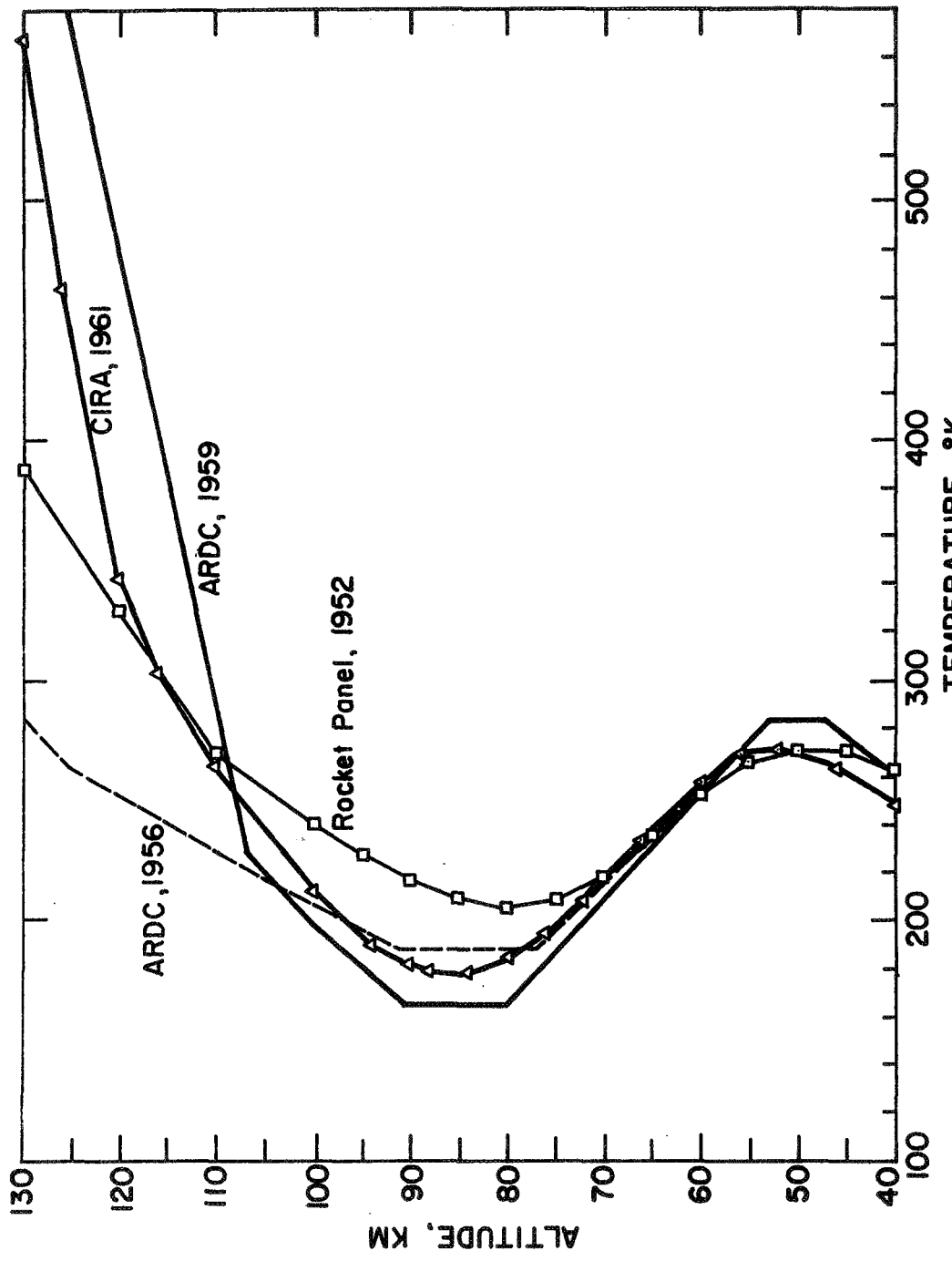

Figure 1. Early model atmospheres

In situ measurements in the mesosphere and lower thermosphere became possible for the first time in the late 1940's when sounding rockets became available for atmospheric research. It is extremely difficult to measure temperature directly at these levels, therefore it is customary to infer the temperature from measurements of pressure or density. This procedure was subject to relatively large uncertainties in the mean molecular weight above the mesopause in this early period. Many of these early measurements were crude according to present standards as indicated by the evolution of early atmospheric temperature models, which are shown in Figure 1.

Atmospheric sounding have become more numerous over the years so that by the 1960's temperature data became available with fairly wide latitude and seasonal coverage. During this period measurement techniques evolved and in situ composition measurements led to improved estimates of the mean molecular weight, both factors contributing to significant decreases in the uncertainty in the temperature. As confidence in the data increased it was possible to obtain a clearer picture of the temperature structure of the mesosphere and lower thermosphere. Significant variations were found to occur with latitude and season, especially near the poles (see Figures 24 and 25). The extremes of temperature at the mesopause are particularly interesting. The warmest mesopause temperatures are found predominantly at the dark winter pole, while the coldest mesopause temperatures are usually measured at the continuously sunlit summer pole. These findings are in sharp contradiction with the radiative processes. Temperature irregularities or perturbations, on the order of 5-25^{o}K over

a few kilometers height range, are often observed especially near the winter pole. These features are superimposed upon the more moderate seasonal and latitudinal variations. The lifetimes of typical irregularities are estimated to be of the order of hours. This is based upon results from the relatively few series of measurements made close to one another in space and time.

Several important theoretical studies have been made to determine radiative sources and sinks of energy in the mesosphere and lower thermosphere in an attempt to understand the undisturbed thermal balance (Murgatroyd, 1957; Murgatroyd and Goody, 1958; Kuhn, 1966, and Kuhn 1968). These studies showed that in general in the region between about 30 Km and 95 Km the atmosphere is relatively near radiative balance at low and mid-latitudes. The radiative imbalances of the winter and summer poles are also apparent in these studies.

Further steps in describing the structure of the mesosphere and lower thermosphere came with studies of motions. Murgatroyd (1957) examined existing wind and temperature data through the thermal wind relation and found them to be reasonably consistent. Hines (1960) identified certain wind profile characteristics as gravity waves and showed theoretically that certain modes could indeed propagate into and through this atmospheric region from the lower atmosphere A comprehensive study of atmospheric tides by Lindzen (1967) showed that the amplitudes of the wind and temperature oscillations would be large at the mesopause and above, especially at low latitudes. Lindzen estimated that the upward flux of tidal energy would have a maximum value of 7 ergs/cm^2/sec near the

equator and if little or no dissipation were present below 100-120 KM, this would represent a very large thermospheric heat source.[1] Simple circulation systems in the meridional-vertical plane have been modelled by Murgatroyd and Singleton (1961) and Leovy(1964). These studies were concerned with the region between about the tropopause and 80 Km and considered the basic differential radiative heating. In general the results indicated ascending motion over the summer pole, northward flow in the mesosphere, and subsidence over the winter pole.

Although each of these features of the overall dynamics can be modelled separately, in principle at least, it remains a formidable challenge to evaluate their combined effect. A very simple vertical eddy[2] transport approach is useful in overcoming this difficulty. Johnson and Wilkins (1965) provided a key step by estimating an upper limit of the vertical eddy transport of heat from the energy imbalance, which was further refined by Johnson (1968). These results complemented the earlier estimates of eddy diffusion from stability arguments made by Lettau (1951) and the values used in compositional studies in the mesosphere and thermosphere by Colgrove, et al (1965, 1966), Shimazaki (1967, 1968), Hesstvedt (1968), Shimazaki and Laird (1970) and Anderson (1970). Thus it became possible to find some very general basis of agreement that vertical eddy diffusion of a magnitude of the order of 10^5 to 10^7 cm^2/sec could provide both the necessary thermal transport and macroscopic mixing consistent with the average thermal and compositional structure of the mesosphere and lower thermosphere.

---

[1] This subject is discussed at length in chapters 2 and 5; also note that the value of energy flux from tides quoted is nearly an order of magnitude larger than that due to the average absorption of solar energy above 120 Km.

[2] This is generally defined as relatively small scale, random motions and is known variously as mixing, turbulence, or eddies.

1.3 STATEMENT OF THE PROBLEM

It was decided to further investigate the premise of Johnson and Wilkins (1965) and Johnson (1968) that vertical eddy transport can balance the gross heating and cooling processes in the mesosphere and lower thermosphere. It was hoped that this simple eddy concept might prove successful in representing the average transport properties of the large scale, interacting, dynamic modes discussed above, which were not specifically included. Also central to the approach was the assumed separability of a long term mean thermal state from local (in space and time) perturbations, which together are the measured atmospheric structure. An assumed mean thermal state was adopted as the basis for each of the thermal models considered. In Chapter 2 the general formulation of the thermal model is presented including the principal heating and cooling mechanisms, both radiative and chemical, molecular and eddy thermal transport, and the derivation of the appropriate energy (conservation) equation.

A global scale thermal model is formulated and discussed in Chapter 3. The global model approximates the average properties and processes of this atmospheric region for the entire earth, as a seasonal and geographical mean. This approximation is quite useful in averaging out horizontal variations in the model and the bulk of the effects of the neglected dynamics. Thus, it was for this thermal model that the most meaningful values of average vertical transport were calculated. The uncertainties in the physical processes included are discussed and the corresponding uncertainties for the model are presented. The response characteristics of the global scale model are presented in Appendix G.

In Chapter 4 the energy budget of the mesosphere and lower thermosphere was considered for various seasons and latitudes. The distribution of heat sources and sinks is presented, as is the vertical transport necessary to balance them. An integral (column) heating imbalance was calculated in order to estimate the heat transported by the large scale motions not specifically contained in the model. This quantity is the sum of contributions both from the integrated net heating rates and the thermal fluxes based upon the global scale vertical eddy transport coefficients adopted in Chapter 3.

Discussion, conclusions, and recommendations for future work are contained in Chapter 5.

CHAPTER 2

THERMAL MODEL

2.1 INTRODUCTION

In this chapter the principal processes which determine the global energy balance of the mesosphere and the lower thermosphere are discussed and incorporated into an appropriate energy (conservation) equation. The processes considered were the following: local deposition of absorbed solar UV energy (solar heating rate); IR radiative transfer by CO_2(15μ bands), O_3(9.6μ bands) and O(63μ line); chemical recombination of O and O_3; dissipation of atmospheric tidal oscillations; and vertical thermal transport by molecular and eddy thermal conductivity.

A general formulation of the energy equation is presented in the first part of the chapter including the adoption of pressure coordinates and boundary conditions. This is followed by discussions of the calculations of molecular thermal conductivity and specific heats. The last part of the chapter describes the calculations of the various heating/cooling rates included in the thermal model.

2.2 THE ENERGY EQUATION

2.2.1 General Formulation

In this section the equation of conservation of energy will be formulated following Haurwitz (1941). Assume a cartesian coordinate system with the z-direction ($\hat{k}$) pointing outward from the earth's center. Assume also that mean motions are described by a generalized velocity $\vec{V} = \hat{i}u + \hat{j}v + \hat{k}w$ and (viscous) frictional forces are described by

$\vec{F} = \hat{i} F_x + \hat{j} F_y + \hat{k} F_z$. If the equations of conservation of momentum are derived in the usual way and then each is multiplied by its respective velocity component and finally these three equations are added together, one obtains:

$$\frac{d}{dt}\left\{\frac{u^2+v^2+w^2}{2} + gz\right\} = -\alpha\left\{u\frac{\partial p}{\partial x} + v\frac{\partial p}{\partial y} + w\frac{\partial p}{\partial z}\right\} + uF_x + vF_y + wF_z \tag{2.2.1}$$

where g is the local gravity, α is the specific volume (inverse of the mass density) and p is the local pressure. We can denote $(u^2+v^2+w^2)/2$ as K_E, the kinetic energy per unit mass and gz as P_E, the potential energy per unit mass. Equation (2.2.1) can be written in a more compact form as:

$$\frac{d}{dt}\left\{K_E + P_E\right\} = -\alpha\,\vec{V}\cdot\nabla p + \vec{V}\cdot\vec{F} \tag{2.2.2}$$

The first law of thermodynamics can be written as:

$$\frac{dq}{dt} = \frac{d\epsilon}{dt} + p\frac{d\alpha}{dt} = \frac{dh}{dt} - \alpha\frac{dp}{dt} \tag{2.2.3}$$

where q is the heat per unit mass, ϵ is the internal energy per unit mass, and h is the enthalpy per unit mass. By the definitions of the specific heats at constant volume and constant pressure, C_v and C_p, respectively, Equation (2.2.3) becomes:

$$\frac{dq}{dt} = C_v\frac{dT}{dt} + p\frac{d\alpha}{dt} = C_p\frac{dT}{dt} - \alpha\frac{dp}{dt} \tag{2.2.4}$$

Choosing the second form of the above equation and adding it to Equation (2.2.2) we get the total (macroscopic and microscopic) equation of conservation of energy in terms of the temperature rate of change as:

$$\rho c_p \frac{dT}{dt} = \rho \frac{dq}{dt} - \rho \frac{d}{dt}\left\{K_E + P_E\right\} - \vec{V}\cdot\nabla p + \vec{V}\cdot\vec{F} + \frac{dp}{dt} \qquad (2.2.5)$$

The total derivatives in the above are the sum of the local and convective rates of change:

$$\frac{d}{dt} = \frac{\partial}{\partial t} + (\vec{V}\cdot\nabla) \qquad (2.2.6)$$

Thus Equation (2.2.5) becomes:[1]

$$\rho c_p \left\{\frac{\partial T}{\partial t} + \vec{V}\cdot\nabla T\right\} = \rho \frac{dq}{dt} + \vec{V}\cdot\vec{F} - \rho\left\{\frac{\partial}{\partial t}\left(K_E + P_E\right) + \vec{V}\cdot\nabla\left(K_E + P_E\right)\right\} - \frac{\partial p}{\partial t} \qquad (2.2.7)$$

The complexity of the above and our meager knowledge of the interaction of the large scale motions necessitated a simpler approach to the problem. Instead of dealing with the motions, $\vec{V}$, directly, a vertical flux of heat was assumed to characterize the overall energy transport. The heat flux becomes part of the general heating term:

$$\rho \frac{dq}{dt} = Q_{TOTAL} - \frac{\partial}{\partial z} \Phi_{TOTAL} \qquad (2.2.8)$$

where Q_{TOTAL} is the total heating rate (per unit volume) and Φ_{TOTAL} is the vertical heat flux composed of both molecular and eddy components, as discussed below.

---

[1] The heating term is not expanded because dq is not an exact differential.

Assuming $\vec{V}=0$ and anticipating the adoption of constant pressure coordinates it was assumed[1] that $\frac{\partial p}{\partial t}=0$. Thus the energy equation can be written as:

$$\rho c_p \frac{\partial T}{\partial t} = Q_{TOTAL} - \frac{\partial}{\partial z} \Phi_{TOTAL} - \rho \frac{\partial}{\partial t}(q z) \qquad (2.2.9)$$

where the last term is the rate of change of P_E .

2.2.2 Molecular and Eddy Thermal Transport

In the smallest scales, individual molecular motion, the heat flux can be expressed by Fick's Law:

$$\Phi_{MOL} = - \lambda \frac{\partial T}{\partial z} \qquad (2.2.10)$$

where λ is the molecular thermal conductivity. The method of calculating the molecular thermal conductivity used in this study is discussed later in this chapter.

Between the molecular scales and those of the mean motions are the random motions that were characterized as eddies. The terms eddies and eddy transport are adopted for descriptive purposes and should not be thought of exclusively as pertaining to the classical concept of turbulence. All that is known is that a process or processes effectively mix the mesosphere and lower thermosphere transporting both constituents and heat. To what extent tidal oscillations, gravity waves, or other phenomena may contribute to this process is unclear at this time.

---

[1] This assumption is necessary in achieving a simple formulation of the energy equation, however, implicit in the neglected term is the transfer bet ween potential and kinetic energy for the atmosphere as a whole (Wiin-Nielsen, 1968; 1970).

In the simplest mixing length formulation the eddy heat flux may be written as:

$$\mathcal{F}_{EDDY} \simeq -\bar{\rho}\,(\overline{w_E \ell})\,\frac{\overline{\partial q}}{\partial z} \qquad (2.2.11)$$

Where ρ is the (mass) density, w_E is an eddy velocity, ℓ is the mixing length, and the bars denote averages over ℓ so that $\bar{\rho}$, $\frac{\overline{\partial q}}{\partial z}$ may be taken as the (mass) density and heat gradient of the undisturbed background gas. $(\overline{w_E \ell})$ is denoted by K_T the eddy diffusion coefficient (cm^2/sec). The heat gradient may be written as:

$$\begin{aligned}\frac{\partial q}{\partial z} &= T\frac{\partial}{\partial z}\eta \\ &= T\left\{C_p\frac{\partial \ln T}{\partial z} - \frac{R}{\bar{M}}\frac{\partial \ln p}{\partial z}\right\} \\ &= C_p\left\{\frac{\partial T}{\partial z} + \frac{g}{C_p}\right\}\end{aligned} \qquad (2.2.12)$$

where η is the entropy per unit mass, R is the gas constant (8.31342×10^7 ergs/(gm mole)/$^\circ$K), $\bar{M}$ is the mean molecular weight, and $\partial \ln p/\partial z = -1/H$ was assumed from the hydrostatic equation, where H is the atmospheric scale height $(RT/\bar{M}g)$. Thus the eddy heat flux is:

$$\begin{aligned}\mathcal{F}_{EDDY} &= -\rho C_p K_T\left(\frac{\partial T}{\partial z} + \frac{g}{C_p}\right) \\ &= -\tilde{K}_T\left(\frac{\partial T}{\partial z} + \frac{g}{C_p}\right)\end{aligned} \qquad (2.2.13)$$

where $\tilde{K}_T = \rho C_p K_T$ was defined as the eddy thermal conductivity (ergs/cm/sec/$^\circ$K).

The total heat flux can now be approximated as:

$$\mathcal{F}_{TOTAL} = \mathcal{F}_{MOL} + \mathcal{F}_{EDDY}$$

$$= -\lambda \frac{\partial T}{\partial z} - K_T \left(\frac{\partial T}{\partial z} + \frac{g}{c_p} \right) \qquad (2.2.14)$$

and Equation (2.2.8) becomes:

$$\rho c_p \frac{\partial T}{\partial t} = Q_{TOTAL} + \frac{\partial}{\partial z} \left\{ \lambda \frac{\partial T}{\partial z} + K_T \left(\frac{\partial T}{\partial z} + \frac{g}{c_p} \right) \right\} \qquad (2.2.15)$$

2.2.3 Pressure Coordinate System

In meteorological studies of the troposphere and stratosphere pressure is generally used as the vertical coordinate, and recently a pressure coordinate has been used in thermospheric studies as well (Mahoney, 1966; Lagos, 1967). The major reason for adopting a pressure coordinate in the present study was that the major physical processes in the atmosphere effecting the thermal state are much more closely tied to pressure surfaces than to height (z) surfaces.

The vertical coordinate chosen was the natural logarithm of p, the pressure, denoted by z_p. The derivatives of z and z_p are related by the following relations:

$$\frac{\partial}{\partial z} z_p = \frac{\partial \ln p}{\partial z} = -\frac{1}{H} \quad \therefore \frac{\partial}{\partial z} = -\frac{1}{H} \frac{\partial}{\partial z_p}$$

$$\frac{\partial^2}{\partial z^2} = -\frac{1}{H} \frac{\partial}{\partial z_p} \left(-\frac{1}{H} \frac{\partial}{\partial z_p} \right) \qquad (2.2.16)$$

$$\simeq \frac{1}{H^2} \left\{ \frac{\partial^2}{\partial z_p^2} - \frac{1}{T} \frac{\partial T}{\partial z_p} \frac{\partial}{\partial z_p} \right\}$$

These derivatives can be applied to the energy equation, Equation (2.2.15), which becomes:

$$\rho C_p^* \frac{\partial T}{\partial t} = Q_{TOTAL} - \frac{1}{H}\frac{\partial}{\partial z_p}\left(-\frac{\lambda+\tilde{K}_T}{H}\frac{\partial T}{\partial z_p} + \tilde{K}_T \frac{g}{C_p}\right) \quad (2.2.17)$$

where the potential energy term has been incorporated in the above through an approximation, discussed in Appendix A, which has the form:

$$\rho C_p^* \frac{\partial T}{\partial t} \simeq \rho C_p \frac{\partial T}{\partial t} + \rho \frac{\partial}{\partial t}(gz) \quad (2.2.18)$$

In evaluating Equation (2.2.17) it was assumed that λ, the molecular thermal conductivity, was far more sensitive to temperature changes than to the relatively small rate of change of composition with height encountered, thus:

$$\frac{\partial \lambda}{\partial z_p} \simeq \frac{\partial \lambda}{\partial T} \cdot \frac{\partial T}{\partial z_p} \quad (2.2.19)$$

Further the temperature dependence implied in Equation (2.3.3) is used to approximate the derivatives of λ :

$$\frac{\partial \lambda}{\partial T} \simeq \frac{\partial}{\partial T} C_\lambda \sqrt{T} = \frac{\lambda}{2T}$$
$$\frac{\partial^2 \lambda}{\partial T^2} \simeq -\frac{\lambda}{4T^2} \quad (2.2.20)$$

where C_λ was considered a constant. With these assumptions Equation (2.2.17) becomes:

$$\rho C_p^* \frac{\partial T}{\partial t} = Q_{TOTAL} + \frac{\lambda+\tilde{K}_T}{H^2}\frac{\partial^2 T}{\partial z_p^2} + \frac{1}{H^2}\frac{\partial \tilde{K}_T}{\partial z_p}\frac{\partial T}{\partial z_p}$$
$$+ \frac{1}{H^2}\left\{\frac{\partial \lambda}{\partial T} - \frac{\lambda+\tilde{K}_T}{T}\right\}\left(\frac{\partial T}{\partial z_p}\right)^2 - \frac{g}{C_p H}\frac{\partial \tilde{K}_T}{\partial z_p} \quad (2.2.21)$$

Thus we are dealing with a second order non-linear partial differential equation, of form:

$$\frac{\partial T}{\partial t} = A + B\frac{\partial T}{\partial z_p} + C\left(\frac{\partial T}{\partial z_p}\right)^2 + D\frac{\partial^2 T}{\partial z_p^2} \qquad (2.2.22)$$

with variable coefficients, given by:

$$\begin{aligned} A &= \left\{ q_{TOTAL} - \frac{g}{c_{pH}}\frac{\partial \tilde{K}_T}{\partial z_p} \right\} / \rho C_p^* \\ B &= \frac{\partial \tilde{K}_T}{\partial z_p} / \rho C_p^* H^2 \\ C &= \left\{ \frac{\partial \lambda}{\partial T} - \frac{\lambda + \tilde{K}_T}{T} \right\} / \rho C_p^* H^2 \\ D &= (\lambda + \tilde{K}_T) / \rho C_p^* H^2 \end{aligned} \qquad (2.2.23)$$

In order to study atmospheric response in real time Equation (2.2.22) was approximated by a stable, implicit finite difference scheme described in Appendix A.

2.2.4 Boundary Conditions

Two boundary conditions must be supplied for Equation (2.2.22), discussed in Appendix A in terms of the necessity of specifying the temperature at points just above and below the nominal boundaries at 50 Km and 120 Km. Some physical justifications for the choices of boundary conditions are discussed in this section; the actual formulation of the boundary conditions into the numerical model are described in Appendix A.

In choosing a boundary condition for the 120 Km level it is useful to briefly consider the gross thermal structure of the thermosphere. Thermospheric thermal studies (see for example Mahoney, 1966; Lagos,

1967) show that the net heating rate in $^{o}K/day$[1] is a monotonically decreasing function of altitude between about 200-300 Km and the mesopause. The rate of decrease of the net heating rate is near maximum at 120 Km. As a result the local thermal state in the region near 120 Km is more sensitive to the relatively large downward flux of heat than to the comparatively small local heating rate. Thus the boundary condition chosen was a constant specified heat flux at 120 Km. This of course places restraints on the temperature and the temperature derivative at that level (see Appendix A.)

The net heating rates near 50 Km are small reflecting a near balance between radiative heating and cooling. This balance represents a potentially large restoring force acting to drive the temperature toward an effective radiative equilibrium value (usually estimated to be not far from average measured values). Thus the tendency of the temperature at 50 Km to remain fairly constant over time periods shorter than those associated with normal seasonal changes is suggested. This argument tends to justify the convenient assumption of a constant temperature lower boundary condition. Unfortunately, this boundary condition has the effect of reducing all atmospheric response to zero in

---

[1] It is customary for discussion purposes to express heating and cooling rates in the units of $^{o}K/day$ in meteorological studies, while in aeronomic studies the common unit is $ergs/cm^3/sec$. The two are related by the following expression: $Q(^{o}K/day) = Q(ergs/cm^3/sec)/\rho C_p \times 86400$ where Q is a general heating/cooling rate, ρ and C_p have their usual meanings, and 86400 is the number of seconds per day. $Q(^{o}K/day)$ may be thought of as the initial response of the temperature profile to the general heat source or sink, $Q(ergs/cm^3/sec)$, if it were the sole process effecting the thermal state.

the limit as the constant temperature point is approached. In practice, however, the effect is essentially limited to the region below about 60 Km and has little effect in the upper mesosphere or lower thermosphere. This limitation is merely an operational aspect of the problem since if the atmospheric response down to 50 Km were required one would for example adopt a model with a lower boundary at 35 Km or 40 Km.

These boundary conditions may be summarized as:

(a) at upper boundary:

$$\frac{\lambda}{H}\frac{\partial T}{\partial z_p} + \frac{\tilde{K}_T}{H}\frac{\partial T}{\partial z_p} - \frac{\tilde{K}_T g}{c_p} = \mathcal{F}_{\text{upper boundary}} \qquad (2.2.24)$$

(b) at lower boundary:

$$T = T_{\text{lower boundary}} \qquad (2.2.25)$$

2.3 PARAMETER SPECIFICATION

2.3.1 Molecular Thermal Conductivity

The temperature dependence of the molecular thermal conductivity has been measured extensively for sea level atmospheric conditions (Hilsenrath, et at, 1955), and this data may be conveniently approximated by the following empirical expression (U. S. Standard Atmosphere, 1962):

$$\lambda_{air} = \frac{264.76 \times T^{3/2}}{T + 245.4 \times 10^{-12/T}} \quad \frac{ergs}{cm\ sec\ ^\circ K} \qquad (2.3.1)$$

This expression is probably a very good approximation to λ up to about the mesospause above which compositional changes must be taken into account.

It is also possible to calculate the value of λ for pure atomic oxygen, a limit the composition approaches in the upper thermosphere, with the expression given by Dalgarno and Smith (1962):

$$\lambda_0 = 67.1 \times T^{0.71} \quad \frac{ergs}{cm\ sec\ ^\circ K} \tag{2.3.2}$$

It is reasonable to assume that as the atmospheric composition varies from predominantly N_2 and O_2 at sea level to predominantly O at several hundred kilometers the molecular thermal conductivity will vary between the values estimated by Equations (2.3.1) and (2.3.2) respectively. A very general expression for λ may be derived from an approximate kinetic model (Jeans, 1925), which takes the composition directly into account:

$$\lambda = \sum_i n_i k \sqrt{\frac{18kT}{\pi m_i}} \left[\sum_j \overline{\sigma_{ij}}\, n_j \left(1 + \frac{m_i}{m_j}\right)^{1/2} \right]^{-1} \tag{2.3.3}$$

where k is Boltzmann's constant, n_i and m_i are the concentration and molecular mass (in grams) of the i^{th} constituent and $\overline{\sigma_{ij}}$ is the viscosity cross section for collisions between the i^{th} and j^{th} constituents. The major difficulty with this expression is the lack of knowledge of the necessary cross sections. Nevertheless, certain assumptions seem qualitatively reasonable and were adopted.

Because of the similarity in size and mass between the N_2 and O_2 molecules the following rough approximation was made:

$$\overline{\sigma_{N_2N_2}} \simeq \overline{\sigma_{O_2O_2}} \simeq \overline{\sigma_{O_2N_2}} = \overline{\sigma_{N_2O_2}} \tag{2.3.4}$$

then with the aid of Equations (2.3.1) and (2.3.3) we estimate the following:

$$\overline{\sigma_{N_2N_2}} \simeq \frac{k\sqrt{\frac{18kT}{\pi m_{N_2}}}}{\sqrt{2}\,\lambda_{air}}$$

$$\simeq 1.52\times10^{-15}\left\{1 + \frac{245.4}{T}10^{-12/T}\right\} cm^2 \qquad (2.3.5)$$

Similarly from Equations (2.3.2) and (2.3.3) we estimate that:

$$\overline{\sigma_{OO}} \simeq \frac{k\sqrt{\frac{18kT}{\pi m_O}}}{\sqrt{2}\,\lambda_O}$$

$$\simeq 7.93\times10^{-15}\,T^{-0.21}\ cm^2 \qquad (2.3.6)$$

These estimates of $\overline{\sigma_{N_2N_2}}$ and $\overline{\sigma_{OO}}$ are shown in Figure 2. Also shown in this figure is the value for:

$$\sigma_{ON_2} = \sigma_{N_2O} \simeq \left\{\frac{\sigma_{N_2N_2} + \sigma_{OO}}{2}\right\} \qquad (2.3.7)$$

which appears to be a particularly good approximation at the temperatures usually coincident in height with high O concentration.

In terms of the above, the adopted expression for the calculation of λ was:

$$\lambda = \frac{\lambda_{air}}{1 + n_O/n_{N_2}\sqrt{44/32}\ \overline{\sigma_{N_2O}}/\overline{\sigma_{N_2N_2}}} + \frac{\lambda_O}{1 + n_{N_2}/n_O\sqrt{44/56}\ \overline{\sigma_{ON_2}}/\overline{\sigma_{OO}}} \qquad (2.3.8)$$

The molecular thermal conductivity calculated with the expression above for the composition given in Appendix B and the temperature profile adopted in Chapter 3 (and shown in Figure 10) is shown in Figure 3. Also shown is λ_{air} as calculated from Equation (2.3.1)

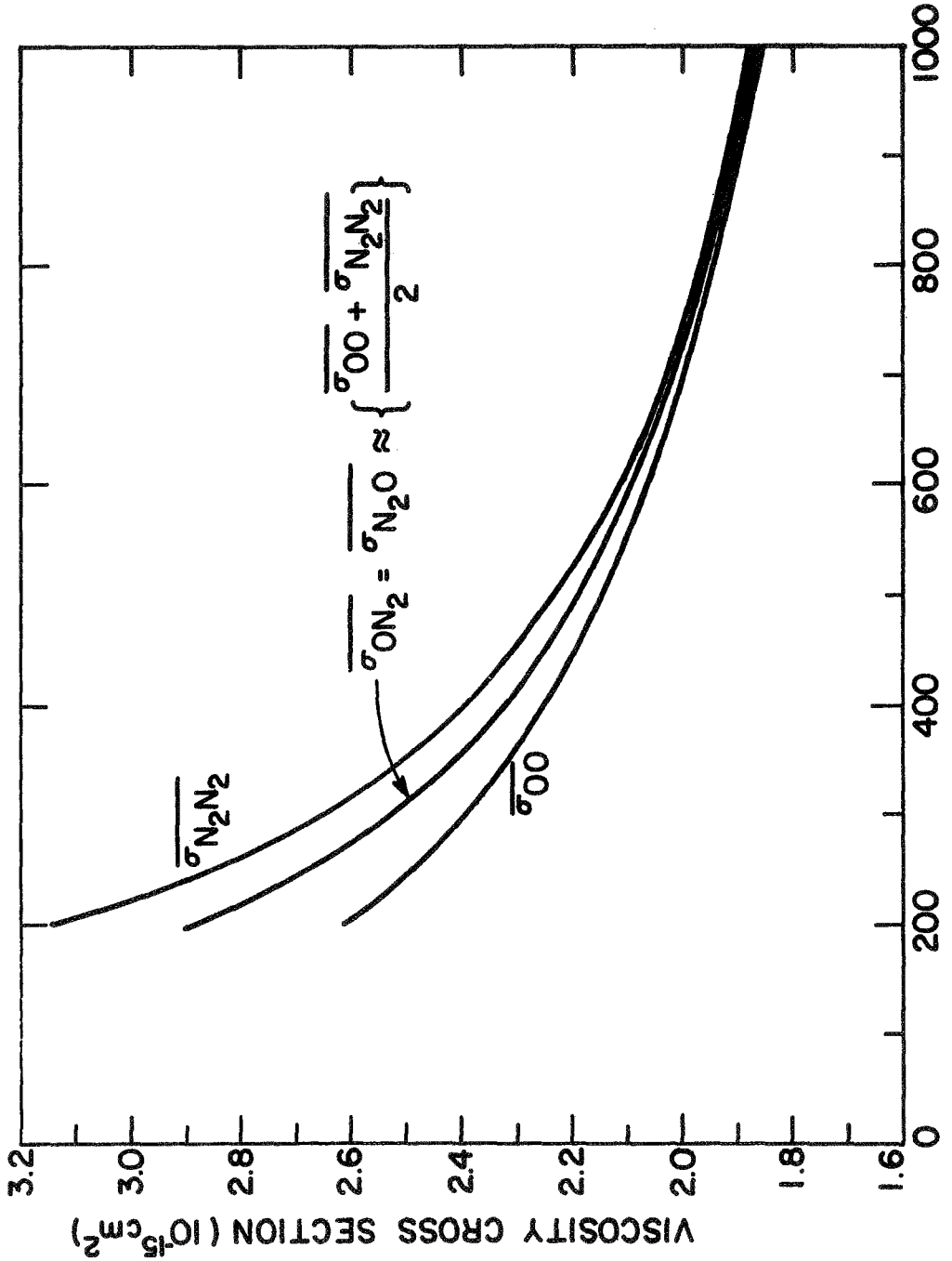

Figure 2. Estimated temperature dependence of viscosity cross sections involving O and N_2

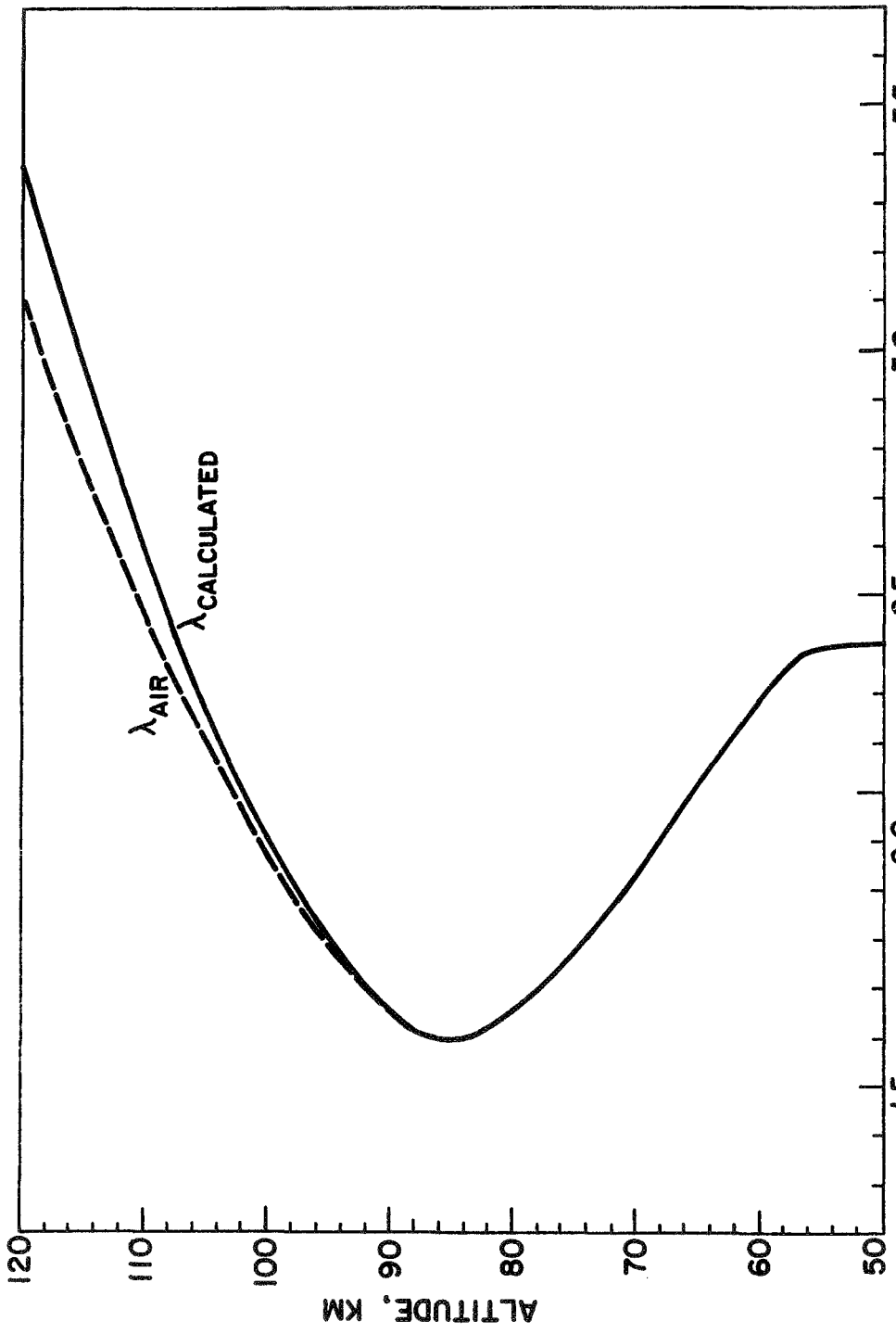

Figure 3. Comparison of adopted moelcular thermal conductivity profile with empirical expression λ_{air}

and the same temperature profile. The difference between the expressions of Equations (2.3.1) and (2.3.8) becomes even greater in the upper thermosphere.

2.3.2 Specific Heats, C_p and C_v

The general expressions for the specific heats in terms of the effective number of degrees of freedom at temperature T, $f(T)$, are the following:

$$C_v = \frac{1}{2} f(T) \frac{R}{M}$$
$$C_p = C_v + \frac{R}{M} = \left\{1 + \frac{1}{2} f(T)\right\} \frac{R}{M} \qquad (2.3.9)$$

Three translational degrees of freedom are obviously applicable and the rotational modes of all multi-atomic species are fully excited, as well, under atmospheric conditions. Thus for $f(T)$ we adopt:

$$f^{N_2,O_2}(T) = f_{trans} + f_{rot} = 5$$
$$f^{o}(T) = f_{trans} = 3 \qquad (2.3.10)$$

In addition vibrational modes for N_2 and O_2 can be excited at somewhat higher temperatures. The following were adopted as given by Davidson (1962):

$$\frac{1}{2} f_{vib}^{N_2}(T) \simeq \left(\frac{3354}{T}\right)^2 \frac{\exp\left(\frac{3354}{T}\right)}{\left[\exp\left(\frac{3354}{T}\right) - 1\right]^2} \qquad (2.3.11)$$

$$\frac{1}{2} f_{vib}^{O_2}(T) \simeq \left(\frac{2258}{T}\right)^2 \frac{\exp\left(\frac{2258}{T}\right)}{\left[\exp\left(\frac{2258}{T}\right) - 1\right]^2}$$

In calculating specific heats all attainable energy states should in principle be included. One such mode which seems to have been overlooked in previous atmospheric studies is the triplet ground state of atomic oxygen, $O(^3P_J)$; with energies: $\epsilon(^3P_2) = \epsilon_2 = 0$; $\epsilon(^3P_1) = \epsilon_1 = 0.020\,eV$; and $\epsilon(^3P_0) = \epsilon_0 = 0.028\,eV$. The populations of the three J levels are given by the partition functions, :

$$P_J = \frac{N_J}{\sum_J N_J} = \frac{\omega_J \exp\{-\epsilon_J/KT\}}{\sum_J \omega_J \exp\{-\epsilon_J/KT\}} \qquad (2.3.12)$$

where N_J is the population of the J^{th} level and ω_J is the multiplicity (or statistical weight) of that level, $\omega_J = 2J+1$. An additional amount of specific heat, $C_V(^3P)$, is appropriate for O because these upper states $(^3P_1, {}^3P_0)$ can be populated at rather low temperatures. Denoting the additional specific heat per molecule by:

$$C_V(^3P) = \frac{\partial}{\partial T}\langle\epsilon\rangle \qquad (2.3.13)$$

where $\langle\epsilon\rangle$ is the ensemble averaged energy:

$$\langle\epsilon\rangle = \frac{\sum_J \epsilon_J P_J}{\sum_J P_J} \qquad (2.3.14)$$

From Equations (2.3.12) and (2.3.14) we get:

$$\frac{\partial}{\partial T}\langle\epsilon\rangle = \frac{1}{KT^2}\left\{\langle\epsilon^2\rangle - \langle\epsilon\rangle^2\right\} \qquad (2.3.15)$$

where:

$$\langle\epsilon^2\rangle = \epsilon_1^2 P_1 + \epsilon_0^2 P_0$$
$$\langle\epsilon\rangle^2 = [\epsilon_1 P_1 + \epsilon_0 P_0]^2 \qquad (2.3.16)$$

Thus the additional degrees of freedom for O for the triplet ground state, $f^{o}_{3p}(T) = 2C_v(^3P)/K$, is just:

$$f^{o}_{3p}(T) = 2\left\{\frac{\epsilon_1^2 P_1 + \epsilon_0^2 P_0 - (\epsilon_1 P_1 + \epsilon_0 P_0)^2}{K^2 T^2}\right\} \qquad (2.3.17)$$

The energy associated with the fine structure levels of the triplet ground state of atomic oxygen is about one tenth the average translational energy at 100°K and becomes an even smaller fraction at higher temperatures; as shown in Figure 4a. The temperature dependence of $f^{o}_{3p}(T)$ is shown in Figure 4b.

The complete expression for the specific heat at constant pressure used in this study is:

$$C_p = \frac{R}{M}\left\{1 + \gamma_{N_2}\frac{1}{2}\left[5 + f^{N_2}_{vib}(T)\right] + \gamma_{O_2}\frac{1}{2}\left[5 + f^{O_2}_{vib}(T)\right] + \gamma_O\frac{1}{2}\left[3 + f^{o}_{3p}(T)\right]\right\} \qquad (2.3.18)$$

where $\gamma_{N_2}, \gamma_{O_2}, \gamma_O$ are the volume mixing ratios of N_2, O_2, O, respectively.

The altitude dependence of C_p for the temperature profile of Figure 10, and composition given in Appendix B., is shown in Figure 5.

2.4 SOLAR HEATING RATE

The solar heating rate refers to the rate at which energy removed from the solar UV energy flux is deposited locally in the atmosphere. The absorbing constituents considered were N_2, O_2, O, and O_3, with O_2 and O_3 being the most important between 50 Km and 120 Km. At 50 Km

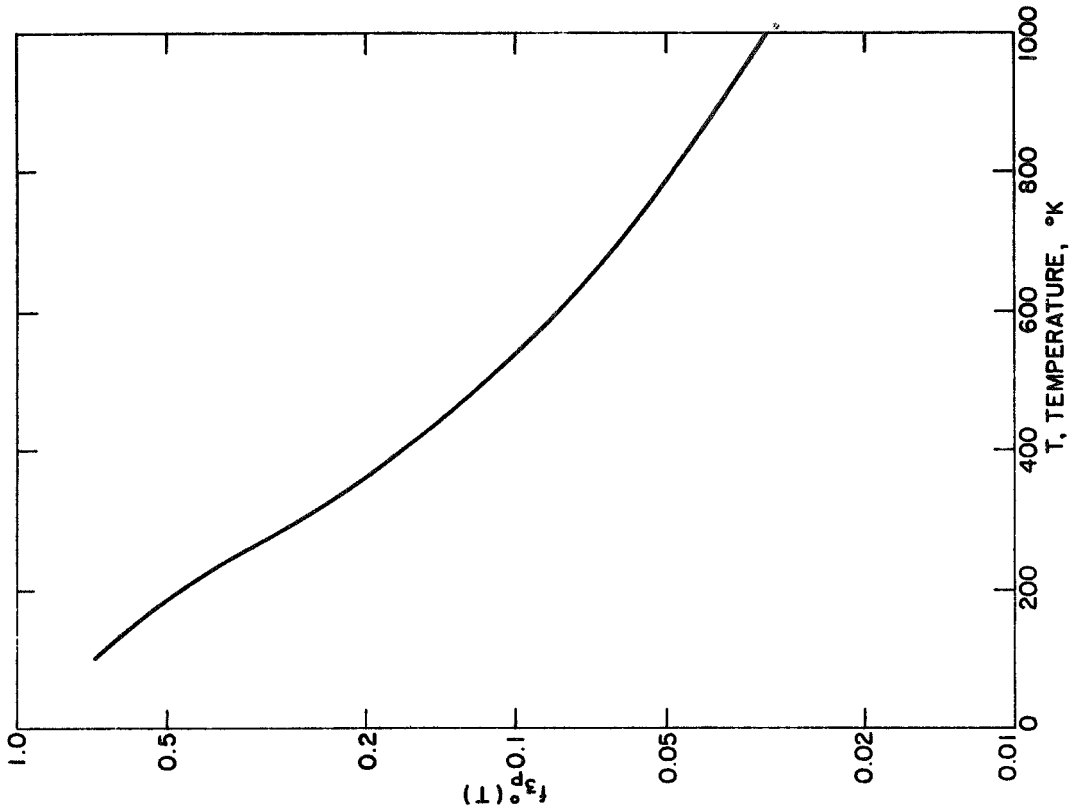

Figure 4. (b) Temperature dependence of the additional degrees of freedom of $O(^3P)$

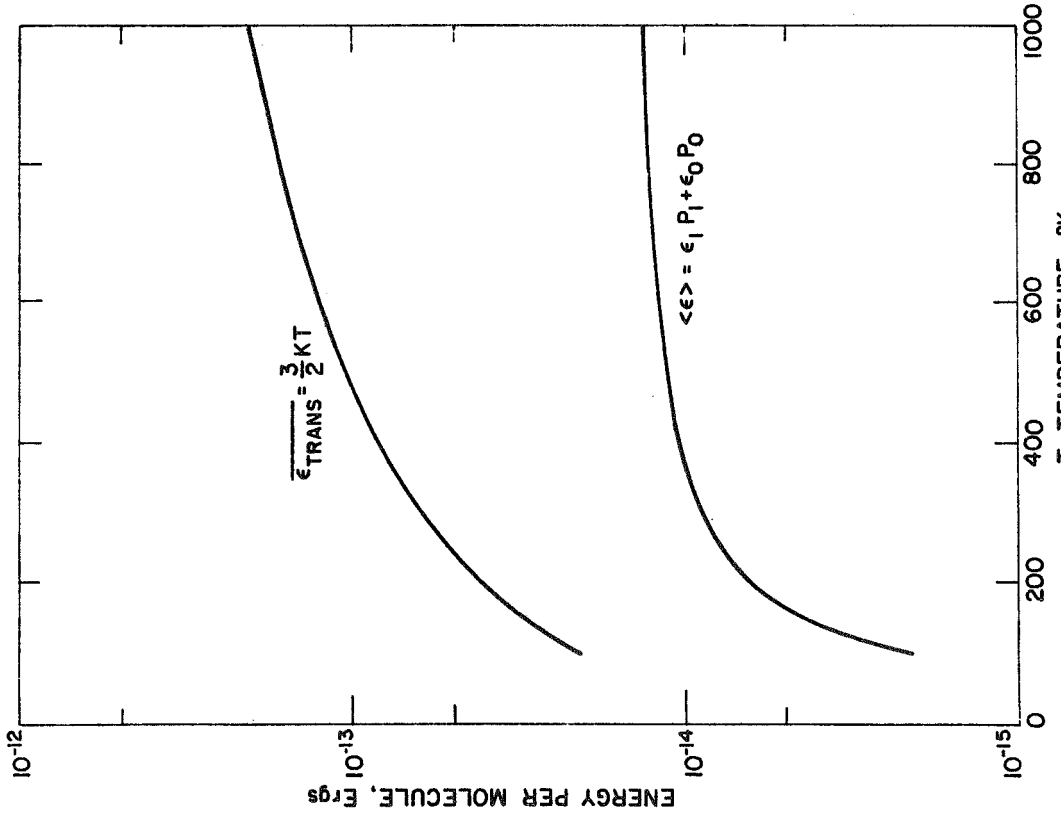

Figure 4. (a) Temperature dependence of the translational and fine structure energy per molecule for $O(^3P)$

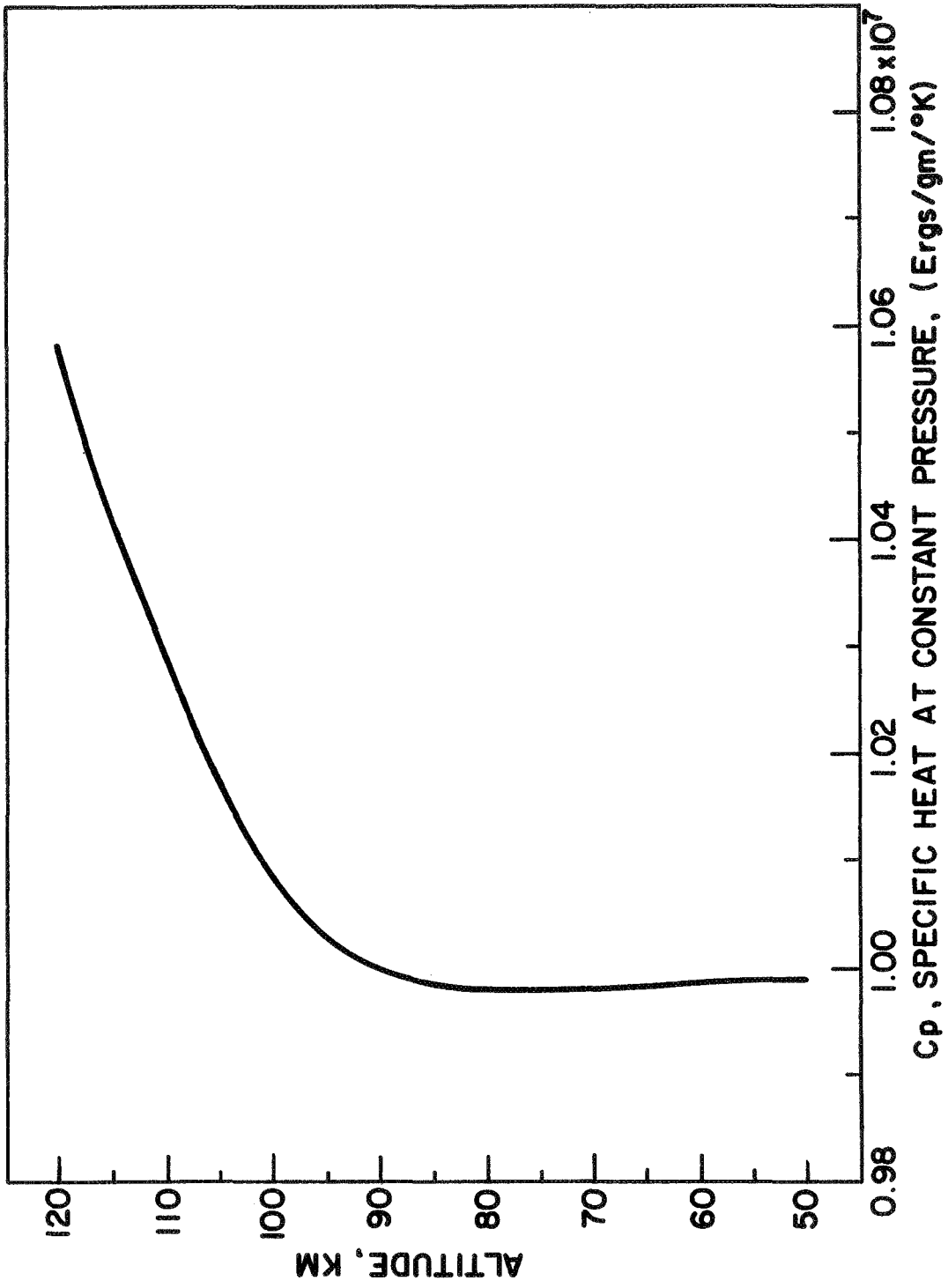

Figure 5. Profile of specific heat at constant pressure

and above solar radiation at wavelengths above about 3000 Å is only absorbed to a negligible extent and has been ignored. In the general case the absorption of a photon at wavelengths below 3000 Å does not lead to the local deposition of the full photon energy and thus heating efficiencies which were in general wavelength and altitude dependent had to be estimated for each constituent. In the first part of this section the general formulation of solar heating rate is presented. The rest of this section is devoted to discussions of the absorption processes and estimates of heating efficiencies.

2.4.1 General Formulation

The solar heating rate at height z for a local zenith angle θ (measured from the vertical) can be expressed from Beer's law as:

$$Q_{SOLAR}(z,\theta) = \int_{\lambda} E^{\lambda} \Phi_{\infty}^{\lambda} \sum_{i} \left[\epsilon_i^{\lambda}(z)\, \sigma_i^{\lambda}\, n_i(z)\right] \times \exp\left\{-\sum_{i} \sigma_i^{\lambda} N_i(z,\theta)\right\} d\lambda \qquad (2.4.1)$$

where: E^{λ} is the photon energy at wavelength λ, in ergs;

Φ_{∞}^{λ} is the solar photon flux at wavelength λ at the 'top' of the atmosphere, in photons/cm^2/sec/Å;

$\epsilon_i^{\lambda}(z)$ is the heating efficiency of the i^{th} constituent at wavelength λ and altitude z, (dimensionless);

$n_i(z)$ is the concentration of the i^{th} constituent at altitude z, in cm^{-3};

σ_i^{λ} is the absorption cross section for the i^{th} constituent at wavelength λ, in cm^2; and

$N_i(z,\theta)$ is the column density of the i^{th} constituent at altitude z taken along the atmospheric path at zenith angle θ, in cm^{-2} (see Appendix C for details).

The above expression was evaluated by a numerical scheme for the range $31\,\text{Å} \leq \lambda \leq 3000\,\text{Å}$. The details of the numerical approximation used as well as tabulated values of the relevant inputs are found in Appendix D.

2.4.2 Molecular Oxygen

The absorption of UV radiation by O_2 at wavelengths below 2424 Å was assumed to result in the following photodissociation processes:

$$O_2 + h\nu \longrightarrow O(^3P) + O(^3P) \qquad (2.4.2)$$
$$1750\text{Å} \leq \lambda \leq 2424\text{Å}$$

$$O_2 + h\nu \longrightarrow O(^1D) + O(^3P) \qquad (2.4.3)$$
$$\lambda < 1750\text{Å}$$

Equation (2.4.2) corresponds to absorption within the Herzberg continuum and the Schumann-Runge band system, which is thought to be at least 99% pre-dissociated (Hudson, et al, 1969). Wallace and McElroy (1966) discussed the dissociation products energetically possible for $\lambda < 1750$Å, and listed the following: $O(^3P) + O(^1D)$ for $\lambda < 1751$Å; $O(^1D) + O(^1D)$ for $\lambda < 1371$Å; $O(^3P) + O(^1S)$ for $\lambda < 1334$Å; and $O(^1D) + O(^1S)$ for $\lambda < 1102$Å. Their findings as well as those of Volman (1963) indicated that Equation (2.4.3) is probably the dominant process for the Schumann-Runge continuum ($1250\text{Å} \leq \lambda \leq 1750$Å). The neglect of ionization for $\lambda < 1027$Å is not felt to be significant because the net solar UV flux at these wavelengths is small, and because the majority of the ionization takes place above 120 Km.

Thus in the lower thermosphere the principal means of depositing solar UV energy are assumed to be the above two processes. The photon energy released in these processes is stored in three parts, in general. First there is the dissociation energy of about 5.12 ev per molecule common to both processes. Above about 100 Km recombination ($O+O+M \rightarrow O_2+M$) proceeds much slower than dissociation and a net downward flux of atomic oxygen results (Colgrove, et al, 1965, 1966). In the present study we consider the liberation of this energy upon recombination as a separate energy source. The second form of energy is the 1.96 ev of excitation energy of $O(^1D)$. An $O(^1D)$ may be de-excited by either of the following processes:

$$O(^1D) \rightarrow O(^3P) + h\nu\ (6300\text{Å}) \qquad (2.4.4)$$

$$O(^1D) + M \rightarrow O(^3P) + M^* + K.E. \qquad (2.4.5)$$

The lifetime of the $O(^1D)$ state against radiative decay, Equation (2.4.4), is about 110 sec. so that this process is only important in the upper thermosphere. Quenching, the process indicated in Equation (2.4.5), is predominant throughout the mesosphere and lower thermosphere. Estimates of the rate coefficient for Equation (2.4.5) are as follows:

$$M \equiv N_2 \qquad 2\times10^{-11} \leq K_Q \leq 1\times10^{-10} \qquad (2.4.6)$$

$$M \equiv O_2 \qquad 1\times10^{-11} \leq K_Q \leq 1.5\times10^{-10}$$

as given by Hunten and McElroy (1966), McGrath and McGarvey (1967), Snelling and Blain (1967), Young and Black (1967), Young, et al (1968), Peterson and Van Zandt (1969), and Noxon (1970). Because of its abundance N_2 must be the dominant quenching molecule. The outcome of quenching will be discussed below.

The third form of energy common to both Equations (2.4.2) and (2.4.3) is the excess kinetic energy shared by the resulting oxygen atoms. Of the three it is the most likely form of energy to be immediately converted into local thermal energy. Thus two of the three forms of energy associated with the processes of Equations (2.4.2) and (2.4.3) are easily dealt with, dissociation energy recovered separately upon recombination, and excess kinetic energy deposited locally. The fate of the $O(^1D)$ excitation energy unfortunately is less certain.

An approximate quenching scheme for $O(^1D)$, based in part upon the arguments of Walker, Stolarski, and Nagy (1969), was adopted in this study. The following are the principal assumptions employed:

(a) The primary quenching process results in vibrational excitation of N_2 molecules from the v=0 to the $v \leq 7$ state (where v is the vibrational quantum number);

(b) at 120 Km and below N_2-N_2 thermalizing collisions redistribute the vibrational energy towards a Boltzmann distribution;

(c) vibrational energy exchange with CO_2 provides an efficient sink for N_2 vibration energy at v=1, by

$$N_2(v=1) + CO_2(\text{ground state}) \longrightarrow N_2(v=0) + CO_2(\nu_3) - 0.002\ eV \qquad (2.4.7)$$

which is nearly energetically resonant; and

(d) above about the mesopause the excitation energy is radiated out of the region of interest at 4.3μ by $CO_2(\nu_3)$. The findings of Walker, et al (1969) indicate that probably not all of the $O(^1D)$ excitation energy is converted to N_2 vibration. Assumption (d) is somewhat arbitrary and will be discussed further in the section concerning ozone below. It is not possible at present to estimate the uncertainties in the above assumptions, or in the overall scheme adopted except in terms of limiting cases; these are discussed in Chapter 3.

In summary, the outcome of this assumed scheme is that for each $O(^1D)$ created an N_2 is excited to the ($v \leq 7$) state leading on the average to 6 or 7 $N_2(v=1)$ molecules. Each of these in turn exchange vibrational energy with a ground state CO_2 molecule, which deactivates by radiation of a 4.3μ photon. Nearly all of the $O(^1D)$ excitation energy is assumed to leave the region of interest as infrared radiation; partly to space and partly to the lower atmosphere where it is probably insignificant because of the much higher local thermal capacity.

When we assign an efficiency for converting solar UV radiation to local thermal energy by the process of Equation (2.4.2) we must subtract from each photon absorbed the dissociation energy, or:

$$\epsilon_2^{\lambda}(z) = \frac{E^{\lambda} - 5.12\,eV}{E^{\lambda}} \quad ; E^{\lambda} \geq 5.12\,eV \qquad (2.4.8)$$

For the process of Equation (2.4.3) both the dissociation energy and the 1.96 ev excitation energy of the (^1D) state must be subtracted from the

photon energy in determining the efficiency, thus:

$$\epsilon_2^{\lambda}(z) = \frac{E^{\lambda} - 7.08\,eV}{E^{\lambda}} \quad ; E^{\lambda} \geq 7.08\,eV \qquad (2.4.9)$$

Figure 6 shows the resulting efficiency for O_2 expressed by Equations (2.4.8) and (2.4.9), as well as in terms of the wavelength intervals discussed in Appendix A. It is also possible to obtain an effective efficiency for O_2 absorption as a function of altitude, as:

$$\overline{\epsilon_2(z)} = \frac{\int_{\lambda} \epsilon_2^{\lambda}(z)\,\sigma_2^{\lambda}\,\mathcal{F}^{\lambda}(z)\,d\lambda}{\int_{\lambda} \sigma_2^{\lambda}\,\mathcal{F}^{\lambda}(z)\,d\lambda} \qquad (2.4.10)$$

where $\mathcal{F}^{\lambda}(z)$ is the solar photon flux reaching height z at wavelength λ. In Figure 7 are plotted the effective O_2 efficiencies for Equations (2.4.8) and the combination of (2.4.8) and (2.4.9) for the earth averaged flux case described in Chapter 3.

2.4.3 Ozone

At wavelengths below about 3100 Å the absorption of solar UV radiation by ozone is thought to occur through the following process (McGrath and Norrish, 1957):

$$O_3 + h\nu \rightarrow O(^1D) + O_2(^1\Delta_g) + K.E. \qquad (2.4.11)$$

Dissociation of O_3 in the Hartley continuum, by the above, typically takes place in the stratosphere and mesosphere where recombination is certain to occur before the products could be transported any distance. Thus the efficiency for deposition of the UV photon energy locally will depend upon the processes which remove the excitation energy of the metastables $O(^1D)$ and $O_2(^1\Delta_g)$.

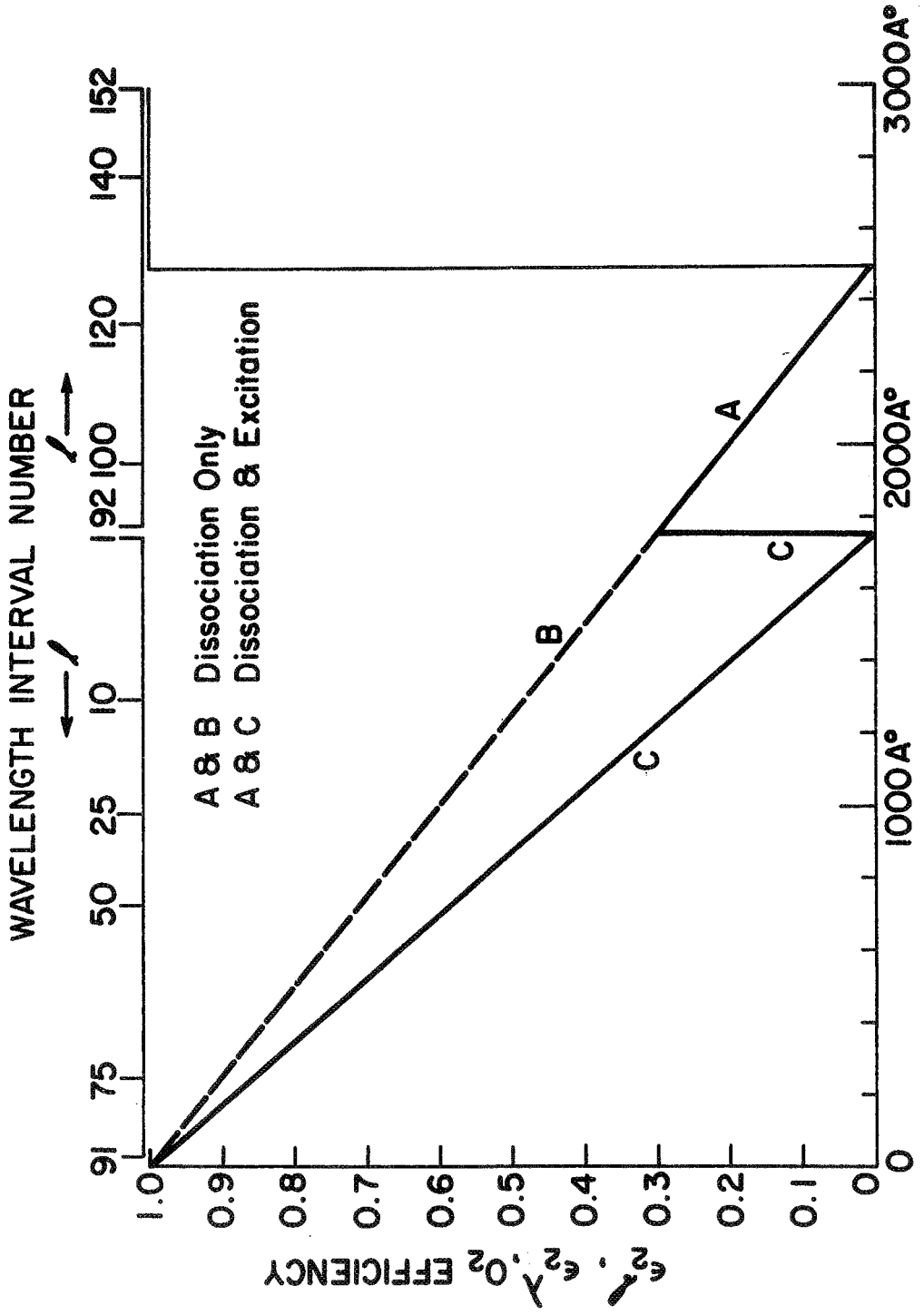

Figure 6. Wavelength dependence of O_2 heating efficiency based on loss of dissociation and $O(^1D)$ excitation energies, and loss of dissociation energy alone

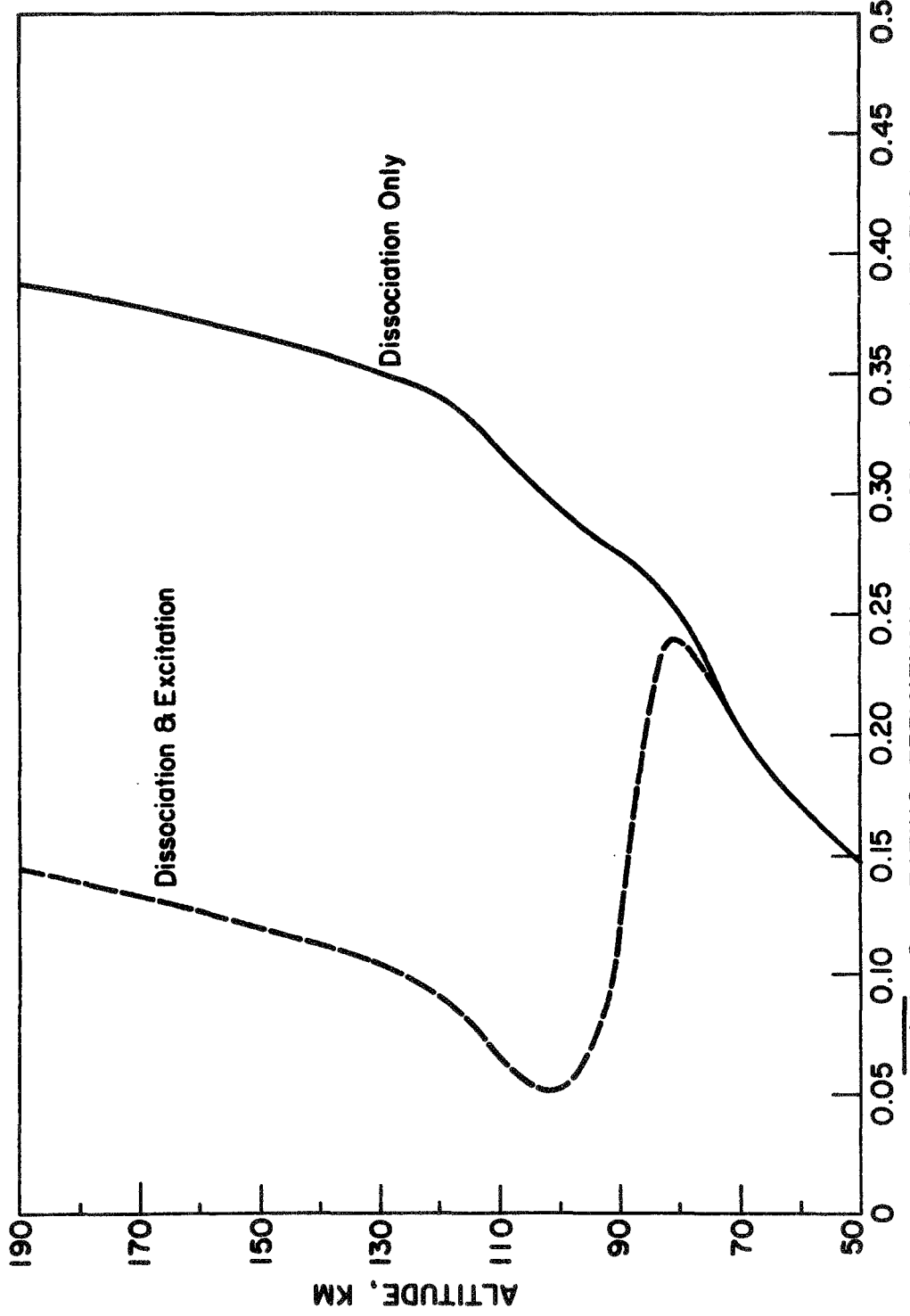

Figure 7. Profiles of wavelength averaged O_2 heating efficiency, based on loss of dissociation and $O(^1D)$ excitation energies, and loss of dissociation energy alone

Consider first the $O(^1D)$ formed in Equation (2.4.11). Assuming the same chain of events, as for O_2 above, leading to 6 or 7 CO_2 (ν_3) molecules per $O(^1D)$ formed we then must ascertain the fate of the ν_3 mode energy. $CO_2(\nu_3)$ can be deactivated by any of the following processes:

$$CO_2(\nu_3) + M \longrightarrow CO_2(\text{ground state}) + M^* + \text{K.E.} \qquad (2.4.12)$$

with a lifetime $\tau_A \simeq 1.2 \times 10^{-5}$ sec at STP;

$$CO_2(\nu_3) \longrightarrow CO_2(\text{ground state}) + h\nu(4.3\mu) \qquad (2.4.13)$$

with a lifetime $\tau_B \simeq 2.4 \times 10^{-3}$ sec; and

$$CO_2(\nu_3) + N_2(V=0) \longrightarrow CO_2(\text{ground state}) + N_2(V=1) \qquad (2.4.14)$$

with a lifetime $\tau_c \simeq \{5 \times 10^{-13} [N_2(V=0)]\ \text{sec}^{-1}\}^{-1}$

With the assumption that Equations (2.4.12) and (2.4.14) are distinct processes we may estimate the likelihood that a given CO_2 (ν_3) molecule will be radiatively deactivated as:

$$P_R = \frac{1/\tau_B}{1/\tau_A + 1/\tau_B + 1/\tau_c} \qquad (2.4.15)$$

Both P_R and $P_Q = 1 - P_R$, the likelihood of quenching are shown in Figure 8. The two processes are equal in magnitude at roughly 75 Km and on that

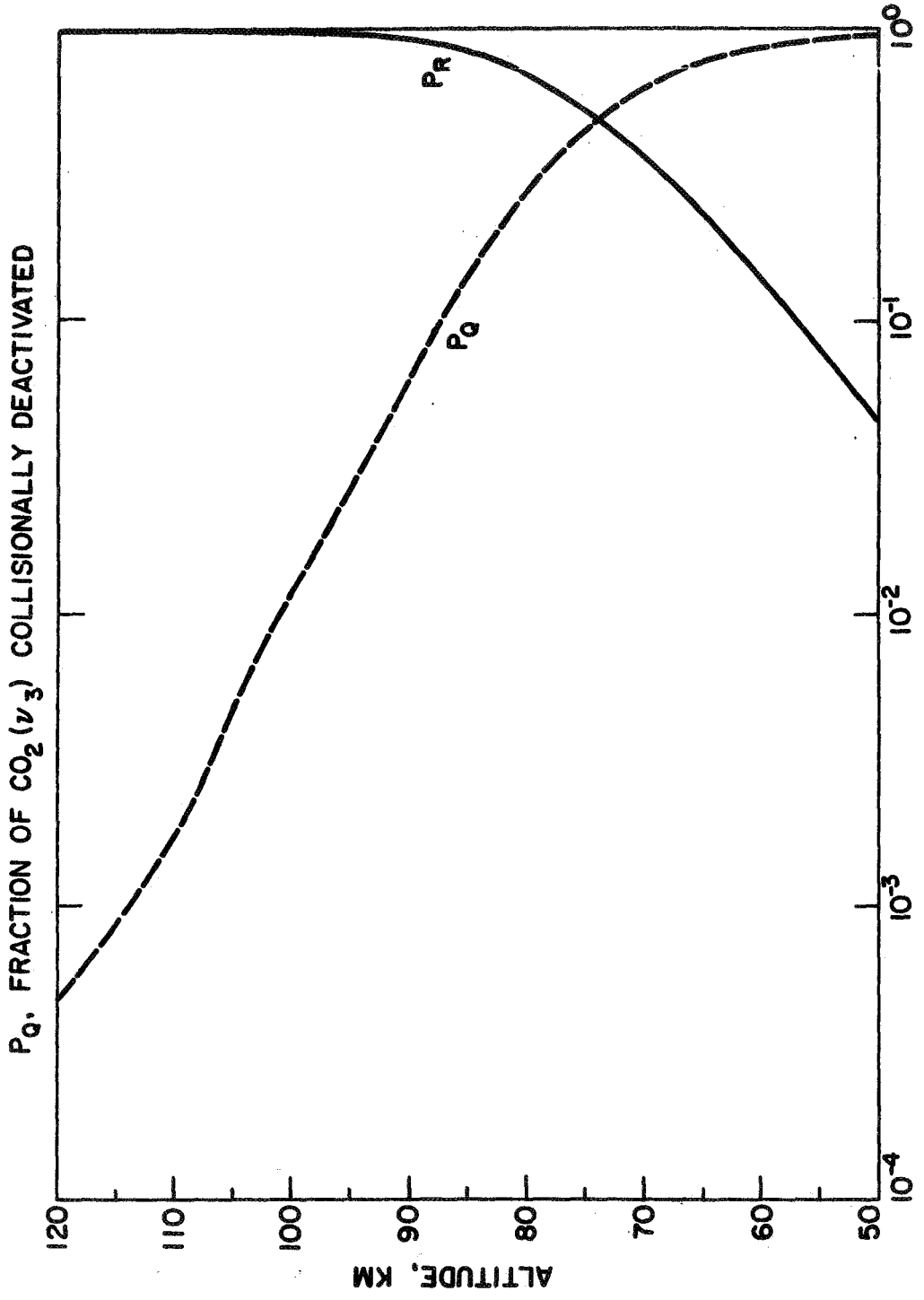

Figure 8. Profiles of de-excitation probabilities for CO_2 (ν_3) for quenching and radiation

basis one could argue that the 4.3μ radiation will in general leave the region down to 75 Km or lower. However, at 75 Km the atmosphere is not optically thin at 4.3μ and the only valid answer would require a full radiative transfer calculation, which is beyond the scope of the present study. (Such a calculation would be of great interest both in settling the present uncertainty but more basically as indicating the kinds of 4.3μ emission features peculiar to the $O(^1D)$-N_2 vibration excitation scheme which might suggest experimental verification.)

Kuhn (1968) considered the problem of $CO_2(\nu_3)$ excitation from absorption of solar 4.3μ radiation. He found that much of this excitation energy was deposited locally throughout the mesosphere, although it decreased quite rapidly near the mesopause. The solar and N_2 vibration excitation sources are qualitatively similar. Thus it can be argued by analogy that the latter source will result in local deposition of energy up to the vicinity of the mesopause. Noting that O_3 absorption is only significant near the mesopause and below we have arbitrarily assumed that in the photolysis of O_3, the $O(^1D)$ excitation energy is always deposited locally. We had previously assumed that this same excitation energy would all leave the region when it was formed as part of the photolysis of O_2; thus the two assumptions are contradictory near the mesopause. It would be difficult to devise significantly improved assumptions without resorting to a 4.3μ IR transfer solution. In any event the uncertainty in the solar heating rate in the vicinity of the mesopause due to the assumptions made on the fate of the $O(^1D)$ energy is not large (Chapter 3.).

On the other hand the radiation from $O_2(^1\Delta_g)$ (the 0-0 band at 1.27μ and the 0-1 band at 1.58μ of the infrared atmospheric bands of O_2) are extremely strong features of the dayglow. So at least part of the $O_2(^1\Delta_g)$ produced by O_3 photolysis must escape the region. Consider the following scheme for deactivation of $O_2(^1\Delta_g)$ (Vallance Jones and Gattinger, 1963):

$$O_2(^1\Delta_g) + M \rightarrow O_2(^3\Sigma_g^-) + M^* \qquad M = N_2, O_2 \qquad (2.4.16)$$

has a lifetime $\tau_D \simeq \{1.7 \times 10^{-21} \sqrt{T}\,[M]\ \text{sec}^{-1}\}^{-1}$ where $[M]$ is essentially the total number density, and T the temperature;

$$O_2(^1\Delta_g) \rightarrow O_2(^3\Sigma_g^-) + h\nu \qquad \text{(IR atmospheric bands)} \qquad (2.4.17)$$

with a lifetime $\tau_E \simeq 6.67 \times 10^3$ sec; and

$$O_2(^1\Delta_g) + O \rightarrow O_2(^3\Sigma_g^-) + O^* \qquad (2.4.18)$$

with a lifetime $\tau_F \simeq \{2 \times 10^{-14}\,[O]\ \text{sec}^{-1}\}^{-1}$ where $[O]$ is the atomic oxygen concentration. Thus the probability of an $O_2(^1\Delta_g)$ being quenched either through Equations (2.4.16) or (2.4.18) is:

$$P_Q = \frac{1/\tau_D + 1/\tau_F}{1/\tau_D + 1/\tau_E + 1/\tau_F} \qquad (2.4.19)$$

and the probability of radiative deactivation is $P_R = 1 - P_Q$. The average UV photon absorbed in the Hartley continuum has a wavelength of about 2500 Å compared with the 1.27μ photon resulting as a secondary

process. Thus at most each IR photon carries off about 0.197 of the original UV photon energy. On this basis we set the efficiency of O_3 for local deposition of absorbed UV radiation to be:

$$\epsilon_4^{\lambda}(z) = 1 - 0.197\, P_R = \overline{\epsilon_4(z)} \quad \text{for all} \tag{2.4.20}$$

The altitude dependence of $\overline{\epsilon_4(z)}$ is shown in Figure 9.

2.4.4 Molecular Nitrogen, Atomic Oxygen

The absorption of solar UV radiation by N_2 and O is predominantly through ionization in the thermosphere. The incident photon energy will generally be divided among the electron and ion gases, possibly in dissociation energy, in the formation of metastable states, in vibrational excitation and even secondary ionization processes. The subject is of great interest but beyond the scope of this study. Fortunately the details of the local heating processes above 120 Km are not as relevant as those below 120 Km for the thermal model.

Most of the solar UV energy absorbed above 120 Km by N_2 and O must appear as a downward flux of heat at 120 Km or be radiated away at 63μ or as part of the airglow spectrum. The approach adopted here was to assume 100% heating efficiency for N_2 and O and estimate the heat lost by radiation above 120 Km. Thus:

$$\epsilon_1^{\lambda}(z) = \epsilon_3^{\lambda}(z) = 1.0 \tag{2.4.21}$$

for all λ, for all z

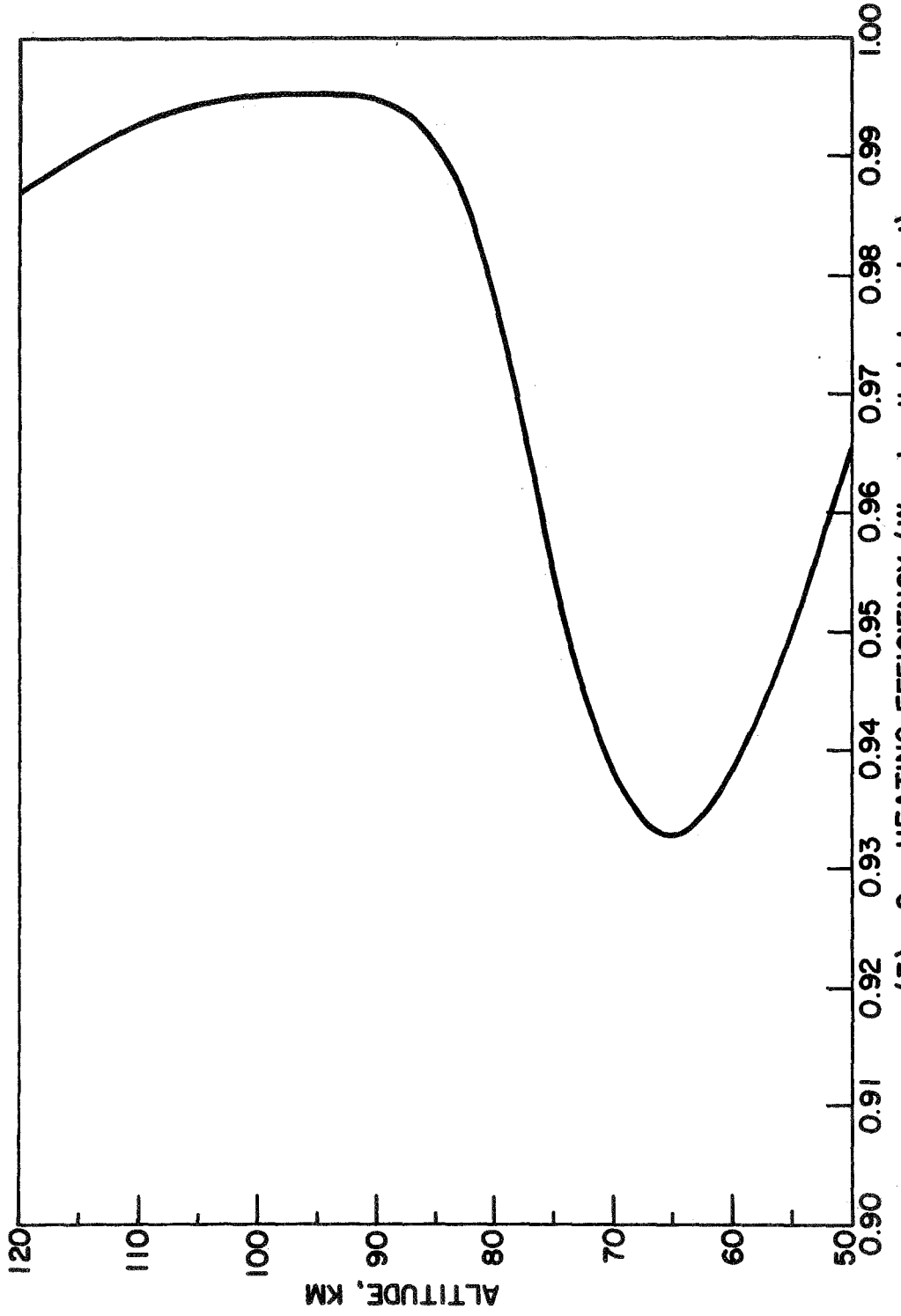

Figure 9. Profile of O_3 heating efficiency

2.5 IR RADIATIVE TRANSFER COOLING RATES

The major IR cooling processes for the mesosphere and lower thermosphere are the radiative flux divergences of CO_2(15μ bands), O_3 (9.6μ bands) and O(63μ line) included in the sections below. Neglected were the extensive bands of H_2O and the 4.3μ and minor bands of CO_2 (at 1.4μ, 1.6μ, 2μ, 2.7μ, 5μ, and 10μ). For these neglected bands the maximum expected contribution to the radiative heating or cooling is on the order of 1^{o}K/day; however they average only a fraction of one ^{o}K/day (Kuhn, 1970).

2.5.1 Carbon Dioxide

The principal feature of IR radiative transfer throughout the mesosphere and lower thermosphere are the 15μ bands of CO_2 [1] arising from transitions to the ν_2 vibration mode. The role of CO_2 (15μ bands) cooling in this region has been studied in detail since methods of handling the breakdown of local thermodynamic equilibrium (LTE) for the various bands were worked out (Curtis and Goody, 1956; Kuhn, 1966; Drayson, 1967).

By neglecting the sphericity and horizontal inhomogeneities of the atmosphere, refraction, scattering, and the non-isotropy of the source function, the basic equation of radiative transfer at frequency ν can be written (Chandrasekhar, 1960):

$$\mu \frac{dI(\nu,\tau,\mu)}{d\tau} = I(\nu,\tau,\mu) - J(\nu,\tau) \qquad (2.5.1)$$

---

[1] The 15μ bands of CO_2 were considered to contain fundamentals and most important overtone bands of the four most abundant isotopes of CO_2.

where: $I(\nu, \tau, \mu)$ is the specific intensity;

$\mu = \cos\theta$, θ is the zenith angle;

$\tau = \tau_\nu$ is the optical depth, $d\tau_\nu = K_\nu du$

u is the optical mass of the absorbing gas;

K_ν is the absorption coefficient;

e_ν is the emission coefficient; and

$J(\nu, \tau) = e_\nu / K_\nu$ is the source function, which equals the Planck black-body function for LTE.

The quantity of interest in terms of the local heating or cooling rate is the divergence of the energy flux at pressure, p, given by:

$$\frac{dF}{dp} = 2\pi \frac{du}{dp} \int_\nu K_\nu \left\{ \int_\tau^{\tau_g} E_2(\tau' - \tau) \frac{dJ}{d\tau'} d\tau' - \int_0^\tau E_2(\tau - \tau') \frac{dJ}{d\tau'} d\tau' - E_2(\tau) J(\nu, 0) \right\} d\nu \qquad (2.5.2)$$

where $E_2(x)$ is the exponential integral of second order resulting from the integration of $I(\nu, \tau, \mu)$ over μ, and τ_g is the optical depth at the lower boundary (taken to be the ground). The flux divergence may also be expressed in a form in which the difference between the source function and the Planck function is explicit (Drayson, 1967, 1970):

$$\frac{dF}{dp} = 4\pi \frac{du}{dp} S \frac{\theta}{\lambda} (J - B) \exp\left(\frac{E_0}{KT}\right) \qquad (2.5.3)$$

where: S is the band strength;

θ is the radiative lifetime;

λ is the vibrational relaxation time.

B is the Planck black - body function; and

E_0 is the energy of the lower vibration state.

From Equations (2.5.2) and (2.5.3) one can calculate the unknown source functions, J, from the Planck functions, B, for the altitude region of interest. The flux divergences are directly temperature dependent because of the dependence on the B's and are also functions of the mixing ratio profile of CO_2 through du/dp.

These calculations are extremely difficult requiring careful investigation of required assumptions and a good deal of analytical and numerical approximation. Some aspects of the calculations, such as line by line integration over frequency (Drayson, 1967), require considerable amounts of computation. This precludes the frequent repetition of these calculations required in the present study for temperature profiles that change with latitude and season (Chapter 4) and with time (Appendix G). So a simplified scheme was worked out by Drayson (1970), for linearizing the flux divergence with temperature perturbations about a standard profile. Thus the flux divergence (or local heating/cooling rate) can be considered as an approximation to be:

$$\frac{dF}{dz} = \left(\frac{dF}{dz}\right)_0 + \int_{z_{min}}^{z_{max}} \Psi(z, z') \cdot \delta T(z')\, dz' \qquad (2.5.4)$$

where: $\left(\frac{dF}{dz}\right)_0$ is the flux divergence for the standard temperature profile $T_0(z)$;

$\Psi(z,z')$ is the Green's function showing the influence of the temperature at height z' on the flux divergence at height z;

$\delta T(z') = T(z') - T_0(z')$ is the temperature perturbation; and

z_{min} and z_{max} are the boundaries (taken to be the earth's surface and the top of the atmosphere, respectively).

The details of this approximation and further discussion of the Drayson (1970) model adopted in this study are found in Appendix F.

This formulation was developed initially for a model atmosphere with a constant CO_2 volume mixing ratio[1], consistent with earlier studies. This assumption has always placed considerable uncertainty on the estimates of CO_2 cooling rates in the lower thermosphere. Since in the present study it was desired to evaluate this quantity with reasonable certainty up to 120 Km a separate investigation into the atmospheric distribution of CO_2 was undertaken. The result is presented in Appendix E. The volume mixing ratio for CO_2 adopted for the present study was a median value given as curve B in Figure 2 (Appendix E). Drayson (1970) showed that the inclusion of a variable CO_2 volume mixing ratio has a significant effect on the cooling rates in the lower thermosphere, reducing them by factors of 2 to 3 (see Chapter 3.).

Another comparable source of uncertainty is the vibrational relaxation time which varies as the collision frequency. The value for sea level condition, λ°, was adopted as 10μ sec; this is discussed in Chapter 3.

2.5.2 Ozone

Kuhn and London (1969) showed that the 9.6μ bands of O_3 provide cooling in the upper stratosphere and lower mesosphere (about 30 Km to

---

[1] The term "volume mixing ratio" is defined to be the ratio of the concentration of a specified constituent to that of the gas as a whole.

70 Km) with a maximum of just over 3 ^{o}K/day near 50 Km in good agreement with the earlier results of Plass (1956). Kuhn and London (1969) also showed that the variation in this cooling rate with latitude and season is quite small. Consequently, it was assumed that seasonal-latitudinal variations were negligible and a mean profile of O_3 cooling rate was adopted from Kuhn and London (1969).

2.5.3 Atomic Oxygen

The only atomic constituent which can participate in IR radiative transfer to an important extent in the atmosphere is oxygen. Bates (1951) pointed out that the 63μ emission arising from the fine structure of the ^{3}P ground state of O should be the most important cooling process in the upper thermosphere. Bates' calculation for the O cooling rate, given by:

$$Q_{BATES} = -\frac{1.67\times10^{-18}[O]\exp\left(-\frac{228}{T}\right)}{1+0.6\exp\left(-\frac{228}{T}\right)+0.2\exp\left(-\frac{325}{T}\right)} \qquad (2.5.5)$$

(where [O] is the atomic oxygen concentration, T is the temperature, and Q_{BATES} has units of ergs/cm^{3}/sec), represents an upper limit and neglects the actual details of the radiative transfer. Recently, Craig and Gillie (1969) solved the transfer problem and obtained significantly reduced cooling rates in the lower thermosphere, compared with those calcualted by Equation (2.4.10) and insignificant heating near the mesopause. However, above about 150 Km they found cooling rates only 10% - 20% lower than those of Bates.

The approach adopted in the present study was to accept the ratios of the cooling rates derived from radiative transfer to those of Bates, which were given by Craig and Gillie (1969), as representative of the role of radiative transfer. Then these ratios were used in conjunction with calculations of Q_{BATES} according to Equation (2.4.10) for local values of [O] and T in determining the O(63μ line) cooling rates, $Q_{63\mu}$. This method is sufficiently accurate for energy balance studies of this type (Gillie, 1970).

2.6 CHEMICAL RECOMBINATIONAL HEATING RATE

The bulk of the solar UV flux absorbed in the lower thermosphere results in the dissociation of O_2 in the Schumann-Runge continuum. Each pair of oxygen atoms thus formed carry 5.12 ev of chemical energy which can be released as heat upon recombination.

Colgrove, et al (1965, 1966) have shown that above about 100 Km recombination by the most likely process:

$$O + O + M \longrightarrow O_2 + M \qquad (2.6.1)$$

cannot compete with dissociation and the excess atomic oxygen formed diffuses downward. This downward flux is augmented by additional dissociation at wavelengths above 1750 Å (Hudson, et al, 1969), principally in the mesosphere. In the mesosphere and below atomic oxygen and ozone continually exchange identities through the processes:

$$O + O_2 + M \longrightarrow O_3 + M \qquad (2.6.2)$$

$$O_3 + h\nu\,(\lambda < 1.1\mu) \longrightarrow O + O_2 \qquad (2.6.3)$$

Indicating that the term "odd oxygen" is more appropriate than O and O_3. Odd oxygen is lost[1] through recombination back to O_2 both through the reaction of Equation (2.6.1) and by:

$$O + O_3 \rightarrow 2O_2 \qquad (2.6.4)$$

In the approximate recombination scheme adopted the details of the intermediate processes, Equations (2.6.2) and (2.6.3) were ignored and the full 5.12 ev chemical energy was assumed to be recovered when either of the reactions of Equations (2.6.1) or (2.6.4) took place. This assumption neglects the possible redistribution of about one fourth of the chemical energy when the recombination actually takes place via Equations (2.6.2) and (2.6.4)

The rate coefficients for Equations (2.6.1) and (2.6.4), K_{11} and K_{13}, respectively, are somewhat uncertain because the highly reactive nature of O and O_3 complicates laboratory analysis of these reactions. In a recent review of these and other reactions of importance in the atmosphere Schiff (1968) recommended the following for K_{13}:

$$K_{13} = 1.2 \times 10^{-11} \exp(-4/RT) \text{ cm}^3/\text{sec} \qquad (2.6.5)$$

---

[1] The present discussion and the assumptions to follow neglect the very complex hydrogen-oxygen chemistry (see, for example Hunt, 1966 and Shimazaki and Laird, 1970). This omission is not considered to be significant.

Where R is the gas constant (1.98717×10^{-3} kcal/(gm mole)/^{o}K) and T is the temperature; this value was adopted in this study. Schiff also discussed K_{11} but without a specific recommendation. In the present work the value obtained by Morgan and Schiff (1963):

$$K_{11} = 2.8 \times 10^{-33} \text{ cm}^6/\text{sec} \tag{2.6.6}$$

was adopted.

The recombinational model adopted was:

$$Q_{CHEM} = 8.264 \times 10^{-12} C_R \left\{ K_{11} [O]^2 [M] + K_{13} [O] [O_3] \right\} \tag{2.6.7}$$

Where Q_{CHEM} is the chemical recombinational heating rate (ergs/cm^3/sec), 8.264×10^{-12} is the chemical energy per recombination (ergs), and C_R is an empirical factor discussed below. In view of the uncertainties in composition (chiefly O_3) and the rate coefficients it was necessary to include in principal the factor C_R to balance the total recombination above 50 Km with the total dissociation above 50 Km. In practice, however, estimates of C_R were always close to unity and a value of C_R=1 was used in all calculations.

2.7 HEAT FLUX AT 120 KM

The downward heat flux at 120 Km must be evaluated in order to specify the upper boundary condition of the energy equation. The time independent (steady state) energy equation may be written as follows:

$$\rho C_p^* \frac{\partial T}{\partial t} = 0 = Q_{TOTAL} - \frac{\partial}{\partial z} \mathcal{F}_{TOTAL} \tag{2.7.1}$$

Integrating the above equation over the limits 120 Km $\leq z' \leq \infty$, one obtains:

$$0 = \int_{120}^{\infty} Q_{TOTAL}\, dz' - \int_{120}^{\infty} d\mathcal{F}_{TOTAL} \qquad (2.7.2)$$

where it is physically appropriate to require the heat flux to vanish in the limit as z approaches ∞. Thus, the heat flux is just:

$$\mathcal{F}_{TOTAL}(120) = -\int_{120}^{\infty} Q_{TOTAL}\, dz' \qquad (2.7.3)$$

The heating and cooling processes assumed to contribute to Q_{TOTAL} were the following: solar heating rate and O(63μ line) cooling rate, as described above; and dissipation of tidal oscillations. Airglow emissions were neglected. The heat flux contributions from absorption of solar UV radiation and the IR radiative transfer at 63μ were calculated by the straightforward integration given in the above equation.

Lindzen (1967) has made extensive calculations of thermally driven diurnal tidal oscillations in the region between the surface and about 100 Km. Included in this study was an estimate of the upward flux of energy due to these oscillations, with a maximum of 6.8 ergs/cm^2/sec at the equator, considerably lower values ($\sim$ 1 erg/cm^2/sec) at mid-latitudes, and zero contribution above 60^o. The hemisphere average of this energy flux is about 1.75 ergs/cm^2/sec. Lindzen's calculations did not include dissipation mechanisms such as IR radiative cooling, viscosity, conductivity (both molecular and eddy) and ion drag.

These mechanisms were discussed in Lindzen and Chapman (1969), and quantitative estimates of the dissipation rates were recently given by Blake and Lindzen (1970), where it was shown that the majority of the dissipation takes place in the upper thermosphere. Other possible mechanisms of dissipation (Lindzen, 1968) and of reflection (Yanowitch, 1967) have been offered; however, there is no definite confirmation that the tidal energy flux is appreciably diminished before reaching 100 Km. This is a tremendous flux of energy nearly $2\frac{1}{2}$ times the energy deposited above 120 Km in absorption of solar UV radiation. Such a significant thermal input could not be ignored and in the absence of a clearer picture of the possible morphology of the tides below 100 Km it had to be included in the basic thermal model.

In the present study it was assumed that all of the upward flux of tidal energy given by Lindzen (1967) was dissipated above 120 Km, that this energy was redistributed by conduction and circulation, and finally that this energy appeared as a downward heat flux at 120 Km at approximately the hemispheric average value. Certainly the effect of introducing a sustained heat flux of nearly 7 ergs/cm^2/sec into the equatorial thermosphere would completely alter our ideas of upper thermospheric models if lateral transport were not in fact important. Inclusion of dissipation energy from the 100 Km - 120 Km region into the downward heat flux at 120 Km should not lead to large errors since the amount of dissipation estimated for this region is small compared to both the local heating/cooling rates, and also to the remainder of the dissipation that takes place above 120 Km.

Thus the heat flux at 120 Km was calculated as follows:

$$\Phi_{TOTAL}(120) = -\int_{120}^{\infty} \{Q_{SOLAR} + Q_{63\mu}\}\, dz' - \overline{\Phi_{TIDE}} \qquad (2.7.4)$$

where $\overline{\Phi_{TIDE}}$ is the hemisphere average of the upward tidal energy flux (~ 1.75 ergs/cm^2/sec). For earth average conditions (Chapter 3) the above quantities have the following values:

$$\int_{120}^{\infty} Q_{SOLAR}\, dz' = 0.73 \text{ ergs/cm}^2\text{/sec}$$

$$\int_{120}^{\infty} Q_{63\mu}\, dz' = -0.085 \text{ ergs/cm}^2\text{/sec} \qquad (2.7.5)$$

$$\Phi_{TOTAL}(120) = -2.40 \text{ ergs/cm}^2\text{/sec}$$

CHAPTER 3

GLOBAL MODEL

3.1 INTRODUCTION AND CONCEPT

The thermal structure of the mesosphere and lower thermosphere is examined on the global scale in this chapter. This is accomplished by adopting a global or earth average model. Such a model is intended to approximate the long term areal average of the diurnal, geographical, and seasonal variations for the earth as a whole. The averaging process acts to completely compress the horizontal extent of the model removing horizontal variations and simplifying the dynamics. Large scale circulatory systems are reduced to quasiconvective transport in the vertical because the horizontal compression reduces a simple cell to its ascending and subsiding elements. The same is true for dynamics on all of the smaller scales including those which have been characterized in Chapter 2 as contributing to eddy transport.

The physical processes at work in the mesosphere and lower thermosphere are critically examined for their influence on the mean thermal state and several of the more prominant sources of uncertainty in these processes are discussed. Also by looking at the global scale it was possible to estimate the overall interdependence of the mean thermal state and the average vertical transport.

3.2 EARTH AVERAGE SOLAR HEATING RATE

The compositional and structural atmospheric model, adopted for earth average conditions, is described in Appendix B. The selection of an earth average temperature profile is discussed below; the profile

adopted in the present study is presented in Figure 10. The only significant parameter remaining in determining the earth average solar heating rate was the zenith angle θ.

If $s(z, \theta)$ is the actual atmospheric path from the point at z to the sun (see Appendix C.) and adopting the commonly used approximation $ds = dz/\cos\theta$, one can express the solar energy flux at wavelength λ, $\Phi_E^\lambda(z)$, as:

$$\Phi_E^\lambda(z) = \Phi_E^\lambda(\infty)\, \mu \exp\{-\tau_z^\lambda/\mu\} \qquad (3.2.1)$$

where $\mu = \cos\theta$ and τ_z^λ, the optical depth, is defined by:

$$\begin{aligned} \tau_z^\lambda &= \sum_i \sigma_i^\lambda N_i(z,0) \\ &= \sum_i \sigma_i^\lambda \int_z^\infty n_i(z')\, dz' \end{aligned} \qquad (3.2.2)$$

This approximation is quite accurate[1] for $\theta \leq 80^\circ$, but as θ approaches 90° the flux calculated as above will tend to zero much more quickly than is the actual case. Thus in averaging the solar energy flux for the earth as a whole the use of the above approximation tends to under-estimate the contributions for $80^\circ < \theta \leq 90^\circ$ where they are quite small already.

An earth average solar energy flux was obtained from a simple geometrical approach. Consider an element of area δA lying in a circular ring of radius r and located a distance R from the center of the earth, as shown in Figure 11, where $R = R_E + z$ and R_E is the earth's radius. SSP is the sub solar point and δA lies in a plane normal to the sun-earth line. Since $r = R \sin\theta$, where θ is the local zenith angle for points on the

[1] The calculation of column densities described in Appendix C. suggest the inaccuracy averages on the order of 3%, at $\theta = 80^\circ$.

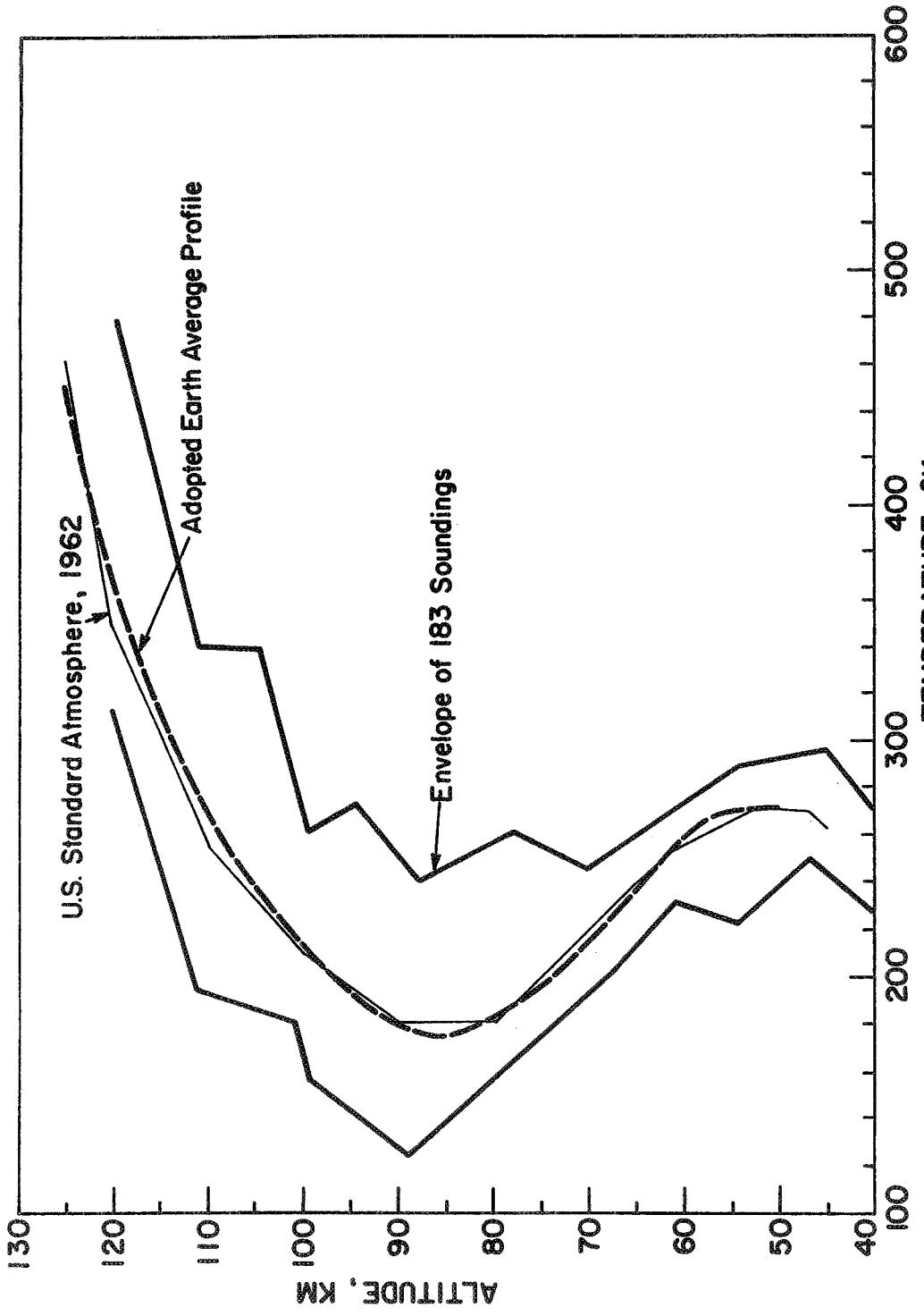

Figure 10. Earth average temperature profile adopted; temperature profile from the U.S. Standard Atmosphere, 1962, and envelopes of 183 soundings included for comparison

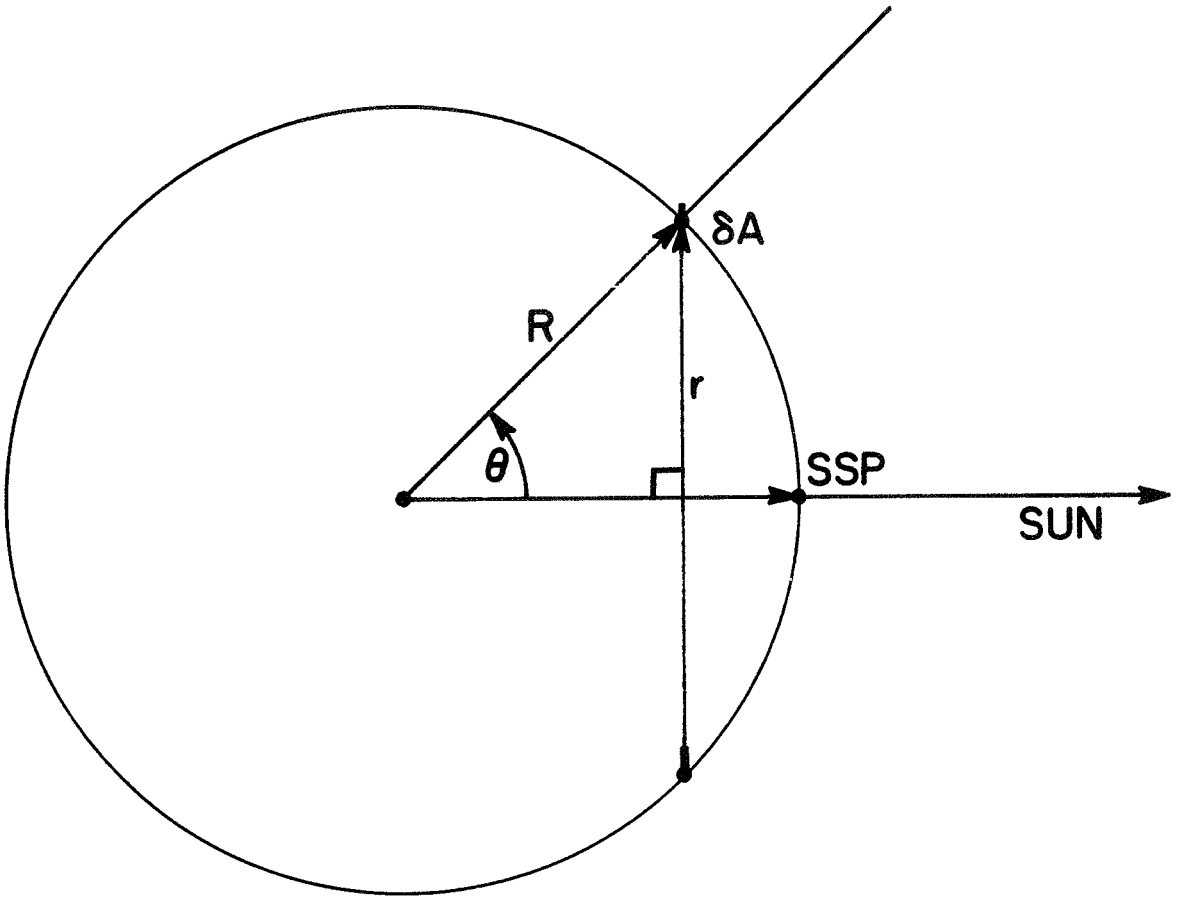

Figure 11. Sun-earth geometry for solar UV flux absorption

circular ring, δA is just:

$$\begin{aligned} \delta A &= 2\pi r\, dr \\ &= 2\pi R^2 \cos\theta\,(-d\cos\theta) \\ &= -2\pi R^2 \mu\, d\mu \end{aligned} \tag{3.2.3}$$

The flux impinging on each element of area δA were then summed and the result divided by the total area of the sphere of radius R, $4\pi R^2$, giving for the earth average flux:

$$\overline{\mathcal{F}_E^{\lambda}(z)} = \frac{1}{4\pi R^2} \int_0^1 \mathcal{F}_E^{\lambda}(z)\ (-2\pi R^2 \mu\, d\mu) \tag{3.2.4}$$

where the integration was performed over the sunlit hemisphere. Since each element δA was normal to the sun-earth line, Equation (3.2.1) became, for this geometry:

$$\mathcal{F}_E^{\lambda}(z) = \mathcal{F}_E^{\lambda}(\infty)\ \exp\{-\tau_z^{\lambda}/\mu\} \tag{3.2.5}$$

thus Equation (3.2.4) was just:

$$\overline{\mathcal{F}_E^{\lambda}(z)} = \frac{1}{2} \int_0^1 \mathcal{F}_E^{\lambda}(\infty)\ \exp\{-\tau_z^{\lambda}/\mu\}\, \mu\, d\mu \tag{3.2.6}$$

then letting $\eta = 1/\mu$, the above equation became:

$$\overline{\mathcal{F}_E^{\lambda}(z)} = \frac{1}{2}\, \mathcal{F}_E^{\lambda}(\infty) \int_1^{\infty} \exp\{-\eta\, \tau_z^{\lambda}\}\, \frac{d\eta}{\eta^3} \tag{3.2.7}$$

or:

$$\overline{\mathcal{F}_E^{\lambda}(z)} = \frac{1}{2}\, \mathcal{F}_E^{\lambda}(\infty)\ E_3(\tau_z^{\lambda}) \tag{3.2.8}$$

where $E_3(\tau_z^{\lambda})$ is the exponential integral of order 3 in the argument τ_z^{λ}.

The earth average solar energy flux, given in the above equation, is zenith angle independent, therefore the earth average rate of absorption of solar energy is just:

$$\overline{\frac{\partial}{\partial z} F_E^{\lambda}(z)} = \frac{\partial}{\partial z} \overline{F_E^{\lambda}(z)} \qquad (3.2.9)$$
$$= -\frac{1}{2} F_E^{\lambda}(\infty) \frac{\partial \tau_z^{\lambda}}{\partial z} E_2(\tau_z^{\lambda})$$

where $E_2(\tau_z^{\lambda})$ is the exponential integral of order 2 in the argument τ_z^{λ}, and from Equation (3.2.2):

$$\frac{\partial \tau_z^{\lambda}}{\partial z} = -\sum_i \sigma_i^{\lambda} n_i(z) \qquad (3.2.10)$$

With the addition of the heating efficiencies as described in Chapter 2, the earth average solar heating rate, analogous to Equation (2.4.1), became:

$$\overline{Q_{SOLAR}(z)} = \int_{\lambda} \left\{ \frac{E^{\lambda} F_{\infty}^{\lambda}}{2} \sum_i \left[\epsilon_i^{\lambda}(z) \sigma_i^{\lambda} n_i(z) \right] \right.$$
$$\left. \times E_2 \left(\sum_i \sigma_i^{\lambda} n_i(z) \right) \right\} d\lambda \qquad (3.2.11)$$

The earth average solar heating rate is shown in Figure 12; also shown are the following heating/cooling rates adopted as part of the global thermal model: CO_2(15μbands); O_3(9.6μbands); O(63μline); chemical recombination; and the total of the above. These quantities are labelled Q_{SOLAR}, $Q_{15\mu}$, $Q_{9.6\mu}$, $Q_{63\mu}$, Q_{CHEM}, and Q_{TOTAL}, respectively in Figure 12.

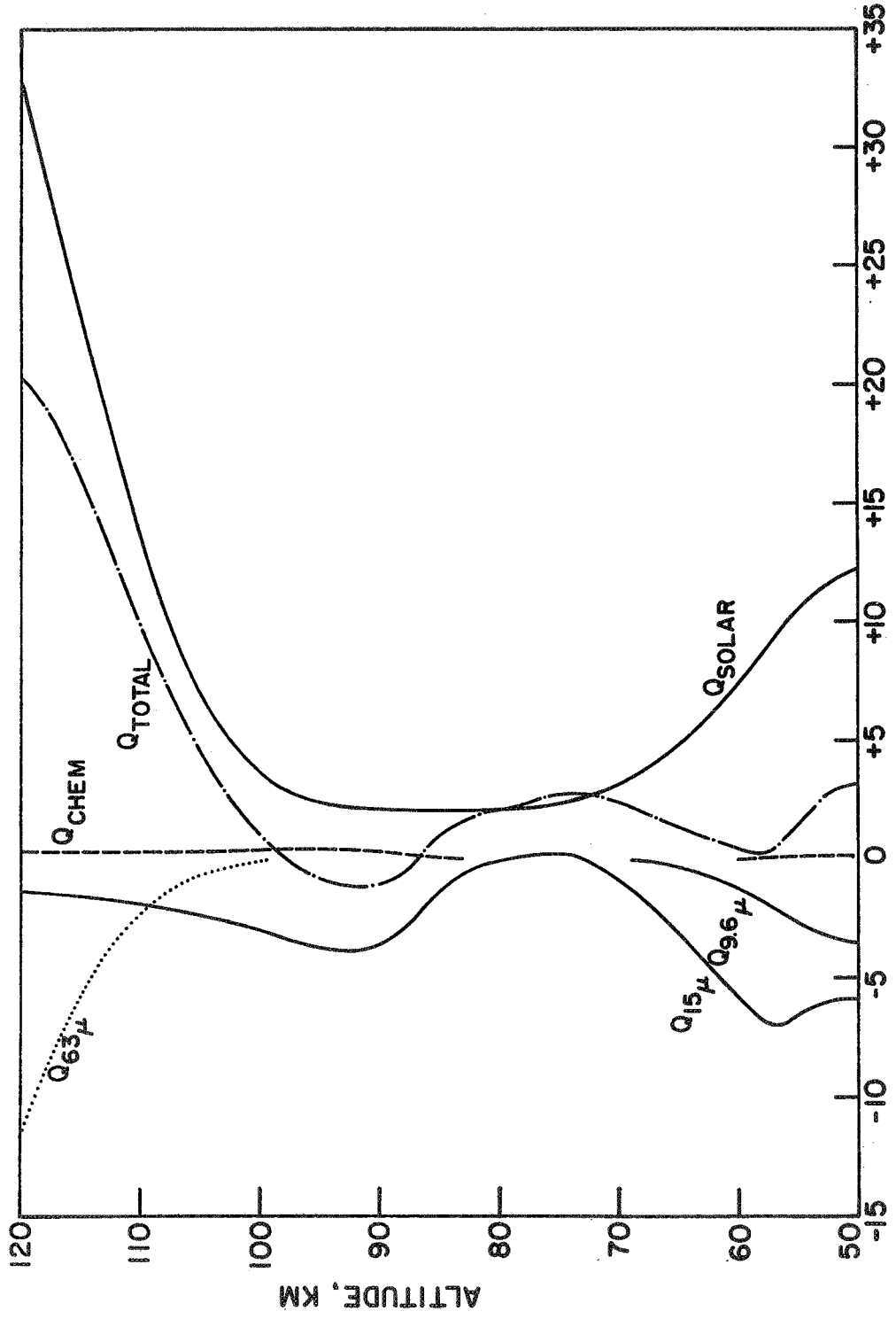

Figure 12. Heating and cooling rates adopted for the global model

3. 3 AN EQUILIBRIUM STATE

As mentioned in Chapter 1 the working hypothesis used in building the time dependent thermal model was the separability of a mean thermal state from perturbed states, which together make up the observable states of the atmosphere. In formulating an earth average mean thermal model, the composition and structural parameters (T, P, ρ) were fixed and a time independent solar heating rate as formulated above, was adopted. This lead to a time independent mean thermal state synonomous with an equilibrium state for the atmosphere.

3. 3. 1 Mean Temperature Profile

No single temperature profile can meaningfully represent the earth as whole at all latitudes, in all seasons and yet in the sense that an average composition and average heating and cooling rates can be formulated for the earth, a single temperature profile is indicative of this thermal model. The two criteria used in choosing an earth average temperature profile were the following: the temperature profile adopted should be smooth; and it should roughly represent a median value of measured temperature profiles for a variety of seasons, geographical locations, and times of day. The first criterion is both practical and physically obvious. Atmospheric processes act to smooth out discontinuities so that a model which includes them would have, for example, exaggerated local effects of CO_2 (15μbands) IR cooling (Drayson and Epstein, 1969), and would also require an extremely discontinuous eddy thermal conductivity profile acting to maintain them.

The second criterion is a weak but straight forward application of the working hypothesis. Actual temperature measurements show the sum of the mean and perturbed states along with local diurnal, seasonal, and geographical variations and include experimental error as well. No attempt was made to extract the earth average temperature profile from them; however, each candidate temperature profile was compared with an ensemble of 183 soundings (Smith, et al, 1964, 1967, 1968, 1969). The profile adopted as an earth average wasa modified CIRA 1961; it is shown in Figure 10 along with envelopes of the extremes of the 183 soundings and the 1962 U. S. Standard Atmosphere for comparison.

3. 3. 2 Equilibrium Eddy Transport

A mean, and therefore equilibrium, thermal state can now be achieved by specifying an equilibrium eddy thermal conductivity, K_T (equil), sufficient to balance the total heating with the adopted temperature profile. This quantity can be derived from the equilibrium form of energy equation, which is:

$$0 = Q_{TOTAL} + (\lambda + \tilde{K}_T)\frac{\partial^2 T}{\partial z^2} + \frac{\partial \lambda}{\partial T}\left(\frac{\partial T}{\partial z}\right)^2 + \frac{\partial \tilde{K}_T}{\partial z}\left(\frac{\partial T}{\partial z} + \frac{g}{C_p}\right) \qquad (3.3.1)$$

The above equation can be formulated in a finite difference scheme with solution by matrix inversion exactly analogous to that described in Appendix A. The resulting K_T(equil.) profile unfortunately reflects the numerical 'noise' in the finite difference approximations to the temperature derivatives. These results can not be used in a phenomenological description of the eddy transport.

A far more realistic eddy thermal conductivity profile can be calculated analytically if Equation (3. 3. 1) is integrated with the assumption that the heat flux at 120 Km is known:

$$\tilde{K}_T(equil) = \frac{\int_z^{120} \rho_{TOTAL}\, dz' - \Phi_{TOTAL}(120) - \lambda \frac{\partial T}{\partial z}}{\left\{ \frac{\partial T}{\partial z} + \frac{g}{C_p} \right\}} \qquad (3.3.2)$$

The equilibrium eddy diffusion coefficient is just:

$$K_T(equil) = \frac{\tilde{K}_T(equil)}{\rho C_p} \qquad (3.3.3)$$

The above equilibrium eddy transport coefficients are given in Figure 13. The results are far more physically reasonable. However, it is not surprising that they do not in general hold for the numerical approximation to Equation (3. 3. 1) (see Appendix A), which is subject to the temperature derivative 'noise' mentioned above.

3. 3. 3 Approach to Equilibrium

The equilibrium thermal state was achieved in the following way. The eddy transport coefficients as given in Equations (3. 3. 2) and (3. 3. 3) were adopted as the appropriate equilibrium values and introduced into the time dependent thermal model (Appendix A) along with the other inputs appropriate to the earth average case, including the adopted temperature profile. Since an equilibrium state did not exist, level for level, in the model, the temperature profile changed with time. After about fifty days no further changes were perceptible although the model was run another one hundred days as a check, the new temperature profile was adopted as the equilibrium temperature profile in all later earth average model studies. The new profile differed from the old by less than 1% at any

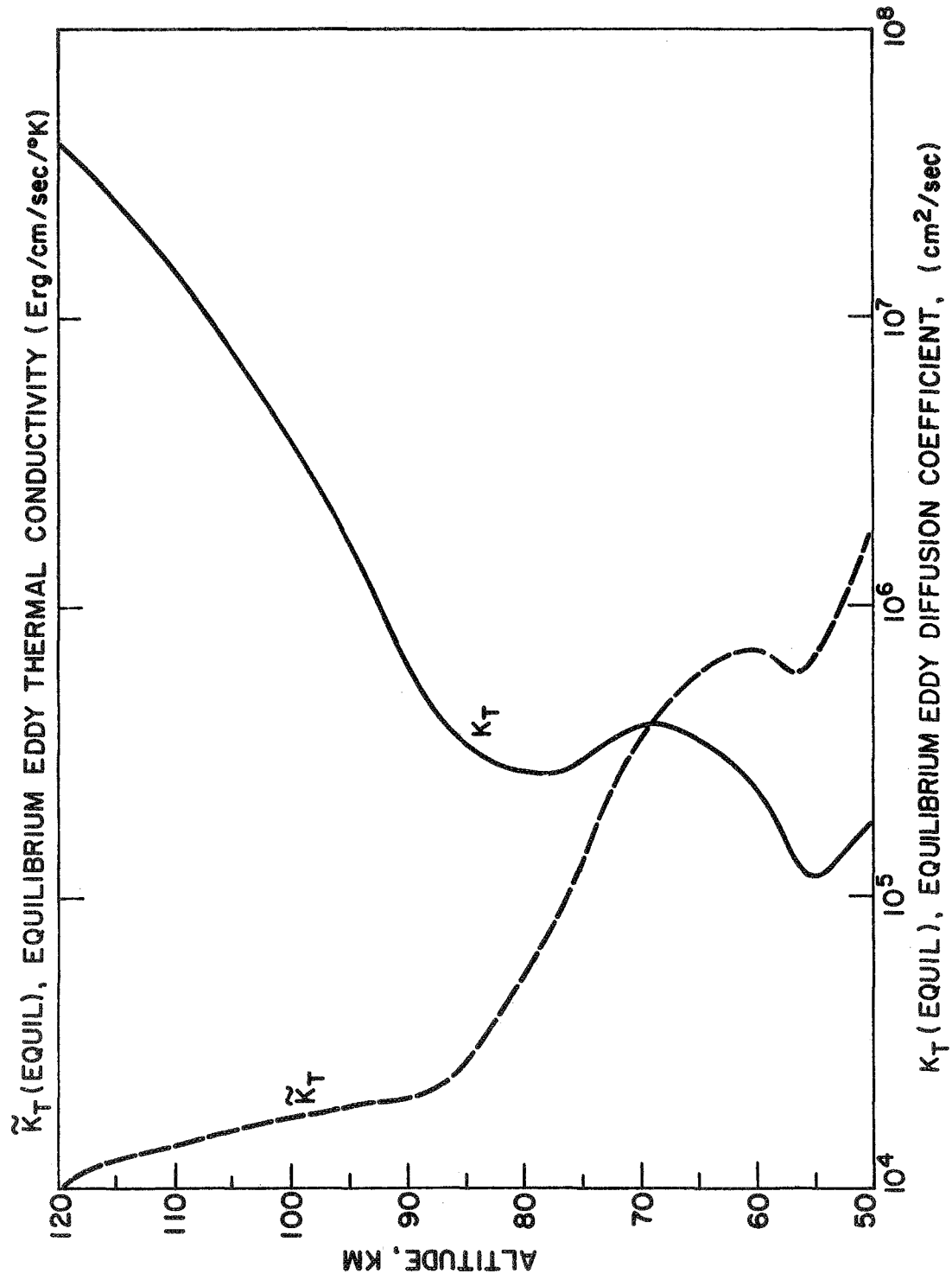

Figure 13. Equilibrium eddy transport coefficients adopted for the global model

point. What in fact had happened in the above procedure was that atmospheric response was used to remove the numerical temperature derivative 'noise' without perceptibly changing the overall temperature profile. This exercise also served as a useful check on the numerical model.

3.4 UNCERTAINTIES IN THE MODEL

The thermal model used in the studies above represents in many ways a reasonable estimate of the mean atmospheric structure and processes, but is in no way definitive. In this section some of the more obvious uncertainties and omissions in the thermal model are discussed and quantitative effects are presented. The principal criterion applied to each uncertainty was its effect on the vertical eddy transport coefficients estimated from the thermal model. A summary of the results are presented at the end of this section.

3.4.1 Ozone Concentration

The thermal model is quite sensitive to the ozone concentration through the absorption of solar UV energy below about 90 Km. Figure 14 summarizes several representative measurements and theoretical calculations of the ozone concentration between 50 Km and 100 Km for daytime conditions. Included are the rocket soundings of Smith (1969), the satellite measurements of Rawcliffe, et al (1963), and Anderson et al (1969), and theoretical estimates of Hunt (1966) and Hesstvedt and Jansson (1969). The curve labelled B is an empirical expression, $[O_3] = 8 \times 10^{10} \exp[-(z-50)/4.53]\ cm^{-3}$ (z in Km), suggested by Evans, et al (1968) to fit their corrected version of the rocket data of Johnson, et al (1952) for the region 40 Km to 70 Km, and used by them to model the

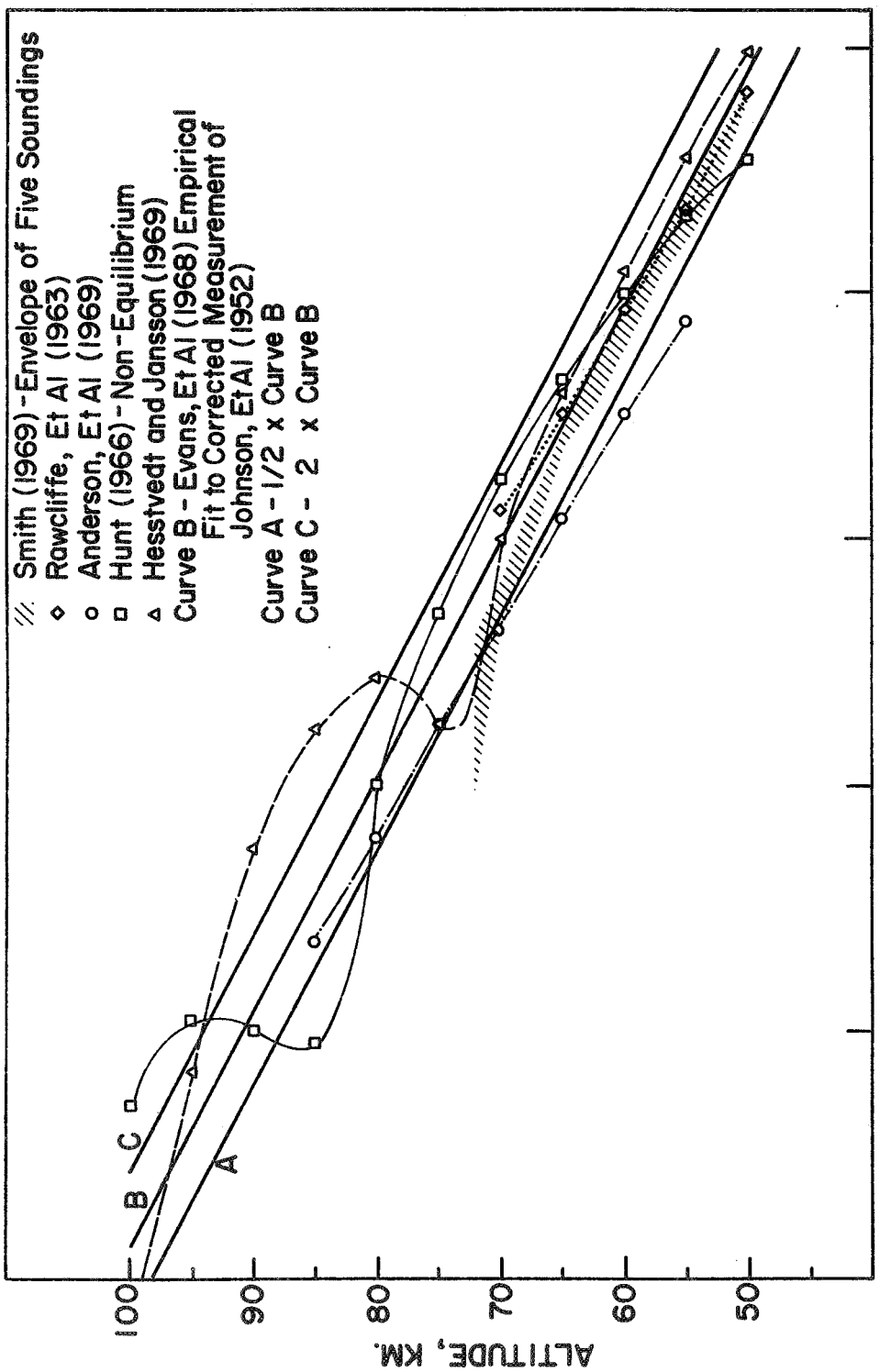

Figure 14. Measurements and theoretical estimates of the O_3 concentration

emission profile of O_2 ($^1\Delta_g$). The profile of curve B was adopted as the standard earth average (daytime) ozone concentration for the thermal model as a reasonable compromise. As crude estimates of the apparent uncertainty in the ozone concentration the following two profiles were chosen: as a lower limit one half the standard value, shown as curve A in Figure 14; and as an upper limit, twice the standard value, shown as curve C in the figure. These limits include the majority of the theoretical estimates and measured data points.

The effect of this uncertainty is directly evident in the calculated solar heating rates shown in Figure 15. These ozone variations are reflected in the equilibrium eddy transport parameters used to balance the thermal model. This variation in the equilibrium eddy diffusion coefficient is shown in Figure 16.

3.4.2 CO_2 (15μ bands) IR Cooling Rate

The two major uncertainties in the CO_2 cooling rates are the actual distribution of CO_2 in the atmosphere and the value of the (vibrational) relaxation time for the ν_2 mode. Appendix E describes a study of the atmospheric distribution of CO_2 from which a median profile was adopted as part of the thermal model (see Chapter 2). In many ways this represents a reasonable lower limit for the CO_2 volume mixing ratio, whereas a fully mixed CO_2 distribution (up to 120-130 Km) would be an extreme but conceivable upper limit. To determine the effect of this uncertainty, the CO_2 cooling rates for the earth average temperature profile were carried out for both the CO_2 distribution adopted in Chapter 2 and for the fully mixed case; and the results are shown in Figure 17. The differences below 60 Km are due to the resolution of

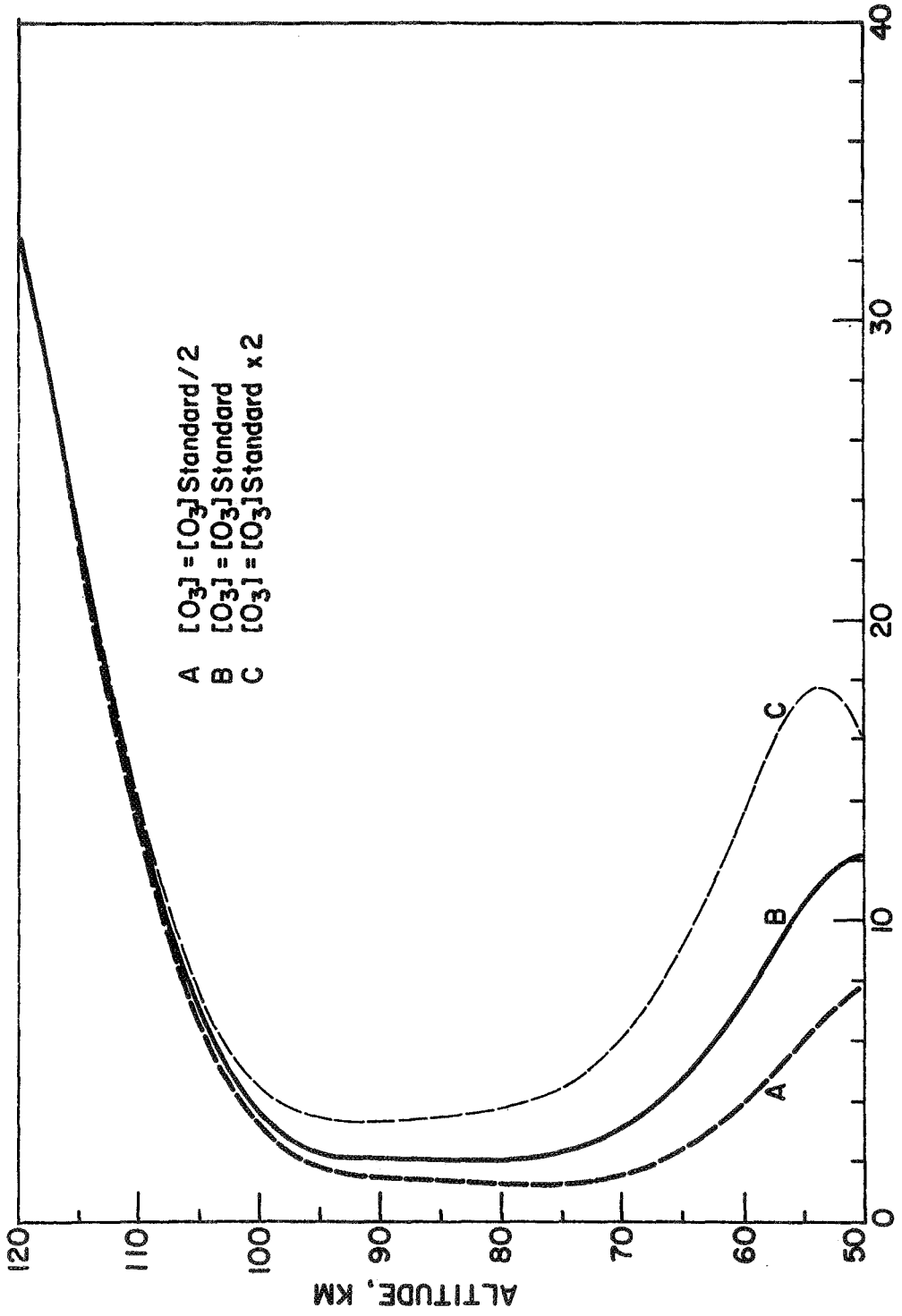

Figure 15. Effect of O_3 concentration uncertainties on the solar heating rate

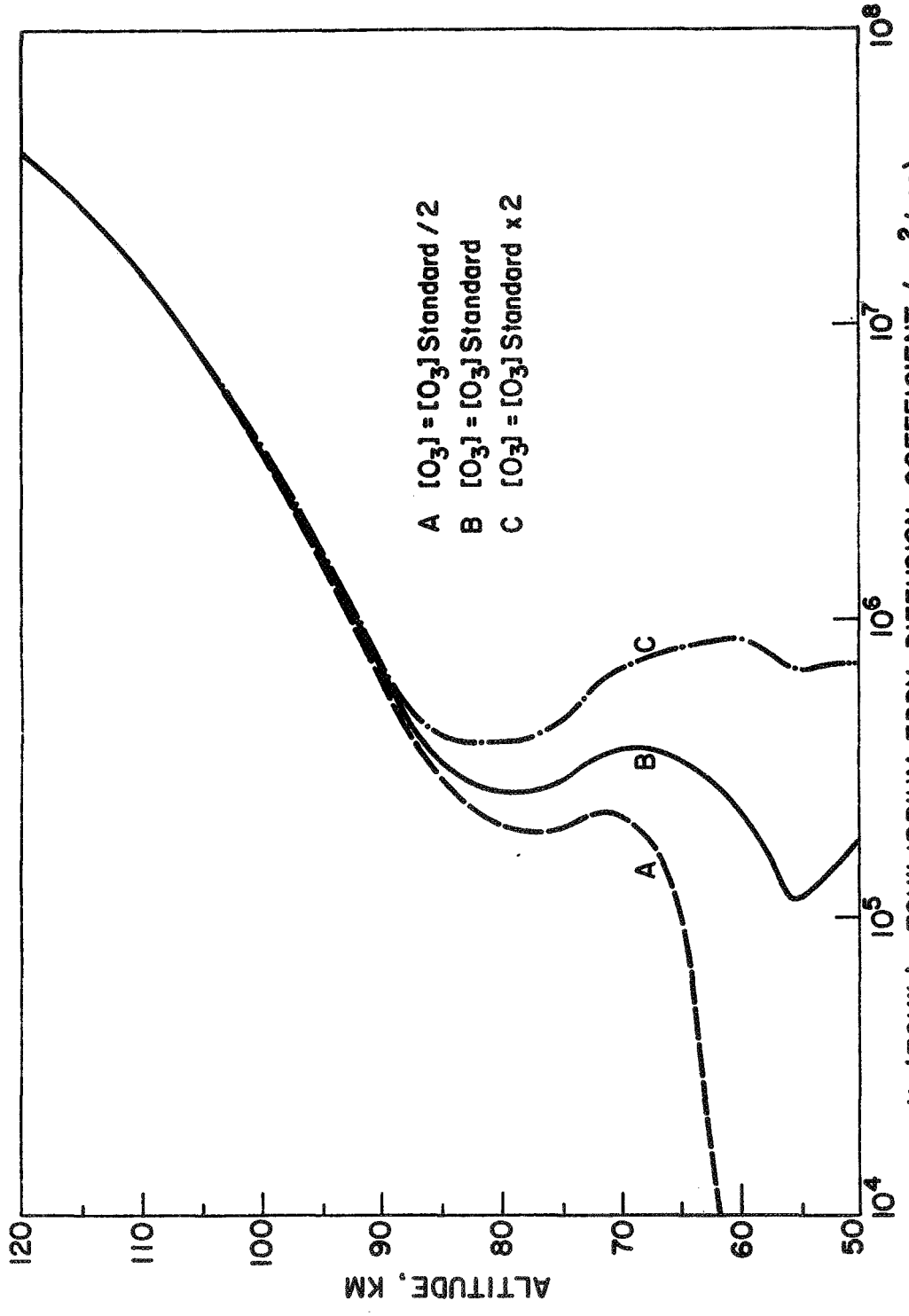

Figure 16. Effect of O_3 concentration uncertainties on the equilibrium eddy diffusion coefficient

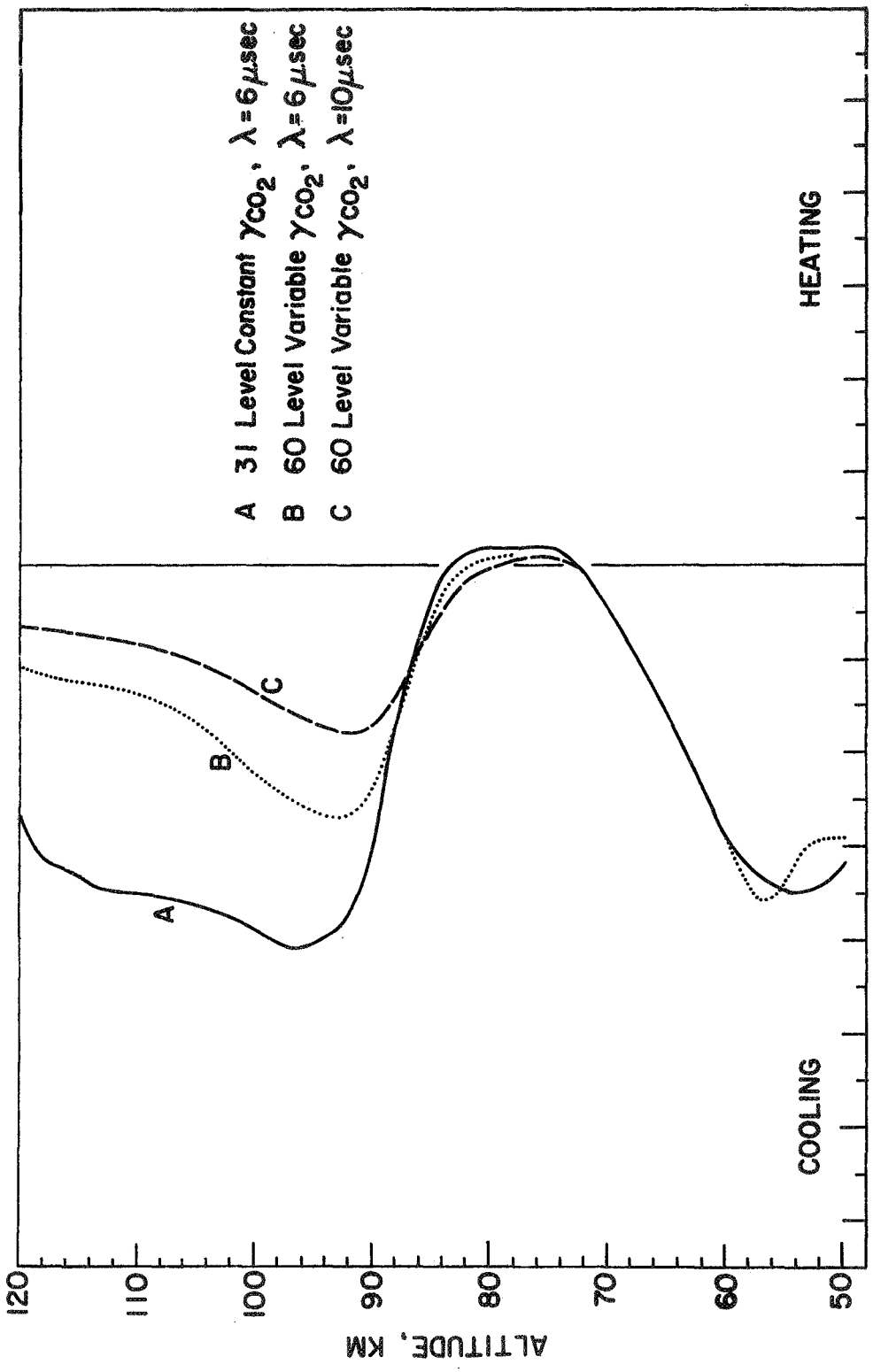

Figure 17. Effect of uncertainties in the CO_2 distribution and vibrational relaxation time on the CO_2 (15μbands) cooling rate

the models, 31 levels versus 60 levels, and not the CO_2 distribution.

Whenever a non-LTE formulation for IR transfer is necessary the results are critically dependent upon the (vibrational) relaxation time (see Chapter 2). Drayson (1967) used the values 2μsec and 20μsec, at 200°K and sea level pressure, to bracket this parameter and showed that this leads to a factor of five or more deviation in the CO_2 cooling rates above about 90 Km. A relaxation time of 10μsec was adopted for the thermal model based on the recent results of Merrill and Amme (1969). Another possible[1] value considered was λ^o=6μsec (where λ^o is the relaxation time at sea level conditions). The CO_2 cooling rates for λ^o=6μ sec and 10μsec are shown in Figure 17. The effect of these heating rates on the equilibrium eddy diffusion coefficients are shown in Figure 18. These uncertainties are probably quite important in some remote sensing applications. However, in the present results, the CO_2 (15μbands) cooling process is shown to be unimportant in the overall energy balance above the mesopause.

3.4.3 Heating Efficiency for Oxygen

In Chapter 2 the efficiency for conversion of absorbed solar UV energy into local translation energy was derived for O_2 and O_3. For O_2 two significant parts of the total absorbed energy, dissociation and $O(^1D)$ excitation were treated separately in determining $\epsilon_{O_2}^{\lambda}(\bar{z})$. There seems to be little doubt that the dissociation energy can be handled consistently and realistically by subtracting it out at absorption and recovering

---

[1] A relaxation time of approximately 6μsec, at 290-300°K and 1 atm., has been fairly well established for CO_2-CO_2 15μdeactivations; see Read (1965) and discussion by Houghton (1967).

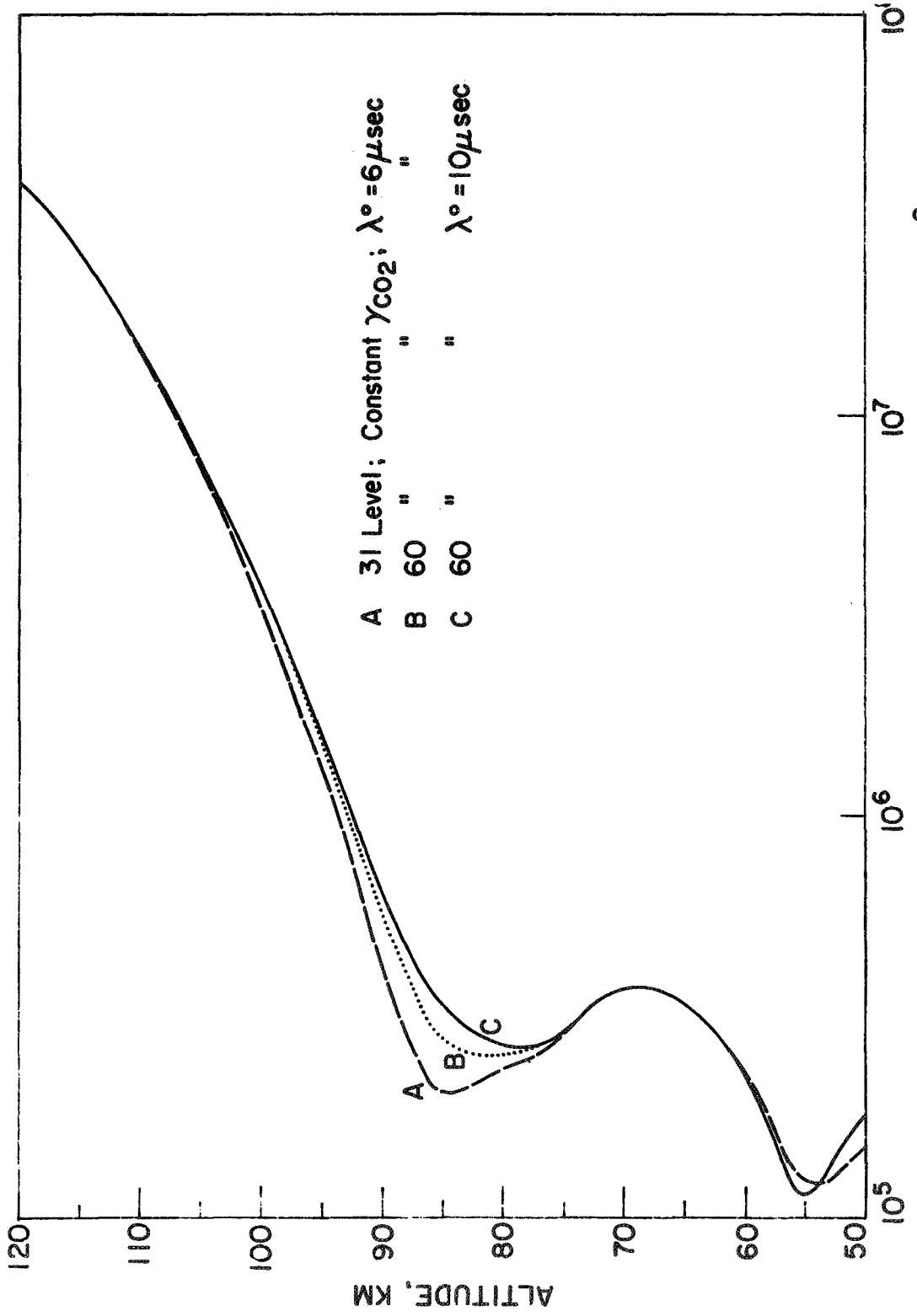

Figure 18. Effect of CO_2 (15μ bands) cooling rate uncertainties on the equilibrium eddy diffusion coefficient

it at recombination. On the other hand, the rather complex procedure outlined in Chapter 2 by which it was suggested that $O(^1D)$ exctiation energy leaves the region through N_2 vibration and the ν_3 mode of CO_2, cannot as yet be critically tested. The impact of this uncertainty in $\epsilon_{O_2}^{\lambda}$, which amounts to the difference between the two curves of Figures 6 and 7, was examined by calculating the appropriate solar heating rates and with these, profiles of equilibrium eddy diffusion coefficient. The solar heating rates are shown in Figure 19 and the equilibrium eddy diffusion coefficients are shown in Figure 20.

3.4.4 Heat Flux at 120 Km

The following assumptions are felt to be the largest sources of uncertainty in the heat flux at 120 Km: the inclusion of the full tidal energy flux proposed by Lindzen (1967); the use of 100% heating efficiencies for N_2 and O; and the neglect of airglow emission. The impact of the last two assumptions is of considerable interest in itself but is beyond the scope of the present study. It is felt however that these uncertainties are insignificant compared with the $\sim$1.75 ergs/cm^2/sec assumed to be continually added on the average throughout the thermosphere by tides.

The heat flux at 120 Km was varied in order to determine its impact on the balancing eddy transport. Profiles of the equilibrium eddy diffusion coefficient are presented in Figure 21 for the following bracketing values of heat flux: 0, -0.6, -1.2, -1.8, -2.4, and -3.0 ergs/cm^2/sec. Larger values of K_T (equil.) are shown to be required near 120 Km as the downward heat flux increases in magnitude. Based on these results an upper limit of roughly 1 erg /cm^2/sec must be placed on the magnitude

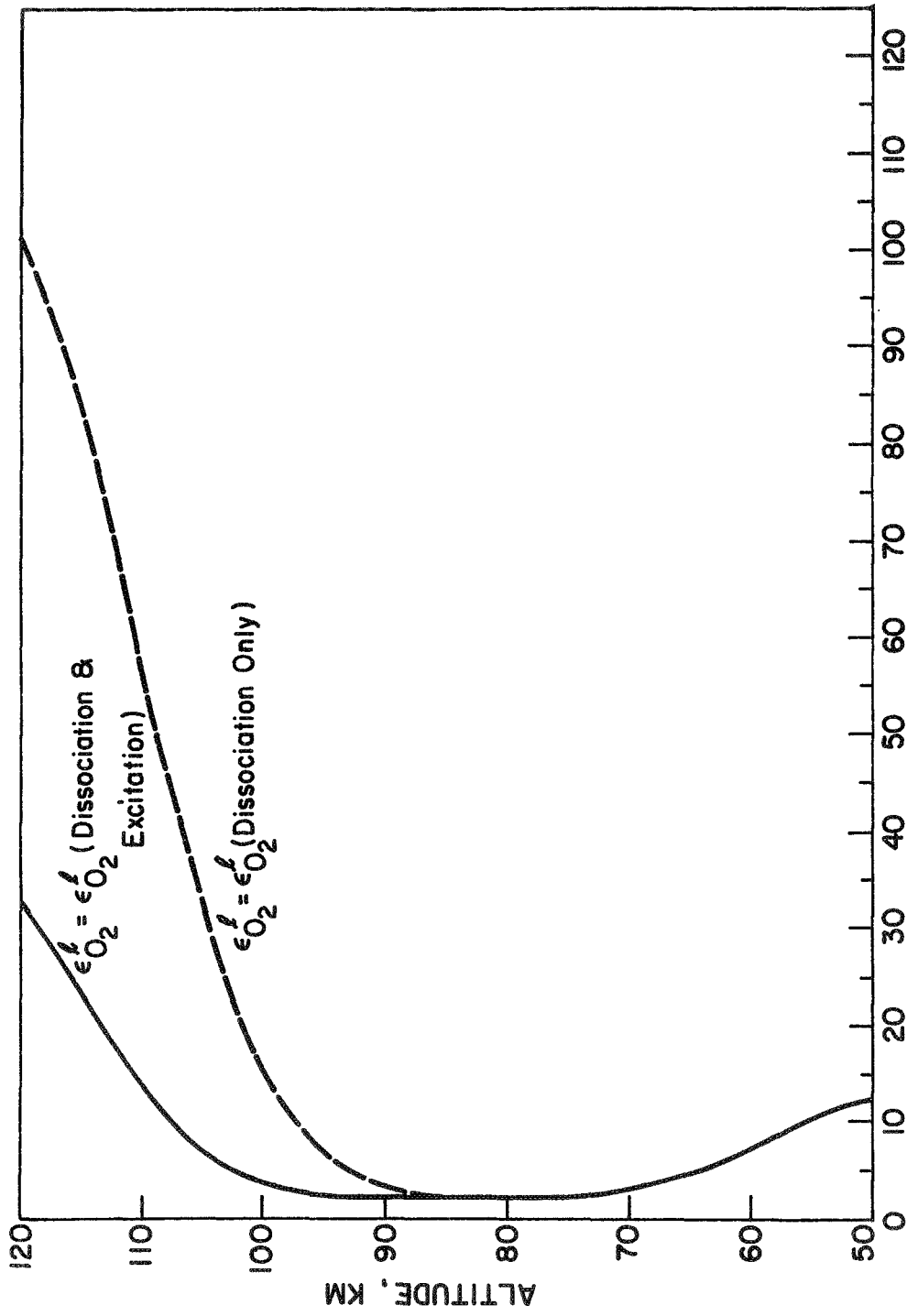

Figure 19. Effect of O_2 heating efficiency uncertainty on the solar heating rate

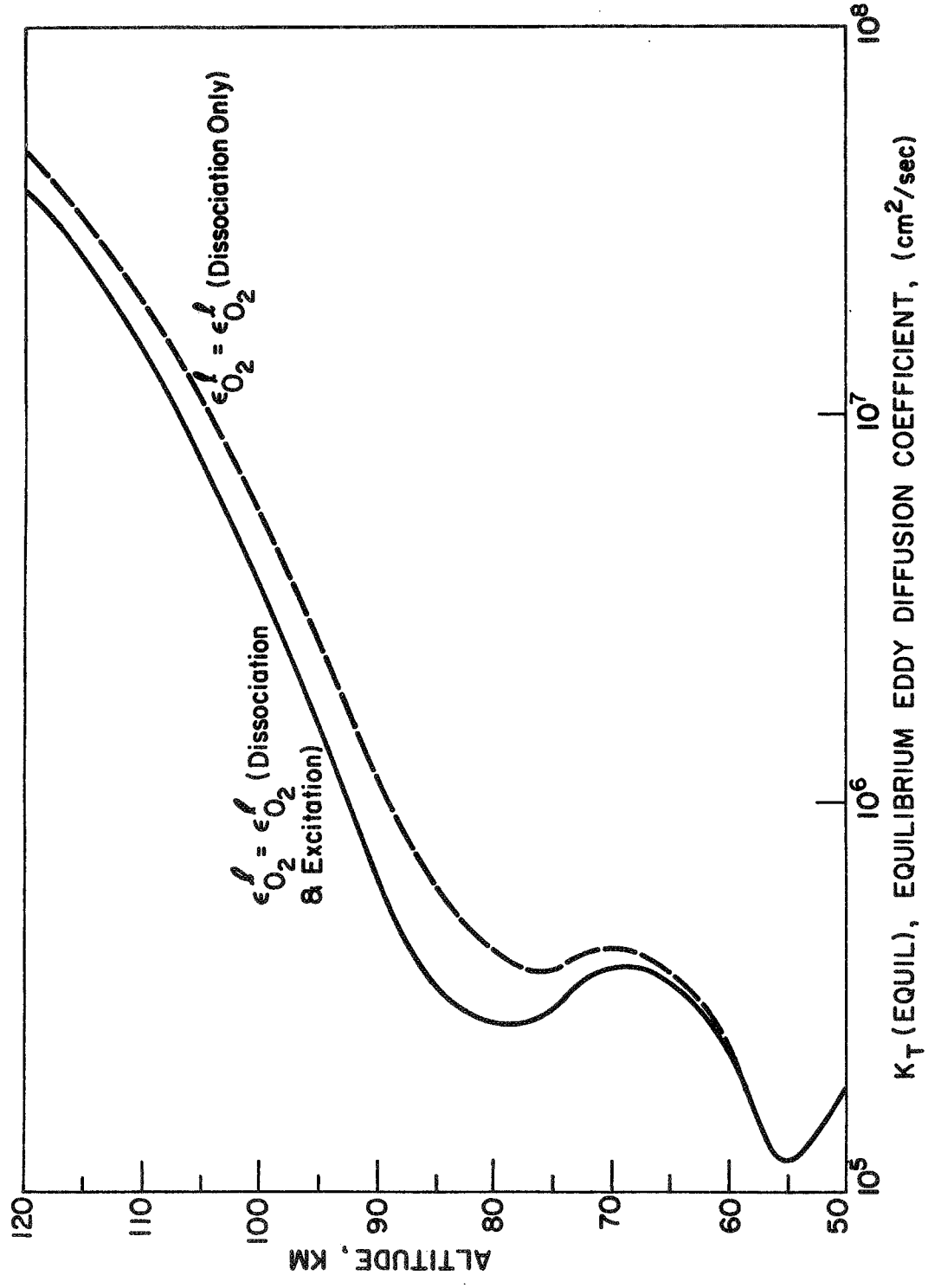

Figure 20. Effect of O_2 heating efficiency uncertainty on the equilibrium eddy diffusion coefficient

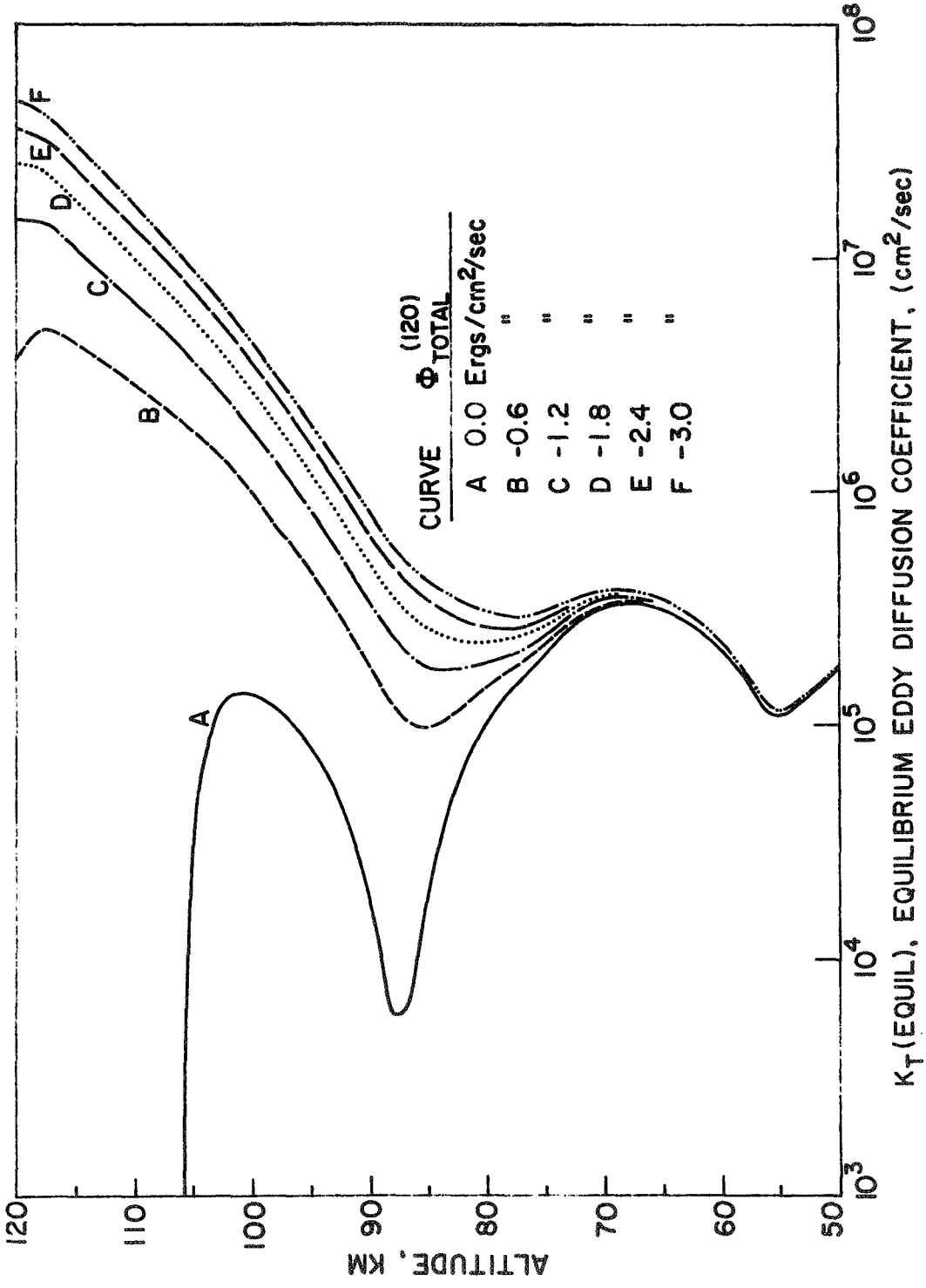

Figure 21. Effect of varying the upper boundary heat flux on the equilibrium eddy diffusion coefficient

of the downward heat flux, in order to limit the eddy transport to values consistent with the compositional studies mentioned in Chapter 1. This observation casts serious doubts on the premise that the tidal energy flux reaches the thermosphere above about 100 Km essentially undiminished. This point will be discussed further in Chapter 5. The eddy transport at levels below the mesopause is shown to be relatively uneffected by the value of the heat flux at 120 Km.

3.4.5 Gravity Wave Dissipation

A possibly important heat source in the mesosphere and lower thermosphere is the dissipation of upwardly propagating gravity waves. Hines (1965) examined the magnitude of this heating source with the aid of the wind data of Kochanski (1964). Hines found that the waves appeared to be losing energy at the following rate:

$$Q_{WAVES} \simeq \frac{1}{2} \frac{\rho U_x^2 V_z}{z_0} \qquad (3.6.1)$$

where ρ is the local mass density, U_x is the horizontal wind speed (taken from Kochanski, 1964), V_z is the vertical phase speed (taken to be 1 m/sec), and $z_0 = 7.6$ Km was the apparent 'scale height' for the decrease of horizontal kinetic energy from Kochanski's data.

This additional heating rate was included in the thermal model by adopting the above expression with the same values of V_z and z_0 and including the horizontal wind data of Kochanski (1964) directly. The winds and calculated heating rate are shown in Figure 22, and in Figure 23 is shown the effect on the equilibrium eddy diffusion coefficient of adding this heat source; in both cases the curves are limited to heights above 70 Km, the lower limit of Kochanski's wind data.

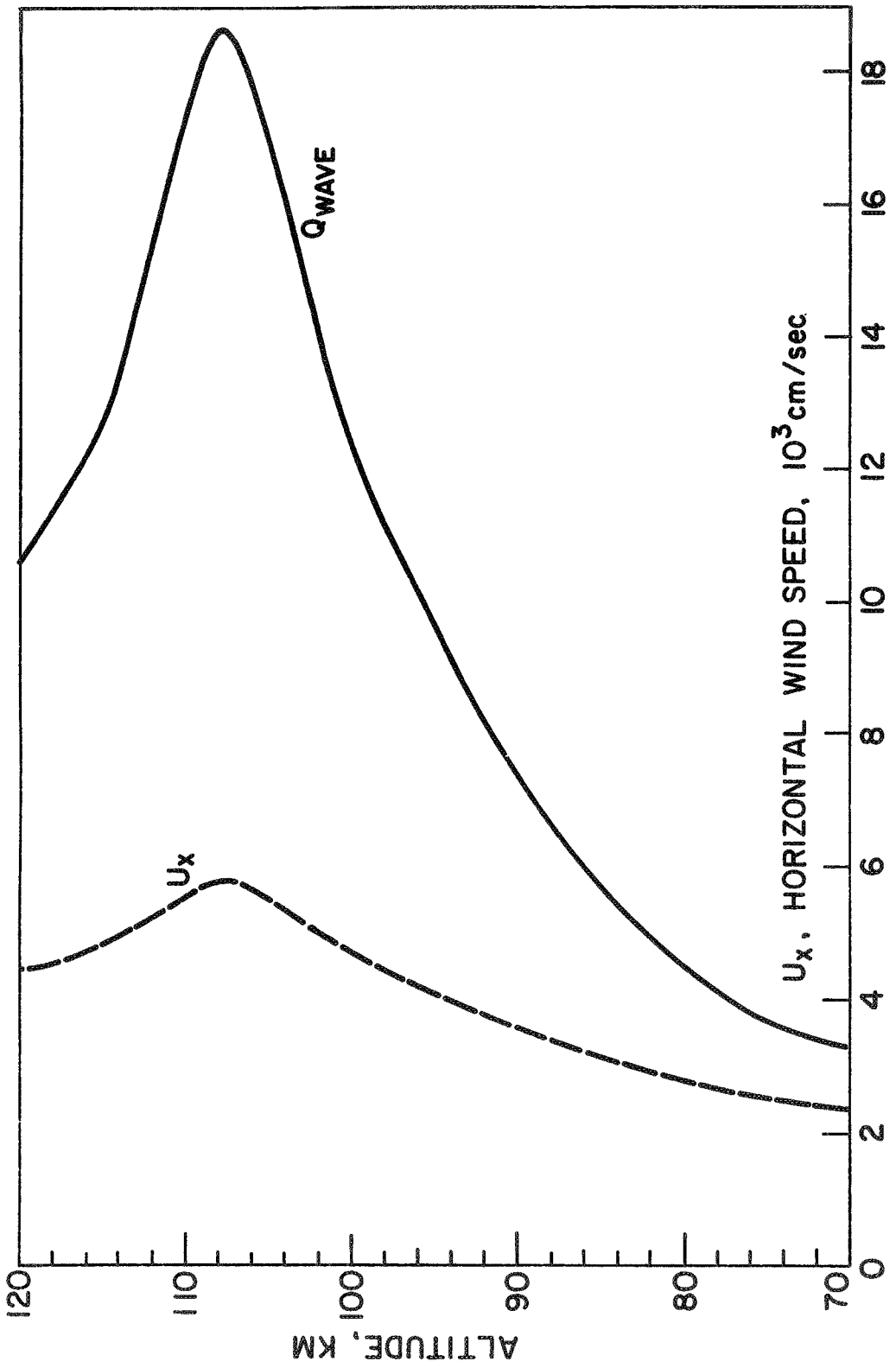

Figure 22. Gravity wave dissipation heating rate and horizontal wind speed on which it is based

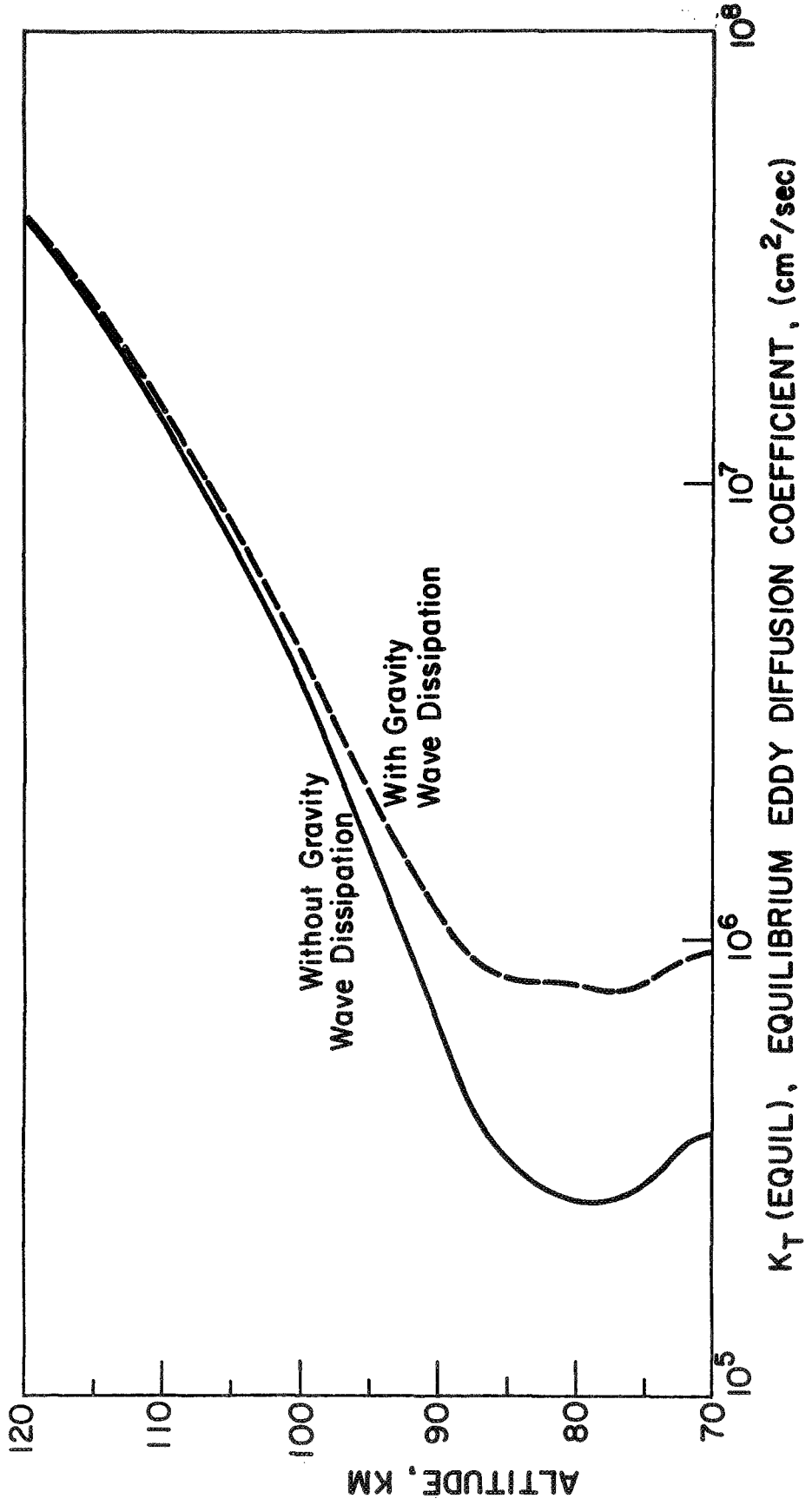

Figure 23. Effect of including gravity wave dissipation on the equilibrium eddy diffusion coefficient

3.4.6 Results

The ozone concentration seems to be the parameter most critical to the thermal model in the mesosphere. By varying this parameter by factors of two the resulting equilibrium eddy diffusion coefficients in the lower mesosphere are changed by orders of magnitude. This seems ironic since the ozone concentration has been considered an important atmospheric quantity for decades and much effort has been spent in measuring it.

Another rather large effect is the inclusion of the energy of dissipation of gravity waves. The extent to which this heat source should be included in the thermal model is presently unknown. Further studies of the frequency and morphology of gravity waves at these heights must first be made for a wider range of latitudes and seasons.

The heat flux at 120 Km has a significant effect on the thermal model above the mesopause. A heat flux much below about .5 ergs/cm^2/sec would correspond to a turbopause below 100 Km. Compositional studies suggest an upper limit as well of about 1 ergs/cm^2/sec.

The uncertainty in the O_2 heating efficiency is manifested in a factor of three uncertainty in the solar heating rate in the lower thermosphere. This uncertainty would be crucial in a radiative equilibrium type calculation; however, in the present thermal model, thermal transport is far more important in the lower thermosphere and the effect is much smaller.

The uncertainties in the CO_2 distribution and relaxation time for the ν_2 mode have a very significant effect on the CO_2 cooling rate in the lower thermosphere. However, this process has almost no effect upon the thermal model above the mesopause in any case.

CHAPTER 4

SEASONAL - LATITUDINAL MODELS

4.1 INTRODUCTION

In Chapter 3 a global thermal model was formulated which unfortunately cannot be attributed to any actual point on the earth in terms of a location and season. Latitudinal and seasonal differences in the heating/cooling rates and temperature structure are particularly interesting in the mesosphere and lower thermosphere and are considered in this chapter.

In order to examine the gross energy balance a separate thermal model was formulated for 10 latitudes, 10^{o} apart (0^{o}, 10^{o}, 20^{o}, 30^{o}, 40^{o}, 50^{o}, 60^{o}, 70^{o}, 80^{o}, 90^{o}) for winter solstice, summer solstice, and equinox conditions. A temperature profile was adopted for each model and the appropriate zenith angle dependence was incorporated into the solar heating rates, which resulted in minor changes in the heat flux at 120 Km. Otherwise the thermal models were identical to those described in Chapter 2. No attempt was made to include latitude or seasonal variations in composition for the following reasons: first, except for ozone the compositional variations are not significant; and second, it seemed inconsistent to adopt estimates of ozone seasonal and latitudinal variations when the basic uncertainty in the ozone concentration above 50 Km remains quite large (see Chapter 3).

4.2 TEMPERATURE STRUCTURE

Temperature data for summer and winter conditions were taken from Newell (1968), which were based upon actual measurements. Newell's data generally does not extend above 70^{o} latitude for very practical reasons, and it was necessary to extrapolate the temperatures

poleward. This extrapolation was based partially upon the temperature data of Murgatroyd (1965) which were determined in part from measured winds and the thermal wind relationship.

The average of the spring and autumn temperature data of Murgatroyd (1965) were adopted for the equinox hemisphere, with minor modification. As was mentioned above, the Murgatroyd data were not based entirely upon actual temperature measurements and thus were considered to contain additional uncertainties. It was felt that a favorable agreement might be expected between the hemisphere averages of spring/autumn conditions with those of summer/winter and this comparison was made between the data of Murgatroyd and Newell, respectively. The agreement was very good, usually to within $1^{o}K$ up to about 105 Km getting progressively poorer with height above that point. This discrepancy was artifically removed by scaling Murgatroyd's data above 105Km with the following factors: 1.026 at 110 Km; 1.063 at 115Km; and 1.11 at 120Km. The adopted meridional temperature cross sections for northern hemisphere summer and winter, and equinox are shown in Figures 24 and 25 respectively.

4.3 DIURNAL AVERAGE SOLAR HEATING RATES AND HEAT FLUXES

The major difference between the solar heating rates for the various seasonal-latitudinal conditions studied were attributed to the local effects of zenith angle and length of day, since possible seasonal-latitudinal composition variations were neglected. Thus for a given latitude, season, and altitude the quantity needed to determine the local heating rate was the zenith angle as a function of local time. This

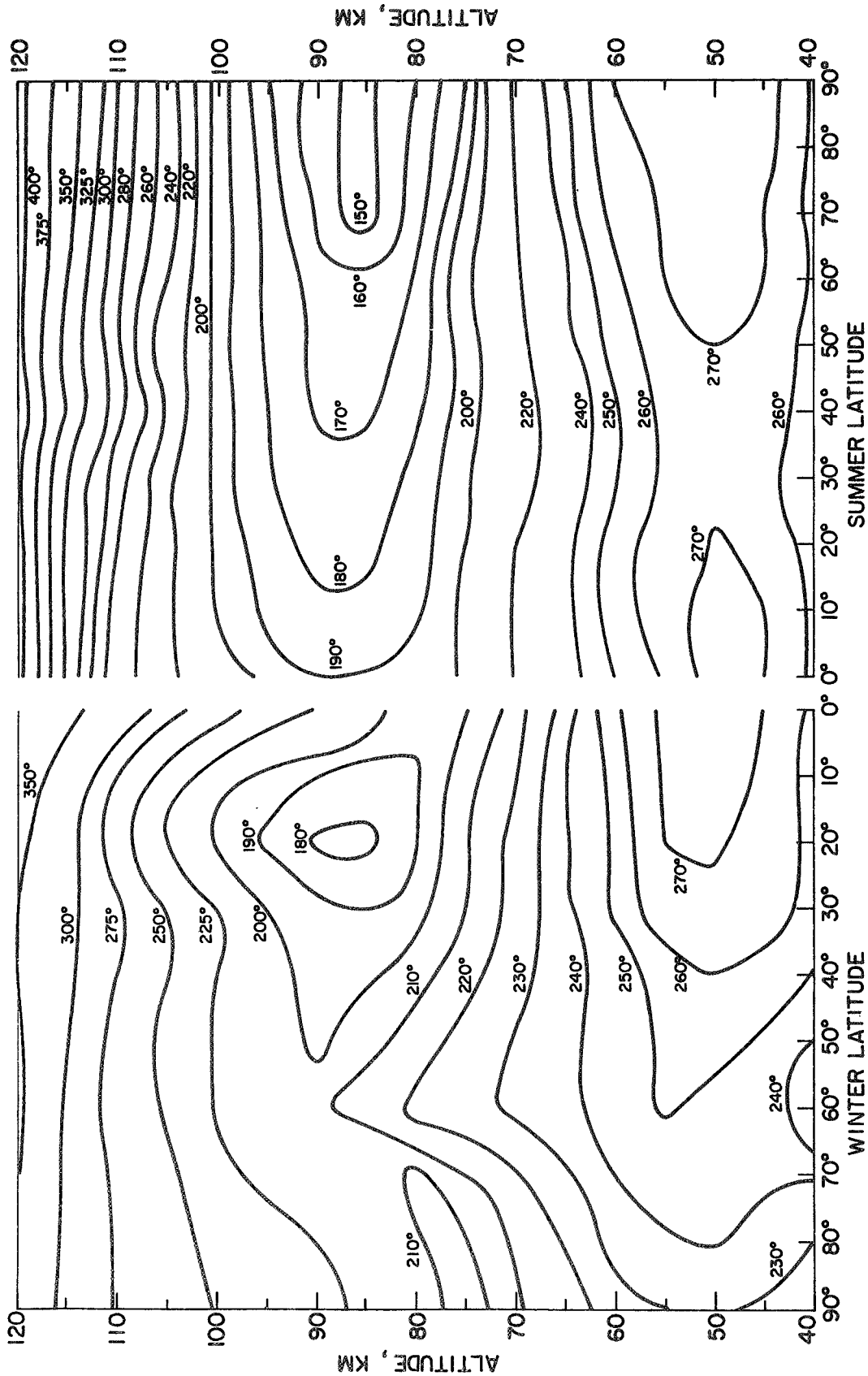

Figure 24. Northern hemisphere temperature profile for winter and summer solstice

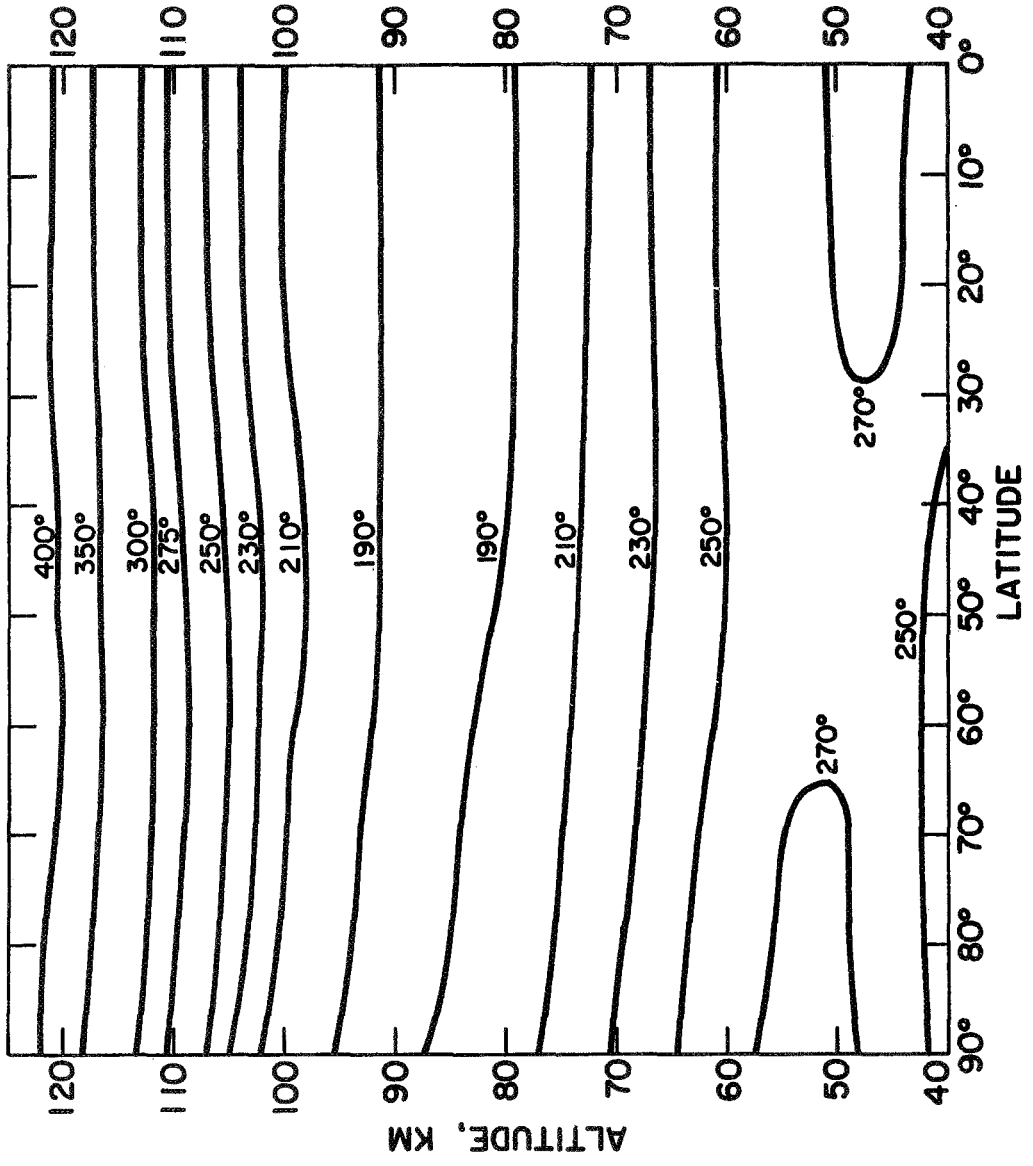

Figure 25. Northern hemisphere temperature profiles for equinox (spring/autumn average)

parameter was calculated with the aid of the formulation of Woolfe (1968) based on the earth-sun geometry with refraction included. The largest zenith angle encountered for altitudes of 120 Km and lower is approximately 103^{o}. The following relationship, discussed in Chapter 3, was found to be quite accurate for zenith angles up to about 80^{o}:

$$N_i(z,\theta) = N_i(z,0)\sec\theta \qquad (4.3.1)$$

Thus the detailed knowledge of column density required to calculate the solar heating rate could be limited to zenith angles between 80^{o} and 103^{o}. It was decided to calculate a library of column densities for the altitude and zenith angle range of interest in sufficient detail that interpolation would be convenient and relatively accurate. The zenith angles covered were 0^{o} to 80^{o} in 10^{o} steps and 80^{o} to 103^{o} in 1^{o} steps. Sixty-two altitude levels were selected as follows: 50 Km to 120 Km in 2 Km steps; 120 Km to 150 Km in 5 Km steps; 150 Km to 200 Km in 10 Km steps; and 200 Km to 500 Km in 20 Km steps. The calculation was made for N_2, O_2, O, and O_3 in the manner described in Appendix C.

In a completely analogous manner a basic library of solar heating rates was compiled for the same thirty-two zenith angles (0^{o}-103^{o}) and sixty-two altitudes (50 Km - 500 Km) as was done for the column densities. For each height-zenith angle pair the local solar heating rate was calculated according to Equation (2.4.1) with the approximations discussed in Appendix D.

The solar heating rates actually used in the seasonal-latitudinal thermal models were diurnal averages obtained by integrating the time

varying heating rate between meridional passage (local noon) and local sunset, and dividing by 12 hours. The calculation details are discussed in Appendix D.

The diurnal average solar heating rates were then integrated as described in Chapter 2. to obtain their contribution to the diurnal average heat flux at 120 Km. Above 120 Km local zenith angles greater than 103^{o} are encountered near sunrise/sunset. For these cases the solar heating rates at 103^{o} were extrapolated exponentially to obtain the necessary values. Below about 200 Km in the model atmosphere used there is no contribution to the solar heating rate from zenith angles of 103^{o} or greater. Thus the above procedure could not have any impact on the integrated heating rates at 120 Km.

In assigning a value to the diurnal average heat flux at 120 Km for a given latitude, a hemispheric average for the appropriate season was used. This was motivated by the assumption that lateral transport in the upper thermosphere should be sufficient to redistribute the energy influx rather uniformly. The hemispheric averages were obtained by adding the contributions from each latitude, weighted by the cosines of the latitudes considered. This procedure was used to calculate the hemisphere averages of the integrated diurnal average solar heating rates and of dissipation of tidal oscillations analogous to that described in Chapter 2. The only other term included in the heat flux was the integrated 63μ emission, and the value obtained in Chapter 3 was assumed in each of the three hemisphere averages. This was a reasonable assumption since the atomic oxygen concentration was not changed and the hemisphere

averaged temperature effects were negligible. The results for the hemisphere averaged heat fluxes are presented in Table I.

Table I

Hemisphere-Season Averaged Heat Fluxes and Contributing Processes

Hemisphere Season Averages (ergs/cm^2/sec)	Winter Solstice	Equinox	Summer Solstice
Integrated diurnal average solar heating rate above 120 Km.	0.5945	0.8368	1.0758
Dissipation of tidal oscillations	1.7535	1.7535	1.7535
Integrated 63μ emission above 120 Km.	-0.0849	-0.0849	-0.0849
Total heat flux at 120 Km.	-2.2631	-2.5054	-2.7444

4.4 DIURNAL AVERAGE TOTAL HEATING RATES

All of the heating and cooling terms described in Chapter 2 were included in the seasonal-latitudinal thermal model. Besides the solar heating rate described above, the largest changes between the various models was in the CO_2(15μbands) cooling rate. The linearized flux

divergence approximation adopted in Chapter 2 with the formulation given in Appendix F was used throughout and the differences in the cooling rates calculated for the various thermal models reflected the differences in the temperature profiles associated with those models. The O (63μ) cooling rate also reflected a small temperature dependent variation through the Bates formulation, Equation (2.4.10). Additionally there was some change in the chemical (recombinational) heating rate because of the temperature dependence of the K_{13} rate coefficient, see Equation (2.6.5). The only heating rate unchanged was that of O_3(9.6μ) as assumed in Chapter 2. All heating rates were assumed to apply to diurnal average conditions.

The diurnal average total heating rates were also assumed to be synonomous with the total of the diurnal average heating rates. These heating rates are plotted in ^{o}K/day units for meridional-vertical cross sections for winter solstice, equinox, and summer solstice in Figures 26, 27, and 28, respectively.

These results may be compared with similar meridional-vertical cross sections for the region 30 Km to 95 Km at solstice given by Murgatroyd and Goody (1958), and Kuhn (1966, 1968). The study by Murgatroyd and Goody included heating from the absorption of solar energy by O_2 and O_3 and cooling by the IR radiative transfer of CO_2 (15μ bands), O_3(9.6μ bands) and H_2O (6.3μ and 80μ bands). Kuhn (1966) adopted the solar heating rates of Murgatroyd and Goody (1958), but recalculated the IR radiative cooling for the same processes. The study by Kuhn (1968) included the same IR radiative cooling calculations as Kuhn (1966), with the exception of neglecting the relatively significant 6.3μ band of H_2O. However Kuhn's 1968 study differed from his

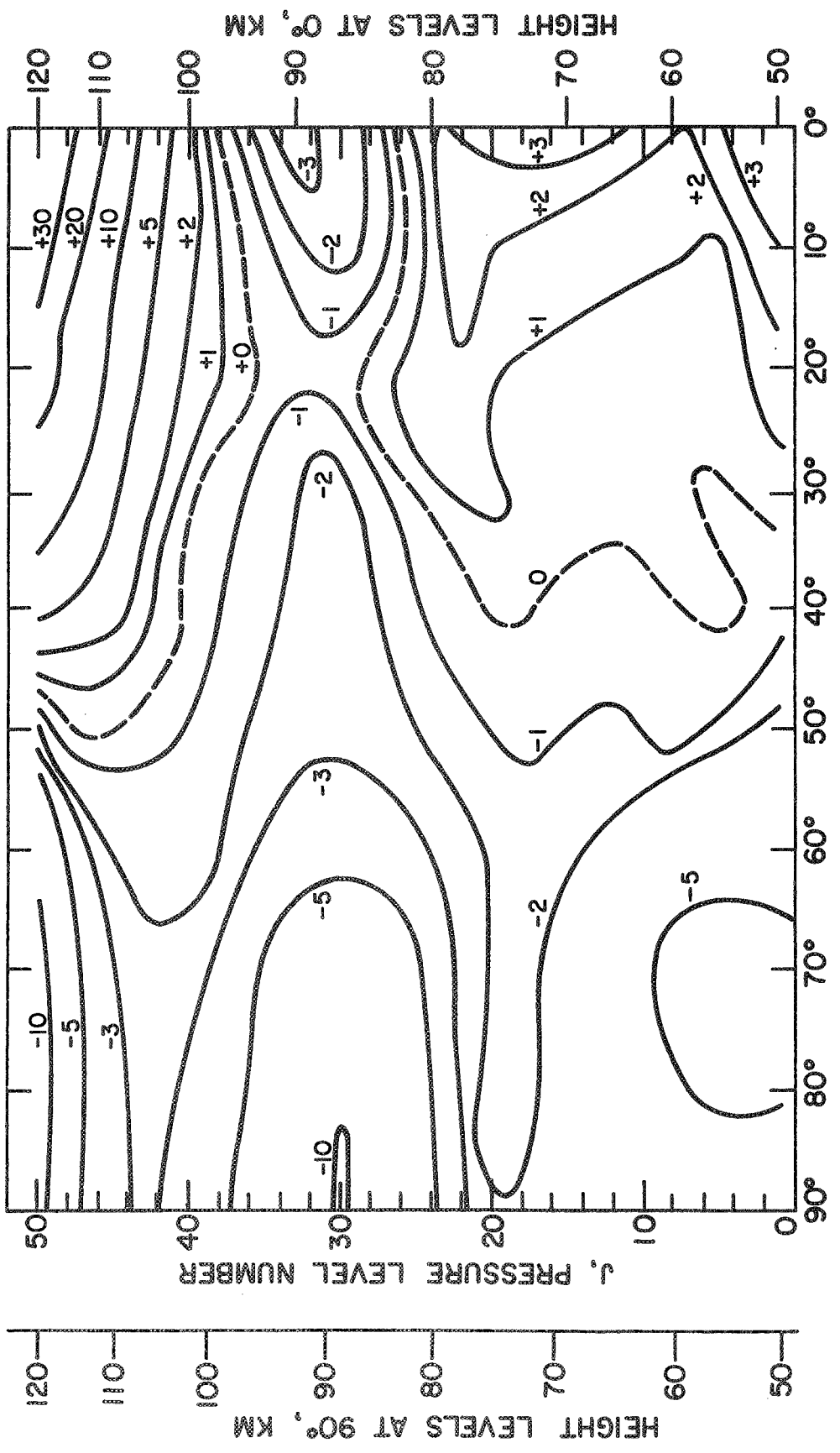

Figure 26. Diurnal average total heating rates, in ^{o}K/day, for winter solstice

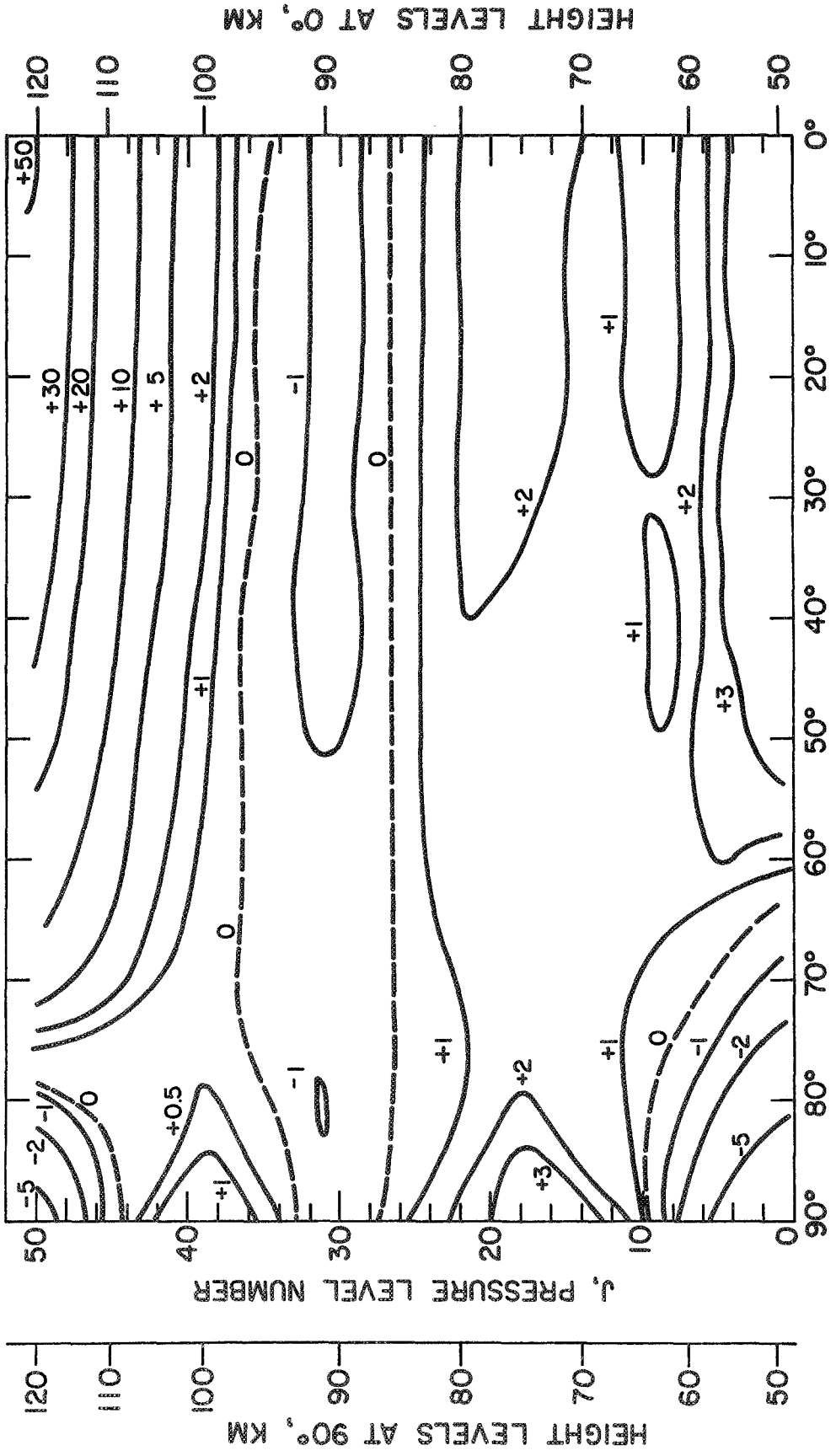

Figure 27. Diurnal average total heating rates, in ^{o}K/day, for equinox (Spring/Autumn average)

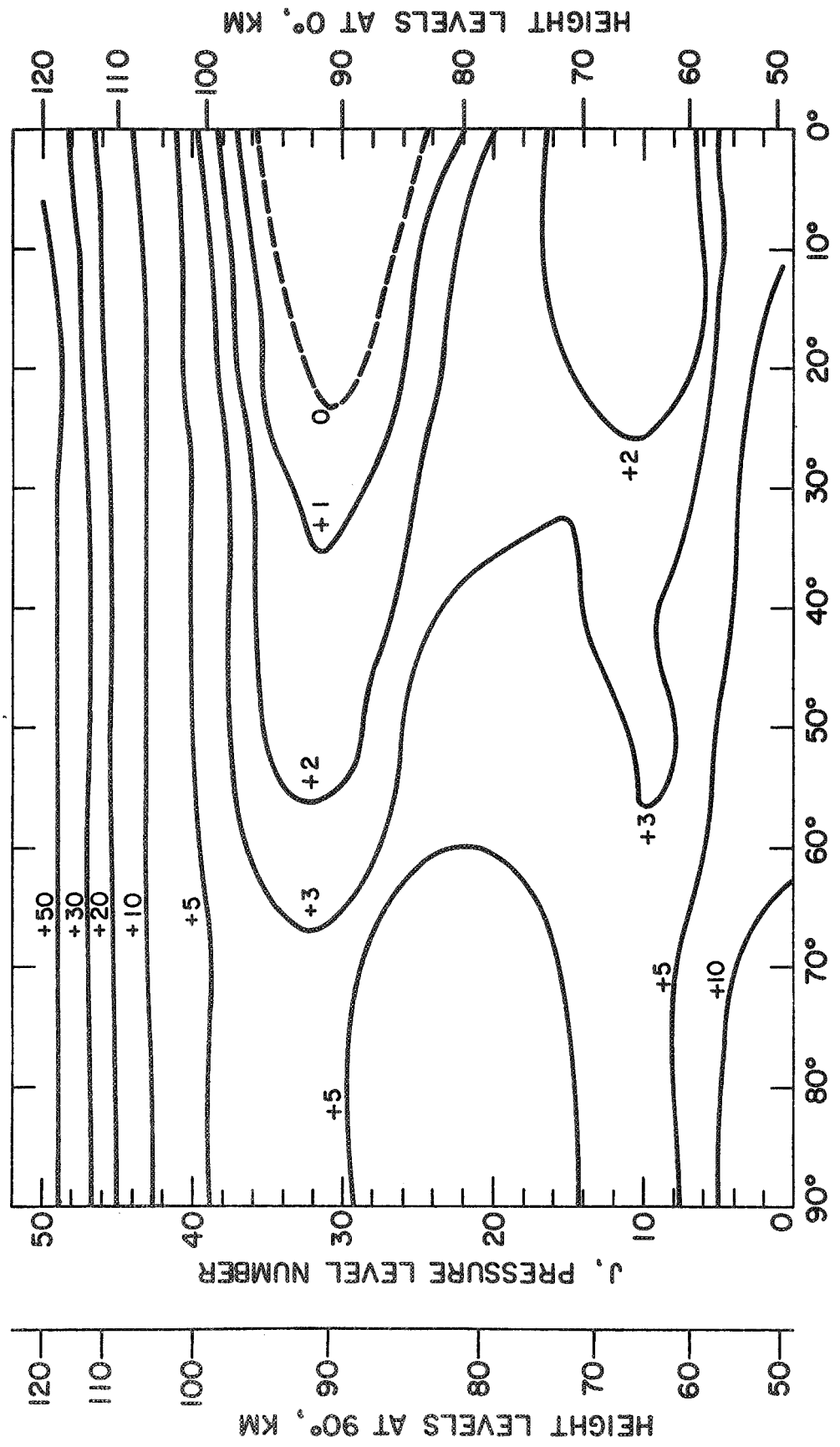

Figure 28. Diurnal average total heating rates, in ^{o}K/day, for summer solstice

1966 work in that he recalculated the solar heating rates using different O_3 concentrations. Murgatroyd and Goody (1958) and Kuhn (1966) used a value of 10 μ sec for the sea level relaxation time of $CO_2(\nu_2)$ while Kuhn (1968) considered the bracketing values 2 μ sec-20 μ sec; comparisons will only be made with the latter case. It is important to note that different temperature data were adopted in each of these studies. These three studies also differed from the present work in the following ways: heating efficiencies for O_2 and O_3 were not employed; chemical recombination of O and O_3 was neglected; more approximate formulations of CO_2 (15 μ bands) were used, and the latter was derived for a fully mixed CO_2 distribution; absorption cross sections and solar UV flux data were adopted from different sources; and perhaps most significantly, different ozone distributions were used. The results of all four studies are qualitatively more similar than the above discussion might suggest, indicating an underlying consistency in describing the major physical processes.

In the present results, in a region centered at about 90 Km, there is a small amount of net cooling from 0°-20° (latitude) in the summer hemisphere and at all latitudes for equinox and winter conditions, although in the latter case the net cooling becomes much larger and spreads to all altitudes considered poleward of about 40° latitude. Murgatroyd and Goody (1958) and Kuhn (1966) show a similar cooling feature with more intense net cooling near the winter pole and extending throughout the summer hemisphere. Kuhn (1968) shows a similar net cooling feature somewhat lower in altitude, extending only to about 15° in

the winter hemisphere, and not at all present in the summer hemisphere.

The summer pole is characterized by net heating at all levels with an approximately 5^{o}K/day magnitude between 60 Km and 100 Km in the present study. This compares favorably with the results of Murgatroyd and Goody (1958) while in general Kuhn (1966) shows less and Kuhn (1968) shows a bit more net heating.

There is net cooling at all levels at the winter pole, for the present results, reaching -10^{o}K/day near the mesopause and again near 120 Km. This agrees best with Kuhn (1968). Murgatroyd and Goody (1958) find far more net cooling throughout the region, and Kuhn (1966) also shows somewhat more net cooling near 60 Km and again near 90 Km.

There are two other points of interest in the present results which cannot be compared with the other studies mentioned above. Above about 100 Km there is a great deal of net heating from equator to pole in the summer hemisphere, from equator to about 80^{o} in the equinox hemisphere and below about 50^{o} latitude for winter conditions. This feature is the result of the strong heating from absorption of solar UV by O_2 at $\lambda \leq 2500$ Å. Also, the equinox pole has a very complex structure with alternating regions of net heating and cooling.

4.5 VERTICAL TRANSPORT

From the heating rate contours discussed above it seems clear that in order to maintain an energy balance on the average heat must be transported vertically and meridionally. Models of meridional flow are beyond the scope of this study; the remainder of this discussion will deal with vertical transport. As mentioned earlier in this study, there is rather general confirmatory evidence that some dynamic processes tend to "mix" the mesosphere and lower thermosphere and that this

process or processes can be modelled by eddy transport. Qualitatively, the results for the global scale model are in agreement in that a similar eddy transport model does indeed provide sufficient cooling by heat transport to balance the mean thermal state.

In this section the extent to which a general eddy transport treatment is able to both balance the energy budget and provide reasonable mixing in the mesosphere and lower thermosphere is examined for the specific seasons and latitudes considered. Since transport by mean motions and by "eddies" are similar processes the transport model will in general reflect the sum of both.

Equilibrium eddy transport coefficient profiles were calculated by the method used in Chapter 3, Equations (3.3.2) and (3.3.3), for each of the seasonal-latitudinal thermal models considered, with the total heating rates, heat fluxes, and temperature profiles presented above. The results are presented as meridional-vertical contours of the equilibrium eddy diffusion coefficient in Figures 29, 30, and 31, for winter solstice, equinox, and summer solstice, respectively. The consistency of the transport above the mesopause is indicative of the similar upper boundary heat fluxes adopted for each model (see Table I). Below the mesopause quite reasonable values of eddy diffusion, consistent with composition modelling studies, were obtained for low and mid-latitudes. However, in all three seasons, significant differences in transport are evident near the pole. Negative eddy diffusion coefficients are inconsistent with the simple mixing length formulation used and these values are undoubtedly indicative of subsidence. Near the

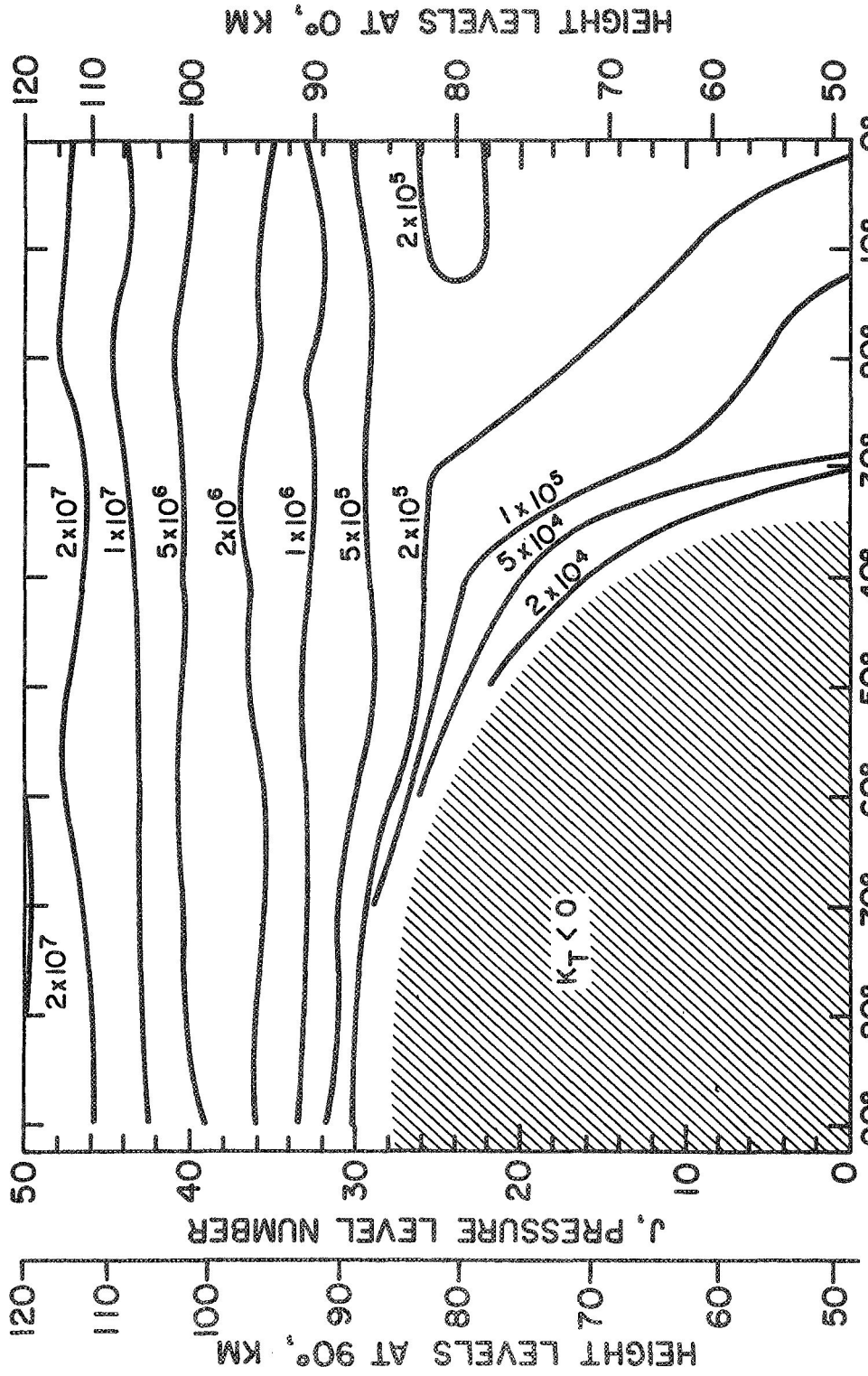

Figure 29. Eddy diffusion coefficients in cm^2/sec, necessary to achieve thermal balance by vertical transport alone for the winter solstice mesosphere and lower thermosphere

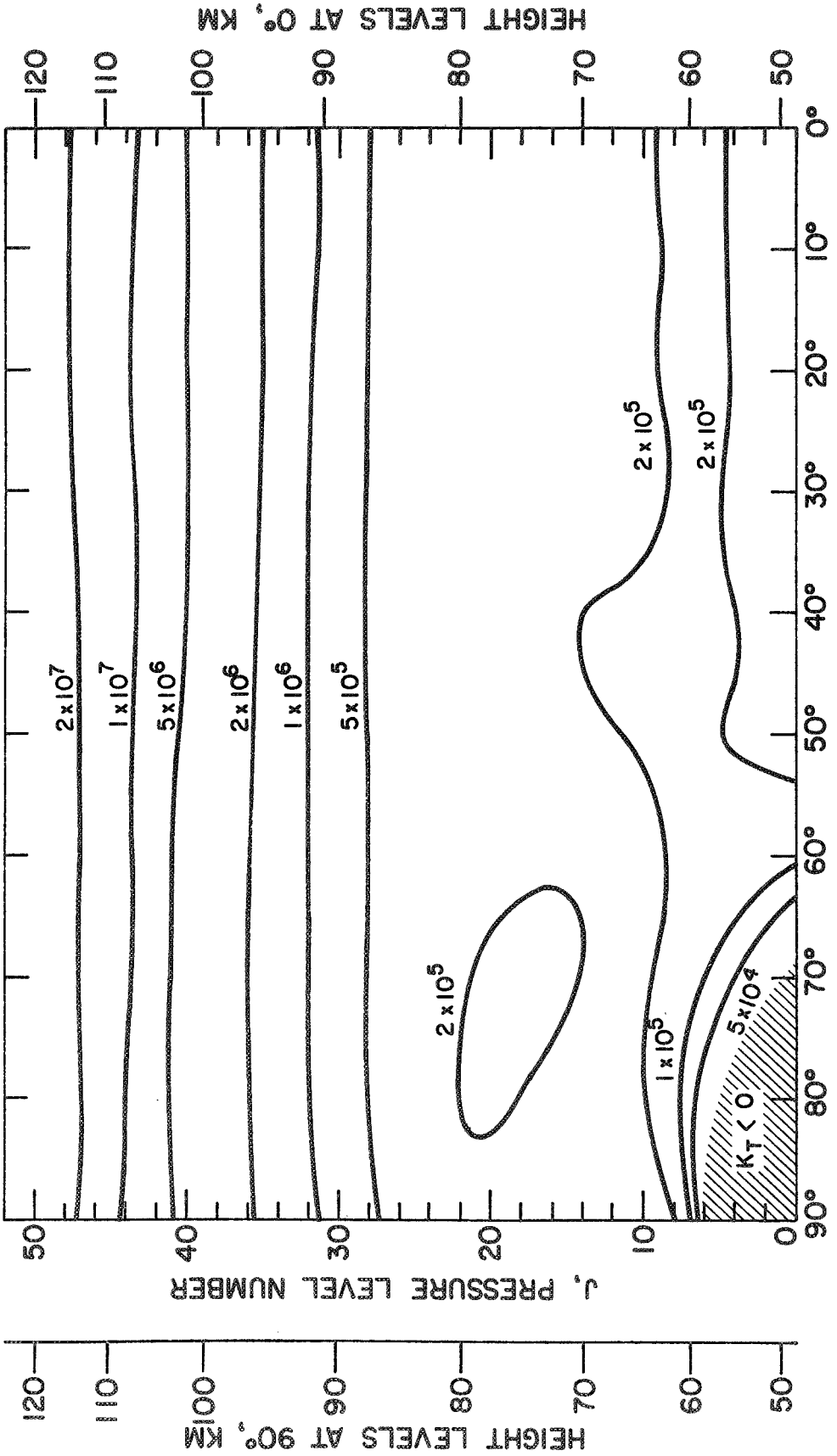

Figure 30. Eddy diffusion coefficients, in cm^2/sec, necessary to achieve thermal balance by vertical transport alone for the equinox mesosphere and lower thermosphere

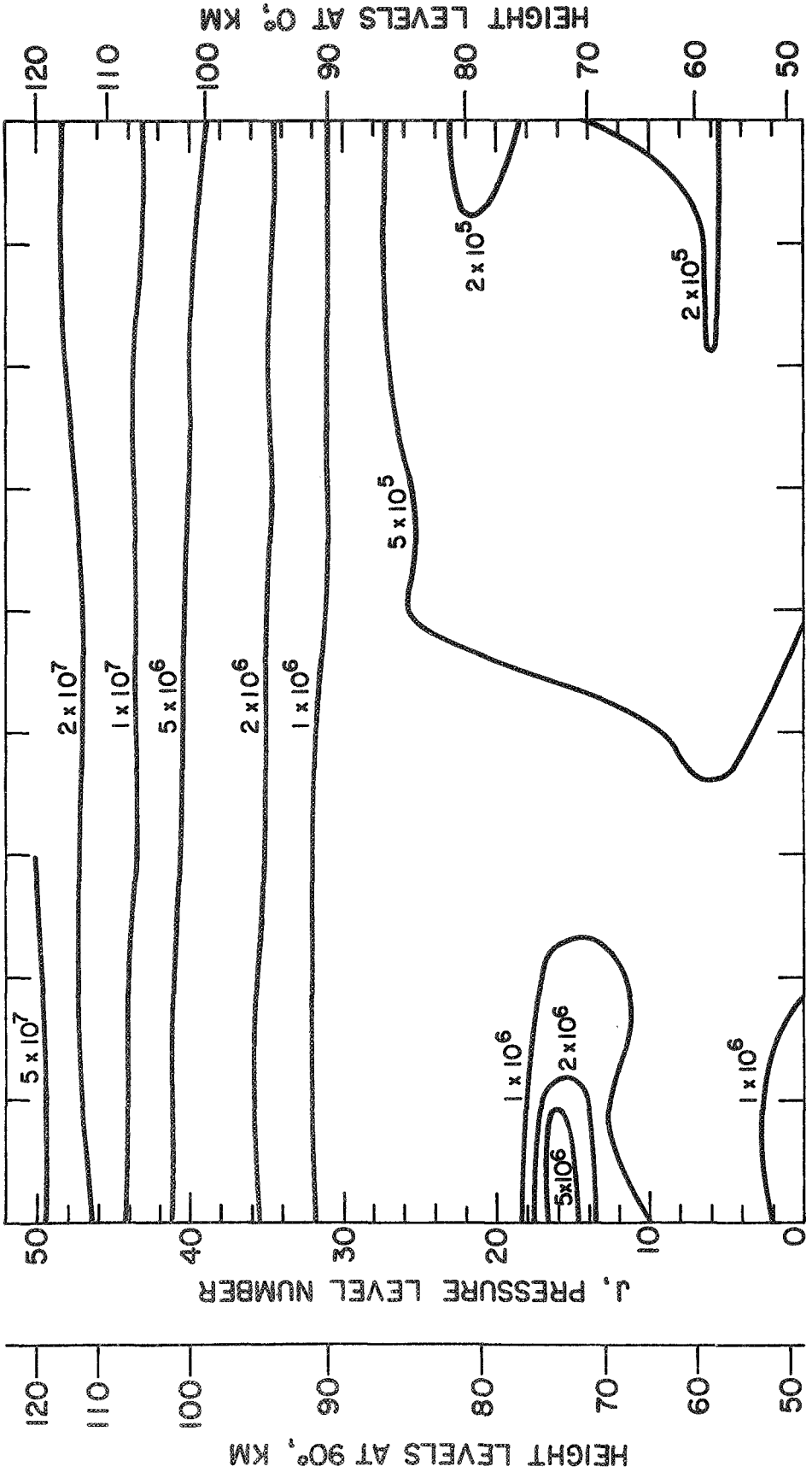

Figure 31. Eddy diffusion coefficients, in cm^2/sec, necessary to achieve thermal balance by vertical transport alone for the summer solstice mesosphere and lower thermosphere

summer solstice pole a localized region of enhanced vertical transport may be attributed by analogy to a balancing upward flow regime.

In general then the energy balance of the mesosphere can be reasonably maintained by vertical eddy transport, qualitatively consistent with compositional requirements, except near the poles. The question of transport near the poles and above the mesopause (at all latitudes) will be considered further below.

4.6 INTEGRAL HEAT SOURCES AND SINKS

The seemingly great energy imbalance between the poles near solstice has been pointed out earlier (Murgatoryd and Goody, 1958) and is not as yet fully understood. Undoubtedly large scale dynamics and circulation must ultimately provide the balance through redistribution of potential, chemical, and kinetic energy (see, for example, Kellogg, 1961, and Young and Epstein, 1962).

Very simple models of mesospheric circulation have been derived by Murgatroyd and Singleton (1961) and Leovy (1964) for differential radiative heating alone which gave qualitatively reasonable results. Hopefully, vastly improved circulation models would be possible if information on the global heating imbalance were known much more precisely. In view of its importance to both the composition and the energy budget of the mesosphere and lower thermosphere globally, vertical thermal transport (predominantly eddy) must be included in heating imbalance estimates.

It was decided to attempt to estimate the gross energy imbalance from the full thermal models including thermal transport. The quantity

of interest was the difference between the total heating rate and a representative value of the divergence of the heat flux, that is:

$$\delta Q = Q_{TOTAL} - \frac{\partial}{\partial z} \mathcal{F}_{TOTAL} \qquad (4.6.1)$$

where δQ is the local heat imbalance (in ergs/cm^3/sec). The equilibrium eddy thermal conductivity for the earth average thermal model (Chapter 3.) was adopted as the most representative, in the sense that it was derived from the thermal model least likely to be significantly influenced by the neglected large scale dynamics. With eddy transport characterized in that manner the local heat flux was calculated with the temperature derivatives and values of (molecular) thermal conductivity appropriate to the various models. Unfortunately this procedure could not be successfully used within the finite difference framework described in Appendix A. The problem was again the 'noise' in the tempera- true derivative approximations, as was the case in an analogous problem in Chapter 3. This 'noise' was greatly enhanced by the resolution of the temperature data, which had been read from the contour plots of Newell (1968) and Murgatroyd (1965) at 5 Km intervals.

In Chapter 3. it was found that integrating the energy equation was quite efficient in averaging over the 'noise'. As a parallel it was decided to calculate the integral heat imbalance instead of δQ. Integrating Equation (4.6.1) in the vertical direction, one obtains:

$$\Delta Q = \int_z^\infty \delta Q \, dz' = \int_z^\infty Q_{TOTAL} \, dz' + \mathcal{F}_{TOTAL} \qquad (4.6.2)$$

Where ΔQ is the integral heat balance in ergs/cm^2/sec. In the above equation the hemisphere average values of the heat flux at 120 Km were incorporated so that the following definition could be made:

$$\int_z^{\infty} Q_{TOTAL}\, dz' = \int_z^{120} Q_{TOTAL}\, dz' - \Phi^{(120)}_{TOTAL} \qquad (4.6.3)$$

The results of the calculations of ΔQ for the three seasons considered are shown in Figures 32, 33, and 34. The equinox hemisphere shows near thermal balance above the mesopause at all latitudes, while in the lower mesosphere, as anticipated, significant net cooling is in evidence at high latitudes. There is however net heating at the same levels at low latitudes sufficient to balance the net cooling at high latitudes through perhaps a single meridional cell. The predominant feature of the solstice hemisphere is still the polar imbalance. An average of about 700-800 ergs/cm^2/sec must be transported from the summer pole to the winter pole, i.e. the region above 65^o, to balance the thermal structure above 50 Km for the earth average thermal model.

These results seem reasonable and hopefully could be incorporated into general circulation models. One of the drawbacks is the lower limit of 50 Km. on the present data. Thus the large amounts of ozone heating in the upper stratosphere are not included. This is presumably a quite important source of energy for driving these global scale wind fields, and would be a useful extension to the present study. Another uncertainty in the present results is the seasonal and latitudinal ozone distribution, which would be expected to have some impact on

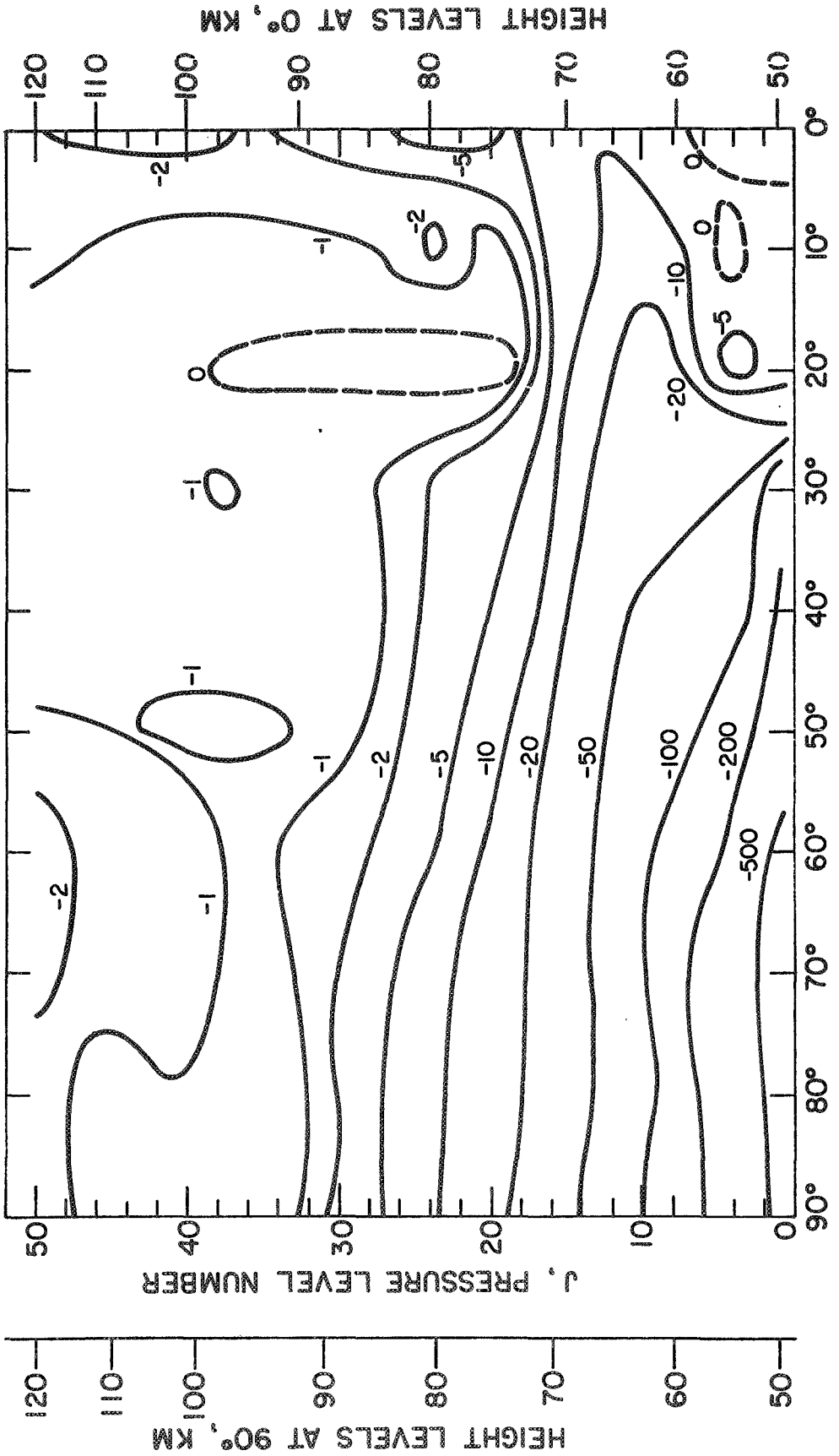

Figure 32. Integral (column) heating imbalance above 50 Km in ergs/cm^2/sec, for winter solstice

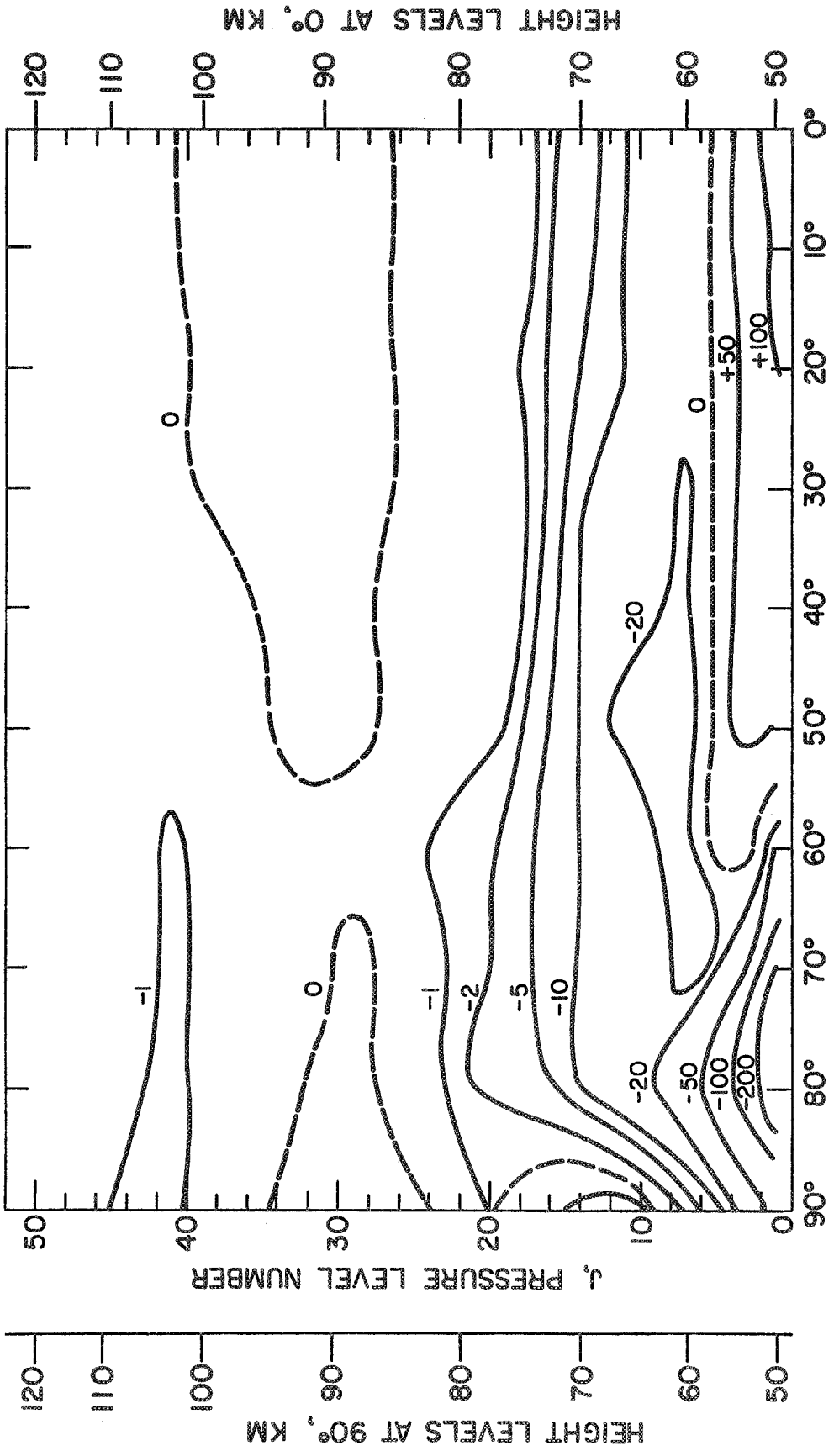

Figure 33. Integral (column) heating imbalance above 50 Km in ergs/cm^2/sec, for equinox

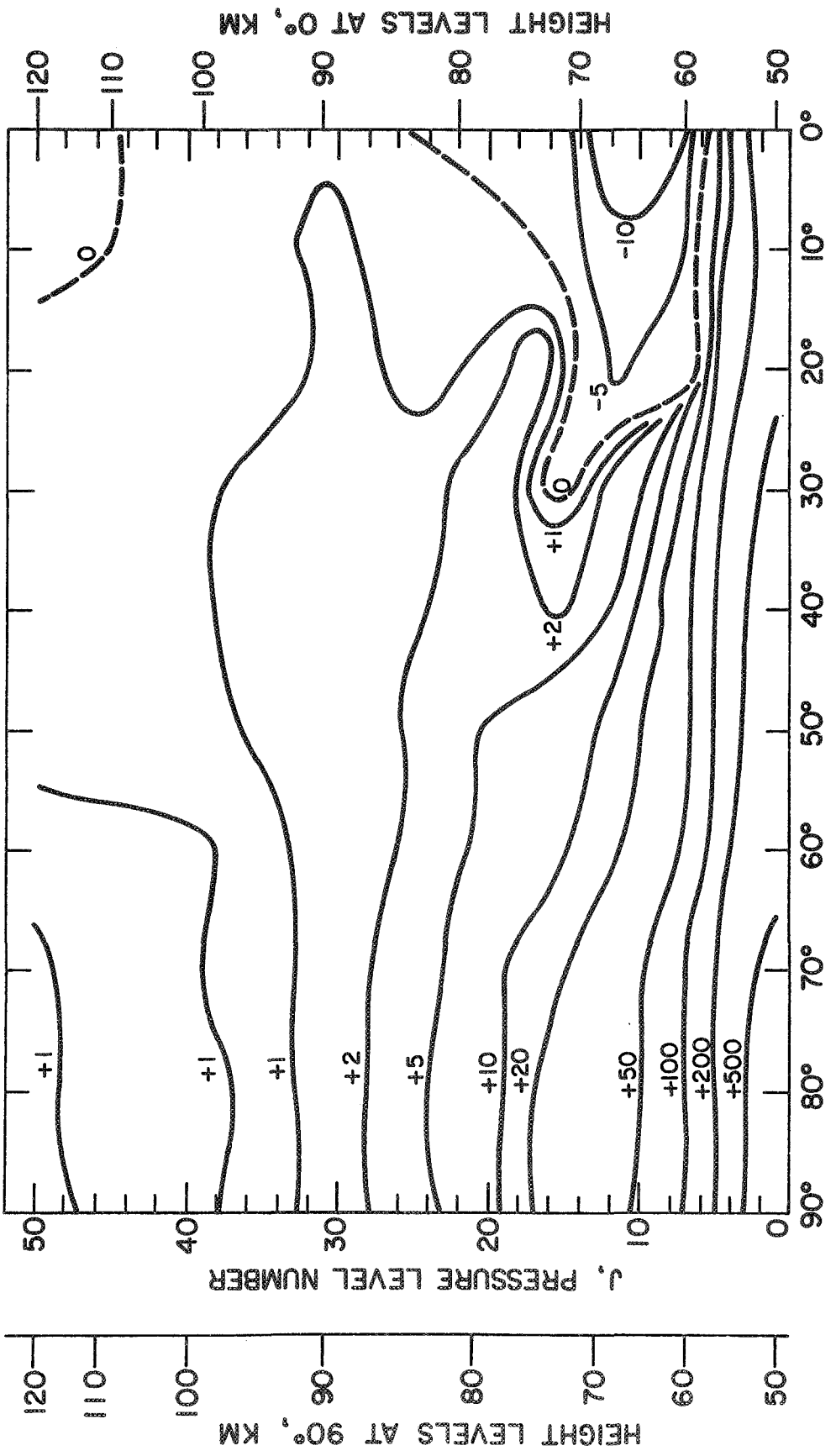

Figure 34. Integral (column) heating imbalance above 50 Km. in ergs/cm^2/sec, for summer solstice

the overall heating imbalances. However, until the large uncertainty in the ozone data above the stratosphere, discussed in Chapter 3., can be resolved the relatively smaller variations are probably unimportant by comparison.

CHAPTER 5

DISCUSSION, CONCLUSIONS, AND RECOMMENDATIONS FOR FUTURE WORK

5.1 DISCUSSION

5.1.1 Vertical Thermal Transport

The assumption of a vertical eddy transport of heat was used in both Chapters 3 and 4 in achieving a balance in the energy budget of the mesosphere and lower thermosphere. The results strongly indicate the necessity of some vertical transport mechanism operative on the average at these levels. The question naturally divides itself into considerations of the regions above and below the mesopause. In the mesosphere the transport necessary for thermal balance is quite consistent with an eddy diffusion interpretation. The values of K_T derived lie at the lower extreme of the range of estimates adopted in compositional studies (Colgrove, et al, 1965, 1966; Shimazaki, 1967, 1968; Hesstvedt, 1968; Shimazaki and Laird, 1970; and Anderson, 1970).

Above the mesopause a quite high level of vertical transport is required, which if interpreted as eddy diffusion would be inconsistent with the estimates used in the compositional studies mentioned above. Near the upper boundary the transport reflects eddy diffusion coefficients which are 5-10 times the values successfully used in modelling composition resulting in an effective turbopause above 120 Km.

It could be argued that the upper portion of the K_T curve in Figure 13 represents the sum of eddy transport and ascending motions.

A vertical velocity, w, obeying the continuity of mass equation, sufficient to provide the necessary transport at the upper boundary can be calculated as:

$$w = \frac{w_{120}\,\rho_{120}}{\rho} = -\frac{\frac{\partial}{\partial z}\left\{\rho C_p K_T \left(\frac{\partial T}{\partial z} + \frac{g}{C_p}\right)\right\}}{\rho C_p \left(\frac{\partial T}{\partial z} + \frac{g}{C_p}\right)} \qquad (5.1.1)$$

The results for w_{120} are of the order of about 10 cm/sec. for the models used in Chapters 3 and 4. Thus, velocities of this kind would have to exist on the average in both hemispheres in all seasons. Besides the obvious problems with conservation of mass globally, velocities of this magnitude are also inconsistent with lower thermospheric composition models.

The predominant factor leading to the large values of transport needed above the mesopause is the magnitude of the heat flux specified at 120 Km. A value of -2.4 ergs/cm^2/sec was used, for example, in the global model. In turn, about 70% of the heat flux adopted results from the assumptions concerning dissipation of tidal oscillations. We are forced to conclude on the basis of the apparent inconsistencies that the bulk of the tidal energy flux does not penetrate much above 90-110 Km on the average.

Two processes which would achieve this end are reflection and the dissipation of the tides at lower levels. Yanowitch (1967) discussed the reflection of waves in a viscous medium but to what extent these calculations might be applicable for the Lindzen (1967) tidal mode is not known. Reflection of the bulk of the upward propagating tidal modes would, of course, be the easiest solution to the immediate problem.

Lindzen (1968) discussed two specific modes of dissipation which act on the temperature fluctuation component of the diurnal tide, Newtonian cooling (with a photochemical interaction), and the production of local regions of instability (Richardson number $\ll$ 0). The first was shown to be of little consequence, and the second could not be explicitly included in the tidal calculations. Lindzen reasoned, however, that in the regions of local instability, about 85-95 Km, the diurnal tides could be effectively dissipated, probably producing gravity waves and turbulence in doing so. This mechanism would be a satisfactory explaination provided that the bulk of the energy resulting from the dissipation did not reach much above 100 Km.

Dissipation by conductivity, viscosity, and ion drag were investigated very recently by Blake and Lindzen (1970). They found essentially no dissipation below about 100 Km, the majority occuring above about 120-130 Km. Thus, the only possible mechanisms for removing the tidal energy flux at 90-100 Km or below are reflection or dissipation in local regions of (tidally induced) instability. In the latter case the diurnal tide may be the process responsible for a good deal of the gravity waves and other smaller scale phenomena observed in the lower thermosphere.

In Figure 35 the equilibrium eddy diffusion coefficients for the global scale model are shown for the tidal dissipation assumptions adopted in Chapter 2, and for the opposite extreme of no energy input from the tides above 50 Km. The values for the latter case labelled "without tidal dissipation" lie well within the range consistent with the compositional studies mentioned earlier. It is possible to speculate on

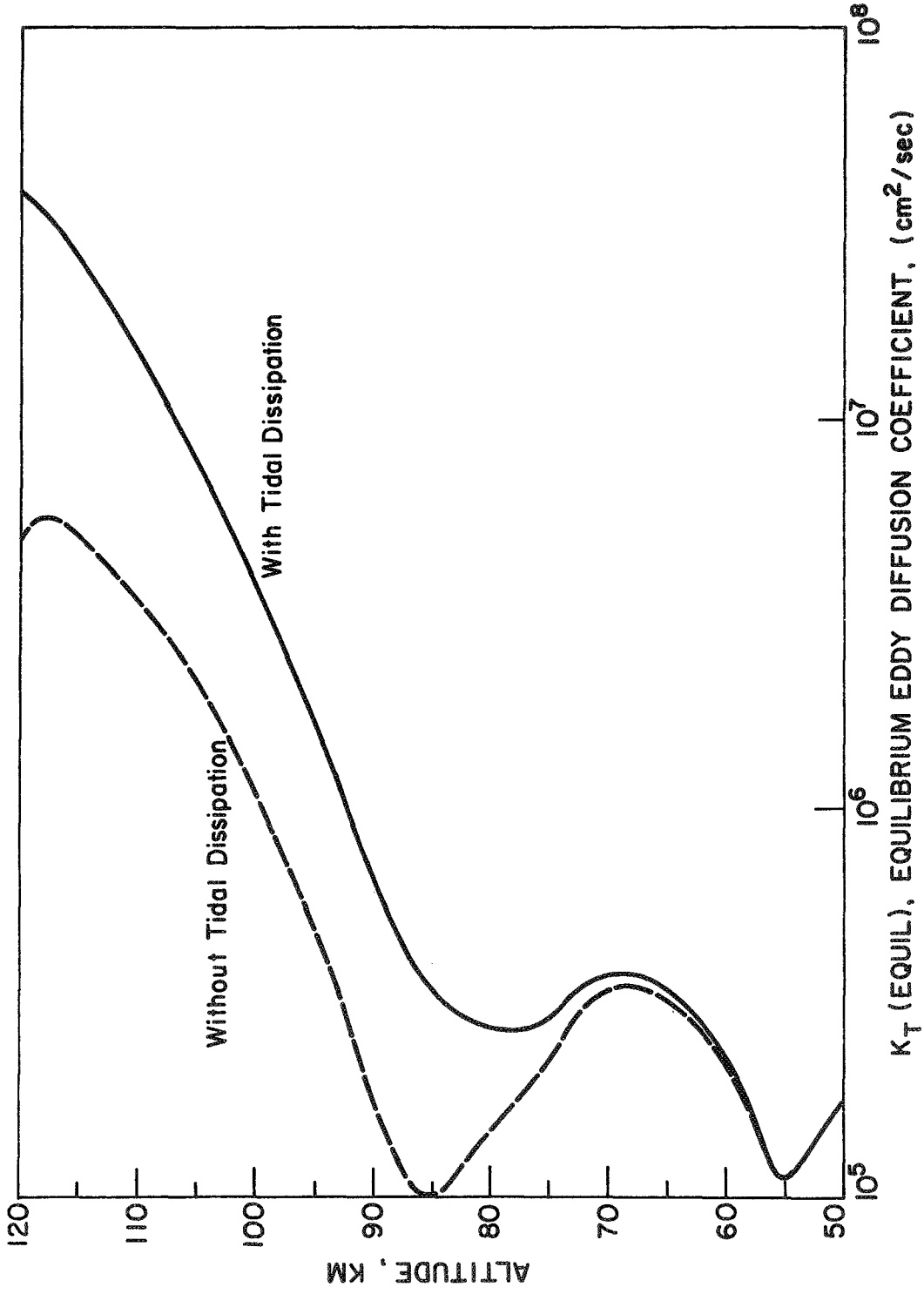

Figure 35. Effect of neglecting the tidal energy dissipation on the equilibrium eddy diffusion coefficient

the effect of dissipating the full tidal energy flux in the mesopause region itself, with reference to Figure 35. The energy involved would lead to increased estimates of eddy transport locally; so that for example, the upper minimum in the K_T (equil) profile might disappear, leaving nearly constant values of $\sim 3 \times 10^5$ cm^2/sec from about 70 Km to 95 Km. This results in a very reasonable eddy transport description throughout the model.

5.1.2 Global Energy Budget

In Chapter 4 the seasonal and latitudinal variations in the energy budget of the mesosphere and lower thermosphere were estimated from the local heating/cooling rates and average values of heat flux at 120 Km and of K_T (equil). These results are presented in Figures 32, 33, and 34 in terms of the integral (column) heating or cooling necessary to balance the local mean thermal state.

For summer and winter solstice the most significant imbalance occurs at high latitudes, which is in keeping with the ability to balance the thermal models with reasonable values of K_T(equil) at the other latitudes (see Figures 29, 30, 31). Near the poles then an average of about 700-800 ergs/cm^2/sec must be deposited in the winter hemisphere, and the same amount removed from the summer pole, or more likely transported from the summer to the winter pole, to achieve a long term balance. The near equality on the energy imbalances for the two hemispheres strongly suggests a global meridional circulation system with a net effect of air ascending over the summer pole and subsiding over the winter pole.

At equinox the imbalances are smaller but may still be significant. As shown in Figure 27 near the equinox pole in the lower mesophere no positive eddy transport coefficient could be expected to balance the large net cooling. Using an average profile of K_T(equil) leads to an integral cooling of just over 200 ergs/cm^2/sec at 80^o. Both poles would require a net influx of heat in this simple spring/autumn average model. At low latitudes (below about 20^o), something over 100 ergs/cm^2/sec is available to balance the energy budget, where the factor of two in magnitudes is compensated by the larger geographical area included in the lower latitudes. Thus, each hemisphere at equinox could balance independently if, for example, a simple hemisphere meridional cell were to exist in the mesosphere with ascending air over the tropics and subsidence at the highest latitudes.

The above considerations of energy imbalances and circulation systems refer to the entire atmosphere above 50 Km. For all practical purposes, however, the results reflect predominantly mesospheric contributions and the uncertainties in the upper boundary heat flux and balancing vertical transport are completely negligible.

5.2 CONCLUSIONS

(a) In the mesosphere the calculated vertical transport requirements of the mean thermal state can be interpreted as resulting from eddy diffusion for values consistent with compositional studies. The same conclusion applies in the lower thermosphere ($\lesssim$ 120 Km) only if the upward energy flux of the diurnal tide can be excluded from that region through either reflection or dissipation lower in the atmosphere.

(b) In the absence of the tidal energy consideration the major uncertainty in the lower thermospheric thermal model is the O_2 heating efficiency. More specifically the uncertainty lies in the ultimate disposition of the $O(^1D)$ excitation energy.

(c) In the mesosphere (and presumeably in the upper stratosphere as well) the ozone concentration is the major uncertainty in the thermal model. However, the profile adopted (Evans, et al, 1968) gives reasonable results in the present application.

(d) The contribution to the thermal balance from CO_2(15μ bands) has been investigated. It is found to be of major importance in the mesosphere. Above the mesopause, the uncertainties in the CO_2 volume mixing ratio and ν_2 vibrational relaxation time must be taken into account. The present results indicate that for reasonable bracketing values of those quantities the CO_2(15μ bands) cooling rate above the mesopause is not very important in the overall energy budget.

5.3 RECOMMENDATIONS FOR FUTURE WORK

(a) The next logical step in estimating the meridional circulation in the mesosphere and lower thermosphere would be to use the integral heating imbalance estimates, Figures 32, 33, and 34, in place of radiative net heating. The present calculation should be extended down to about 20Km - 30 Km. to include the majority of the solar heating due to ozone.

(b) The derivation of a vertical eddy transport profile consistent with composition and the energy balance simultaneously should be attempted. Specifically the effects of transport on composition and of composition on the heating/cooling rates should be considered. This

was done in an approximate way for CO_2 in the present work.

(c) A great deal remains to be done in studies of the thermal structure of the thermosphere as a whole. The following are areas in which the need for further work is obvious: (i) derive (solar UV) heating efficiencies on the basis of the physical processes involved rather than accepting empirically fitted constant values; (ii) obtain better estimates of the airglow emission especially in the near IR and far UV; (iii) investigate the average heating by particle bombardment especially in the auroral zone; (iv) consider the upward energy flux associated with atmospheric tides and gravity waves, and their ultimate deposition by reflection and dissipation; and (v) attempt to estimate the lateral transport by conduction and gross circulation.

(d) A radiative transfer study of the 4.3μ bands of CO_2 should be made, including the postulated additional excitation mechanism from N_2 vibration. An immediate outcome of such a study would be the determination of the spatial redistribution of the $O(^1D)$ excitation energy, from the photolysis of O_2 and O_3, assumed in Chapter 2 to be transmitted to $CO_2(\nu_3)$ through N_2 vibration. In addition if the IR flux characteristics were modified sufficiently by the additional source the latter's existence might be experimentally verifiable.

APPENDIX A

NUMERICAL FORMULATION OF THE THERMAL MODEL

An approximate numerical model of the time dependent energy equation, Equation (2.2.22), is presented in this appendix. The finite difference scheme and general procedure used in approximating the partial differential equation are discussed in the first part. This is followed by a recasting of the boundary conditions, discussed in Chapter 2, in terms of the finite difference formulation. The next section deals with a matrix representation for the system of simultaneous equations and the method of solution is presented. The final section includes the evaluation of various parameters and other numerical approximations necessary to establish the overall numerical model.

A.1 FINITE DIFFERENCE FORMULATION

A suitable spatial and temporal grid must be established in order to use a finite difference scheme for approximating Equation (2.2.22). Let us divide the pressure (z_p) field into 50 levels such that:

$$z_p(m) = z_p^o + (m-1)\,\Delta z_p \qquad m=1,2\ldots,50 \tag{A.1}$$

where m denotes the level, z_p^o is the lower boundary at 50 km. The upper boundary at approximately 120 km is given by:

$$z_p(50) = z_p^o + 49\,\Delta z_p \tag{A.2}$$

The time scale can be expressed in increments of Δt, as:

$$t_n = n\,\Delta t \qquad n = 0, 1, 2, \cdots \tag{A.3}$$

where n represents the number of the time step and hence a measure of the time from an arbitrary starting point. Thus we have set up a $z_p(m)$, t_n grid at each point of which the energy equation is either already known or must yet be evaluated.

If t_n is the latest time at which the temperatures, T_n^m, and the coefficients, A_n^m, B_n^m, C_n^m, D_n^m are known, then in solving for the unknown temperatures, T_{n+1}^m, we should consider the basic equation evaluated at the midpoint $t_{n+\frac{1}{2}} = t_n + \frac{1}{2}\Delta t$. Thus we express the coefficients in terms of the midpoint temperatures, $T_{n+\frac{1}{2}}^m = T_n^m + \frac{1}{2}\Delta T_n^m$, where $\Delta T_n^m = T_{n+1}^m - T_n^m$, as $A_{n+\frac{1}{2}}^m$, $B_{n+\frac{1}{2}}^m$, $C_{n+\frac{1}{2}}^m$, $D_{n+\frac{1}{2}}^m$. These coefficients can be obtained by expansion about the n^{th} time step as follows:

$$A_{n+\frac{1}{2}}^m \approx A_n^m + \frac{\Delta T_n^m}{2}\left(\frac{\partial A}{\partial T}\right)_n \qquad C_{n+\frac{1}{2}}^m \approx C_n^m + \frac{\Delta T_n^m}{2}\left(\frac{\partial C}{\partial T}\right)_n \tag{A.4}$$

$$B_{n+\frac{1}{2}}^m \approx B_n^m + \frac{\Delta T_n^m}{2}\left(\frac{\partial B}{\partial T}\right)_n \qquad D_{n+\frac{1}{2}}^m \approx D_n^m + \frac{\Delta T_n^m}{2}\left(\frac{\partial D}{\partial T}\right)_n$$

Thus the basic equation at time $t_{n+\frac{1}{2}}$ becomes:

$$\frac{\partial T_{n+\frac{1}{2}}^m}{\partial t} = A_{n+\frac{1}{2}}^m + B_{n+\frac{1}{2}}^m \frac{\partial T_{n+\frac{1}{2}}^m}{\partial z_p} + C_{n+\frac{1}{2}}^m \left(\frac{\partial T_{n+\frac{1}{2}}^m}{\partial z_p}\right)^2 + D_{n+\frac{1}{2}}^m \frac{\partial^2 T_{n+\frac{1}{2}}^m}{\partial z_p^2}$$

$$\frac{\partial T_{n+\frac{1}{2}}^m}{\partial t} = \left\{A_n^m + \frac{\Delta T_n^m}{2}\left(\frac{\partial A}{\partial T}\right)_n\right\} + \left\{B_n^m + \frac{\Delta T_n^m}{2}\left(\frac{\partial B}{\partial T}\right)_n\right\}\left\{\frac{\partial T_n^m}{\partial z_p} + \frac{1}{2}\frac{\partial \Delta T_n^m}{\partial z_p}\right\}$$

$$+ \left\{C_n^m + \frac{\Delta T_n^m}{2}\left(\frac{\partial C}{\partial T}\right)_n\right\}\left\{\frac{\partial T_n^m}{\partial z_p} + \frac{1}{2}\frac{\partial \Delta T_n^m}{\partial z_p}\right\}^2$$

$$+\left\{D_n^m+\frac{\Delta T_n^m}{2}\frac{\partial D}{\partial T}\right)_n\right\}\left\{\frac{\partial^2 T_n^m}{\partial z_p^2}+\frac{1}{2}\frac{\partial^2 \Delta T_n^m}{\partial z_p^2}\right\} \qquad \text{(A.5)}$$

When fully expanded, this becomes:

$$\begin{aligned}\frac{\partial T_{n+\frac{1}{2}}^m}{\partial t} &= A_m^n+\frac{\Delta T_n^m}{2}\frac{\partial A}{\partial T}\Big)_n+B_n^m\frac{\partial T_n^m}{\partial z_p}+\frac{1}{2}B_n^m\frac{\partial \Delta T_n^m}{\partial z_p}\\ &+\frac{1}{2}\Delta T_n^m\frac{\partial B}{\partial T}\Big)_n\frac{\partial T_n^m}{\partial z_p}+\frac{1}{4}\Delta T_n^m\frac{\partial B}{\partial T}\Big)_n\frac{\partial \Delta T_n^m}{\partial z_p}+C_n^m\left(\frac{\partial T_n^m}{\partial z_p}\right)^2\\ &+C_n^m\frac{\partial T_n^m}{\partial z_p}\frac{\partial \Delta T_n^m}{\partial z_p}+\frac{1}{4}C_n^m\left(\frac{\partial \Delta T_n^m}{\partial z_p}\right)^2+\frac{1}{2}\Delta T_n^m\frac{\partial C}{\partial T}\Big)_n\left(\frac{\partial T_n^m}{\partial z_p}\right)^2\\ &+\frac{1}{2}\Delta T_n^m\frac{\partial C}{\partial T}\Big)_n\frac{\partial T_n^m}{\partial z_p}\frac{\partial \Delta T_n^m}{\partial z_p}+\frac{1}{8}\Delta T_n^m\frac{\partial C}{\partial T}\Big)_n\left(\frac{\partial \Delta T_n^m}{\partial z_p}\right)^2 \qquad \text{(A.6)}\\ &+D_n^m\frac{\partial^2 T_n^m}{\partial z_p^2}+\frac{1}{2}D_n^m\frac{\partial \Delta T_n^m}{\partial z_p^2}+\frac{1}{2}\Delta T_n^m\frac{\partial D}{\partial T}\Big)_n\frac{\partial^2 T_n^m}{\partial z_p^2}\\ &+\frac{1}{4}\Delta T_n^m\frac{\partial D}{\partial T}\Big)_n\frac{\partial^2 \Delta T_n^m}{\partial z_p^2}\end{aligned}$$

Let us now neglect terms of order $(\Delta T_n^m)^2$, that is:

$$\Delta T_n^m\frac{\partial \Delta T_n^m}{\partial z_p},\ \Delta T_n^m\frac{\partial^2 \Delta T_n^m}{\partial z_p^2},\ \Delta T_n^m\left(\frac{\partial \Delta T_n^m}{\partial z_p}\right),\ \left(\frac{\partial \Delta T_n^m}{\partial z_p}\right)^2 \qquad \text{(A.7)}$$

The remaining equation is then:

$$\begin{aligned}\frac{\partial T_{n+\frac{1}{2}}^m}{\partial t} &= \left\{A_n^m+B_n^m\frac{\partial T_n^m}{\partial z_p}+C_n^m\left(\frac{\partial T_n^m}{\partial z_p}\right)^2+D_n^m\frac{\partial^2 T_n^m}{\partial z_p^2}\right\}\\ &+\left\{\frac{1}{2}B_n^m+C_n^m\frac{\partial T_n^m}{\partial z_p}\right\}\frac{\partial \Delta T_n^m}{\partial z_p}+\frac{1}{2}D_n^m\frac{\partial^2 \Delta T_n^m}{\partial z_p^2} \qquad \text{(A.8)}\\ &+\frac{1}{2}\Delta T_n^m\left\{\frac{\partial A}{\partial T}\Big)_n+\frac{\partial B}{\partial T}\Big)_n\frac{\partial T_n^m}{\partial z_p}+\frac{\partial C}{\partial T}\Big)_n\left(\frac{\partial T_n^m}{\partial z_p}\right)^2\right.\\ &+\left.\frac{\partial D}{\partial T}\Big)_n\frac{\partial^2 T_n^m}{\partial z_p^2}\right\}\end{aligned}$$

The evaluation of the quantities $\partial A/\partial T)_n$, $\partial B/\partial T)_n$, etc. will be found in a later section of this appendix.

The following scheme was used to express the derivatives in terms of stable, implicit finite differences:

$$
\begin{aligned}
\frac{\partial T_{n+\frac{1}{2}}^{m}}{\partial t} &\simeq \frac{T_{n+1}^{m} - T_{n}^{m}}{\Delta t} \\
\frac{\partial \Delta T_{n}^{m}}{\partial z_p} &= \frac{\partial T_{n+1}^{m}}{\partial z_p} - \frac{\partial T_{n}^{m}}{\partial z_p} \\
\frac{\partial^2 \Delta T_{n}^{m}}{\partial z_p^2} &= \frac{\partial^2 T_{n+1}^{m}}{\partial z_p^2} - \frac{\partial^2 T_{n}^{m}}{\partial z_p^2} \\
\frac{\partial T_{n}^{m}}{\partial z_p} &\simeq \frac{T_{n}^{m+1} - T_{n}^{m-1}}{2\Delta z_p} \\
\frac{\partial T_{n+1}^{m}}{\partial z_p} &\simeq \frac{T_{n+1}^{m+1} - T_{n+1}^{m-1}}{2\Delta z_p} \\
\frac{\partial^2 T_{n}^{m}}{\partial z_p^2} &\simeq \frac{T_{n}^{m+1} - 2T_{n}^{m} + T_{n}^{m-1}}{\Delta z_p^2} \\
\frac{\partial^2 T_{n+1}^{m}}{\partial z_p^2} &\simeq \frac{T_{n+1}^{m+1} - 2T_{n+1}^{m} + T_{n+1}^{m-1}}{\Delta z_p^2}
\end{aligned}
\qquad \text{(A. 9)}
$$

The derivatives $\partial T_n^m/\partial z_p$ and $\partial^2 T_n^m/\partial z_p^2$ will not be expressed as finite differences since they do not involve unknown quantities. In terms of the above set of approximations, the basic equation may be written as:

$$
\begin{aligned}
\frac{T_{n+1}^{m} - T_{n}^{m}}{\Delta t} = &\left\{ A_n^m + B_n^m \frac{\partial T_n^m}{\partial z_p} + C_n^m \left(\frac{\partial T_n^m}{\partial z_p}\right)^2 + D_n^m \frac{\partial^2 T_n^m}{\partial z_p^2} \right\} \\
&+ \left\{ \frac{1}{2} B_n^m + C_n^m \frac{\partial T_n^m}{\partial z_p} \right\} \left\{ \frac{T_{n+1}^{m+1} - T_{n+1}^{m-1}}{2\Delta z_p} - \frac{\partial T_n^m}{\partial z_p} \right\}
\end{aligned}
$$

$$+\frac{1}{2}D_n^m\left\{\frac{T_{n+1}^{m+1}-2T_{n+1}^{m}+T_{n+1}^{m-1}}{\Delta z_p^2}-\frac{\partial^2 T_n^m}{\partial z_p^2}\right\}$$

$$+\frac{1}{2}(T_{n+1}^m-T_n^m)\left\{\frac{\partial A}{\partial T}\right)_n+\frac{\partial B}{\partial T}\Big)_n\frac{\partial T_n^m}{\partial z_p} \tag{A.10}$$

$$+\frac{\partial C}{\partial T}\Big)_n\left(\frac{\partial T_n^m}{\partial z_p}\right)^2+\frac{\partial D}{\partial T}\Big)_n\frac{\partial^2 T_n^m}{\partial z_p^2}\Big\}$$

A new variable, E_n^m, is defined by the following:

$$E_n^m=\frac{1}{2}\left\{\frac{\partial A}{\partial T}\right)_n+\frac{\partial B}{\partial T}\Big)_n\frac{\partial T_n^m}{\partial z_p}+\frac{\partial C}{\partial T}\Big)_n\left(\frac{\partial T_n^m}{\partial z_p}\right)^2+\frac{\partial D}{\partial T}\Big)_n\frac{\partial^2 T_n^m}{\partial z_p^2}\right\} \tag{A.11}$$

Equation (A.10) may now be written as:

$$T_{n+1}^{m-1}\left\{\frac{\Delta t}{2\Delta z_p}\left(\frac{1}{2}B_n^m+C_n^m\frac{\partial T_n^m}{\partial z_p}-\frac{D_n^m}{\Delta z_p}\right\}+T_{n+1}^m\left\{1\right.\right.$$

$$\left.-\Delta t\left(E_n^m-\frac{D_n^m}{\Delta z_p}\right)\right\}+T_{n+1}^{m+1}\left\{-\frac{\Delta t}{2\Delta z_p}\left(\frac{1}{2}B_n^m\right.\right. \tag{A.12}$$

$$\left.\left.+C_n^m\frac{\partial T_n^m}{\partial z_p}+\frac{D_n^m}{\Delta z_p}\right\}=T_n^m(1-\Delta t\,E_n^m)\right.$$

$$+\Delta t\left\{A_n^m+\frac{B_n^m}{2}\frac{\partial T_n^m}{\partial z_p}+\frac{D_n^m}{2}\frac{\partial^2 T_n^m}{\partial z_p^2}\right\}$$

This is now a set of equations of the form:

$$\alpha(m)\,T_{n+1}^{m-1}+\beta(m)\,T_{n+1}^m+\gamma(m)\,T_{n+1}^{m+1}=F(m) \tag{A.13}$$

where the following substitutions have been made:

$$\alpha(m) = \frac{\Delta t}{2\Delta z_p}\left(\frac{1}{2}B_n^m + C_n^m\frac{\partial T_n^m}{\partial z_p} - \frac{D_n^m}{\Delta z_p}\right)$$

$$\beta(m) = 1 - \Delta t\left(E_n^m - \frac{D_n^m}{\Delta z_p}\right)$$

$$\gamma(m) = -\frac{\Delta t}{2\Delta z_p}\left(\frac{1}{2}B_n^m + C_n^m\frac{\partial T_n^m}{\partial z_p} + \frac{D_n^m}{\Delta z_p}\right) \qquad \text{(A.14)}$$

$$F(m) = T_n^m(1 - \Delta t\, E_n^m) + \Delta t\left\{A_n^m + \frac{1}{2}B_n^m\frac{\partial T_n^m}{\partial z_p} + \frac{1}{2}D_n^m\frac{\partial^2 T_n^m}{\partial z_p^2}\right\}$$

As m ranges from 1 to 50, there are 50 equations in the following 52 unknowns:

$$T_{n+1}^0, T_{n+1}^1, T_{n+1}^2, \ldots, T_{n+1}^{49}, T_{n+1}^{50}, T_{n+1}^{51} \qquad \text{(A.15)}$$

Two of these unknowns, the first and last can be eliminated through the boundary conditions.

A.2 BOUNDARY CONDITIONS

The points m=0 and m=51 are pseudo points lying outside the established grid and therefore unreachable and unknowable. By means of an upper and a lower boundary condition these pseudo points can be expressed in terms of constants and points within the boundaries, that is $1 \leq m \leq 50$.

A.2.1 Lower Boundary Condition

The elimination of the unknown temperature point below the lower boundary, T_{n+1}^o, was discussed in Chapter 2 and the boundary

condition adopted was a constant temperature at that point. Thus, at m=0, $z_p(0) = z_p^o - \Delta z_p$, the temperature for all n was considered a constant:

$$T_n^o = T_{\text{lower boundary}} = \text{constant} \tag{A.16}$$

A.2.2 Upper Boundary Condition

At the upper boundary of 120 km (m=50) a constant, specified heat flux was adopted as the boundary condition (Chapter 2). Since the temperature gradients are part of the heat flux term, the pseudo point at m=51, $z_p(51) = z_p(50) + \Delta z_p$, is included in the flux at m=50. The flux at the upper boundary was considered a constant for all n:

$$\Phi_{TOTAL}(50,n) = \Phi_{\text{upper boundary}} = \text{constant} \tag{A.17}$$

but $\Phi_{\text{upper boundary}}$ can be expressed as:

$$\Phi_{\text{upper boundary}} = \frac{(\lambda+\tilde{K}_T)}{H}\frac{\partial T_n^{50}}{\partial z_p} - \tilde{K}_T\frac{g}{C_p}$$

$$\Phi_{\text{upper boundary}} = -\int_{120}^{\infty} Q_{TOTAL}\, dz \tag{A.18}$$

Let us introduct the quantity ψ as:

$$\psi_n = \frac{H\left(\Phi_{\text{upper boundary}} + \tilde{K}_T\frac{g}{C_p}\right)}{(\lambda+\tilde{K}_T)} \tag{A.19}$$

$$= \frac{\partial T_n^{50}}{\partial z_p}$$

Expanding about the temperature at t_n and expressing the above in terms of the mid-point, at $t_{n+\frac{1}{2}} = t_n + \frac{1}{2}\Delta t$:

$$\frac{\partial T^{50}_{n+\frac{1}{2}}}{\partial z_p} = \frac{1}{2}\frac{\partial T^{50}_{n+1}}{\partial z_p} + \frac{1}{2}\frac{\partial T^{50}_{n}}{\partial z_p} = \psi_{n+\frac{1}{2}}$$

$$\simeq \psi_n + \frac{1}{2}\Delta T^{50}_n \frac{\partial \psi}{\partial T}\Big)_n \qquad \text{(A.20)}$$

$$\frac{\partial T^{50}_{n+1}}{\partial z_p} = \psi_n + \Delta T^{50}_n \frac{\partial \psi}{\partial T}\Big)_n$$

Using the finite difference scheme already employed leads to:

$$\frac{T^{51}_{n+1} - T^{49}_{n+1}}{2\Delta z_p} = \psi_n + \left(T^{50}_{n+1} - T^{50}_n\right)\frac{\partial \psi}{\partial T}\Big)_n$$

$$T^{51}_{n+1} = T^{49}_{n+1} + 2\Delta z_p\,\psi_n \qquad \text{(A.21)}$$

$$+ 2\Delta z_p \left(T^{50}_{n+1} - T^{50}_n\right)\frac{\partial \psi}{\partial T}\Big)_n$$

Thus the pseudo point temperature T^{51}_{n+1} has been expressed in terms of the boundary point temperature T^{50}_{n+1}, an interior point temperature T^{49}_{n+1} and various constants and other known quantities, central to which is of course $\Phi_{\text{upper boundary}}$. Equation (A.21) can be re-written in a more compact form as:

$$T^{51}_{n+1} = T^{49}_{n+1} + \delta\, T^{50}_{n+1} + \epsilon$$

$$\delta = 2\Delta z_p \left(\frac{\partial \psi}{\partial T}\right)_n$$

$$\epsilon = 2\Delta z_p \left\{ \psi_n - T_n^{50} \left(\frac{\partial \psi}{\partial T}\right)_n \right\} \qquad \text{(A.22)}$$

A.3 MATRIX REPRESENTATION

With the inclusion of the boundary conditions as suitable substitutions for the pseudo point temperatures, the 50 equations in 50 unknowns are as follows:

$$\begin{aligned}
&\alpha(1)\, T_{\text{lower boundary}} + \beta(1)\, T_{n+1}^{1} + \gamma(1)\, T_{n+1}^{2} \\
&\qquad = F(1) \qquad\qquad m=1 \\
&\alpha(m)\, T_{n+1}^{m-1} + \beta(m)\, T_{n+1}^{m} + \gamma(m)\, T_{n+1}^{m+1} \qquad \text{(A.23)} \\
&\qquad = F(m) \qquad\qquad m=2,3,\ldots,48,49 \\
&\alpha(50)\, T_{n+1}^{49} + \beta(50)\, T_{n+1}^{50} + \gamma(50)\left\{ T_{n+1}^{49} + \delta\, T_{n+1}^{50} \right. \\
&\qquad \left. + \epsilon \right\} = F(50) \qquad\qquad m=50
\end{aligned}$$

For symmetry the m=1 and m=50 equations can be written as:

$$\begin{aligned}
&\beta(1)\, T_{n+1}^{1} + \gamma(1)\, T_{n+1}^{2} = \widetilde{F(1)} \\
&\widetilde{\alpha(50)}\, T_{n+1}^{49} + \widetilde{\beta(50)}\, T_{n+1}^{50} = \widetilde{F(50)}
\end{aligned} \qquad \text{(A.24)}$$

where we define:

$$\begin{aligned}
\tilde{F}(1) &= F(1) - \alpha(1)\, T_{\text{lower boundary}} \\
\tilde{\alpha}(50) &= \alpha(50) + \gamma(50) \\
\tilde{\beta}(50) &= \beta(50) + \delta\,\gamma(50) \\
\tilde{F}(50) &= F(50) - \epsilon\,\gamma(50)
\end{aligned} \tag{A.25}$$

Thus the complete set of equations has the form:

$$\begin{aligned}
\beta(1)T^1 + \gamma(1)T^2 &= \tilde{F}(1) \\
\alpha(2)T^1 + \beta(2)T^2 + \gamma(2)T^2 &= F(2) \\
\alpha(3)T^2 + \beta(3)T^3 + \gamma(3)T^4 &= F(3) \\
&\vdots \\
\alpha(49)T^{48} + \beta(49)T^{49} + \gamma(49)T^{50} &= F(49) \\
\tilde{\alpha}(50)T^{49} + \tilde{\beta}(50)T^{50} &= \tilde{F}(50)
\end{aligned} \tag{A.26}$$

and it can be written symbolically as:

$$\mathbf{A}\,\bar{T} = \bar{F} \tag{A.27}$$

Where $\bar{T}$ and $\bar{F}$ are 50 element column vectors (50x1 matrices) and $\mathbf{A}$ is a 50x50 square matrix. Provided that $\mathbf{A}$ is non-singular the system of

equations can be solved for the unknown T^m_{n+1}'s, that is $\bar{T}$, as:

$$\bar{T} = A^{-1} \bar{F} \tag{A.28}$$

Where A^{-1} is the inverse of the matrix A.

The elements of the square matrix A, are:

$$\begin{aligned}
a_{ii} &= \beta(i) && 1 \le i \le 49 \\
a_{ii} &= \beta(i) + \delta\gamma(i) && i = 50 \\
a_{ii-1} &= \alpha(i) && 2 \le i \le 49 \\
a_{ii-1} &= \alpha(i) + \gamma(i) && i = 50 \\
a_{ii+1} &= \gamma(i) && 1 \le i \le 49 \\
a_{ii+1} &= 0 && i = 50 \\
a_{ii-1} &= 0 && i = 1 \\
a_{ij} &= 0 \qquad j > i+1, \; j < i-1 && : \; 1 \le i \le 50
\end{aligned} \tag{A.29}$$

Since each row and column of A has a maximum of three elements, and these are centered on the main diagonal of the matrix, it is known as a tri-diagonal matrix. A particularly efficient method of solving systems of simultaneous equations of this type has been given by Dingle and Young (1965), based on prior work by Richtmyer (1957) and Henrici (1962). First, it is necessary to define two auxiliary matrices. L and U, and the vector $\bar{Y}$ such that the following relationships will be applicable:

$$L U = A$$

$$L\bar{Y} = \bar{F}$$
$$U\bar{T} = \bar{Y} \qquad \text{(A. 30)}$$

Then it follows that:

$$\bar{T} = U^{-1}\bar{Y}$$
$$= U^{-1}L^{-1}\bar{F} \qquad \text{(A. 31)}$$
$$= A^{-1}\bar{F}$$

Since:

$$U^{-1}L^{-1} = (LU)^{-1} \qquad \text{(A. 32)}$$

The above will be accomplished if L and U have the forms:

$$L = \begin{pmatrix} 1 & 0 & 0 & 0 & \cdots & & \\ \ell_{21} & 1 & 0 & 0 & \cdots & & \\ 0 & \ell_{32} & 1 & 0 & \cdots & & \\ 0 & 0 & \ell_{43} & 1 & & & \\ \vdots & & & & & & \\ \cdots & & & & & & \\ & & & & & \vdots & \\ & & & & & \vdots & \\ & & & & \cdots\ 0 & \ell_{4948}\ 1 & 0 \\ & & & & \cdots\ 0 & 0\ \ell_{5049} & 1 \end{pmatrix}$$

(A. 33)

$$U = \begin{bmatrix} u_{11} & u_{12} & 0 & 0 & 0 & \cdot & \cdot & & & & \\ 0 & u_{22} & u_{23} & 0 & 0 & \cdot & \cdot & & & & \\ 0 & 0 & u_{33} & u_{34} & 0 & \cdot & \cdot & & & & \\ \cdot & \cdot & & & & & & & & & \\ \cdot & \cdot & & & & & & & & & \\ & & & & & & & & \cdot & \cdot & \\ & & & & & & & & 0 & 0 & \\ & & & & & \cdot & 0 & u_{4848} & u_{4849} & 0 & \\ & & & & & \cdot & 0 & 0 & u_{4949} & u_{4950} & \\ & & & & & \cdot & 0 & 0 & 0 & u_{5050} & \end{bmatrix}$$

Then since LU = A the following are true:

$$a_{11} = u_{11}$$

$$\left.\begin{aligned} a_{ii-1} &= l_{ii-1}\, u_{i-1\,i-1} \\ a_{ii} &= l_{ii-1}\, u_{ii-1} + u_{ii} \end{aligned}\right\} \quad 2 \le i \le 50 \qquad \text{(A. 34)}$$

$$a_{ii+1} = u_{ii+1} \qquad 1 \le i \le 49$$

This leads to the following expressions for the elements of L and U:

$$u_{11} = a_{11}$$

$$\left.\begin{aligned} l_{ii-1} &= a_{ii-1} / u_{i-1} u_{i-1} \\ u_{ii} &= a_{ii} - l_{ii-1}\, u_{i-1i} \\ &= a_{ii} - l_{ii-1}\, a_{i-1i} \end{aligned}\right\} \quad 2 \le i \le 50$$

$$u_{ii+1} = a_{ii+1} \qquad 1 \le i \le 49 \tag{A. 35}$$

The other two relations of Equations (A. 30) give us:

$$\begin{aligned} y_1 &= f_1 \\ y_i &= f_i - l_{ii-1}\, y_{i-1} \qquad 2 \le i \le 50 \\ u_{ii}\, t_i &= y_i \qquad i = 50 \\ u_{ii}\, t_i + u_{ii+1}\, t_{i+1} &= y_i \qquad 1 \le i \le 49 \end{aligned} \tag{A. 36}$$

These can be solved for the unknown t's as:

$$\begin{aligned} t_i &= y_i / u_{ii} \qquad i = 50 \\ t_i &= \frac{y_i - u_{ii+1}\, t_{i+1}}{u_{ii}} \qquad 1 \le i \le 49 \end{aligned} \tag{A. 37}$$

This series of algebraic expressions accomplishes the goal of evaluating the elements of $\bar{T}$ in terms of $\bar{F}$.

A.4 PARAMETER EVALUATION AND APPROXIMATIONS

In the above formulation several coefficients and parameters were defined but not evaluated; they are given here. Let us assume the following:

$$\frac{\partial C_p}{\partial T} = 0 \qquad \frac{\partial K_T}{\partial T} = 0$$

$$\frac{\partial g}{\partial T} = 0 \qquad \frac{\partial}{\partial T}\left(\frac{\partial K_T}{\partial z_p}\right) = 0 \tag{A.38}$$

Strictly speaking none of the above is correct. The specific heat, C_p is of 0(2) in the temperature, but the value of the derivative is certainly negligible. The quantities g, K_T and $\partial K_T / \partial z_p$ are all altitude dependent, and the altitude in our constant pressure level system is directly temperature dependent. However the basic energy equation we have used assumes that the height levels are either constant or slowly varying with time. Consistent with that premise we assume Equation (A.38) is approximately true.

In addition, note the following relations which follow from the assumptions of the perfect gas law and the definitions of H and K_T:

$$\frac{\partial}{\partial T}\left(\frac{1}{\rho}\right) = \frac{1}{\rho T} \tag{A.39}$$

$$\frac{\partial}{\partial T}\left(\frac{1}{\rho H}\right) = 0 \tag{A.40}$$

$$\frac{\partial}{\partial T}\left(\frac{1}{\rho H^2}\right) = -\frac{1}{\rho H^2 T} \tag{A.41}$$

$$\frac{\partial}{\partial T}\left(\frac{1}{H}\right) = -\frac{1}{HT} \tag{A.42}$$

$$\frac{\partial}{\partial T}\tilde{K}_T = \frac{\partial}{\partial T}(\rho C_p K_T) = -\frac{\tilde{K}_T}{T} \tag{A.43}$$

$$\frac{\partial}{\partial T}\left(\frac{\partial \tilde{K}_T}{\partial z_p}\right) = C_p \frac{\partial \tilde{K}_T}{\partial z_p}\frac{\partial \rho}{\partial T} = -\frac{1}{T}\frac{\partial \tilde{K}_T}{\partial z_p} \tag{A.44}$$

A.4.1 Parameter Evaluation

The following are the parameters which must be evaluated (A, B, C, and D are derived in Chapter 2):

1. $$\left.\frac{\partial A}{\partial T}\right)_n = \frac{\partial}{\partial T}\left\{\frac{1}{\rho C_p}\left(Q_{TOTAL} - \frac{q}{C_p H}\frac{\partial \tilde{K}_T}{\partial z_p}\right)\right\}_n$$

$$= \frac{1}{\rho C_p T}\left\{Q_{TOTAL} - \frac{q}{C_p H}\frac{\partial \tilde{K}_T}{\partial z_p}\right\} \tag{A.45}$$

$$+\frac{1}{\rho C_p}\left\{\frac{\partial Q_{TOTAL}}{\partial T} + \frac{q}{C_p H T}\frac{\partial \tilde{K}_T}{\partial z_p} + \frac{q}{C_p H T}\frac{\partial \tilde{K}_T}{\partial z_p}\right\}$$

$$\left.\frac{\partial A}{\partial T}\right)_n = \frac{1}{\rho C_p}\left\{\frac{Q_{TOTAL}}{T} + \frac{\partial Q_{TOTAL}}{\partial T} + \frac{q}{C_p H T}\frac{\partial \tilde{K}_T}{\partial z_p}\right\}$$

where:

$$\frac{\partial Q_{TOTAL}}{\partial T} \approx \frac{\partial Q_{ISM}}{\partial T}$$

2. $$\left.\frac{\partial B}{\partial T}\right)_n = \frac{\partial}{\partial T}\left\{\frac{1}{\rho C_p H^2}\frac{\partial \tilde{K}_T}{\partial z_p}\right\}_n$$

$$= -\frac{1}{\rho C_p H^2 T}\frac{\partial \tilde{K}_T}{\partial z_p} - \frac{1}{\rho C_p H^2 T}\frac{\partial \tilde{K}_T}{\partial z_p} \qquad \text{(A.46)}$$

$$\left.\frac{\partial B}{\partial T}\right)_n = -\left.\frac{2B}{T}\right)_n$$

3. $$\left.\frac{\partial C}{\partial T}\right)_n = \frac{\partial}{\partial T}\left\{\frac{1}{\rho C_p H^2}\left(\frac{\partial \lambda}{\partial T} - \frac{(\lambda+\tilde{K}_T)}{T}\right)\right\}_n$$

$$= \frac{1}{\rho C_p H^2}\left\{\frac{\partial^2 \lambda}{\partial T^2} - \frac{1}{T}\left(\frac{\partial \lambda}{\partial T} + \frac{\partial \tilde{K}_T}{\partial z_p}\right)\right.$$

$$\left. + \frac{(\lambda+\tilde{K}_T)}{T^2}\right\} - \frac{1}{\rho C_p H^2 T}\left\{\frac{\partial \lambda}{\partial T} - \frac{(\lambda+\tilde{K}_T)}{T}\right\}$$

$$\left.\frac{\partial C}{\partial T}\right)_n = -\left.\frac{C}{T}\right)_n + \frac{1}{\rho C_p H^2}\left\{\frac{\partial^2 \lambda}{\partial T^2}\right. \qquad \text{(A.47)}$$

$$\left. - \frac{1}{T}\left(\frac{\partial \lambda}{\partial T} - \frac{\tilde{K}_T}{T}\right) + \frac{(\lambda+\tilde{K}_T)}{T^2}\right\}$$

$$4.\quad \left(\frac{\partial D}{\partial T}\right)_n = \frac{\partial}{\partial T}\left\{\frac{1}{\rho C_p H^2}\,(\lambda+\tilde{K}_T)\right\}_n$$

$$= -\frac{1}{\rho C_p H^2 T}\,(\lambda+\tilde{K}_T)$$

$$+\frac{1}{\rho C_p H^2}\left\{\frac{\partial\lambda}{\partial T}+\frac{\partial\tilde{K}_T}{\partial T}\right\} \qquad \text{(A.48)}$$

$$\left(\frac{\partial D}{\partial T}\right)_n = -\left(\frac{D}{T}\right)_n + \frac{1}{\rho C_p H^2}\left\{\frac{\partial\lambda}{\partial T}-\frac{\tilde{K}_T}{T}\right\}$$

$$5.\quad \left(\frac{\partial\psi}{\partial T}\right)_n = \frac{\partial}{\partial T}\left\{\frac{H(\mathcal{F}_{\text{upper boundary}}+\tilde{K}_T\, g/c_p)}{(\lambda+\tilde{K}_T}\right\}$$

$$= \left(\frac{\mathcal{F}_{\text{upper boundary}}+\tilde{K}_T\, g/c_p}{(\lambda+\tilde{K}_T)}\right)\left\{\frac{H}{T}-\frac{H}{(\lambda+\tilde{K}_T)}\right.\times$$

$$\left.\left[\frac{\partial\lambda}{\partial T}+\frac{\partial\tilde{K}_T}{\partial T}\right]\right\}+\frac{H}{(\lambda+\tilde{K}_T)}\frac{g}{c_p}\frac{\partial\tilde{K}_T}{\partial T} \qquad \text{(A.49)}$$

$$\left(\frac{\partial\psi}{\partial T}\right)_n = \psi_n\left\{\frac{1}{T}-\frac{1}{(\lambda+\tilde{K}_T)}\left[\frac{\partial\lambda}{\partial T}-\frac{\tilde{K}_T}{T}\right]\right\}-\frac{g\,H\,\tilde{K}_T}{c_p T(\lambda+\tilde{K}_T)}$$

A.4.2 General Approximations

A special procedure is necessary for expressing finite difference approximations to derivatives at boundaries. In general, the

following is assumed:

$$\frac{\partial}{\partial \rho}\theta^i \simeq \frac{\theta^{i+1} - \theta^{i-1}}{2\Delta\rho} \tag{A.50}$$

where θ, ρ are arbitrary variables. If however, either the i+1 or i-1 point lies outside the boundary, the above cannot in general be used. Instead, if i is the upper boundary:

$$\frac{\partial\theta^i}{\partial\rho} \simeq \frac{\partial\theta^{i-1}}{\partial\rho} - \Delta\rho\,\frac{\partial^2\theta^{i-1}}{\partial\rho^2}$$

$$\simeq \frac{\theta^i - \theta^{i-2}}{2\Delta\rho} - \Delta\rho\,\frac{\theta^i - 2\theta^{i-1} + \theta^{i-2}}{\Delta\rho^2} \tag{A.51}$$

$$\frac{\partial\theta^i}{\partial\rho} \simeq \frac{3\theta^i + \theta^{i-2} - 4\theta^{i-1}}{\Delta\rho}$$

or, if i is the lower boundary:

$$\frac{\partial\theta^i}{\partial\rho} \simeq \frac{\partial\theta^{i+1}}{\partial\rho} - \Delta\rho\,\frac{\partial^2\theta^{i+1}}{\partial\rho^2}$$

$$\simeq \frac{\theta^{i+1} - \theta^i}{2\Delta\rho} - \Delta\rho\,\frac{\theta^{i+2} - 2\theta^{i+1} + \theta^i}{\Delta\rho^2} \tag{A.52}$$

$$\frac{\partial\theta^i}{\partial\rho} \simeq \frac{4\theta^{i+1} - 3\theta^i - \theta^{i+2}}{\Delta\rho}$$

The evaluation of g, the gravity, in pressure coordinates is necessary since the atmospheric scale height must be determined before the altitude levels can be calculated; therefore assume:

$$g(z) = g_o \left(\frac{R_E}{R_E+z}\right)^2 \tag{A.53}$$

where $g_o = g(z=o)$ and R_E is the earth's radius, and:

$$g(z_j) \simeq g(z_{j-1}) + \frac{\partial g}{\partial z}\Big)_{j-1} (z_j - z_{j-1}) \tag{A.54}$$

then in pressure coordinates, z_{pj}:

$$g(z_{p_j}) = g(z_{p_{j-1}}) + \frac{\partial g}{\partial z_p}\Big)_{j-1} (z_{p_j} - z_{p_{j-1}}) \tag{A.55}$$

If (z_j, z_{pj}) and $(z_{j-1}\ a_{pj-1})$ refer to the same levels respectively, then:

$$(z_j - z_{j-1}) \frac{\partial}{\partial z}\Big)_{j-1} = (z_{p_j} - z_{p_{j-1}}) \frac{\partial}{\partial z_p}\Big)_{j-1} \tag{A.56}$$

$$\frac{\partial g}{\partial z_p}\Big)_{j-1} = \frac{\Delta z}{\Delta z_p}\Big)_{j-1} \frac{\partial g}{\partial z}\Big)_{j-1} = -H_{j-1} \frac{\partial g}{\partial z}\Big)_{j-1}$$

$$= H_{j-1} \left(\frac{2g}{R_E+z}\right)_{j-1} \simeq H_{j-1} \left(\frac{2g}{R_E}\right)_{j-1} \tag{A.57}$$

but:

$$H_{j-1} = \left(\frac{RT}{\bar{M} g}\right)_{j-1} \tag{A.58}$$

where R is the gas constant. Therefore:

$$\left(\frac{\partial g}{\partial z_p}\right)_{j-1} = \left(\frac{2RT}{\bar{M} R_E}\right)_{j-1} \tag{A.59}$$

and:

$$g(z_{p_j}) = g(z_{p_{j-1}}) + \left(\frac{2RT}{\bar{M} R_E}\right)_{j-1} (z_{p_j} - z_{p_{j-1}}) \tag{A.60}$$

so that only $T=T(z_p)$, $\bar{M}=\bar{M}(z_p)$ and $g(z_{p1})$ need initially be known.

Finally, it was necessary to approximate the potential energy term for the constant pressure levels. This term may be written as:

$$\rho \frac{\partial}{\partial T}(gz)_{z_p} = \rho \frac{\partial}{\partial z}(gz)_{z_p} \frac{\partial z}{\partial T}\Big)_{z_p} \frac{\partial T}{\partial t}\Big)_{z_p} \tag{A.61}$$

The first term is just:

$$\frac{\partial}{\partial z}(gz)_{z_p} = \frac{\partial}{\partial z}\left\{ \frac{g_0 R_E^2 z}{(R_E+z)^2} \right\}_{z_p} \tag{A.62}$$

$$= g(z_p)\left[\frac{R_E - z}{R_E + z}\right]$$

and the height $z(z_p)$ is given by:

$$z(z_p) = z(z_p^\circ) - \int_{z_p^\circ}^{z_p} H(z_p')\, dz_p'$$

$$\simeq z(z_p^\circ) - \sum_j^{\uparrow} \left\{ \left(\frac{RT}{\bar{M} g}\right)_{z_{p_{j+1}}'} + \left(\frac{RT}{\bar{M} g}\right)_{z_{p_j}'} \right\} \frac{z_{p_{j+1}}' - z_{p_j}'}{2} \tag{A.63}$$

and thus:

$$\left.\frac{\partial z}{\partial T}\right)_{z_p} = \left.\overline{\frac{\partial z}{\partial T}}\right)_{z_{p_j'}}$$

$$\simeq -\left.\frac{R}{\bar{M} g}\right)_{z_{p_j'}} \cdot (z_{p_{j+1}'} - z_{p_j'}) \qquad \text{(A. 64)}$$

The potential energy term can now be written in terms of all of the above as:

$$\rho \frac{\partial}{\partial T}(gz)_{z_p} \simeq -\rho g \frac{(R_E - z)}{(R_E + z)} \frac{R}{\bar{M} g} \Delta z_p \left.\frac{\partial T}{\partial t}\right)_{z_p} \qquad \text{(A. 65)}$$

or:

$$\rho \frac{\partial}{\partial T}(gz)_{z_p} = -\rho \frac{R (R_E - z)}{\bar{M} (R_E + z)} \left.\frac{\partial T}{\partial t}\right)_{z_p} \Delta z_p$$

This term, because of its $\partial T/\partial t$ dependence, was most easily incorporated into a modified specific heat term, C_p^*, as follows:

$$\rho C_p \frac{\partial T}{\partial t} = Q_{TOTAL} - \frac{\partial}{\partial z} \Phi_{TOTAL} + \rho \frac{R (R_E - z)}{\bar{M} (R_E + z)} \Delta z_p \frac{\partial T}{\partial t}$$

$$\rho C_p^* \frac{\partial T}{\partial t} = Q_{TOTAL} - \frac{\partial}{\partial z} \Phi_{TOTAL} \qquad \text{(A. 66)}$$

$$C_p^* = C_p - \frac{R (R_E - z)}{\bar{M} (R_E + z)} \Delta z_p$$

APPENDIX B

MODEL ATMOSPHERE

A very convenient and natural choice for use in the upper thermosphere is an analytic model built around an exponential temperature profile. Such a temperature profile was defined by Jacchia (1964) for a static diffusion model through the expressions:

$$T(z) = T_\infty - (T_\infty - T_{120}) \exp\left[-\lambda (z-120)\right] \tag{B.1}$$

$$\lambda = 0.029 \exp\left\{-\frac{1}{2}\left[\frac{(T_\infty - 800)}{750 + 1.7\times10^{-4}(T_\infty - 800)^2}\right]^2\right\} \tag{B.2}$$

where T_∞ and T_{120} are the temperatures assumed in the exosphere and at 120 Km, the lower limit of applicability of the expression, respectively. Walker (1965) developed analytic expressions for the temperature and concentrations based on the above and on the work of Bates (1959) and Stein and Walker (1965) by incorporating the geopotential height. If z is the geometrical height and R_E is the radius of the earth (R_E = 6356.77 Km), then ζ is the geopotential height[1] given by:

$$\zeta = \frac{(z-120)(R_E + 120)}{(R_E + z)} \tag{B.3}$$

The temperature becomes:

$$T(z) = T_\infty \left[1 - \alpha \exp(-\sigma \zeta)\right] \tag{B.4}$$

where $\sigma = \lambda + 0.00015$ and $\alpha = (T_\infty - T_{120})/T_\infty$.

[1] This expression for geopotential height uses a reference level at z=120 Km rather than the standard levels of z=0, or where g≡ 980 cm/sec^2.

Walker gives as the concentration of the i^{th} constituent at altitude z, $n_i(z)$, the following expression:

$$n_i(z) = n_i(120) \left\{ \frac{1-\alpha}{1-\alpha \exp(-\sigma \beta)} \right\}^{1+\gamma_i'} \exp(-\sigma \gamma_i' \beta) \qquad (B.5)$$

where:

$$\gamma_i' = \frac{m_i g(120)}{\sigma k T_\infty} \qquad (B.6)$$

and m_i is the mass of the i^{th} constituent, g(120) is the gravity at 120 Km and k is Boltzmann's constant (1.38053×10^{-16} erg/^oK). The concentrations at 120 Km, $n_i(120)$, must be specified in the model, along with T_∞, T_{120}, and g(120).

In the above, the thermal diffusion factor was omitted since in the present study only N_2, O_2 and O were calculated from the above. The pressure, p, mean molecular weight, $\bar{M}$, density, ρ, and atmospheric scale height, H, were calculated from the concentrations and temperature in the usual manner. An exospheric temperature of 1000^oK was used for all the thermal models considered in this study.

Below 120 Km a different procedure was adopted. The temperature and concentrations, N_2, O_2, and O were specified at selected levels and an empirical expression for the O_3 concentrations was incorporated as discussed below (see also Chapter 3). Intermediate values were obtained by linear interpolation of the temperature and logarithmic interpolation of the N_2, O_2, and O concentrations. From the concentrations, volume mixing ratios and the mean molecular weights were then calculated. The atmospheric scale heights were calculated

in the usual way and with them the pressures and densities were obtained by integration upward from the reference level: p (50 Km) = 797.8 dynes/cm^2; or, when the model was extended below 50 Km, $p(0) = 1.013 \times 10^6$ dynes/cm^2. The total number density at each height was derived from the calculated pressure, through the perfect gas law. From the calculated total number density and volume mixing ratios the composition was adjusted slightly for internal consistency.

The temperature profile used in the model was the earth average temperature shown in Figure 10 for the region 50 Km to 120 Km, with the U. S. Standard Atmosphere, 1962, used below 50 Km. In Table II are presented the input concentrations and their sources for the atmospheric model below 120 Km. The sources are as follows:

(a) Colgrove, Johnson, and Hanson (1966), Table 2, photochemical and transport model with $K_T = 2.3 \times 10^6$ cm^2/sec for "average temperatures"

(b) Hunt (1966), "wet" photochemical model with no transport; equilibrium case

(c) U. S. Standard Atmosphere, 1962; based on tabulated total number densities and constant volume mixing ratios for N_2 and O_2 of 0.78084 and 0.20948, respectively (Glueckauf, 1951).

The ozone distribution adopted was a composite of two empirical profiles. Above 40 Km Evans, et al (1968) used the following expression to fit the (corrected) data of Johnson, et al (1952):

$$[O_3] = 8 \times 10^{10} \exp\left\{-\frac{(z-50)}{4.53}\right\} \text{ cm}^{-3} \qquad \text{(B. 7)}$$

TABLE II

Adopted Concentrations of N_2, O_2, and O Below 120 Km

z (Km)	N_2 (cm^{-3})	Ref.	O_2 (cm^{-3})	Ref.	O (cm^{-3})	Ref.
120	3.85(11)[1]	(a)	5.24(10)	(a)	1.05(11)	(a)
115	7.77(11)	"	1.23(11)	"	1.56(11)	"
110	1.62(12)	"	3.01(11)	"	2.21(11)	"
105	3.53(12)	"	7.56(11)	"	2.89(11)	"
100	8.10(12)	"	1.93(12)	"	3.37(11)	"
95	1.97(13)	"	4.98(12)	"	3.47(11)	"
90	5.18(13)	"	1.35(13)	"	3.03(11)	"
85	1.30(14)	"	3.45(13)	"	1.61(11)	(a)
80	3.28(14)	(a)	8.74(13)	(a)	6.20(10)	(b)
75	7.04(14)	(c)	1.89(14)	(c)	2.40(10)	"
70	1.42(15)	"	3.81(14)	"	1.40(10)	"
65	2.71(15)	"	7.26(14)	"	9.80(9)	"
60	4.97(15)	"	1.33(15)	"	8.00(9)	"
55	9.10(15)	"	2.44(15)	"	6.60(9)	"
50	1.67(16)	"	4.47(15)	"	5.70(9)	"
45	3.05(16)	"	8.19(15)	"	5.00(9)	"
40	6.25(16)	"	1.68(16)	"	4.00(9)	"
35	1.37(17)	"	3.69(16)	"	1.30(9)	"
30	2.99(17)	"	8.02(16)	"	1.20(8)	"
25	6.51(17)	"	1.75(17)	"	1.30(7)	"
20	1.44(18)	"	3.87(17)	"	1.10(6)	"
15	3.16(18)	"	8.48(17)	"	1.00(5)	"
10	6.71(18)	"	1.80(18)	"	7.60(3)	"
5	1.20(19)	"	3.21(18)	"	5.90(2)	"
0	1.99(19)	"	5.34(18)	"	5.10(1)	"

[1] 3.85(11) denotes 3.85×10^{11}

As explained in Chapter 3, this profile was considered to be a reasonable representation of measurements and theoretical estimates of O_3 concentrations above 40 Km, see Figure 14. Below 40 Km an analytic expression given by Green (1966):

$$[O_3] = \frac{4[O_3]_{max} \exp\left(\frac{z-z_m}{h}\right)}{\left[1+\exp\left(\frac{z-z_m}{h}\right)\right]^2} \text{ cm}^{-3} \qquad \text{(B.8)}$$

was adopted with $[O_3]_{max}=4.14\text{x}10^{12}$ cm^{-3}, $z_m=22$ Km, and h=6 Km. This is probably reasonable at least for the stratosphere.

The model atmosphere was extended from 50 Km down to the surface chiefly for the purpose of calculating column densities at zenith angles greater than 90^o for use in the solar heating rate calculations of Chapter 4, (see also Appendix C.). Thus for the long slant paths involved, where there is little contribution to the solar heating rates, the thermal models are rather insensitive to the uncertainty in the lower atmospheric composition. The other use of the lower atmospheric model was in the CO_2 and CO distribution study (see Appendix D.) In those calculations the results are relatively insensitive to the details of the composition below about 50 Km.

APPENDIX C

COLUMN DENSITY CALCULATIONS

In general the calculation of the column density of the i^{th} constituent, at altitude z, for zenith angle θ, $N_i(z, \theta)$ was made through an appropriate numerical integration technique. The integration was approximated in a usual manner from z to an arbitrary z_{max} chosen high enough so that the remainder of the actual atmospheric path would make no significant contribution to $N_i(z, \theta)$. Further, at $z=z_{max}$ (typically chosen as 500 Km) the actual remaining contribution to the column density was approximated by:

$$N_i(z_{max}, \theta) \simeq n_i(z_{max})\, H_i(z_{max}) \left(\frac{\partial s}{\partial z}\right)_{z_{max}} \qquad (C.1)$$

and added to $N_i(z, \theta)$; where $n_i(z_{max})$ and $H_i(z_{max})$ are the concentration and specific scale heights of the i^{th} constituent at z_{max} and $\partial s/\partial z)\, z_{max}$ is a crude estimate of the ratio of the remaining atmospheric path at zenith angle θ to that for $\theta=0^{o}$ (discussed further below).

For the earth average solar heating rate calculations of Chapter 3 only vertical column densities were required. For this case $\partial s/\partial z=1$ and the atmospheric path, $z_{max}-z$, was broken up into intervals $\Delta s=\Delta z$ of 5 Km above 120 Km and 1 Km below 120 Km. Above 150 Km, the distributions of the species considered were assumed to approach diffusive equilibrium. Thus the following approximations were made:

$$N_i(z,0) = \sum_j \int_{z_j}^{z_{j+1}} n_i(z)\, dz$$

$$n_i(z) = n_i(z_j) \exp\left\{ \frac{\ln\left[n_i(z_{j+1}) / n_i(z_j)\right]}{(z_{j+1} - z_j)} (z - z_j) \right\} \qquad (C.2)$$

the latter being restricted to $z_j \leq z \leq z_{j+1}$. The result of the indicated integration is just:

$$N_i(z,0) = \sum_j \frac{(z_{j+1}-z_j)\left[n_i(z_{j+1}) - n_i(z_j)\right]}{\ln\left[n_i(z_{j+1}) / n_i(z_j)\right]} \qquad (C.4)$$

The approximations used above served to divide the entire integration interval into a finite number of small intervals $\Delta z = z_{j+1} - z_j$, inside each of which the concentration of the i^{th} constituent was approximated by an exponential function of constant scale length (or e-folding distance) and forced to match the model concentrations at the interval boundaries; Equation (C. 3).

Below 150 Km a more general numerical integration scheme was needed (to handle the O peak at about 95 Km for example) and a standard Simpson's rule scheme was adopted. Thus the column densities below 150 Km were approximated by:

$$N_i(z,0) \simeq N_i(150,0) + \sum_j \left\{ n_i(z_j) + 4\, n_i(z_{j+\frac{1}{2}}) + n_i(z_{j+1}) \right\} \frac{z_{j+1}-z_j}{6} \qquad (C.5)$$

where the summation over j covered the altitude range $z \leq z_j \leq 150$ Km.

For the studies of Chapter 4, column densities were calculated for 32 selected zenith angles (0^o-103^o). For the general case of a non-zero zenith angle the geometry of Figure C-1 is appropriate with $s = s(z, \theta)$ is the independent variable. Therefore the column density at z of the i^{th} constituent was just:

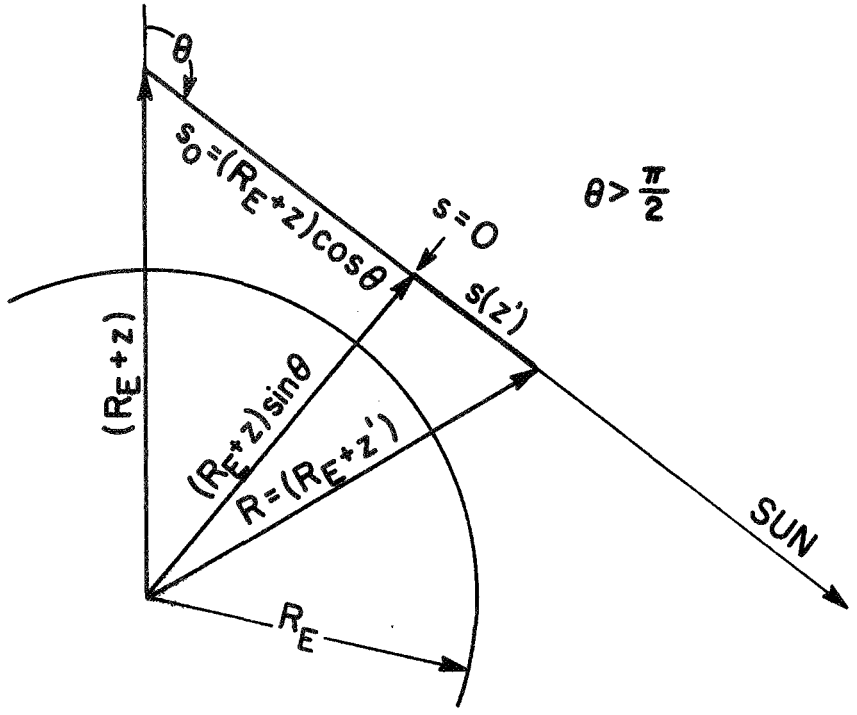

(a)

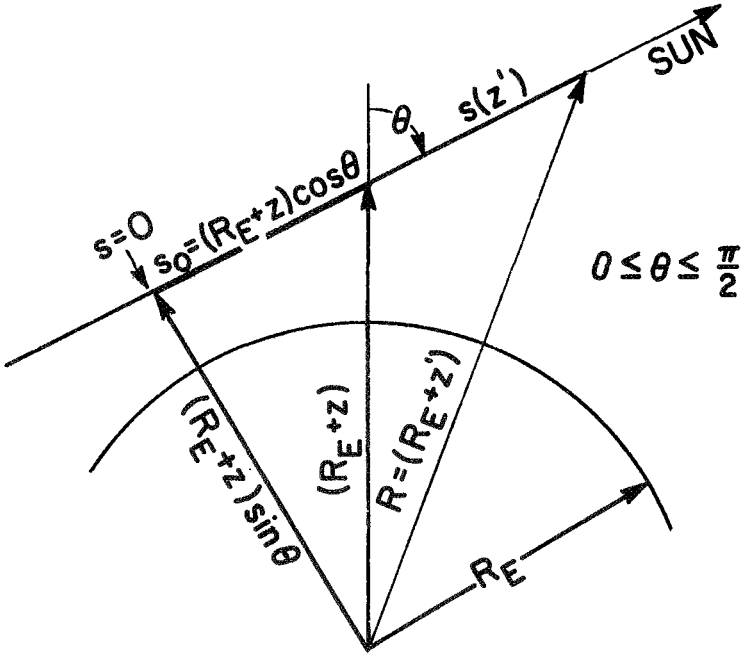

(b)

Figure C-1. Integration path geometry for column density calculations

$$N_i(z,\theta) = \int_{S_0(z,\theta)}^{\infty} n_i(s')\, ds' \qquad \text{(C.6)}$$

Assuming a spherically symmetrical atmosphere and considering the geometry of Figure C-1, it was apparent that the following relations held:

$$z' = R - R_E \qquad \text{(C.7)}$$

$$R^2 = S(z',\theta)^2 + (R_E+z)^2 \sin^2\theta \qquad \text{(C.8)}$$

$$z' = \sqrt{S(z',\theta)^2 + (R_E+z)^2 \sin^2\theta} - R_E \qquad \text{(C.9)}$$

and:

$$n_i(s') = n_i(z') \qquad \text{(C.10)}$$

$$= n_i\left[\sqrt{S(z',\theta)^2 + (R_E+z)^2 \sin^2\theta} - R_E\right]$$

For these cases Simpson's rule was used throughout the altitude range of interest and the column densities were approximated by the following:

$$N_i(z,\theta) \simeq \sum_j \left\{ n_i(z_j) + 4\, n_i(z_{j+\frac{1}{2}}) + n_i(z_{j+1}) \right\} \frac{\Delta s_j}{6} \qquad \text{(C.11)}$$

where $\Delta s_j = s_{j+1} - s_j$ and s_j and z_j' were given by:

$$S_j = S_o(z, \theta) + \sum_j \Delta S_j \qquad \text{(C.12)}$$

$$S_o(z, \theta) = (R_E + z) \cos\theta \qquad \text{(C.13)}$$

$$z_j' = \sqrt{S_j^2 + (R_E + z)^2 \sin^2\theta} - R_E \qquad \text{(C.14)}$$

Thus the integration was started from s_o with intervals of size Δs_j and the necessary concentrations being evaluated at z_j' heights, which are direct functions of the S_j's. The distinction in integrating over ds rather than dz must be maintained, since:

$$\frac{\partial s'}{\partial z'} = - \frac{(R_E + z) \sin^2\theta}{s'} \qquad \text{(C.15)}$$

based on Equation (C.8), and it is obvious that the above blows up at the tangent point, $s' = 0$, which lies in the integration path for $\theta \geq 90^o$. Consequently integration over dz would greatly underestimate the contributions to the column densities near the tangent point.

Note also that the atmospheric path will intersect the earth for $(R_E + z) \sin\theta \leq R_E$ and $\theta > \pi/2$. In these cases the column densities were assumed infinite.

APPENDIX D

CALCULATION OF THE SOLAR HEATING RATE

The general character of the solar heating rate calculation was described in Chapter 2 based upon Equation (2.4.1). It would be impractical to actually carry out the integration over wavelength in that equation even if the detailed spectral features of the solar energy flux and absorption cross sections were known much more precisely then they are at present. Instead the usual procedure of approximating the integration over finite wavelength intervals and summing the results was adopted. The wavelength range from 31 Å to 3000 Å was divided into 152 intervals of width varying between 0-50 Å.

Thus Equation (2.4.1) was replaced by:

$$Q_{SOLAR}(z,\theta) = \sum_{\ell} \left\{ E^{\ell} F_{\infty}^{\ell} \sum_{i} \left(\epsilon_i^{\ell}(z) \sigma_i^{\ell} \eta_i(z) \right) \exp\left[-\sum_{i} \sigma_i^{\ell} N_i(z,\theta) \right] \right\} \tag{D.1}$$

where the ℓ^{th} wavelength interval extends from $\lambda_1(\ell)$ to $\lambda_2(\ell)$, $\epsilon_i^{\ell}(z)$ and σ_i^{ℓ} are the effective heating efficiency and cross section, respectively, for the i^{th} constituent (discussed below), E^{ℓ} is the effective photon energy (in ergs) given by:

$$E^{\ell} = \frac{1}{\lambda_2(\ell) - \lambda_1(\ell)} \int_{\lambda_1(\ell)}^{\lambda_2(\ell)} \frac{hc\, d\lambda}{\lambda} \times 10^8 \frac{\text{Å}}{\text{cm}}$$

$$E^{\ell} = \frac{hc}{\lambda_2(\ell) - \lambda_1(\ell)} \ln\left[\frac{\lambda_2(\ell)}{\lambda_1(\ell)}\right] \times 10^8 \frac{\text{Å}}{\text{cm}} \qquad \text{(D. 2)}$$

which collapses to:

$$E^{\ell} = E^{\lambda}$$
$$E^{\ell} = \frac{hc}{\lambda} \times 10^8 \frac{\text{Å}}{\text{cm}} \qquad \text{(D. 3)}$$

for $\lambda_2(\ell) = \lambda_1(\ell)$, (single solar lines), where h is Planck's constant (6.6255×10^{-27} erg sec) and c is the speed of light in a vacuum (2.998×10^{10} cm/sec), and Φ_{∞}^{ℓ} is the solar photon flux at the "top" of the atmosphere integrated over the ℓ^{th} wavelength interval.

The first 91 intervals, covering 31 Å - 1775 Å, were taken as a compromise between those given by Hinteregger, et al (1965), and Hinteregger (1969) in order to use flux and cross section data from both of these sources. The advantage to using this data was that the absorption cross sections given in Hinteregger, et al (1965) are already effective cross sections obtained as (Hinteregger, 1962):

$$\sigma_i^{\ell}(z) = \frac{\int_{\lambda_1(\ell)}^{\lambda_2(\ell)} \sigma_i^{\lambda} \Phi^{\lambda}(z)\, d\lambda}{\int_{\lambda_1(\ell)}^{\lambda_2(\ell)} \Phi^{\lambda}(z)\, d\lambda} \qquad \text{(D. 4)}$$

where $\sigma_i^{\ell}(z)$ is the effective absorption cross section in the ℓ^{th} wavelength interval. The z dependence in this quantity comes from the detailed correlation of the spectral characteristics of σ_i^{λ} with those of the flux. In Hinteregger, et al (1965) the z dependence of the effective cross sections was denoted by a range of values corresponding to the extrema for actual atmospheric conditions, but was limited to 15 intervals from 796 Å to 1027 Å. Mean values for the indicated ranges were adopted on the basis that sample calculations of solar heating rates made from them and from both extremes of the ranges gave negligible differences.

In addition 61 other wavelength intervals were adopted, 1775Å - 1800 Å, and 20 Å steps from 1800 Å to 3000 Å. For these intervals the effective absorption cross sections were approximated by the following:

$$\sigma_i^{\ell} = \frac{1}{\lambda_2(\ell) - \lambda_1(\ell)} \int_{\lambda_1(\ell)}^{\lambda_2(\ell)} \sigma_i^{\lambda} \, d\lambda \qquad (D.5)$$

with the exception of the Schumann-Runge bands of O_2 (1775 Å - 2000 Å). For this rather complex absorption spectrum the concept of an effective cross section is not as valid as in the Hartley continuum of O_3 or the Herzberg continuum of O_2. However, approximate values were adopted for the Schumann-Runge bands from estimates of band maxima and band minima (Blake, et al, 1966) and adjusted to give good agreement in terms of calculated O_2 photodissociation rates with those of Hudson, et al (1969) for which a far more accurate spectral treatment was used.

The following are presented in Table III: the wavelength interval number, ℓ; the limits of the ℓ^{th} interval in $\mathring{A}$, λ_1 and λ_2; the effective-photon energy in ergs, E^{ℓ}; the integrated solar photon flux above the atmosphere in photons/cm^2/sec, Φ_{∞}^{ℓ}; and the effective absorption cross sections, σ_i^{ℓ}. The sources of the flux and cross section data are presented at the end of Table III.

In Chapter 4 diurnal average solar heating rates were calculated for specific latitudes and seasons. This was accomplished by integrating the time dependent heating rate between meridional passage (local noon) and local sunset, and dividing by 12 hours, i.e.,

$$\overline{Q_{SOLAR}(z)} = \frac{1}{12hr.} \int_0^{\Delta t_s} Q_{SOLAR}[z, \theta(t)]\, dt \qquad (D.6)$$

where $\overline{Q_{SOLAR}(z)}$ is the diurnal average, Δt_s is the time between meridional passage and sunset (one half the number of daylight hours), and $\theta(t)$ is the appropriate zenith angle for time t measured from meridional passage. The integration was performed by Simpson's rule with Δt_s divided into 6 parts (giving a minimum resolution of 2 hours for continuous daylight conditions) based on the solar heating rate evaluated at 13 points:

$$\overline{Q_{SOLAR}(z)} = \frac{1}{12} \sum_{n=1}^{n=6} [Q_n + 4Q_{n+\frac{1}{2}} + Q_{n+1}] \frac{\Delta t_s/6}{6} \qquad (D.7)$$

where the time step was $\Delta t_s/6$ and Q_n's are:

$$Q_n = Q_{SOLAR}[z, \theta(t_n)]$$
$$t_n = \frac{n-1}{6} \Delta t_s \qquad (D.8)$$

Table III. Parameters Adopted in Solar Heating Rate Approximation

l	λ_1	λ_2	E^l	F^l_∞	$\sigma^l_{N_2}$	$\sigma^l_{O_2}$	σ^l_O	$\sigma^l_{O_3}$
1	1725.0	1775.0	1.136E-11 *	1.06E 12 (1)	0.0	1.70E-19 (1)	0.0	0.0
2	1675.0	1725.0	1.169E-11	7.00E 11	0.0	8.60E-19	0.0	0.0
3	1625.0	1675.0	1.205E-11	4.20E 11	0.0	2.20E-18	0.0	0.0
4	1575.0	1625.0	1.242E-11	2.60E 11	0.0	5.20E-18	0.0	0.0
5	1525.0	1575.0	1.282E-11	1.33E 11	0.0	8.00E-18	0.0	0.0
6	1475.0	1525.0	1.325E-11	7.30E 10	0.0	1.13E-17	0.0	0.0
7	1425.0	1475.0	1.371E-11	3.70E 10	0.0	1.43E-17	0.0	0.0
8	1375.0	1425.0	1.420E-11	1.83E 10	0.0	1.43E-17	0.0	0.0
9	1325.0	1375.0	1.472E-11	1.77E 10	0.0	5.80E-18 (1)	0.0	0.0
10	1275.0	1325.0	1.529E-11	1.18E 10	0.0	7.00E-19 (3)	0.0	0.0
11	1220.0	1275.0	1.593E-11	2.60E 10	0.0	6.50E-19	0.0	0.0
12	1215.7	1215.7	1.635E-11	2.70E 11	0.0	1.00E-20	0.0	0.0
13	1206.5	1206.5	1.647E-11	4.30E 09	0.0	1.72E-17	0.0	0.0
14	1200.0	1220.0	1.643E-11	7.40E 09	0.0	6.00E-18	0.0	0.0
15	1180.0	1200.0	1.670E-11	5.50E 09	0.0	4.00E-19	0.0	0.0
16	1175.7	1175.7	1.690E-11	2.50E 09	0.0	1.04E-18	0.0	0.0
17	1130.0	1180.0	1.721E-11	5.80E 09	0.0	1.00E-18	0.0	0.0
18	1090.0	1130.0	1.791E-11	4.40E 09	0.0	1.50E-18	0.0	0.0
19	1085.7	1085.7	1.831E-11	4.80E 08	0.0	1.00E-18	0.0	0.0
20	1040.0	1090.0	1.867E-11	4.20E 09	0.0	1.20E-18	0.0	0.0
21	1037.6	1037.6	1.915E-11	1.23E 09	0.0	7.80E-19	0.0	0.0
22	1031.9	1031.9	1.926E-11	1.89E 09	0.0	1.04E-18	0.0	0.0
23	1027.0	1040.0	1.923E-11	6.90E 08 (1)	0.0	1.30E-18 (5)	0.0	0.0
24	1025.7	1025.7	1.938E-11	2.70E 09 (2)	0.0	1.60E-18 (4)	0.0	0.0
25	991.5	991.5	2.005E-11	4.00E 08	1.40E-18 (1)	1.90E-18	0.0	0.0
26	990.0	1027.0	1.971E-11	1.50E 09	2.30E-19	1.90E-18	0.0	0.0
27	977.0	977.0	2.034E-11	4.00E 09	2.60E-18	4.00E-18	0.0	0.0
28	972.5	972.5	2.044E-11	6.50E 08	2.50E-16	4.00E-17	0.0	0.0
29	950.0	990.0	2.049E-11	6.00E 08	1.70E-18	8.30E-18	0.0	0.0
30	949.7	949.7	2.093E-11	3.50E 08	4.30E-18	5.90E-18	0.0	0.0
31	937.8	937.8	2.119E-11	2.00E 08	5.40E-18	5.20E-18	0.0	0.0
32	920.0	950.0	2.126E-11	6.90E 08	3.40E-18	7.00E-18	0.0	0.0
33	911.0	920.0	2.171E-11	8.10E 08	3.80E-18	7.40E-18	0.0	0.0
34	890.0	911.0	2.207E-11	4.00E 09	4.40E-18	9.30E-18	2.70E-18 (1)	0.0
35	860.0	890.0	2.272E-11	3.80E 09	5.00E-18	8.90E-18	2.90E-18	0.0
36	840.0	860.0	2.338E-11	1.80E 09	5.00E-18	1.17E-17	3.10E-18	0.0
37	832.0	835.0	2.385E-11	6.50E 08	1.11E-17	1.35E-17	3.20E-18	0.0
38	810.0	840.0	2.409E-11	1.60E 09	3.40E-18	2.60E-17	3.20E-18	0.0
39	796.0	810.0	2.475E-11	7.00E 08	6.80E-18	4.00E-17	3.30E-18	0.0
40	790.1	790.1	2.516E-11	3.60E 08	2.80E-17	3.30E-17	3.30E-18	0.0
41	787.7	787.7	2.523E-11	2.80E 08	9.70E-18	2.80E-17	3.30E-18	0.0
42	780.3	780.3	2.547E-11	1.60E 08	1.38E-17	3.30E-17	3.30E-18	0.0
43	780.0	756.0	2.522E-11	5.00E 08	2.60E-17	2.80E-17	3.30E-18	0.0
44	770.4	770.4	2.580E-11	3.20E 08	1.38E-17	2.00E-17	3.40E-18	0.0
45	765.1	765.1	2.598E-11	2.30E 08	7.10E-17	2.50E-17	3.40E-18	0.0
46	760.0	780.0	2.581E-11	6.00E 08	2.40E-17	2.20E-17	3.40E-18	0.0
47	740.0	760.0	2.650E-11	4.00E 08	2.50E-17	2.20E-17	3.40E-18	0.0
48	732.0	740.0	2.700E-11	1.50E 08	2.50E-17	4.10E-17	3.50E-18	0.0
49	703.8	703.8	2.824E-11	2.00E 08	2.60E-17	3.30E-17	8.10E-18	0.0
50	700.0	732.0	2.776E-11	3.50E 08	2.20E-17	3.50E-17	7.70E-18	0.0
51	665.0	700.0	2.913E-11	7.00E 09 (2)	2.70E-17 (1)	2.70E-17 (1)	8.30E-18 (1)	0.0

Table III. (continued)

l	λ_1	λ_2	E^l	Φ_∞^l	$\sigma_{N_2}^l$	$\sigma_{O_2}^l$	σ_O^l	$\sigma_{O_3}^l$
104	2020.0	2040.0	9.795E-12	2.98E 12 (7)	0.0	1.21E-23 (5)	0.0	3.16E-19 (6)
105	2040.0	2060.0	9.695E-12	3.55E 12	0.0	1.14E-23	0.0	3.42E-19
106	2060.0	2080.0	9.601E-12	3.98E 12	0.0	1.07E-23	0.0	3.94E-19
107	2080.0	2100.0	9.505E-12	6.02E 12	0.0	1.00E-23	0.0	4.88E-19
108	2100.0	2120.0	9.415E-12	7.95E 12	0.0	9.20E-24	0.0	5.99E-19
109	2120.0	2140.0	9.331E-12	8.10E 12	0.0	8.40E-24	0.0	7.52E-19
110	2140.0	2160.0	9.244E-12	1.02E 13	0.0	7.70E-24	0.0	9.71E-19
111	2160.0	2180.0	9.159E-12	9.89E 12	0.0	7.00E-24	0.0	1.24E-18
112	2180.0	2200.0	9.074E-12	1.29E 13	0.0	6.40E-24	0.0	1.56E-18
113	2200.0	2220.0	8.993E-12	1.23E 13	0.0	5.80E-24	0.0	1.94E-18
114	2220.0	2240.0	8.912E-12	1.67E 13	0.0	5.10E-24	0.0	2.36E-18
115	2240.0	2260.0	8.833E-12	1.61E 13	0.0	4.60E-24	0.0	2.90E-18
116	2260.0	2280.0	8.755E-12	1.26E 13	0.0	4.10E-24	0.0	3.48E-18
117	2280.0	2300.0	8.679E-12	1.50E 13	0.0	3.50E-24	0.0	4.12E-18
118	2300.0	2320.0	8.604E-12	1.54E 13	0.0	3.00E-24	0.0	4.79E-18
119	2320.0	2340.0	8.530E-12	1.48E 13	0.0	2.40E-24	0.0	5.48E-18
120	2340.0	2360.0	8.457E-12	1.40E 13	0.0	1.90E-24	0.0	6.23E-18
121	2360.0	2380.0	8.386E-12	1.45E 13	0.0	1.60E-24	0.0	6.97E-18
122	2380.0	2400.0	8.315E-12	1.32E 13	0.0	1.20E-24	0.0	7.68E-18
123	2400.0	2420.0	8.247E-12	1.46E 13	0.0	9.50E-25	0.0	8.40E-18
124	2420.0	2440.0	8.178E-12	2.01E 13	0.0	7.80E-25	0.0	9.17E-18
125	2440.0	2460.0	8.111E-12	1.81E 13	0.0	5.80E-25	0.0	9.84E-18
126	2460.0	2480.0	8.047E-12	1.78E 13	0.0	4.40E-25	0.0	1.04E-17
127	2480.0	2500.0	7.982E-12	1.78E 13	0.0	3.40E-25	0.0	1.08E-17
128	2500.0	2520.0	7.918E-12	1.84E 13	0.0	2.60E-25	0.0	1.11E-17
129	2520.0	2540.0	7.856E-12	1.80E 13	0.0	2.00E-25	0.0	1.13E-17
130	2540.0	2560.0	7.794E-12	2.38E 13	0.0	1.50E-25	0.0	1.14E-17
131	2560.0	2580.0	7.733E-12	2.60E 13	0.0	1.00E-25 (5)	0.0	1.11E-17
132	2580.0	2600.0	7.673E-12	3.69E 13	0.0	0.0	0.0	1.11E-17
133	2600.0	2620.0	7.614E-12	3.21E 13	0.0	0.0	0.0	1.07E-17
134	2620.0	2640.0	7.557E-12	4.56E 13	0.0	0.0	0.0	1.02E-17
135	2640.0	2660.0	7.499E-12	7.76E 13	0.0	0.0	0.0	9.71E-18
136	2660.0	2680.0	7.444E-12	7.55E 13	0.0	0.0	0.0	8.89E-18
137	2680.0	2700.0	7.388E-12	7.48E 13	0.0	0.0	0.0	8.11E-18
138	2700.0	2720.0	7.334E-12	7.20E 13	0.0	0.0	0.0	7.38E-18
139	2720.0	2740.0	7.280E-12	5.73E 13	0.0	0.0	0.0	6.51E-18
140	2740.0	2760.0	7.227E-12	5.00E 13	0.0	0.0	0.0	5.71E-18
141	2760.0	2780.0	7.175E-12	7.76E 13	0.0	0.0	0.0	4.93E-18
142	2780.0	2800.0	7.123E-12	6.20E 13	0.0	0.0	0.0	4.19E-18
143	2800.0	2820.0	7.072E-12	5.16E 13	0.0	0.0	0.0	3.48E-18
144	2820.0	2840.0	7.022E-12	1.04E 14	0.0	0.0	0.0	2.91E-18
145	2840.0	2860.0	6.973E-12	6.03E 13	0.0	0.0	0.0	2.39E-18
146	2860.0	2880.0	6.924E-12	1.14E 14	0.0	0.0	0.0	1.92E-18
147	2880.0	2900.0	6.876E-12	1.32E 14	0.0	0.0	0.0	1.54E-18
148	2900.0	2920.0	6.829E-12	2.02E 14	0.0	0.0	0.0	1.21E-18
149	2920.0	2940.0	6.783E-12	1.78E 14	0.0	0.0	0.0	9.45E-19
150	2940.0	2960.0	6.737E-12	1.82E 14	0.0	0.0	0.0	7.33E-19
151	2960.0	2980.0	6.691E-12	1.87E 14	0.0	0.0	0.0	5.58E-19 (6)
152	2980.0	3000.0	6.647E-12	1.64E 14 (7)	0.0	0.0	0.0	0.0

Table III. (continued)

l	λ_1	λ_2	E^l	Φ^l_∞	$\sigma^l_{N_2}$	$\sigma^l_{O_2}$	σ^l_O	$\sigma^l_{O_3}$
52	630.0	665.0	3.070E-11	3.50E 08 (2)	2.60E-17 (1)	3.30E-17 (1)	1.15E-17 (1)	0.0
53	629.7	629.7	3.156E-11	1.00E 09	2.30E-17	3.50E-17	1.20E-17	0.0
54	625.0	625.0	3.180E-11	2.00E 08	2.30E-17	3.50E-17	1.20E-17	0.0
55	600.0	630.0	3.232E-11	8.00E 08	2.20E-17	3.90E-17	1.25E-17	0.0
56	584.3	584.3	3.402E-11	1.00E 09	2.30E-17	2.90E-17	1.30E-17	0.0
57	580.0	600.0	3.369E-11	2.50E 08	2.30E-17	2.70E-17	1.29E-17	0.0
58	540.0	580.0	3.551E-11	8.00E 08	2.60E-17	3.00E-17	1.30E-17	0.0
59	510.0	540.0	3.787E-11	5.00E 08	2.60E-17	2.90E-17	1.30E-17	0.0
60	500.0	510.0	3.936E-11	5.00E 08	2.50E-17	2.80E-17	1.30E-17	0.0
61	480.0	500.0	4.057E-11	6.00E 08	2.50E-17	2.70E-17	1.29E-17	0.0
62	460.0	480.0	4.229E-11	4.00E 08	2.40E-17	2.60E-17	1.21E-17	0.0
63	435.0	460.0	4.442E-11	3.50E 08	2.20E-17	2.50E-17	1.05E-17	0.0
64	400.0	435.0	4.763E-11	6.00E 08	1.70E-17	2.40E-17	1.25E-17	0.0
65	370.0	400.0	5.165E-11	4.00E 08	1.31E-17	2.30E-17	1.11E-17	0.0
66	368.1	368.1	5.359E-11	4.00E 08	1.13E-17	2.20E-17	1.03E-17	0.0
67	355.0	370.0	5.484E-11	7.00E 08	1.06E-17	2.20E-17	1.00E-17	0.0
68	340.0	355.0	5.720E-11	6.00E 08	9.10E-18	2.20E-17	9.30E-18	0.0
69	325.0	340.0	5.978E-11	4.00E 08	7.70E-18	2.10E-17	8.70E-18	0.0
70	310.0	325.0	6.261E-11	4.00E 08	6.40E-18	2.00E-17	8.10E-18	0.0
71	303.8	303.8	6.542E-11	4.00E 09	5.00E-18	1.95E-17	9.80E-18	0.0
72	280.0	310.0	6.743E-11	8.00E 08	4.90E-18	1.87E-17	9.20E-18	0.0
73	260.0	280.0	7.364E-11	5.00E 08	4.20E-18	1.60E-17	8.00E-18	0.0
74	256.3	257.0	7.744E-11	3.00E 08	3.80E-18	1.44E-17	7.20E-18	0.0
75	240.0	260.0	7.954E-11	4.00E 08	3.60E-18	1.34E-17	6.70E-18	0.0
76	220.0	240.0	8.647E-11	4.00E 08	3.10E-18	1.12E-17	5.60E-18	0.0
77	205.0	220.0	9.357E-11	3.00E 08	2.80E-18	9.40E-18	4.70E-18	0.0
78	190.0	205.0	1.007E-10	1.60E 09	2.40E-18	8.00E-18	4.00E-18	0.0
79	180.0	190.0	1.075E-10	2.20E 09	2.20E-18	6.80E-18	3.40E-18	0.0
80	165.0	180.0	1.153E-10	3.20E 09	1.90E-18 (1)	5.70E-18 (1)	2.90E-18 (1)	0.0
81	130.0	165.0	1.354E-10	4.00E 08	1.20E-18 (4)	4.00E-18 (4)	2.00E-18 (4)	0.0
82	120.0	130.0	1.591E-10	5.00E 06	9.00E-19	2.20E-18	1.10E-18	0.0
83	110.0	120.0	1.729E-10	1.60E 07	9.00E-19	2.20E-18	1.10E-18	0.0
84	100.0	110.0	1.894E-10	5.00E 07	8.00E-19	2.20E-18	1.10E-18	0.0
85	90.0	100.0	2.054E-10	8.00E 07	5.50E-19	1.40E-18	1.00E-18	0.0
86	80.0	90.0	2.341E-10	8.00E 07	4.70E-19	1.20E-18	6.50E-19	0.0
87	70.0	80.0	2.654E-10	6.00E 07	3.70E-19	8.00E-19	4.00E-19	0.0
88	60.0	70.0	3.064E-10	6.00E 07	3.00E-19	7.00E-19	4.00E-19	0.0
89	50.0	60.0	3.624E-10	6.00E 07	1.80E-19	4.40E-19	2.00E-19	0.0
90	40.0	50.0	4.435E-10	3.00E 07	1.60E-19	4.40E-19	2.00E-19	0.0
91	31.0	40.0	5.629E-10	3.00E 07 (2)	7.00E-20 (4)	2.00E-19 (4)	1.00E-19 (4)	0.0
92	1775.0	1800.0	1.112E-11	3.75E 11 (7)	0.0	1.90E-20 (8)	0.0	8.19E-19 (6)
93	1800.0	1820.0	1.098E-11	4.24E 11	0.0	1.20E-20	0.0	7.44E-19
94	1820.0	1840.0	1.086E-11	4.77E 11	0.0	5.96E-21	0.0	7.44E-19
95	1840.0	1860.0	1.074E-11	4.59E 11	0.0	3.25E-21	0.0	6.70E-19
96	1860.0	1880.0	1.063E-11	6.54E 11	0.0	1.87E-21	0.0	5.95E-19
97	1880.0	1900.0	1.052E-11	8.08E 11	0.0	1.04E-21	0.0	5.58E-19
98	1900.0	1920.0	1.041E-11	9.75E 11	0.0	5.56E-22	0.0	4.84E-19
99	1920.0	1940.0	1.030E-11	9.95E 11	0.0	2.90E-22	0.0	4.09E-19
100	1940.0	1960.0	1.019E-11	1.68E 12	0.0	1.30E-22	0.0	3.91E-19
101	1960.0	1980.0	1.009E-11	1.90E 12	0.0	4.27E-23	0.0	3.72E-19
102	1980.0	2000.0	9.987E-12	2.05E 12	0.0	1.63E-23 (8)	0.0	3.35E-19
103	2000.0	2020.0	9.887E-12	2.59E 12 (7)	0.0	1.27E-23 (5)	0.0	3.16E-19 (6)

TABLE III (continued)

Sources

(1) Hinteregger, et al (1965)

(2) Hinteregger, (1969)

(3) Watanabe, et al (1956, 1958), and Watanabe (1958)

(4) Data of Hinteregger, et al (1965) adjusted to intervals of Hinteregger (1969)

(5) Ditchburn & Young (1962)

(6) Inn & Tanaka (1959)

(7) Brinkman, et al (1966)

(8) Estimated from Hudson, et al (1969) and Blake, et al (1966)

---

* 1.136 E-11 means 1.136×10^{-11}

Solar heating rates for the necessary $\theta(t)$'s were obtained from the library[1] by interpolation (logarithmic) between the tabulated zenith angles. Except when continuous daylight conditions prevailed Q_7 was set equal to zero as an operational definition of local sunset.

[1] The library of solar heating rates for a specified set of zenith angles and altitudes was discussed in Chapter 4.

APPENDIX E

CARBON DIOXIDE AND MONOXIDE ABOVE THE TROPOSPHERE

This appendix contains a pre-print of a paper, co-authored with Paul B. Hays, which has been accepted for publication in Planetary and Space Science.

CARBON DIOXIDE AND MONOXIDE ABOVE THE TROPOSPHERE

Abstract

The dependence of the atmospheric distributions of CO_2 and CO upon the combined effects of photochemical production and loss, and transport is examined. It is found that, for CO_2, deviations from complete mixing are possible in the mesosphere and upper stratosphere. Further, sufficient quantities of CO may be maintained, as a product of CO_2 photodissociation, to be aeronomically significant.

The role of carbon dioxide as a major participant in the transfer of infrared radiation through the Earth's atmosphere has been apparent for many years (Gold, 1909). Moreover, both the recent suggestion of using the 4.3μ and 15μ bands of CO_2 as means by which to remotely measure atmospheric temperature (Kaplan, 1959), and the recognition of the role played by CO_2 in the thermal budget of the mesosphere (Curtis and Goody, 1956) have greatly increased our understanding of its importance. Ultimately, the accuracy of such studies must depend upon a knowledge of the distribution of CO_2 in the upper atmosphere. This discussion briefly considers the factors which influence the distribution of CO_2 in the stratosphere, mesosphere, and lower thermosphere.

Carbon monoxide has been measured at concentrations of between 0.1 and 0.2 ppm in the troposphere (Robinson and Robbins, 1967). Thought to be chiefly the product of automobile exhausts, it has become a major air pollutant in this century. Little is known of its abundance in the upper atmosphere and the proximity of its molecular mass to that of N_2 precludes mass spectrometric identification.

Carbon dioxide is continuously produced at or near the earth's surface by combustion and biological decay, and is also released from the oceans (Robinson and Robbins, 1967). Turbulent mixing within the troposphere should be sufficiently rapid that complete mixing is a valid assumption. In the past it has been assumed that this is true for the stratosphere, mesosphere, and lower thermosphere as well. However, in both the mesosphere and thermosphere CO_2 is dissociated and/or ionized by solar (UV) radiation. Thus, either a vertical flux must be maintained or the resulting CO must recombine locally in order to balance this loss. Recombination is thought to occur both by the three body process:

a) $CO + O + M \rightarrow CO_2 + M$ $\qquad K_a = 10^{-34} cm^6/sec$ at 300^oK (Kaufman, 1968)

and by the two body process:

b) $CO + OH \rightarrow CO_2 + H$ $\qquad K_b = 1.5 \times 10^{-13} cm^3/sec$ at 300^oK (Kaufman, 1968)

Estimates of process a) suggest a significant effect on the vertical flux below about 60 km. The effect of process b) is much less clear due to the present state of uncertainty in the OH distribution. Using the time constants for transport and recombination as a basis for comparison, and assuming an OH concentration as large as given by Hesstvedt (1967), as an upper limit, one finds that above 70 km transport dominates but local photochemical equilibrium will prevail below that level. Because of the uncertainties the following two limiting cases were considered: (1) no recombination; and (2) full recombination of CO below 70 km and none above. These cases should encompass the possible variations of CO_2 and CO in the atmosphere.

The general method employed here in calculating the distributions of CO_2 and CO is similar to that used by Colegrove, Hanson, and Johnson (1965,

1966), where both molecular and eddy diffusion as well as photochemical production and loss are considered. It is found that the problem can be simplified by introducing a parameter, λ, which equals the ratio of the actual mixing ratio of a species to that for the zero flux case. A brief discussion of the formulation is contained in the appendix.

The dissociation rate for CO_2 used in these calculations is a global average obtained from CO_2 cross sections as listed in Table 1., with values for solar UV flux and total absorption cross sections taken from Hinteregger, Hall, and Schmidtke (1963). An atmospheric model essentially the same as the CIRA-1965 model is used.

The molecular diffusion coefficients for CO_2 and CO were taken from Chapman and Cowling (1939) and Lettau (1951). The eddy diffusion coefficients, K_T, used in this study fall naturally into the categories of stratospheric and upper atmospheric values. In the stratosphere, the maximum, minimum, and global averages of the seasonal-latitudinal values of K_T, given by Gudiksen, et. al. (1968) were adopted. These three mixing profiles were extrapolated from 27 km to 50 km. to match the upper atmospheric value; they are shown in Fig. 1, labelled C, D, and E. Between 50 km and 120 km an equilibrium eddy diffusion coefficient was determined from an earth-averaged thermal model (Olivero, 1970) in a manner similar to Johnson and Wilkins (1965) and Johnson (1968). Above 120 km K_T was allowed to decrease exponentially. The eddy diffusion profile adopted as well as the range of values associated with the uncertainties in the inputs to the thermal model are shown in Fig. 1. Thus three models of eddy diffusion were chosen and used in all calculations corresponding to maximum, minimum and average mixing in the stratosphere and average mixing above 50 km.

The time independent continuity equation was integrated between the tropopause (12km) and 200 km for each of the combinations of the three eddy diffusion profiles and two characterizations of recombination. The CO_2 volume mixing ratio was set at 3.145×10^{-4}, the average sea level value (Bolin and Keeling, 1963) at the tropopause and the CO volume mixing ratio was set at 1×10^{-7} (Robinson and Robbins, 1967) at the tropopause.

The results of the calculations for CO_2 and CO are shown in Fig. 2. It is apparent that the question of recombination is not significant for CO_2 within the limits of eddy diffusion considered. On the other hand, the CO mixing ratio is critically dependent upon recombination. The limits of eddy diffusion and recombination used in these calculations lead to more than two orders of magnitude uncertainty in the CO mixing ratio in the upper stratosphere and lower mesosphere. However, in the thermosphere the uncertainty is reduced to less than a factor of two, and CO is shown to be a significant minor constituent. Because of the importance of these results to aeronomical studies confirming experimental evidence would be highly desirable.

Any measurement of CO in our atmosphere will be quite difficult in practice to accomplish. One might observe the Cameron or the fourth positive bands which arise from transitions to the a $^3\Pi$ and a$'\Pi$ levels respectively. But these transitions are either forbidden or hidden by nitric oxide and molecular oxygen bands in the same region of the spectrum. However, if actual measurements of the carbon monoxide concentration in the mesosphere and thermosphere could be made and were to give results significantly below the minimum profile of Fig. 2 the assumed CO_2 dissociation rate would be seriously questioned. Such a result would suggest that the apparent CO_2 absorption continua above

the 903 Å ionization threshold are partially made up of unresolved band systems which do not lead to appreciable dissociation. This conclusion might shed new light on the low atomic oxygen concentration in the Martian atmosphere.

TABLE I.

Sources of Carbon Dioxide Cross Sections

Wavelength	Reference
165Å-580Å (except 303.8Å solar line)	Romand (1966)
Solar lines: 303.8Å, 765.1Å, 708.7Å, etc.	Cairns and Samson (1965)
580Å - 1675Å (except solar lines)	Nakata, Watanabe and Matsunaga (1965)
1675Å - 1775Å	Thompson, Harteck and Reeves (1963)

References

Bolin, B. and Keeling, C. D. 1963. J. Geophys. Res. 68, 3899.

Cairns, R. B. and Samson, J. A. R. 1965. J. Geophys. Res. 70, 99.

Chapman, S. and Cowling, T. G. 1939. The Mathematical Theory of Non-Uniform Gases, University Press, Cambridge.

Colgrove, F. D., Hanson, W. B. and Johnson, F. S. 1965. J. Geophys. Res. 70, 4931.

Colgrove, F. D., Johnson, F. S. and Hanson, W. B. 1966. J. Geophys. Res. 71, 2227.

Curtis, A. R. and Goody, R. M. 1956. Proc. Roy. Soc. A236, 193.

Gold, E. 1909. Proc. Roy. Soc. London. A82, 43.

Gudiksen, P. H., Fairhall, A. W., and Reed, R. H. 1968. J. Geophys. Res. 73, 4461.

Hesstvedt, E. 1967. Geofysiske Publikasjoner. 27, 1.

Hinteregger, H. E., Hall, L. A. and Schmidtke, G. 1965. Space Research V. North-Holland.

Johnson, F. S. and Wilkins, E. M. 1965. J. Geophys. Res. 70, 1281.

Johnson, F. S. 1968. Physical Processes Influencing the Chemistry of Planetary Atmopsheres. Fourth Western Regional Meeting, American Chemical Society, San Francisco.

Kaplan, L. D. 1959. J Opt. Soc. A. 49, 1004.

Kaufman, F. 1968. Symposium on Laboratory Measurements of Aeronomic Interest. I. A. G. A. Toronto.

Lettau, H. 1951. Diffusion in the Upper Atmosphere, in Compendium of Meteorology (Ed. T. F. Malone), p. 320. Waverly Press, Inc. Baltimore.

Nakata, R. S., Watanabe, K. and Matsunaga, F. M. 1965. Science of Light. 14, 54.

Olivero, J. J. 1970. Ph. D. Dissertation (in preparation).

Robinson, E. and Robbins R. C. 1967. Sources, Abundance, and Fate of Gaseous Atmospheric Pollutants. Final Report, SRI Project PR-6755, 123 pp.

Rommand, J. 1966. NASA CR-371, A Congeries of Absorption Cross Sections for Wavelengths Less Than 3000 A (Ed. J. O. Sullivan and A. C. Holland), p. 50, Clearinghouse for Federal Scientific and Technical Information. Springfield, Va.

Thompson, B. A., Harteck, P. and Reeves, R. R., Jr. 1963. J. Geophys. Res. 68, 6431.

APPENDIX

The CO_2 and CO distributions are described by the following equations, respectively:

$$\frac{d\mathcal{J}}{dz} = \frac{d}{dz}\left(\frac{\gamma_2}{\tilde{\gamma}_2}\right) = -\frac{\varphi_{dis} + \varphi_{ion}}{\tilde{\gamma}_2 N(D_2+K_T)} \tag{1}$$

$$\frac{d\gamma_1}{dz} = \frac{\varphi_{dis}}{N(D_1+K_T)} - \frac{\gamma_1 D_1}{(D_1+K_T)}\left(\frac{H-H_1}{HH_1}\right) \tag{2}$$

where: $\mathcal{J} = \gamma_2/\tilde{\gamma}_2$

γ_2 is the actual CO_2 mixing ratio

$\tilde{\gamma}_2$ is the zero flux CO_2 mixing ratio

$$= \tilde{\gamma}_2^{o} \exp\left\{-\int_{z_o}^{z} \frac{D_2}{(D_2+K_T)}\left(\frac{(H-H_2)}{HH_2}\right) dz\right\}$$

φ_{dis} is the photochemical induced flux from dissociation

$$= \int_{z}^{\infty} \tilde{\gamma}_2 \, N \, \mathcal{J} \, J_{dis} \, dz$$

J_{dis} is the dissociation rate, per molecule

φ_{ion} is the photochemical induced flux from ionization

$$= \int_{z}^{\infty} \tilde{\gamma}_2 \, N \, \mathcal{J} \, J_{ion} \, dz$$

J_{ion} is the ionization rate, per molecule

N is the total number density

D_2 is the effective molecular diffusion coefficient for CO_2

K_T is the eddy diffusion coefficient

H is the atmospheric scale height

H_2 is the specific scale height for CO_2

γ_1 is the actual CO mixing ratio

D_1 is the effective molecular diffusion coefficient for CO

H_1 is the specific scale height for CO

Both equations were integrated between the tropopause (12 km) and the arbitrary upper boundry at 200 km for each of the combinations of mixing and recombination. The following boundary conditions were employed:

a) $\gamma_2^o = 3.145 \times 10^{-4}$ at z = 12 km

b) $\gamma_1^o = 1.0 \times 10^{-7}$ at z = 12 km

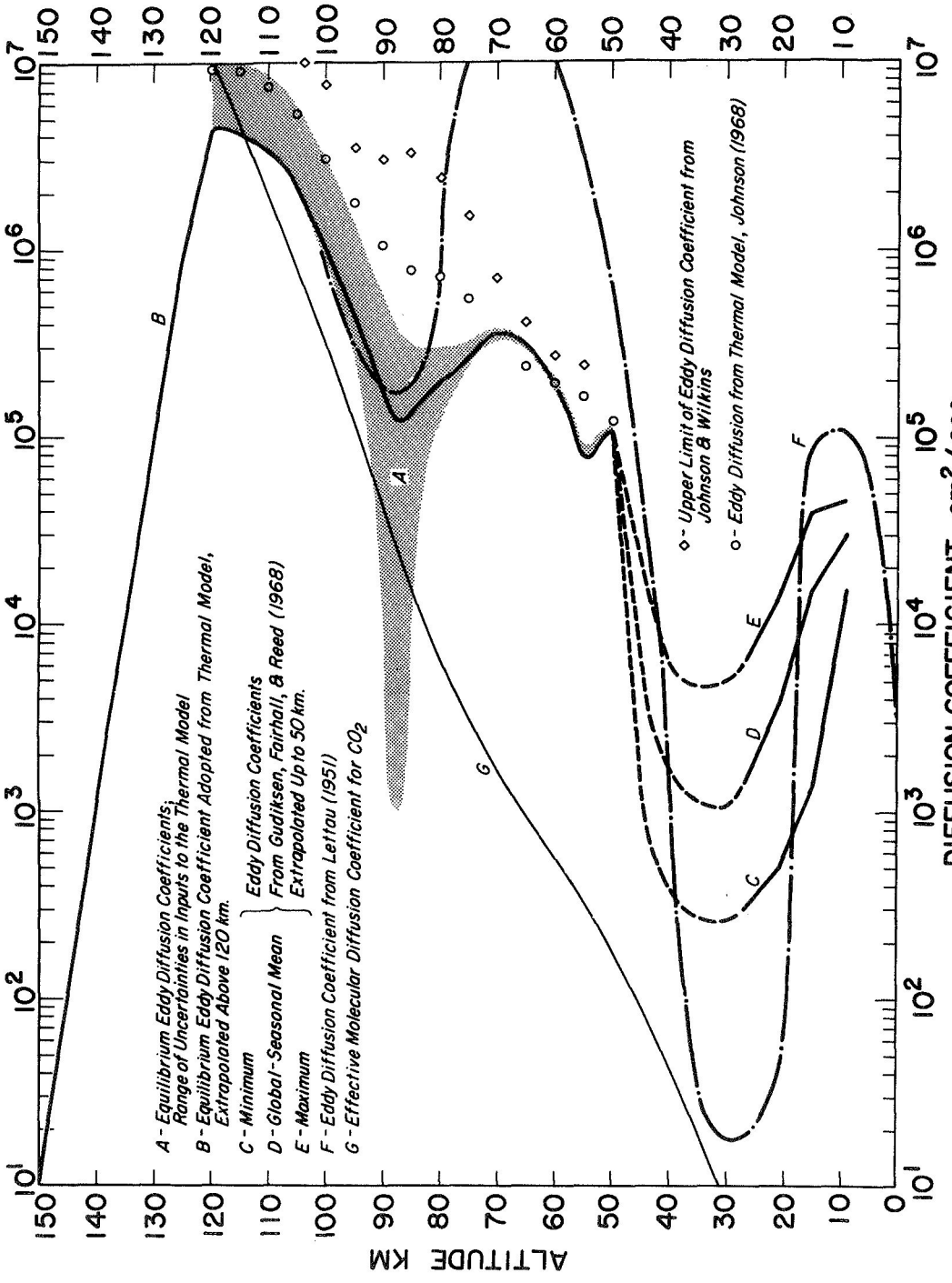

Figure 1. Eddy diffusion coefficients used along with other estimates

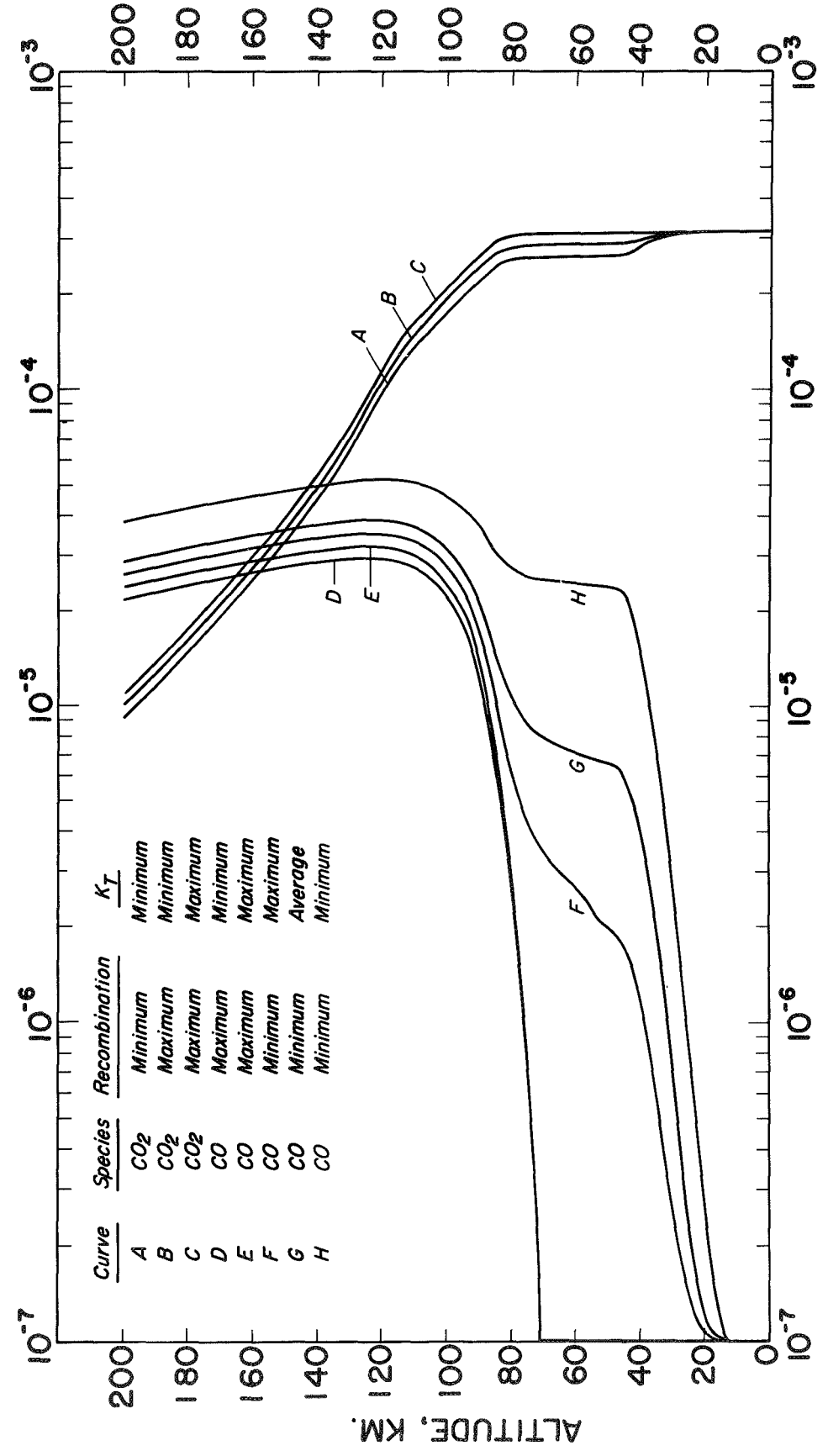

Figure 2. Calculated profiles of the volume mixing ratios of CO_2 and CO

APPENDIX F

LINEARIZED IR TRANSFER OF CARBON DIOXIDE (15μ Bands)

For the present study a model of the CO_2 (15μ bands) cooling rate specifically tailored to the thermal model adopted was formulated by Drayson (1970), as described in Chapter 2. The Drayson model utilized direct numerical integration over each line in the bands, in the basic IR transfer formulation,[1] instead of resorting to one of the customary band models. There is a considerable gain in flexibility and accuracy associated with this approach but at the expense of long computing times required in the calculations. The following were also assumed (Drayson, 1967):

(a) The entire atmosphere was divided into L_{max} layers within each of which a Curtis-Godson- type approximation (Curtis, 1952; Godson, 1953) was made for the effective pressure, temperature and CO_2 concentration;

(b) The source function, $J(\nu, T)$ was assumed linear with pressure between adjacent levels; and in regions of large temperature gradients the layer separation was decreased;

(c) The small frequency dependence of the source function over an individual band was neglected with the value at the mid-band frequency, ν_0, used throughout the band; and

(d) It was assumed that the lines of individual bands were non-overlapping in the regions of the atmosphere where deviations from Kirchoff's law became important.

---

[1] This refers to calculations such as Equation (2.5.2). Further details of the line by line integration and band model approachs can be found in Drayson (1967) and Kuhn (1966), respectively.

From the general equation of transfer one can infer a linear relationship between the source functions, J(I), and the radiative flux difference between the L^{th} and $(L+1)^{th}$ levels, $\Delta F(L)$, which can be expressed as:

$$\Delta F(L) = \sum_{I} a(L,I)\ J(I) \qquad \text{(F.1)}$$

The flux difference between adjacent levels may also be derived from the non-LTE transfer equation:

$$\Delta F(L) = b(L)\left[J(L) - B(L)\right] \qquad \text{(F.2)}$$

where B(L) is the Planck (blackbody) function and b(L) is an expression involving the ratio of the statistical weights of the two energy states (ν_2 mode and ground state), and the relaxation time. From Equation (F.1) and (F.2) the source functions were derived as linear polynomials in the B's:

$$J(L) = \sum_{K} c(I,K)\ B(K) \qquad \text{(F.3)}$$

and Equation (2.4.1) became:

$$\Delta F(L) = \sum_{I} a(L,I)\ \sum_{K} c(I,K)\ B(K) \qquad \text{(F.4)}$$

The Planck function was linearly approximated about a standard temperature profile, To(k), as:

$$B(K) \simeq d(K) + e(K)\left[T(K) - T_o(K)\right] \qquad \text{(F.5)}$$

The cooling rates were obtained by summing the flux divergences of each of the CO_2 (isotope fundamental and overtone) bands:

$$Q_{15\mu} \simeq \sum_{n}' \left(\frac{\Delta F(L)}{\Delta z(L)}\right)_n \qquad \text{(F. 6)}$$

The flux divergences were expressed in terms of Equations (F. 4) and (F. 5) and summed as above, leading to the following quantities:

$$HZERO(L) = \sum_{n}' \left\{ \frac{1}{\Delta z(L)} \sum_{I} a(L,I) \sum_{K}' c(I,K)\, d(K) \right\} \qquad \text{(F. 7)}$$

$$DH(L,K) = \sum_{n}' \left\{ \frac{1}{\Delta z(L)} \sum_{I}' a(L,I)\, c(I,K)\, e(K) \right\} \qquad \text{(F. 8)}$$

thus the CO_2 (15 bands) cooling rate was just:

$$Q_{15\mu}(z(L)) = HZERO(L) + \sum_{K}' DH(L,K)\left[T(K) - T_0(K)\right] \qquad \text{(F. 9)}$$

The following parameters are given in Table IV: the level designation, K; its height in Km, Z(K); the pressure in dynes/cm^2, P(K); the standard temperature in ^{o}K, T_o(K); the interval center designation, L; its height in Km, Z(L); and the unperturbed cooling rate in ^{o}K/day, H ZERO (L). The interval centers in Table IV., for $4 \leq L \leq 53$, correspond to the nominal height levels in the numerical model (Appendix A.). The (59x60) matrix, DH (L, K), is presented in Table V. Each element of this matrix may be interpreted as a relationship between the temperature at level K and the cooling rate at the L^{th} interval center; the elements of DH (L, K) have units (^{o}K/day) per ^{o}K. The three intervals above 120 Km and six intervals below 50 Km. serve to determine the radiative flux at these boundaries. Once the

Table IV. Standard Profile Parameters for the Linearized CO_2 (15 bands) Cooling Rate

LEVEL				INTERVAL CENTER		
K	Z(K) (Km)	P(K) (dynes/cm^2)	To(K) (°K)	L	Z(L) (Km)	HZERO(L) (°K/day)
1		0.0	1000.00			
				1	160.0	-0.187
2	150.3	5.828(-3)*	713.40			
				2	140.5	-0.758
3	134.0	1.159(-2)	563.33			
				3	127.5	-1.261
4	123.8	2.306(-2)	404.60			
				4	120.03	-1.340
5	118.8	3.167(-2)	357.75			
				5	117.54	-1.404
6	116.4	3.903(-2)	335.40			
				6	115.27	-1.511
7	114.2	4.810(-2)	314.44			
				7	113.17	-1.581
8	112.2	5.927(-2)	294.50			
				8	111.22	-1.638
9	110.3	7.305(-2)	277.96			
				9	109.39	-1.735
10	108.5	9.002(-2)	264.35			
				10	107.66	-1.832
11	106.8	1.109(-1)	253.14			
				11	106.02	-1.978
12	105.2	1.367(-1)	243.62			
				12	104.44	-2.139
13	103.7	1.685(-1)	235.16			
				13	102.93	-2.315
14	102.2	2.077(-1)	227.43			
				14	101.48	-2.503
15	100.8	2.559(-1)	220.46			
				15	100.08	-2.700
16	99.4	3.154(-1)	214.17			
				16	98.72	-2.912
17	98.1	3.887(-1)	208.30			
				17	97.40	-3.092

*5.828(-3) denotes 5.828×10^{-3}

Table IV. (continued)

LEVEL				INTERVAL CENTER		
K	Z(K) (Km)	P(K) (dynes/cm^2)	To(K) (^{o}K)	L	Z(L) (Km)	HZERO(L) (^{o}K/day)
18	96.7	4.790(-1)	202.68			
				18	96.12	-3.262
19	95.5	5.903(-1)	197.51			
				19	94.87	-3.422
20	94.3	7.275(-1)	193.14			
				20	93.66	-3.551
21	93.1	8.966(-1)	189.33			
				21	92.46	-3.617
22	91.8	1.105(0)	185.72			
				22	91.29	-3.589
23	90.7	1.362(0)	182.48			
				23	90.15	-3.471
24	89.6	1.678(0)	179.72			
				24	89.01	-3.145
25	88.5	2.068(0)	177.55			
				25	87.90	-2.700
26	87.3	2.549(0)	175.88			
				26	86.79	-2.158
27	86.2	3.141(0)	174.95			
				27	85.69	-1.584
28	85.1	3.871(0)	174.81			
				28	84.59	-1.075
29	84.0	4.771(0)	175.39			
				29	83.49	-0.657
30	82.9	5.879(0)	176.60			
				30	82.37	-0.358
31	81.8	7.246(0)	178.40			
				31	81.25	-0.168
32	80.7	8.929(0)	180.65			
				32	80.12	-0.042
33	79.5	1.100(1)	183.23			
				33	78.97	+0.053
34	78.4	1.356(1)	186.08			
				34	77.80	+0.135

Table IV. (continued)

LEVEL				INTERVAL CENTER		
K	Z(K) (Km)	P(K) (dynes/cm^2)	To(K) (^{o}K)	L	Z(L) (Km)	HZERO(L) (^{o}K/day)
35	77.2	1.671(1)	189.15			
				35	76.61	+0.214
36	76.0	2.060(1)	192.47			
				36	75.41	+0.255
37	74.8	2.538(1)	196.19			
				37	74.18	+0.204
38	73.6	3.128(1)	200.46			
				38	72.92	+0.026
39	72.3	3.855(1)	205.32			
				39	71.64	-0.292
40	71.0	4.751(1)	210.74			
				40	70.32	-0.736
41	69.6	5.855(1)	216.55			
				41	68.97	-1.273
42	68.3	7.216(1)	222.64			
				42	67.58	-1.900
43	66.9	8.893(1)	228.97			
				43	66.15	-2.612
44	65.4	1.096(2)	235.46			
				44	64.68	-3.371
45	63.9	1.351(2)	242.01			
				45	63.17	-4.143
46	62.4	1.665(2)	248.54			
				46	61.62	-4.949
47	60.8	2.051(2)	255.06			
				47	60.02	-5.876
48	59.2	2.528(2)	261.49			
				48	58.39	-6.805
49	57.6	3.116(2)	266.95			
				49	56.73	-7.128
50	55.9	3.840(2)	269.71			
				50	55.05	-6.631
51	54.2	4.732(2)	270.34			
				51	53.37	-6.062

Table IV. (continued)

LEVEL				INTERVAL CENTER		
K	Z(K) (Km)	P(K) (dynes/cm^2)	To(K) (^{o}K)	L	Z(L) (Km)	HZERO(L) (^{o}K/day)
52	52.5	5.831(2)	270.75			
				52	51.68	-5.834
53	50.8	7.187(2)	271.00			
				53	50.0	-5.771
54	49.3	8.774(2)	270.65			
				54	47.0	-4.998
55	43.6	1.785(3)	260.85			
				55	41.0	-3.722
56	38.4	3.570(3)	245.37			
				56	35.2	-2.306
57	32.0	8.891(3)	228.49			
				57	28.4	-1.086
58	24.7	2.669(4)	221.25			
				58	18.4	-0.345
59	12.0	1.939(5)	216.65			
				59	6.0	+0.308
60	0.0	1.013(6)	288.15			

Table V. Matrix Elements, DH (L, K), for the Linearized CO_2 (15μ bands) Cooling Rate

DH(1,1).....DH(1,6)

-1.8686E-04	-1.7378E-04	1.[illegible]E-05	1.7[illegible]E-[illegible]	1.[illegible]E-[illegible]	2.4[illegible]E-[illegible]	4.5650E-09	5.1066E-09	7.3069E-09	1.0167E-08
1.4231E-08	1.9778E-08	2.[illegible]E-08	3.7479E-[illegible]	5.[illegible]E-[illegible]	6.9263E-08	9.2900E-08	1.2365E-07	1.6398E-07	2.1453E-07
2.7777E-07	3.5455E-07	4.4471E-07	5.4591E-07	6.4696E-07	7.4585E-07	8.3029E-07	8.9121E-07	9.2522E-07	9.2882E-07
9.0611E-07	8.6427E-07	8.1569E-07	7.6968E-07	7.3242E-07	7.0689E-07	6.9327E-07	6.8488E-07	6.7553E-07	6.5900E-07
6.3308E-07	6.0077E-07	5.7701E-07	5.[illegible]E-07	5.0426E-07	6.3280E-07	6.6143E-07	6.7105E-07	6.4028E-07	5.6454E-07
4.5687E-07	3.4200E-07	2.3241E-07	2.8105E-07	1.4790E-07	7.7551E-08	2.4479E-08	4.1511E-09	3.0014E-09	5.3827E-10

DH(2,1).....DH(2,6)

2.6619E-1[illegible]	-1.2[illegible]E-[illegible]	-1.[illegible]E-[illegible]	1.[illegible]E-08	1.1932E-08	1.5197E-[illegible]	2.1971E-08	3.0918E-08	4.3268E-08	5.9334E-08
8.2386E-08	1.1340E-07	1.5549E-07	2.1233E-07	2.8719E-07	3.8757E-07	5.1840E-07	6.8625E-07	9.0750E-07	1.1863E-06
1.5339E-06	1.9598E-06	2.4667E-06	3.[illegible]E-06	3.5794E-06	4.1284E-06	4.6106E-06	4.9586E-06	5.1611E-06	5.2100E-06
5.1248E-06	4.9400E-06	4.7366E-06	4.5689E-06	4.4894E-06	4.5329E-06	4.7340E-06	5.0986E-06	5.6140E-06	6.2328E-06
6.9039E-06	7.5791E-06	8.[illegible]E-06	8.6977E-06	8.9720E-06	9.0551E-06	8.8618E-06	8.3379E-06	7.4562E-06	6.2745E-06
5.0561E-06	4.0237E-06	3.1335E-06	5.2185E-06	4.0691E-06	1.7937E-06	3.7509E-07	5.4427E-08	2.3735E-08	1.9513E-08

DH(3,1).....DH(3,6)

5.2276E-1[illegible]	3.5519E-[illegible]	-3.[illegible]E-[illegible]	-2.[illegible]E-[illegible]	3.8971E-08	4.9657E-08	6.9700E-08	9.9213E-08	1.3767E-07	1.8605E-07
2.5237E-07	3.4965E-07	4.7894E-07	6.5253E-07	8.8176E-07	1.1891E-06	1.5894E-06	2.1093E-06	2.7854E-06	3.6584E-06
4.7445E-06	6.0677E-06	7.6597E-06	9.4236E-06	1.1251E-05	1.3062E-05	1.4684E-05	1.5941E-05	1.6710E-05	1.7007E-05
1.6838E-05	1.6348E-05	1.5717E-05	1.5144E-05	1.4704E-05	1.4556E-05	1.4773E-05	1.5466E-05	1.6522E-05	1.7758E-05
1.9073E-05	2.0420E-05	2.1532E-05	2.2165E-05	2.2343E-05	2.2116E-05	2.1347E-05	1.9877E-05	1.7602E-05	1.4682E-05
1.1825E-05	9.4756E-06	7.4109E-06	1.2003E-05	9.0681E-06	4.1654E-06	1.5538E-06	6.1229E-07	3.3170E-07	1.1866E-06

DH(4,1).....DH(4,6)

9.6792E-1[illegible]	6.5392E-09	3.9346E-08	-5.[illegible]E-[illegible]	-4.6433E-[illegible]	1.1901E-07	1.5634E-07	2.2652E-07	3.1149E-07	4.2505E-07
5.7042E-07	7.9220E-07	1.[illegible]E-06	1.4706E-06	1.9855E-06	2.6618E-06	3.5622E-06	4.7298E-06	6.2162E-06	8.1253E-06
1.0518E-05	1.3434E-05	1.6972E-05	2.0782E-05	2.4734E-05	2.8623E-05	3.2009E-05	3.4496E-05	3.5966E-05	3.6376E-05
3.5704E-05	3.4335E-05	3.2669E-05	3.[illegible]E-05	2.9536E-05	2.8547E-05	2.8270E-05	2.8622E-05	2.9549E-05	3.0755E-05
3.1930E-05	3.3177E-05	3.[illegible]E-05	3.[illegible]E-[illegible]	3.3119E-05	3.1901E-05	3.0059E-05	2.7358E-05	2.3695E-05	1.9364E-05
1.5386E-05	1.2311E-05	9.5902E-06	1.5157E-05	1.1274E-05	5.2468E-06	2.2555E-06	1.0590E-06	6.5823E-07	2.5545E-06

DH(5,1).....DH(5,6)

1.3337E-08	8.7933E-09	5.[illegible]E-08	1.[illegible]E-07	-6.4384E-[illegible]	-5.[illegible]E-[illegible]	2.6385E-07	3.4975E-07	4.7078E-07	6.4659E-07
8.7804E-07	1.1926E-06	1.6219E-06	2.[illegible]E-06	2.9663E-06	3.9823E-06	5.3224E-06	7.0435E-06	9.2549E-06	1.2084E-05
1.5589E-05	1.9892E-05	2.5[illegible]E-05	3.[illegible]E-05	3.6149E-05	4.1693E-05	4.6406E-05	4.9782E-05	5.1571E-05	5.1776E-05
5.0469E-05	4.8105E-05	4.5[illegible]E-05	4.[illegible]E-05	3.9864E-05	3.8342E-05	3.7116E-05	3.7004E-05	3.7579E-05	3.8529E-05
3.9417E-05	4.0202E-05	4.[illegible]E-05	4.[illegible]E-[illegible]	3.8338E-05	3.6242E-05	3.3804E-05	3.0780E-05	2.5856E-05	2.0895E-05
1.6586E-05	1.3121E-05	9.[illegible]E-06	1.5644E-05	1.1617E-05	5.4615E-06	2.1689E-06	9.8079E-07	8.6121E-07	2.2625E-06

DH(6,1).....DH(6,6)

1.7125E-[illegible]	1.1276E-08	6.5[illegible]E-08	1.2674E-07	1.7161E-07	-7.8726E-[illegible]	-7.2472E-[illegible]	5.0710E-07	6.7753E-07	9.1285E-07
1.2371E-06	1.6682E-06	2.2[illegible]E-06	3.[illegible]E-06	4.1375E-06	5.5566E-06	7.4180E-06	9.7734E-06	1.2860E-05	1.6761E-05
2.1619E-05	2.7464E-05	3.4465E-05	4.1[illegible]E-05	4.9509E-05	5.6820E-05	6.3004E-05	6.7227E-05	6.9424E-05	6.9218E-05
6.7136E-05	6.3537E-05	5.[illegible]E-05	5.4911E-05	5.1140E-05	4.8204E-05	4.6489E-05	4.5843E-05	4.6093E-05	4.6762E-05
4.7403E-05	4.7502E-05	4.[illegible]E-05	4.6292E-05	4.4323E-05	4.1139E-05	3.7675E-05	3.3359E-05	2.8221E-05	2.2592E-05
1.7780E-05	1.3918E-05	1.[illegible]E-[illegible]	1.6799E-05	1.2429E-05	5.6256E-06	2.2118E-06	9.4351E-07	4.9221E-07	2.0031E-06

Table V. (continued)

DH(7,1).....DH(7,60)

2.1913E-09	1.4207E-08	8.1849E-08	1.5641E-07	2.9605E-07	3.0903E-07	-9.3969E-03	-8.5519E-03	9.8363E-07	1.2962E-06
1.7280E-06	2.3341E-06	3.153 E-06	4.2609E-06	5.7048E-06	7.6751E-06	1.0190E-05	1.3438E-05	1.7619E-05	2.2928E-05
2.9442E-05	3.7344E-05	4.6723E-05	5.6719E-05	6.6715E-05	7.6355E-05	8.4126E-05	8.9436E-05	9.1796E-05	9.1168E-05
8.7664E-05	8.2411E-05	7.6098E-05	6.9837E-05	6.4174E-05	5.9838E-05	5.6963E-05	5.5522E-05	5.5265E-05	5.5364E-05
5.5467E-05	5.5066E-05	5.3646E-05	5.1817E-05	4.9931E-05	4.5086E-05	4.0788E-05	3.5781E-05	3.0088E-05	2.4016E-05
1.8645E-05	1.4320E-05	1.0796E-05	1.7475E-05	1.2913E-05	5.6962E-06	2.4095E-06	1.0034E-06	1.7519E-07	1.6621E-06

DH(8,1).....DH(8,60)

2.7797E-09	1.7827E-08	1.0136E-07	1.9229E-07	2.5007E-07	3.6571E-07	6.1014E-07	-1.1018E-02	-1.0045E-02	1.8833E-06
2.4574E-06	3.2716E-06	4.3905E-06	5.8682E-06	7.8572E-06	1.0485E-05	1.3921E-05	1.8299E-05	2.3984E-05	3.1087E-05
3.9885E-05	5.0381E-05	6.2921E-05	7.6054E-05	8.9238E-05	1.0154E-04	1.1150E-04	1.1789E-04	1.2048E-04	1.1872E-04
1.1371E-04	1.0585E-04	9.7028E-05	8.7969E-05	8.0016E-05	7.3596E-05	6.9343E-05	6.6807E-05	6.5692E-05	6.5073E-05
6.4442E-05	6.3157E-05	6.0595E-05	5.7298E-05	5.3752E-05	4.9264E-05	4.3912E-05	3.8101E-05	3.1779E-05	2.5315E-05
1.9590E-05	1.4821E-05	1.1178E-05	1.7844E-05	1.3046E-05	5.9557E-06	2.4372E-06	1.0015E-06	1.0643E-07	1.3717E-06

DH(9,1).....DH(9,60)

3.5151E-09	2.2213E-08	1.2551E-07	2.3699E-07	3.0596E-07	4.4208E-07	7.1754E-07	1.1803E-06	-1.3026E-02	-1.1927E-02
3.6069E-06	4.6575E-06	6.1482E-06	8.1746E-06	1.0846E-05	1.4434E-05	1.9082E-05	2.5070E-05	3.2687E-05	4.2328E-05
5.4143E-05	6.8291E-05	8.5012E-05	1.0253E-04	1.1971E-04	1.3580E-04	1.4843E-04	1.5639E-04	1.5883E-04	1.5591E-04
1.4815E-04	1.3716E-04	1.2455E-04	1.1209E-04	1.0087E-04	9.1812E-05	8.5341E-05	8.1352E-05	7.9070E-05	7.7629E-05
7.5798E-05	7.3331E-05	6.9861E-05	6.5426E-05	6.0508E-05	5.4746E-05	4.8435E-05	4.1625E-05	3.4441E-05	2.7372E-05
2.1154E-05	1.6153E-05	1.2129E-05	1.9312E-05	1.4298E-05	6.5429E-06	2.4190E-06	9.0975E-07	1.9933E-07	1.2079E-06

DH(10,1).....DH(10,60)

4.3091E-09	2.7064E-08	1.5171E-07	2.8544E-07	3.6678E-07	5.2636E-07	8.4361E-07	1.3440E-06	2.2401E-06	-1.5170E-02
-1.3970E-02	6.6078E-06	8.5726E-06	1.1190E-05	1.4791E-05	1.9500E-05	2.5738E-05	3.3595E-05	4.3747E-05	5.6415E-05
7.2116E-05	9.0520E-05	1.1256E-04	1.3514E-04	1.5751E-04	1.7797E-04	1.9414E-04	2.0340E-04	2.0605E-04	2.0078E-04
1.9007E-04	1.7446E-04	1.5770E-04	1.4049E-04	1.2550E-04	1.1291E-04	1.0407E-04	9.8112E-05	9.4662E-05	9.1782E-05
8.8467E-05	8.4664E-05	8.1307E-05	7.4781E-05	6.7959E-05	6.0594E-05	5.3478E-05	4.5706E-05	3.7693E-05	2.9949E-05
2.3005E-05	1.7637E-05	1.3530E-05	2.1707E-05	1.6252E-05	7.4327E-06	2.8040E-06	1.0139E-06	5.1150E-07	1.1107E-06

DH(11,1).....DH(11,60)

5.2828E-09	3.2993E-08	1.8394E-07	3.4518E-07	4.4210E-07	6.3180E-07	1.0053E-06	1.5831E-06	2.5199E-06	4.2003E-06
-1.7898E-02	-1.6552E-02	1.2461E-05	1.5777E-05	2.0406E-05	2.6816E-05	3.4954E-05	4.5641E-05	5.9002E-05	7.6092E-05
9.6618E-05	1.2132E-04	1.4995E-04	1.8002E-04	2.0859E-04	2.3562E-04	2.5536E-04	2.6727E-04	2.6880E-04	2.6168E-04
2.4552E-04	2.2510E-04	2.0127E-04	1.7879E-04	1.5770E-04	1.4121E-04	1.2861E-04	1.2068E-04	1.1508E-04	1.1076E-04
1.0586E-04	9.9980E-05	9.3607E-05	8.6817E-05	7.8638E-05	6.9596E-05	6.0436E-05	5.1435E-05	4.2423E-05	3.3513E-05
2.5668E-05	1.9837E-05	1.5181E-05	2.4532E-05	1.8646E-05	8.5529E-06	3.4638E-06	1.3876E-06	6.2089E-07	1.0818E-06

DH(12,1).....DH(12,60)

6.4422E-09	3.9703E-08	2.2965E-07	4.1332E-07	5.2812E-07	7.5251E-07	1.1918E-06	1.8574E-06	2.9338E-06	4.6506E-06
7.7826E-06	-2.1062E-02	-1.9507E-02	2.2865E-05	2.8713E-05	3.6818E-05	4.7876E-05	6.1697E-05	7.9796E-05	1.0193E-04
1.2956E-04	1.6148E-04	1.9973E-04	2.3826E-04	2.7624E-04	3.0964E-04	3.3569E-04	3.4861E-04	3.5084E-04	3.3838E-04
3.1780E-04	2.8819E-04	2.5776E-04	2.2589E-04	1.9907E-04	1.7595E-04	1.5975E-04	1.4796E-04	1.4040E-04	1.3382E-04
1.2734E-04	1.1922E-04	1.1051E-04	1.0104E-04	9.0911E-05	7.9845E-05	6.8819E-05	5.8330E-05	4.8010E-05	3.7841E-05
2.9288E-05	2.2901E-05	1.7357E-05	2.8288E-05	2.1788E-05	9.9073E-06	3.8064E-06	1.4816E-06	3.9459E-07	1.0888E-06

Table V. (continued)

DH(13,1).....DH(13,60)

7.7522E-08	4.7594E-08	2.6251E-07	4.8277E-07	6.2837E-07	8.9345E-07	1.4103E-06	2.1883E-06	3.4177E-06	5.3530E-06
8.5285E-06	1.4361E-05	-2.4772E-02	-2.2335E-02	4.1719E-05	5.2033E-05	6.5841E-05	8.4629E-05	1.0787E-04	1.3800E-04
1.7357E-04	2.1671E-04	2.6565E-04	3.1742E-04	3.6503E-04	4.0986E-04	4.4041E-04	4.5830E-04	4.5629E-04	4.4135E-04
4.0937E-04	3.7238E-04	3.2824E-04	2.8851E-04	2.5025E-04	2.2140E-04	1.9808E-04	1.8318E-04	1.7162E-04	1.6283E-04
1.5288E-04	1.4277E-04	1.3114E-04	1.1864E-04	1.0506E-04	9.1691E-05	7.9118E-05	6.6832E-05	5.4636E-05	4.3283E-05
3.3766E-05	2.6495E-05	2.0166E-05	3.2713E-05	2.5372E-05	1.1733E-05	4.3176E-06	1.4193E-06	5.2825E-07	1.1182E-06

DH(14,1).....DH(14,60)

9.2479E-08	5.6793E-08	3.1327E-07	5.8493E-07	7.4471E-07	1.0570E-06	1.6643E-06	2.5725E-06	3.9948E-06	6.1910E-06
9.7359E-06	1.5594E-05	2.6299E-05	-2.9087E-02	-2.6963E-02	7.5969E-05	9.3465E-05	1.1678E-04	1.4860E-04	1.8709E-04
2.3570E-04	2.9092E-04	3.5747E-04	4.2261E-04	4.8715E-04	5.4146E-04	5.8367E-04	6.0042E-04	6.0012E-04	5.7273E-04
5.3419E-04	4.7813E-04	4.2412E-04	3.6618E-04	3.1929E-04	2.7713E-04	2.4857E-04	2.2627E-04	2.1186E-04	1.9825E-04
1.8549E-04	1.7061E-04	1.5588E-04	1.3954E-04	1.2249E-04	1.0639E-04	9.1649E-05	7.7076E-05	6.2866E-05	4.9726E-05
3.8902E-05	3.0377E-05	2.3353E-05	3.8158E-05	2.9988E-05	1.4177E-05	4.8980E-06	1.3020E-06	1.0754E-06	1.1723E-06

DH(15,1).....DH(15,60)

1.1008E-08	6.7076E-08	3.6958E-07	6.8929E-07	8.7628E-07	1.2418E-06	1.9512E-06	3.0062E-06	4.6508E-06	7.1630E-06
1.1135E-05	1.7569E-05	2.8259E-05	4.7820E-05	-3.4063E-02	-3.1619E-02	1.3697E-04	1.6628E-04	2.0547E-04	2.5817E-04
3.1992E-04	3.9564E-04	4.7985E-04	5.6886E-04	6.4784E-04	7.2273E-04	7.6938E-04	7.9529E-04	7.8363E-04	7.5268E-04
6.9018E-04	6.2313E-04	5.4185E-04	4.7201E-04	4.0278E-04	3.5213E-04	3.0952E-04	2.8271E-04	2.6048E-04	2.4392E-04
2.2534E-04	2.0607E-04	1.8577E-04	1.6526E-04	1.4444E-04	1.2553E-04	1.0649E-04	8.9473E-05	7.2907E-05	5.7669E-05
4.5191E-05	3.5399E-05	2.7267E-05	4.5841E-05	3.6053E-05	1.6972E-05	5.7048E-06	1.4427E-06	9.9660E-07	1.2543E-06

DH(16,1).....DH(16,60)

1.3041E-08	7.9028E-08	4.3490E-07	8.1040E-07	1.0288E-06	1.4558E-06	2.2833E-06	3.5106E-06	5.4112E-06	8.2965E-06
1.2805E-05	1.9982E-05	3.1566E-05	5.0982E-05	8.6822E-05	-4.0013E-02	-3.7104E-02	2.4618E-04	2.9545E-04	3.6000E-04
4.4526E-04	5.4062E-04	6.5749E-04	7.6779E-04	8.7806E-04	9.6546E-04	1.0334E-03	1.0515E-03	1.0441E-03	9.8400E-04
9.1191E-04	8.0513E-04	7.0924E-04	6.0243E-04	5.2061E-04	4.4389E-04	3.9387E-04	3.5211E-04	3.2621E-04	3.0049E-04
2.7752E-04	2.5062E-04	2.2491E-04	1.9744E-04	1.7163E-04	1.4716E-04	1.2496E-04	1.0457E-04	8.5618E-05	6.7699E-05
5.3117E-05	4.1857E-05	3.2836E-05	5.5158E-05	4.3507E-05	2.0487E-05	6.8787E-06	1.8028E-06	1.1946E-06	1.3623E-06

DH(17,1).....DH(17,60)

1.5236E-08	9.1943E-08	5.0582E-07	9.4144E-07	1.1935E-06	1.6862E-06	2.6403E-06	4.0526E-06	6.2244E-06	9.5069E-06
1.4618E-05	2.2639E-05	3.5344E-05	5.6033E-05	9.0949E-05	1.5642E-04	-4.6613E-02	-4.3089E-02	4.3829E-04	5.1860E-04
6.2073E-04	7.5376E-04	8.9687E-04	1.0515E-03	1.1812E-03	1.3065E-03	1.3731E-03	1.4092E-03	1.3699E-03	1.3071E-03
1.1912E-03	1.0601E-03	9.0635E-04	7.8457E-04	6.5701E-04	5.6355E-04	4.9109E-04	4.4452E-04	4.0237E-04	3.7286E-04
3.3918E-04	3.0570E-04	2.6993E-04	2.3663E-04	2.0221E-04	1.7230E-04	1.4611E-04	1.2229E-04	1.0005E-04	7.9454E-05
6.2205E-05	4.9443E-05	3.9263E-05	6.6164E-05	5.2282E-05	2.4800E-05	8.4474E-06	2.2656E-06	1.1277E-06	1.4822E-06

DH(18,1).....DH(18,60)

1.7714E-08	1.0675E-07	5.8711E-07	1.0917E-06	1.3817E-06	1.9491E-06	3.0467E-06	4.6632E-06	7.1540E-06	1.0895E-05
1.6670E-05	2.5691E-05	3.9823E-05	6.2350E-05	9.9266E-05	1.6258E-04	2.8113E-04	-5.4356E-02	-5.0221E-02	7.8053E-04
9.0723E-04	1.0623E-03	1.2653E-03	1.4485E-03	1.6364E-03	1.7702E-03	1.8775E-03	1.8812E-03	1.8536E-03	1.7188E-03
1.5834E-03	1.3735E-03	1.2038E-03	1.0024E-03	8.6076E-04	7.1903E-04	6.3268E-04	5.5454E-04	5.0918E-04	4.6020E-04
4.2082E-04	3.7274E-04	3.2908E-04	2.8370E-04	2.4250E-04	2.0436E-04	1.7347E-04	1.4431E-04	1.1840E-04	9.4365E-05
7.4800E-05	5.9656E-05	4.7321E-05	7.9586E-05	6.3484E-05	3.0271E-05	1.0576E-05	2.8718E-06	3.1806E-07	1.6355E-06

Table V. (continued)

DH(19,1).....DH(19,60)

2.0337E-08	1.2362E-07	6.7479E-07	1.2533E-06	1.5836E-06	2.2298E-06	3.4791E-06	5.3153E-06	8.1318E-06	1.2348E-05
1.8846E-05	2.8939E-05	4.4562E-05	6.8255E-05	1.0884E-04	1.7463E-04	2.8729E-04	5.0075E-04	-6.3243E-02	-5.8733E-02
1.3786E-03	1.5467E-03	1.7354E-03	2.0573E-03	2.2603E-03	2.4648E-03	2.5438E-03	2.5830E-03	2.4664E-03	2.3341E-03
2.0709E-03	1.8474E-03	1.5491E-03	1.3332E-03	1.0917E-03	9.4056E-04	7.9309E-04	7.1317E-04	6.3283E-04	5.8176E-04
5.1851E-04	4.6334E-04	4.1040E-04	3.4604E-04	2.9228E-04	2.4707E-04	2.0636E-04	1.7239E-04	1.4084E-04	1.1304E-04
8.9883E-05	7.2652E-05	5.7554E-05	9.7427E-05	7.8014E-05	3.7341E-05	1.3163E-05	3.7399E-06	2.7650E-07	1.8306E-06

DH(20,1).....DH(20,60)

2.3106E-08	1.3778E-07	7.6103E-07	1.4125E-06	1.7812E-06	2.5028E-06	3.8973E-06	5.9413E-06	9.0647E-06	1.3740E-05
2.0886E-05	3.1048E-05	4.9023E-05	7.5703E-05	1.1806E-04	1.8691E-04	3.0095E-04	4.9853E-04	8.8059E-04	-7.3331E-02
-6.8226E-02	2.3986E-03	2.6537E-03	2.9147E-03	3.2691E-03	3.3865E-03	3.5341E-03	3.4672E-03	3.3755E-03	3.0668E-03
2.8022E-03	2.3802E-03	2.0747E-03	1.6887E-03	1.4431E-03	1.1750E-03	1.0300E-03	8.8271E-04	8.0644E-04	7.1554E-04
6.4929E-04	5.6507E-04	4.9356E-04	4.1749E-04	3.5523E-04	2.9531E-04	2.4733E-04	2.0464E-04	1.6859E-04	1.3489E-04
1.0794E-04	8.7206E-05	7.0166E-05	1.1895E-04	9.5723E-05	4.5844E-05	1.6440E-05	4.9601E-06	1.4030E-06	2.0657E-06

DH(21,1).....DH(21,60)

2.5420E-08	1.5304E-07	8.4597E-07	1.5687E-06	1.9737E-06	2.7671E-06	4.2990E-06	6.5368E-06	9.9531E-06	1.5036E-05
2.2812E-05	3.4761E-05	5.3144E-05	8.1717E-05	1.2654E-04	1.9870E-04	3.1559E-04	5.1109E-04	8.5676E-04	1.5345E-03
-8.4967E-02	-7.8657E-02	4.0981E-03	4.3483E-03	4.5641E-03	4.8362E-03	4.8483E-03	4.8338E-03	4.5006E-03	4.2076E-03
3.6427E-03	3.2267E-03	2.6382E-03	2.2621E-03	1.8031E-03	1.5488E-03	1.2714E-03	1.1399E-03	9.8953E-04	9.0676E-04
7.9257E-04	7.0362E-04	5.9751E-04	5.1105E-04	4.2448E-04	3.5689E-04	2.9435E-04	2.4601E-04	2.0107E-04	1.6283E-04
1.2987E-04	1.0559E-04	8.4315E-05	1.4519E-04	1.1637E-04	5.5536E-05	2.0033E-05	5.9778E-06	2.1886E-06	2.3468E-06

DH(22,1).....DH(22,60)

2.7881E-08	1.6698E-07	9.2770E-07	1.7184E-06	2.1565E-06	3.0154E-06	4.6735E-06	7.0876E-06	1.0761E-05	1.6220E-05
2.4527E-05	3.7277E-05	5.6789E-05	8.6952E-05	1.3399E-04	2.0892E-04	3.2871E-04	5.2486E-04	8.5895E-04	1.4570E-03
2.6468E-03	-9.8162E-02	-9.0495E-02	6.8167E-03	6.9227E-03	6.9312E-03	7.0038E-03	6.6290E-03	6.3311E-03	5.5695E-03
5.0370E-03	4.1438E-03	3.6023E-03	2.8354E-03	2.4263E-03	1.9083E-03	1.6767E-03	1.3931E-03	1.2758E-03	1.1053E-03
1.0027E-03	8.5393E-04	7.4306E-04	6.1610E-04	5.2031E-04	4.2676E-04	3.5745E-04	2.9417E-04	2.4381E-04	1.9577E-04
1.5856E-04	1.2861E-04	1.0391E-04	1.7861E-04	1.4498E-04	6.9041E-05	2.4032E-05	6.7338E-06	2.4395E-06	2.6908E-06

DH(23,1).....DH(23,60)

2.9779E-08	1.7994E-07	1.0013E-06	1.8525E-06	2.3180E-06	3.2318E-06	4.9949E-06	7.5521E-06	1.1433E-05	1.7180E-05
2.5910E-05	3.9270E-05	5.9614E-05	9.0922E-05	1.3949E-04	2.1622E-04	3.3776E-04	5.3367E-04	8.6004E-04	1.4216E-03
2.4381E-03	4.5042E-03	-1.1353E-01	-1.0442E-01	1.1130E-02	1.0758E-02	1.0143E-02	9.7282E-03	8.6756E-03	7.9324E-03
6.6061E-03	5.7959E-03	4.5624E-03	3.9094E-03	2.9953E-03	2.5822E-03	2.0407E-03	1.8394E-03	1.5484E-03	1.4255E-03
1.2175E-03	1.0821E-03	8.9948E-04	7.6894E-04	6.2706E-04	5.2571E-04	4.3056E-04	3.6152E-04	2.9494E-04	2.4107E-04
1.9348E-04	1.5950E-04	1.2836E-04	2.2407E-04	1.8082E-04	8.6508E-05	2.9876E-05	8.1838E-06	2.6293E-06	3.1334E-06

DH(24,1).....DH(24,60)

3.0329E-08	1.8319E-07	1.0257E-06	1.8950E-06	2.3637E-06	3.2841E-06	5.0600E-06	7.6261E-06	1.1506E-05	1.7238E-05
2.5929E-05	3.9153E-05	5.9268E-05	9.0044E-05	1.3755E-04	2.1216E-04	3.2927E-04	5.1606E-04	8.2212E-04	1.3363E-03
2.2284E-03	3.8736E-03	7.3552E-03	-1.2750E-01	-1.1675E-01	1.7222E-02	1.5589E-02	1.3749E-02	1.2488E-02	1.0466E-02
9.1907E-03	7.2601E-03	6.2233E-03	4.7137E-03	4.0138E-03	3.0373E-03	2.6699E-03	2.1453E-03	1.9718E-03	1.6661E-03
1.5170E-03	1.2677E-03	1.1035E-03	9.0965E-04	7.6079E-04	6.1633E-04	5.1905E-04	4.2586E-04	3.5591E-04	2.8678E-04
2.3479E-04	1.9139E-04	1.5665E-04	2.7078E-04	2.2174E-04	1.0634E-04	3.6783E-05	9.9354E-06	2.2605E-06	3.5938E-06

Table V. (continued)

DH(25,1).....DH(25,60)

2.9903E-08	1.3177E-07	1.0706E-06	1.8821E-06	2.3392E-06	3.2380E-06	4.9716E-06	7.4654E-06	1.1224E-05	1.6759E-05
2.5122E-05	3.7823E-05	5.7956E-05	8.6387E-05	1.3142E-04	2.0178E-04	3.1133E-04	4.8446E-04	7.6477E-04	1.2273E-03
2.0089E-03	3.3823E-03	6.0356E-03	1.1611E-02	-1.4257E-01	-1.2967E-01	2.5619E-02	2.1566E-02	1.7616E-02	1.5199E-02
1.1897E-02	1.0157E-02	7.5802E-03	6.4545E-03	4.6920E-03	4.0673E-03	3.0572E-03	2.7890E-03	2.2581E-03	2.1067E-03
1.7504E-03	1.5724E-03	1.2816E-03	1.1044E-03	8.8817E-04	7.5259E-04	6.1089E-04	5.1780E-04	4.2232E-04	3.5010E-04
2.8191E-04	2.3442E-04	1.8962E-04	3.3432E-04	2.7008E-04	1.3164E-04	4.5058E-05	1.2048E-05	2.5818E-06	4.1731E-06

DH(26,1).....DH(26,60)

2.8893E-08	1.7326E-07	9.7479E-07	1.7944E-06	2.2211E-06	3.0614E-06	4.6825E-06	7.0027E-06	1.0487E-05	1.5601E-05
2.3394E-05	3.4074E-05	5.2574E-05	7.9291E-05	1.2015E-04	1.8362E-04	2.8185E-04	4.3565E-04	6.8221E-04	1.0833E-03
1.7476E-03	2.8799E-03	4.9324E-03	8.8270E-03	1.7521E-02	-1.5753E-01	-1.4283E-01	3.6473E-02	2.8202E-02	2.1223E-02
1.7375E-02	1.2757E-02	1.0631E-02	7.5653E-03	6.4209E-03	4.5730E-03	4.0630E-03	3.0992E-03	2.8996E-03	2.3631E-03
2.1991E-03	1.7871E-03	1.5809E-03	1.2695E-03	1.0889E-03	8.7372E-04	7.4614E-04	6.1031E-04	5.1732E-04	4.1777E-04
3.4689E-04	2.8377E-04	2.3390E-04	4.0683E-04	3.3344E-04	1.5909E-04	5.5432E-05	1.4761E-05	3.6013E-06	4.8963E-06

DH(27,1).....DH(27,60)

2.5100E-08	1.5490E-07	8.8184E-07	1.6176E-06	1.9928E-06	2.7338E-06	4.1631E-06	6.1982E-06	9.2412E-06	1.3694E-05
2.0376E-05	3.0469E-05	4.5635E-05	6.8565E-05	1.0347E-04	1.5741E-04	2.4037E-04	3.6924E-04	5.7381E-04	9.0278E-04
1.4387E-03	2.3307E-03	3.8914E-03	6.6731E-03	1.2102E-02	2.5072E-02	-1.7060E-01	-1.5428E-01	4.8925E-02	3.4351E-02
2.3688E-02	1.8513E-02	1.2778E-02	1.0504E-02	7.1556E-03	6.1600E-03	4.3636E-03	4.0228E-03	3.1165E-03	2.9618E-03
2.3955E-03	2.1648E-03	1.7621E-03	1.5471E-03	1.2345E-03	1.0631E-03	8.6140E-04	7.4304E-04	6.0667E-04	5.0966E-04
4.1204E-04	3.4677E-04	2.7935E-04	4.9959E-04	4.0361E-04	1.9456E-04	6.7061E-05	1.7830E-05	4.9467E-06	5.7534E-06

DH(28,1).....DH(28,60)

2.1806E-08	1.3255E-07	7.5907E-07	1.3916E-06	1.7051E-06	2.3272E-06	3.5263E-06	5.2238E-06	7.7501E-06	1.1434E-05
1.6944E-05	2.5239E-05	3.7651E-05	5.6344E-05	8.4669E-05	1.2821E-04	1.9473E-04	2.9744E-04	4.5890E-04	7.1588E-04
1.1286E-03	1.8021E-03	2.9478E-03	4.9023E-03	8.4434E-03	1.5694E-02	3.4096E-02	-1.8292E-01	-1.6473E-01	6.2303E-02
3.9326E-02	2.4833E-02	1.8634E-02	1.2196E-02	9.0661E-03	6.6301E-03	5.8461E-03	4.2005E-03	3.9981E-03	3.1367E-03
2.9781E-03	2.3829E-03	2.1614E-03	1.7232E-03	1.5125E-03	1.2139E-03	1.0566E-03	8.6442E-04	7.4341E-04	6.0140E-04
5.0498E-04	4.1438E-04	3.4449E-04	5.9381E-04	4.9175E-04	2.3493E-04	8.2016E-05	2.1541E-05	5.3862E-06	6.8465E-06

DH(29,1).....DH(29,60)

1.7800E-08	1.0759E-07	6.2335E-07	1.1394E-06	1.3883E-06	1.8826E-06	2.8375E-06	4.1801E-06	6.1679E-06	9.0548E-06
1.3359E-05	1.9815E-05	2.9435E-05	4.3867E-05	6.5612E-05	9.8926E-05	1.4945E-04	2.2690E-04	3.4775E-04	5.3817E-04
8.3995E-04	1.3244E-03	2.1203E-03	3.4550E-03	5.7317E-03	9.9981E-03	1.9307E-02	4.3875E-02	-1.9290E-01	-1.7279E-01
7.5029E-02	4.2248E-02	2.4588E-02	1.7937E-02	1.1150E-02	9.1857E-03	6.0502E-03	5.5634E-03	4.0982E-03	3.9717E-03
3.1303E-03	2.0443E-03	2.3444E-03	2.1154E-03	1.6918E-03	1.4924E-03	1.2129E-03	1.0609E-03	8.6721E-04	7.3590E-04
5.9533E-04	5.0414E-04	4.0619E-04	7.3058E-04	5.8868E-04	2.8473E-04	9.8331E-05	2.6204E-05	5.9769E-06	8.1999E-06

DH(30,1).....DH(30,60)

1.3799E-08	8.4418E-08	4.9241E-07	8.9721E-07	1.0857E-06	1.4622E-06	2.1904E-06	3.2054E-06	4.7019E-06	6.8653E-06
1.0078E-05	1.4893E-05	2.2038E-05	3.2644E-05	4.8621E-05	7.2910E-05	1.0963E-04	1.6546E-04	2.5192E-04	3.8689E-04
5.9851E-04	9.3286E-04	1.4777E-03	2.3491E-03	3.7839E-03	6.3040E-03	1.1077E-02	2.1650E-02	5.3663E-02	-2.0051E-01
-1.7892E-01	8.6034E-02	4.3148E-02	2.3389E-02	1.6617E-02	1.0046E-02	8.4222E-03	5.6820E-03	5.3804E-03	4.0835E-03
3.0463E-03	3.1265E-03	2.9065E-03	2.3282E-03	2.0939E-03	1.6947E-03	1.4999E-03	1.2316E-03	1.0676E-03	8.6409E-04
7.2844E-04	5.9696E-04	4.9790E-04	8.6542E-04	7.1036E-04	3.3977E-04	1.1870E-04	3.1294E-05	7.6367E-06	9.9216E-06

Table V. (continued)

DH(31,1).....DH(31,60)

1.0240E-08	6.3930E-08	3.7558E-07	6.9147E-07	3.1814E-07	1.0930E-06	1.6258E-06	2.3616E-06	3.4406E-06	4.9930E-06
7.2901E-06	1.0709E-05	1.5761E-05	2.3266E-05	3.4481E-05	5.1472E-05	7.6954E-05	1.1549E-04	1.7472E-04	2.6642E-04
4.0867E-04	6.3260E-04	9.8593E-04	1.5407E-03	2.4235E-03	3.8996E-03	6.4841E-03	1.1506E-02	2.3170E-02	6.2218E-02
-2.0431E-01	-1.8167E-01	9.3938E-02	4.1989E-02	2.1525E-02	1.4990E-02	9.0831E-03	7.7953E-03	5.5050E-03	5.2716E-03
4.1101E-03	3.9087E-03	3.1373E-03	2.9841E-03	2.3414E-03	2.0964E-03	1.7215E-03	1.5153E-03	1.2429E-03	1.0550E-03
8.5298E-04	7.2134E-04	5.8050E-04	1.0434E-03	8.3828E-04	4.0620E-04	1.4059E-04	3.7504E-05	9.3628E-06	1.2019E-05

DH(32,1).....DH(32,60)

7.3991E-09	4.7304E-08	2.8074E-07	5.0657E-07	6.0222E-07	7.9738E-07	1.1761E-06	1.6942E-06	2.4487E-06	3.5291E-06
5.1206E-06	7.4798E-06	1.0950E-05	1.6081E-05	2.3701E-05	3.5201E-05	5.2342E-05	7.8095E-05	1.1740E-04	1.7780E-04
2.7062E-04	4.1372E-04	6.3951E-04	9.8521E-04	1.5202E-03	2.3812E-03	3.8049E-03	6.3313E-03	1.1359E-02	2.3601E-02
6.8906E-02	-2.0468E-01	-1.8124E-01	9.8352E-02	3.9451E-02	1.9484E-02	1.3475E-02	8.4361E-03	7.4102E-03	5.5044E-03
5.2382E-03	4.1775E-03	3.8992E-03	3.1068E-03	2.9010E-03	2.3875E-03	2.1230E-03	1.7570E-03	1.5194E-03	1.2304E-03
1.0321E-03	8.4429E-04	7.0093E-04	1.2169E-03	9.9341E-04	4.7605E-04	1.6695E-04	4.4245E-05	1.1043E-05	1.4584E-05

DH(33,1).....DH(33,60)

5.6638E-09	3.5478E-08	2.0858E-07	3.7252E-07	4.3783E-07	5.7336E-07	8.3790E-07	1.1952E-06	1.7120E-06	2.4481E-06
3.5269E-06	5.1187E-06	7.4481E-06	1.0874E-05	1.5943E-05	2.3531E-05	3.4794E-05	5.1585E-05	7.7063E-05	1.1592E-04
1.7509E-04	2.6541E-04	4.0619E-04	6.1778E-04	9.3819E-04	1.4391E-03	2.2317E-03	3.5529E-03	5.9286E-03	1.0775E-02
2.3056E-02	7.3059E-02	-2.0159E-01	-1.7812E-01	9.9391E-02	3.6182E-02	1.7647E-02	1.2790E-02	8.1438E-03	7.2479E-03
5.6281E-03	5.2639E-03	4.2989E-03	3.9574E-03	3.2811E-03	2.9439E-03	2.4498E-03	2.1482E-03	1.7671E-03	1.4874E-03
1.2003E-03	1.0077E-03	8.3979E-04	1.4447E-03	1.1547E-03	5.5938E-04	1.9500E-04	5.2411E-05	1.3006E-05	1.7667E-05

DH(34,1).....DH(34,60)

3.8626E-09	2.6216E-08	1.5513E-07	2.7406E-07	3.1766E-07	4.1111E-07	5.9423E-07	8.3869E-07	1.1889E-06	1.6850E-06
2.4082E-06	3.4702E-06	5.0155E-06	7.2718E-06	1.0599E-05	1.5548E-05	2.2838E-05	3.3643E-05	4.9918E-05	7.4553E-05
1.1179E-04	1.6831E-04	2.5463E-04	3.8299E-04	5.7374E-04	8.6446E-04	1.3104E-03	2.0188E-03	3.2092E-03	5.3850E-03
9.9168E-03	2.1766E-02	7.4634E-02	-1.9588E-01	-1.7297E-01	9.7633E-02	3.2809E-02	1.6228E-02	1.1539E-02	8.1505E-03
7.2590E-03	5.8314E-03	5.3697E-03	4.4678E-03	4.0445E-03	3.3864E-03	2.9936E-03	2.4953E-03	2.1365E-03	1.7282E-03
1.4329E-03	1.1688E-03	9.6182E-04	1.6649E-03	1.3455E-03	6.4589E-04	2.2795E-04	6.1206E-05	1.5365E-05	2.1340E-05

DH(35,1).....DH(35,60)

3.1104E-09	1.9580E-08	1.1692E-07	2.0372E-07	2.3253E-07	2.9676E-07	4.2434E-07	5.9140E-07	8.2976E-07	1.1638E-06
1.6495E-06	2.3578E-06	3.3827E-06	4.8705E-06	7.0477E-06	1.0267E-05	1.4985E-05	2.1920E-05	3.2296E-05	4.7883E-05
7.1267E-05	1.0621E-04	1.5959E-04	2.3738E-04	3.5122E-04	5.2139E-04	7.7523E-04	1.1645E-03	1.7867E-03	2.8426E-03
4.7986E-03	8.9331E-03	2.0054E-02	7.3873E-02	-1.8859E-01	-1.6680E-01	9.3999E-02	2.9805E-02	1.5322E-02	1.1219E-02
8.3694E-03	7.4052E-03	6.1055E-03	5.5262E-03	4.6578E-03	4.1410E-03	3.4779E-03	3.0176E-03	2.4842E-03	2.0631E-03
1.6576E-03	1.3758E-03	1.1023E-03	1.9447E-03	1.5430E-03	7.4667E-04	2.6271E-04	7.1466E-05	1.8229E-05	2.5681E-05

DH(36,1).....DH(36,60)

2.4386E-09	1.6352E-08	9.8899E-08	1.5432E-07	1.7283E-07	2.1776E-07	3.0737E-07	4.2369E-07	5.8710E-07	8.1574E-07
1.1452E-06	1.6236E-06	2.3110E-06	3.3032E-06	4.7446E-06	6.8663E-06	9.9470E-06	1.4447E-05	2.1129E-05	3.1114E-05
4.5936E-05	6.7950E-05	1.0113E-04	1.4908E-04	2.1815E-04	3.1971E-04	4.6786E-04	6.8910E-04	1.0287E-03	1.5752E-03
2.5095E-03	4.2404E-03	7.9738E-03	1.8179E-02	7.1292E-02	-1.8106E-01	-1.6095E-01	8.9455E-02	2.7458E-02	1.4962E-02
1.1270E-02	8.7513E-03	7.6835E-03	6.4401E-03	5.7305E-03	4.8376E-03	4.2230E-03	3.5253E-03	2.9768E-03	2.3956E-03
1.9576E-03	1.5867E-03	1.2915E-03	2.2228E-03	1.7734E-03	8.5234E-04	3.0328E-04	8.2841E-05	2.1317E-05	3.0894E-05

Table V. (continued)

				DH(37,1)……..DH(37,60)					
1.6136E-09	1.0718E-08	6.3338E-08	1.1944E-07	1.3137E-07	1.6294E-07	2.2759E-07	3.0973E-07	4.2440E-07	5.8356E-07
8.1194E-07	1.1417E-06	1.6127E-06	2.2873E-06	3.2612E-06	4.6857E-06	6.7438E-06	9.7197E-06	1.4124E-05	2.0637E-05
3.0277E-05	4.4428E-05	6.5429E-05	9.5915E-05	1.3998E-04	2.0166E-04	2.9161E-04	4.2278E-04	6.1913E-04	9.2246E-04
1.4119E-03	2.2477E-03	3.8375E-03	7.1481E-03	1.6388E-02	6.7647E-02	-1.7495E-01	-1.5676E-01	8.4819E-02	2.5997E-02
1.5134E-02	1.1654E-02	9.2998E-03	9.0866E-03	6.8082E-03	5.9413E-03	4.9887E-03	4.2627E-03	3.4901E-03	2.8509E-03
2.2711E-03	1.8584E-03	1.4798E-03	2.5747E-03	2.0199E-03	9.7593E-04	3.4745E-04	9.6312E-05	2.5067E-05	3.7352E-05
				DH(38,1)……..DH(38,60)					
1.4858E-09	9.4049E-09	5.6745E-08	9.4117E-08	1.0156E-07	1.2408E-07	1.7155E-07	2.3024E-07	3.1244E-07	4.2483E-07
5.8646E-07	8.1681E-07	1.1455E-06	1.6125E-06	2.2836E-06	3.2576E-06	4.6564E-06	6.6669E-06	9.6209E-06	1.3972E-05
2.0360E-05	2.9695E-05	4.3548E-05	6.3208E-05	9.2874E-05	1.3089E-04	1.8762E-04	2.6929E-04	3.8921E-04	5.6992E-04
8.5020E-04	1.3019E-03	2.0722E-03	3.4940E-03	6.5121E-03	1.4849E-02	6.3613E-02	-1.7105E-01	-1.5462E-01	8.0583E-02
2.5443E-02	1.5774E-02	1.2325E-02	9.9721E-03	8.5508E-03	7.1505E-03	6.1161E-03	5.0659E-03	4.2025E-03	3.3432E-03
2.6845E-03	2.1523E-03	1.7294E-03	2.0439E-03	2.3105E-03	1.1101E-03	3.9954E-04	1.1183E-04	2.9635E-05	4.5508E-05
				DH(39,1)……..DH(39,60)					
6.9867E-10	6.8555E-09	4.5438E-08	7.5242E-08	7.9233E-08	9.5698E-08	1.3036E-07	1.7351E-07	2.3213E-07	3.1305E-07
4.2744E-07	5.9128E-07	8.2210E-07	1.1492E-06	1.6156E-06	2.2900E-06	3.2496E-06	4.6243E-06	6.6270E-06	9.5674E-06
1.3856E-05	2.0088E-05	2.9296E-05	4.2287E-05	6.0534E-05	8.6631E-05	1.2347E-04	1.7626E-04	2.5294E-04	3.6686E-04
5.4213E-04	8.0945E-04	1.2437E-03	1.9784E-03	3.3178E-03	6.1130E-03	1.3744E-02	5.9890E-02	-1.6988E-01	-1.5485E-01
7.7191E-02	2.5820E-02	1.6840E-02	1.3220E-02	1.0688E-02	8.9919E-03	7.4225E-03	6.2046E-03	5.0075E-03	4.0096E-03
3.1437E-03	2.5321E-03	1.9938E-03	3.4110E-03	2.6326E-03	1.2686E-03	4.5822E-04	1.3075E-04	3.5332E-05	5.5975E-05
				DH(40,1)……..DH(40,60)					
8.1717E-10	7.1456E-09	3.8407E-08	6.0365E-08	6.2150E-08	7.3832E-08	9.9345E-08	1.3062E-07	1.7270E-07	2.3059E-07
3.1194E-07	4.2750E-07	5.9334E-07	8.1822E-07	1.1414E-06	1.6069E-06	2.2642E-06	3.1994E-06	4.5561E-06	6.5364E-06
9.4146E-06	1.3571E-05	1.9692E-05	2.8292E-05	4.0326E-05	5.7520E-05	8.1764E-05	1.1642E-04	1.6675E-04	2.4113E-04
3.5312E-04	5.2432E-04	7.9254E-04	1.2242E-03	1.9504E-03	3.2630E-03	5.9668E-03	1.3169E-02	5.6853E-02	-1.7124E-01
-1.5709E-01	7.4996E-02	2.7032E-02	1.8183E-02	1.4176E-02	1.1321E-02	9.3269E-03	7.5478E-03	6.1135E-03	4.7683E-03
3.7511E-03	2.9587E-03	2.3433E-03	3.9226E-03	3.0182E-03	1.4465E-03	5.2863E-04	1.5324E-04	4.2408E-05	6.9357E-05
				DH(41,1)……..DH(41,60)					
4.0700E-10	4.7606E-09	3.0268E-08	4.7943E-08	4.8269E-08	5.6641E-08	7.5348E-08	9.7754E-08	1.2765E-07	1.6836E-07
2.2577E-07	3.0645E-07	4.1952E-07	5.7665E-07	7.9830E-07	1.1146E-06	1.5599E-06	2.1870E-06	3.0926E-06	4.4093E-06
6.3114E-06	9.0474E-06	1.3066E-05	1.8688E-05	2.6567E-05	3.7798E-05	5.3697E-05	7.6479E-05	1.0966E-04	1.5882E-04
2.3268E-04	3.4504E-04	5.1876E-04	7.9181E-04	1.2320E-03	1.9740E-03	3.3189E-03	6.0664E-03	1.3143E-02	5.4770E-02
-1.7441E-01	-1.6243E-01	7.4213E-02	2.8867E-02	1.9551E-02	1.4996E-02	1.1756E-02	9.4518E-03	7.4143E-03	5.7859E-03
4.4362E-03	3.5076E-03	2.7196E-03	4.5663E-03	3.4526E-03	1.6579E-03	6.0943E-04	1.8084E-04	5.1046E-05	8.6174E-05
				DH(42,1)……..DH(42,60)					
4.8241E-10	5.0834E-09	2.5277E-08	3.7904E-08	3.7245E-08	4.3045E-08	5.6548E-08	7.2402E-08	9.3392E-08	1.2180E-07
1.6160E-07	2.1737E-07	2.9476E-07	4.0173E-07	5.5099E-07	7.6364E-07	1.0588E-06	1.4732E-06	2.0681E-06	2.9260E-06
4.1633E-06	5.9331E-06	8.5212E-06	1.2150E-05	1.7215E-05	2.4477E-05	3.4782E-05	4.9668E-05	7.1493E-05	1.0401E-04
1.5314E-04	2.2783E-04	3.4283E-04	5.2164E-04	8.0442E-04	1.2636E-03	2.0482E-03	3.4814E-03	6.3897E-03	1.3640E-02
5.3761E-02	-1.7885E-01	-1.6460E-01	7.4782E-02	3.0782E-02	2.0719E-02	1.5561E-02	1.1898E-02	9.2512E-03	6.9839E-03
5.3554E-03	4.1312E-03	3.2219E-03	5.2815E-03	3.9791E-03	1.9006E-03	7.0738E-04	2.1389E-04	6.1787E-05	1.0723E-04

Table V. (continued)

DH(43,1).....DH(43,6)

2.3672E-11	3.2436E-09	1.8063E-08	2.9604E-08	2.8515E-08	3.2515E-08	4.2127E-08	5.3208E-08	6.7857E-08	8.7296E-08
1.1475E-07	1.5278E-07	2.0511E-07	2.7701E-07	3.7691E-07	5.1711E-07	7.1175E-07	9.8107E-07	1.3670E-06	1.9187E-06
2.7109E-06	3.8403E-06	5.4988E-06	7.7929E-06	1.1019E-05	1.5661E-05	2.2300E-05	3.1970E-05	4.6271E-05	6.7805E-05
1.0052E-04	1.5051E-04	2.2755E-04	3.4691E-04	5.3344E-04	8.3125E-04	1.3233E-03	2.1760E-03	3.7436E-03	6.9044E-03
1.4556E-02	5.3888E-02	-1.8431E-01	-1.6921E-01	7.6512E-02	3.2706E-02	2.1604E-02	1.5797E-02	1.1649E-02	8.7084E-03
6.4468E-03	4.9771E-03	3.7778E-03	6.2150E-03	4.5916E-03	2.1982E-03	8.2393E-04	2.5593E-04	7.5381E-05	1.3449E-04

DH(44,1).....DH(44,60)

5.4845E-10	3.8320E-09	1.6423E-08	2.2378E-08	2.1504E-08	2.4193E-08	3.0896E-08	3.8561E-08	4.8539E-08	6.1791E-08
8.0357E-08	1.0597E-07	1.4118E-07	1.8861E-07	2.5482E-07	3.4653E-07	4.7305E-07	6.4693E-07	8.9320E-07	1.2458E-06
1.7478E-06	2.4621E-06	3.4998E-06	4.9522E-06	6.9816E-06	9.9409E-06	1.4193E-05	2.0451E-05	2.9816E-05	4.4022E-05
6.5817E-05	9.9204E-05	1.5101E-04	2.3098E-04	3.5555E-04	5.5214E-04	8.7110E-04	1.4073E-03	2.3439E-03	4.0689E-03
7.5134E-03	1.5698E-02	5.5099E-02	-1.8957E-01	-1.7329E-01	7.8876E-02	3.4275E-02	2.1991E-02	1.5482E-02	1.0935E-02
8.0207E-03	5.9730E-03	4.5593E-03	7.2661E-03	5.3501E-03	2.5459E-03	9.6780E-04	3.0691E-04	9.2261E-05	1.6847E-04

DH(45,1).....DH(45,60)

-3.3129E-10	3.5963E-09	1.3499E-08	1.7234E-08	1.5873E-08	1.7661E-08	2.2207E-08	2.7472E-08	3.4117E-08	4.3048E-08
5.5423E-08	7.2555E-08	9.5717E-08	1.2711E-07	1.7008E-07	2.3019E-07	3.1141E-07	4.2305E-07	5.8032E-07	8.0411E-07
1.1212E-06	1.5722E-06	2.2252E-06	3.1406E-06	4.4289E-06	6.3053E-06	9.0345E-06	1.3090E-05	1.9211E-05	2.8604E-05
4.3074E-05	6.5446E-05	1.0007E-04	1.5369E-04	2.3678E-04	3.6705E-04	5.7604E-04	9.2053E-04	1.5048E-03	2.5281E-03
4.3999E-03	8.1167E-03	1.6912E-02	5.6873E-02	-1.9379E-01	-1.7608E-01	8.1396E-02	3.5147E-02	2.1602E-02	1.4540E-02
1.0040E-02	7.4123E-03	5.4355E-03	8.6749E-03	6.2299E-03	2.9723E-03	1.1377E-03	3.7085E-04	1.1270E-04	2.0976E-04

DH(46,1).....DH(46,60)

5.8755E-10	1.8068E-09	8.9362E-09	1.2794E-08	1.1537E-08	1.2493E-08	1.5783E-08	1.9053E-08	2.3661E-08	2.9387E-08
3.7731E-08	4.8766E-08	6.4293E-08	8.4437E-08	1.1281E-07	1.5130E-07	2.0406E-07	2.7528E-07	3.7608E-07	5.1814E-07
7.2077E-07	1.0052E-06	1.4209E-06	2.0008E-06	2.8231E-06	4.0266E-06	5.7893E-06	8.4313E-06	1.2454E-05	1.8658E-05
2.8279E-05	4.3175E-05	6.6274E-05	1.0200E-04	1.5724E-04	2.4339E-04	3.8020E-04	6.0280E-04	9.7277E-04	1.6013E-03
2.6941E-03	4.6834E-03	8.6470E-03	1.8040E-02	5.9078E-02	-1.9652E-01	-1.7728E-01	8.3402E-02	3.4890E-02	2.0379E-02
1.3382E-02	9.2803E-03	6.7749E-03	1.0309E-02	7.3486E-03	3.4739E-03	1.3486E-03	4.4791E-04	1.3767E-04	2.5963E-04

DH(47,1).....DH(47,60)

-6.5703E-10	1.0156E-09	7.0155E-09	9.1934E-09	8.1787E-09	8.8005E-09	1.0902E-08	1.3120E-08	1.5936E-08	1.9885E-08
2.5080E-08	3.2610E-08	4.2356E-08	5.5795E-08	7.3940E-08	9.8997E-08	1.3284E-07	1.7894E-07	2.4334E-07	3.3497E-07
4.6417E-07	6.4719E-07	9.1253E-07	1.2863E-06	1.8164E-06	2.5971E-06	3.7482E-06	5.4818E-06	8.1395E-06	1.2246E-05
1.8647E-05	2.8543E-05	4.3901E-05	6.7598E-05	1.0412E-04	1.6071E-04	2.5004E-04	3.9375E-04	6.2910E-04	1.0204E-03
1.6792E-03	2.8173E-03	4.8948E-03	9.0475E-03	1.8920E-02	6.1235E-02	-1.9784E-01	-1.7728E-01	8.4042E-02	3.3440E-02
1.8924E-02	1.2432E-02	8.4855E-03	1.2690E-02	8.7024E-03	4.1068E-03	1.6025E-03	5.4661E-04	1.6835E-04	3.2079E-04

DH(48,1).....DH(48,60)

7.6865E-10	1.4865E-09	4.6484E-09	6.4826E-09	5.6094E-09	6.0054E-09	7.3189E-09	8.7654E-09	1.0553E-08	1.3063E-08
1.6354E-08	2.1287E-08	2.7386E-08	3.6180E-08	4.7729E-08	6.3984E-08	8.5422E-08	1.1553E-07	1.5657E-07	2.1540E-07
2.9869E-07	4.1677E-07	5.8781E-07	8.3003E-07	1.1751E-06	1.6849E-06	2.4395E-06	3.5833E-06	5.3368E-06	8.0631E-06
1.2285E-05	1.9846E-05	2.9074E-05	4.4556E-05	6.8468E-05	1.0536E-04	1.6304E-04	2.5506E-04	4.0399E-04	6.4754E-04
1.0482E-03	1.7173E-03	2.8741E-03	4.9857E-03	9.2087E-03	1.9339E-02	6.2850E-02	-1.9662E-01	-1.7493E-01	8.2182E-02
3.1425E-02	1.7682E-02	1.1422E-02	1.5707E-02	1.0473E-02	4.8500E-03	1.9143E-03	6.6271E-04	2.0373E-04	3.8832E-04

Table V. (continued)

DH(49,1).....DH(49,60)

-6.0348E-10	6.3437E-10	3.0384E-09	4.2914E-09	3.8629E-09	3.9494E-09	4.6563E-09	5.5994E-09	6.8466E-09	8.3067E-09
1.0331E-08	1.3422E-08	1.7444E-08	2.3111E-08	2.9915E-08	4.0725E-08	5.4439E-08	7.3549E-08	9.9451E-08	1.3845E-07
1.8079E-07	2.6761E-07	3.7059E-07	5.3639E-07	7.6126E-07	1.0947E-06	1.5936E-06	2.3529E-06	3.5083E-06	5.3055E-06
8.1028E-06	1.2416E-05	1.9352E-05	2.9221E-05	4.4749E-05	6.8521E-05	1.0543E-04	1.6378E-04	2.5704E-04	4.0759E-04
6.5089E-04	1.0474E-03	1.7183E-03	2.8482E-03	4.9214E-03	9.0860E-03	1.9263E-02	6.3403E-02	-1.9102E-01	-1.6785E-01
7.8271E-02	2.0327E-02	1.6122E-02	2.1288E-02	1.2593E-02	5.7310E-03	2.2610E-03	7.9430E-04	2.3687E-04	4.4412E-04

DH(50,1).....DH(50,60)

8.3941E-10	5.4239E-10	1.7248E-09	2.8490E-09	2.4046E-09	2.4904E-09	2.9213E-09	3.5356E-09	4.1559E-09	5.2890E-09
6.3942E-09	8.3209E-09	1.0735E-08	1.4505E-08	1.9100E-08	2.5182E-08	3.4581E-08	4.6389E-08	6.4136E-08	8.8095E-08
1.2262E-07	1.7355E-07	2.4423E-07	3.4904E-07	4.9813E-07	7.1967E-07	1.0488E-06	1.5539E-06	2.3238E-06	3.5186E-06
5.3682E-06	8.2183E-06	1.2575E-05	1.9222E-05	2.9291E-05	4.4538E-05	6.8246E-05	1.0514E-04	1.6359E-04	2.5669E-04
4.0501E-04	6.4213E-04	1.0275E-03	1.6666E-03	2.7619E-03	4.7546E-03	8.8121E-03	1.8863E-02	6.2383E-02	-1.8034E-01
-1.5698E-01	7.3541E-02	2.6691E-02	2.7223E-02	1.5389E-02	6.7201E-03	2.6534E-03	9.3036E-04	2.6320E-04	4.7390E-04

DH(51,1).....DH(51,60)

-1.1047E-09	-9.3335E-10	1.3129E-09	1.7551E-09	1.5126E-09	1.5519E-09	1.9413E-09	2.0512E-09	2.7617E-09	3.0525E-09
4.0489E-09	5.2062E-09	6.7145E-09	8.9225E-09	1.2314E-08	1.5791E-08	2.2372E-08	2.9447E-08	4.1549E-08	5.6745E-08
8.1194E-08	1.1126E-07	1.6245E-07	2.2938E-07	3.3373E-07	4.7593E-07	7.0032E-07	1.0393E-06	1.5595E-06	2.3556E-06
3.6029E-06	5.4035E-06	8.4031E-06	1.2785E-05	1.9417E-05	2.9415E-05	4.4705E-05	6.8404E-05	1.0559E-04	1.6410E-04
2.5623E-04	4.0147E-04	6.3291E-04	1.0069E-03	1.6223E-03	2.6743E-03	4.6059E-03	8.5605E-03	1.8249E-02	5.9675E-02
-1.6843E-01	-1.4621E-01	6.7371E-02	4.1496E-02	1.9378E-02	7.9594E-03	3.1087E-03	1.0886E-03	2.8731E-04	4.8973E-04

DH(52,1).....DH(52,60)

1.4761E-10	1.1529E-09	1.7114E-09	1.1520E-09	9.7603E-10	8.9484E-10	1.2629E-09	1.3001E-09	1.7624E-09	1.8978E-09
2.5328E-09	3.1713E-09	4.7244E-09	5.4046E-09	7.9041E-09	1.0149E-08	1.4810E-08	1.8908E-08	2.6932E-08	3.7607E-08
5.3414E-08	7.3879E-08	1.0747E-07	1.5247E-07	2.2149E-07	3.2116E-07	4.6991E-07	7.0120E-07	1.0546E-06	1.5992E-06
2.4343E-06	3.7142E-06	5.6587E-06	8.5885E-06	1.2997E-05	1.9626E-05	2.9656E-05	4.5130E-05	6.9130E-05	1.0667E-04
1.6517E-04	2.5642E-04	3.9375E-04	6.2700E-04	9.9108E-04	1.5881E-03	2.6148E-03	4.4991E-03	8.2646E-03	1.7207E-02
5.6063E-02	-1.5814E-01	-1.3893E-01	9.1088E-02	2.6319E-02	9.5542E-03	3.6787E-03	1.2785E-03	3.1557E-04	5.0439E-04

DH(53,1).....DH(53,60)

-3.4366E-09	-2.7449E-09	6.1203E-10	7.0523E-10	6.0253E-10	6.8635E-10	6.7629E-10	9.9379E-10	1.0375E-09	1.3563E-09
1.4176E-09	2.3784E-09	2.7816E-09	3.7274E-09	4.8909E-09	6.7720E-09	9.5822E-09	1.3259E-08	1.7776E-08	2.4765E-08
3.5479E-08	5.0542E-08	7.3306E-08	1.0459E-07	1.4902E-07	2.1817E-07	3.2195E-07	4.8004E-07	7.2484E-07	1.0911E-06
1.6712E-06	2.5374E-06	3.8509E-06	5.8587E-06	8.8203E-06	1.3283E-05	1.9983E-05	3.0274E-05	4.6116E-05	7.0710E-05
1.0877E-04	1.6757E-04	2.5916E-04	4.0236E-04	6.2750E-04	9.8691E-04	1.5795E-03	2.5959E-03	4.4060E-03	7.8696E-03
1.6151E-02	5.3997E-02	-1.5118E-01	-6.9232E-02	4.2968E-02	1.1666E-02	4.3564E-03	1.5063E-03	3.4636E-04	5.1535E-04

DH(54,1).....DH(54,60)

1.0875E-09	9.6874E-10	2.5820E-10	2.4071E-10	2.3679E-10	2.8291E-10	2.4548E-10	2.8848E-10	3.6212E-10	4.3674E-10
8.5713E-10	7.4494E-10	1.1402E-09	1.2884E-09	2.0928E-09	3.1107E-09	3.7472E-09	5.2192E-09	7.2964E-09	1.0271E-08
1.5181E-08	2.3655E-08	3.0154E-08	4.4547E-08	6.4304E-08	9.1753E-08	1.3887E-07	2.0480E-07	3.0850E-07	4.6374E-07
7.1213E-07	1.0738E-06	1.6393E-06	2.4714E-06	3.7135E-06	5.5596E-06	8.3145E-06	1.2490E-05	1.8861E-05	2.8652E-05
4.3580E-05	6.6454E-05	1.0153E-04	1.5553E-04	2.3877E-04	3.6767E-04	5.7099E-04	8.9707E-04	1.4186E-03	2.2533E-03
3.7195E-03	6.0972E-03	1.7589E-02	-9.0089E-02	-4.0606E-02	2.4252E-02	6.8826E-03	2.2282E-03	4.1874E-04	4.8049E-04

Table V. - (continued)

DH(55,1).....DH(55,60)

-7.0179E-10	-6.1990E-10	3.1103E-11	3.9093E-11	5.8673E-11	4.7223E-11	6.8544E-11	4.3624E-11	1.0786E-10	1.1258E-10
1.2802E-10	1.9155E-10	2.6831E-10	3.2451E-10	5.0147E-10	6.2860E-10	1.0402E-09	1.2225E-09	1.8569E-09	2.5927E-09
3.7867E-09	5.3699E-09	7.8626E-09	1.2913E-08	1.5829E-08	2.3977E-08	3.6856E-08	5.0751E-08	7.8460E-08	1.2442E-07
1.8043E-07	2.8201E-07	4.2503E-07	6.3536E-07	9.5101E-07	1.4182E-06	2.1151E-06	3.1633E-06	4.7581E-06	7.1553E-06
1.9781E-05	1.6322E-05	2.4707E-05	3.7478E-05	5.6933E-05	8.6497E-05	1.3180E-04	2.0136E-04	3.0517E-04	4.5332E-04
6.6897E-04	1.0059E-03	1.5109E-03	1.3661E-02	-6.7271E-02	-2.5223E-02	1.6378E-02	3.9893E-03	5.5806E-04	3.9540E-04

DH(56,1).....DH(56,60)

6.1633E-10	5.4469E-10	-2.2532E-11	8.0413E-12	2.8136E-12	3.9779E-12	2.0674E-11	5.9460E-12	1.1231E-11	7.6879E-12
7.5856E-11	1.6954E-11	5.8148E-11	2.0633E-11	9.5083E-11	8.8955E-11	2.2757E-10	2.1906E-10	3.4016E-10	4.9704E-10
6.6310E-10	8.9076E-10	1.4509E-09	2.1062E-09	2.7766E-09	4.2985E-09	7.5556E-09	9.1205E-09	1.5525E-08	2.0436E-08
3.5997E-08	5.1627E-08	7.6037E-08	1.1928E-07	1.7512E-07	2.6547E-07	4.0019E-07	5.9034E-07	8.9159E-07	1.3605E-06
2.0497E-06	3.1050E-06	4.7311E-06	7.2142E-06	1.0986E-05	1.6780E-05	2.5655E-05	3.9233E-05	5.9307E-05	8.7429E-05
1.2700E-04	1.8561E-04	2.6520E-04	1.5737E-03	9.7073E-03	-5.0076E-02	-1.2362E-02	1.0286E-02	9.1322E-04	3.3936E-04

DH(57,1).....DH(57,60)

-1.0374E-09	-9.1668E-10	3.8387E-11	-9.0107E-13	-3.1319E-13	4.7227E-13	-4.5856E-13	6.6496E-13	-5.7933E-13	8.9519E-13
4.6680E-12	1.5529E-13	4.5120E-13	8.0959E-12	7.9943E-12	8.3131E-13	5.8217E-11	1.5725E-11	3.4409E-11	2.2924E-11
5.2397E-11	5.4758E-11	2.4031E-10	1.1062E-10	2.4923E-10	3.7827E-10	4.9465E-10	7.7040E-10	1.2445E-09	1.6449E-09
3.2880E-09	4.1211E-09	9.9406E-09	9.6245E-09	1.9206E-08	2.5749E-08	3.7336E-08	5.6958E-08	9.5447E-08	1.3615E-07
2.1133E-07	3.3008E-07	5.0743E-07	7.9548E-07	1.2373E-06	1.9181E-06	2.9812E-06	4.6371E-06	7.1125E-06	1.0535E-05
1.5330E-05	2.2342E-05	3.1682E-05	1.7810E-04	7.2041E-04	5.8976E-03	-2.8470E-02	-2.7605E-03	2.3943E-03	4.0170E-04

DH(58,1).....DH(58,60)

6.1840E-10	5.4351E-10	-2.4255E-11	5.9528E-13	3.6142E-13	-4.2554E-13	5.0440E-13	-5.7472E-13	6.6029E-13	-7.3930E-13
8.5387E-13	-9.5133E-13	1.1067E-12	-1.2247E-12	1.4246E-12	-1.5635E-12	1.8589E-12	-1.9818E-12	2.4026E-12	-2.4876E-12
3.1582E-12	-3.0851E-12	2.8549E-11	-8.4511E-12	1.1915E-11	-1.0320E-11	1.0199E-10	-2.8035E-11	3.8931E-11	3.8143E-11
4.2514E-11	7.8417E-11	1.6918E-10	4.1477E-10	2.1366E-10	8.2388E-10	1.4875E-09	1.5958E-09	2.8378E-09	3.8683E-09
6.6113E-09	1.1436E-08	1.6250E-08	2.7714E-08	4.3384E-08	6.9240E-08	1.1196E-07	1.7558E-07	2.7216E-07	4.0789E-07
5.8766E-07	8.4302E-07	1.1856E-06	6.3325E-06	2.2976E-05	1.1140E-04	1.2032E-03	-9.9584E-03	-8.4499E-04	1.4990E-03

DH(59,1).....DH(59,60)

4.0054E-04	3.4891E-04	-1.9216E-05	4.7973E-07	1.3815E-07	-1.7671E-07	2.1258E-07	-2.4514E-07	2.8173E-07	-3.1597E-07
3.6511E-07	-4.0666E-07	4.7430E-07	-5.2564E-07	6.1004E-07	-6.7261E-07	7.9956E-07	-8.6036E-07	1.0347E-06	-1.0948E-06
1.3525E-06	-1.3954E-06	1.7587E-06	-1.7742E-06	2.2887E-06	-2.2899E-06	2.9876E-06	-3.0211E-06	3.8949E-06	-3.9821E-06
4.9258E-06	-5.0569E-06	5.9127E-06	-6.0797E-06	6.6610E-06	-6.9574E-06	7.0427E-06	-7.7730E-06	6.9674E-06	-8.6572E-06
6.3139E-06	-9.3472E-06	5.0065E-06	-9.1048E-06	3.8146E-06	-7.7462E-06	2.9928E-06	-5.3763E-06	2.5943E-06	-2.6959E-06
2.4451E-06	-6.0219E-07	2.5571E-06	2.1780E-06	7.4893E-06	9.2005E-06	1.5370E-05	5.7831E-04	-2.2695E-03	8.8084E-07

arrays H ZERO (L) and To(K) and the matrix DH(L, K) were established it was trivial to calculate CO_2 (15μ bands) cooling rates for each new temperature profile, T(K), by means of Equation (F. 9).

APPENDIX G

GLOBAL MODEL RESPONSE CHARACTERISTICS

G.1 INTRODUCTION

In Chapter 3 an equilibrium mean thermal state was formulated as a balance of the heating/cooling rates, the heat flux at the upper boundary, an earth average temperature profile, and parameterized eddy transport. Several of the thermal inputs were varied, as a means of representing the uncertainties in those quantities, and the new equilibrium states were calculated in terms of new total heating rates and equilibrium eddy transport for a fixed temperature profile.

In this appendix we consider the unsteady response of the thermal model to idealized perturbations or variations of the thermal inputs. The basic global thermal model was adopted including the heating/cooling rates, equilibrium eddy transport, and earth average temperature profile, as the initial condition. The time dependent numerical formulation of the energy equation, described in Appendix A, was used to examine the unsteady temperature profile. In general if one adds a localized heat source, for example, to the mean thermal model the temperature profile will reflect the approach in time to a new equilibrium state.

The temporal response and new equilibrium state are indicative of the influence of changes in the basic physical processes on the structure of the mesosphere and lower thermosphere on a global scale. These response characteristics are quite different in nature from those which apply to limited geographical regions. In the latter case localized heat sources give rise to circulation systems which redistribute the

heat over much larger areas. On the global scale such a heat source is localized only in the vertical dimension and acts uniformly over the entire earth, thus having a significant effect on the thermal model. Hopefully, the results will be useful in estimating the effects of including in the thermal model either processes not considered, or variations in the thermal inputs (heating/cooling rates, heat fluxes, or thermal transport) which were considered. An example might be the inclusion of gravity wave dissipation globally (as discussed in Chapter 3) if further studies should show wide spread evidence of this process in the mesosphere and lower thermosphere.

In order to better unify the results, the following practices were adopted: all perturbations originating inside the region of interest 50 Km $\leq$ z $\leq$ 120 Km, were applied at the pressure levels nearest 70 Km, 85 Km, and 100 Km; and a 'temperature perturbation factor' was defined as the ratio of temperature difference from equilibrium to either the magnitude or the maximum of the perturbation process.

G.2 TEMPERATURE PERTURBATION

Consider a perturbation in the mean thermal state consisting of an instantaneous excursion of the temperature profile. Such an excursion might be the result of impulsive heating, or of the passage of a single wave. The temperature excursion modelled was a Gaussian of form:

$$T = T(equil) + \Delta_{max} \exp\left\{ - \left(\frac{z - z_0}{2} \right)^2 \right\} \qquad (G.1)$$

Where Δ_{max} was the maximum of the perturbation, z_o was one of the three selected levels, and 2 Km was the e-folding distance for the profile. The temperature perturbation factor used was:

$$(TPF) = \frac{T - T(equil)}{\Delta_{max}} \qquad (G.2)$$

The values of Δ_{max} used in the study were: 5^oK, 10^oK, 20^oK, 50^oK.

In Figures G-1, G-2, and G-3 are shown typical response curves for the levels 70, 85, and 100 Km respectively, for $\Delta_{max}=10^oK$. The response is quite linear, in that (TPF) is approximately independent of Δ_{max}. The damping out of the temperature spike is accomplished predominantly through the resulting perturbation of the heat flux. In Figure G-4 a region near 70 Km is shown with the heat flux both for the equilibrium and perturbation temperature profiles; the latter is plotted at the left. As indicated at the right the instantaneous perturbation heat flux is such that its vertical derivative acts to cool the temperature spike itself and heat the adjoining levels. This results directly in smoothing the temperature profile. To a lesser extent the CO_2(15μ bands) cooling rate also contributes to the damping process.

Figure G-5 shows the decay of the perturbation in terms of (TPF) at z_o for each of the z_o's, at both extremes of Δ_{max}. Although the decay curves are not pure exponentials it is still reasonable to consider the e^{-1} points as approximate time constants. These are shown as the solid circles at the intersections of the decay curves and the e^{-1} line. They range from just over 8 hours for $\Delta_{max}=5^oK$ at $z_o=100$ Km

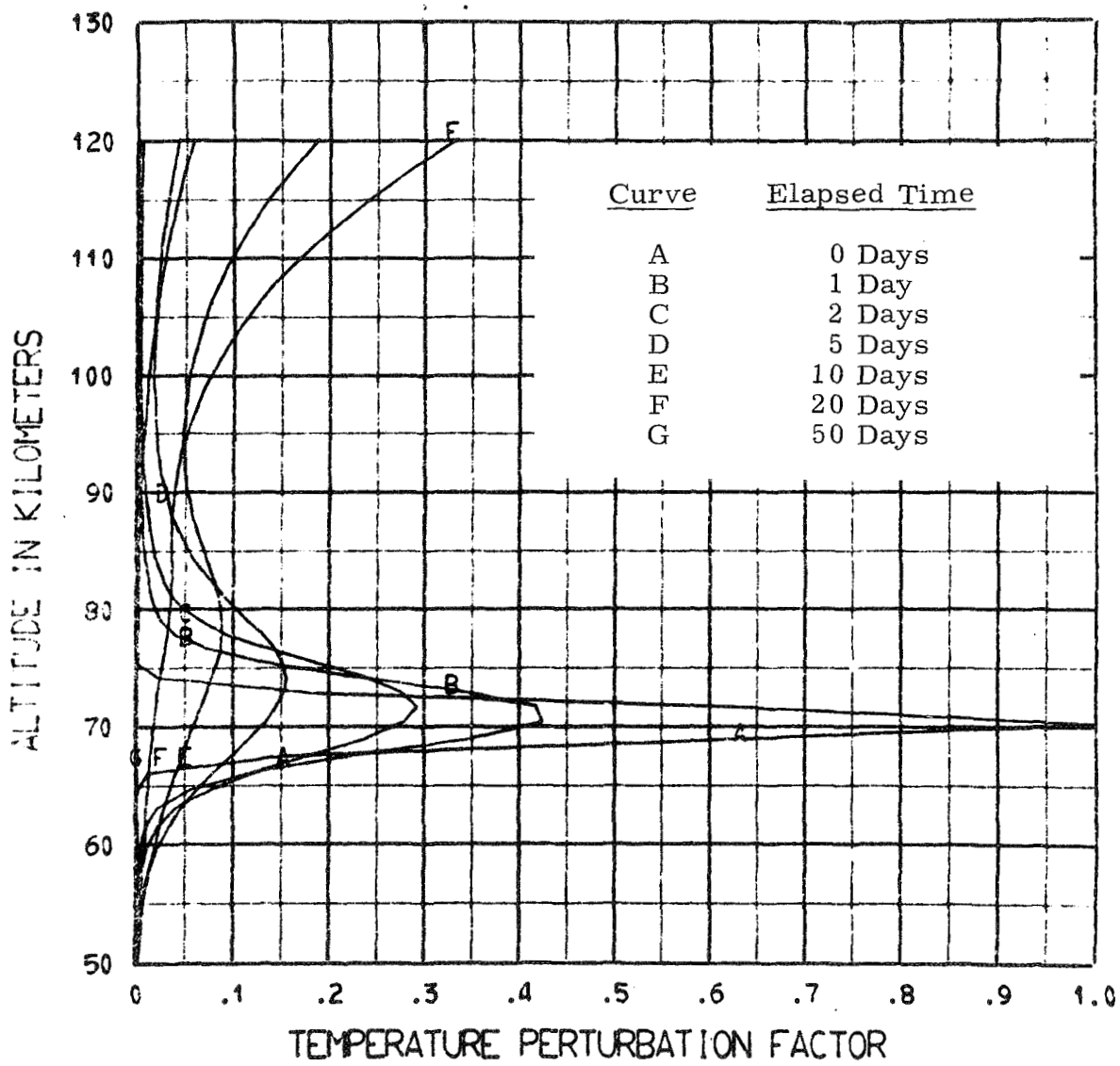

Figure G-1. Response to an instantaneous temperature perturbation at 70 Km. ; $\Delta_{max}=10^{o}K$

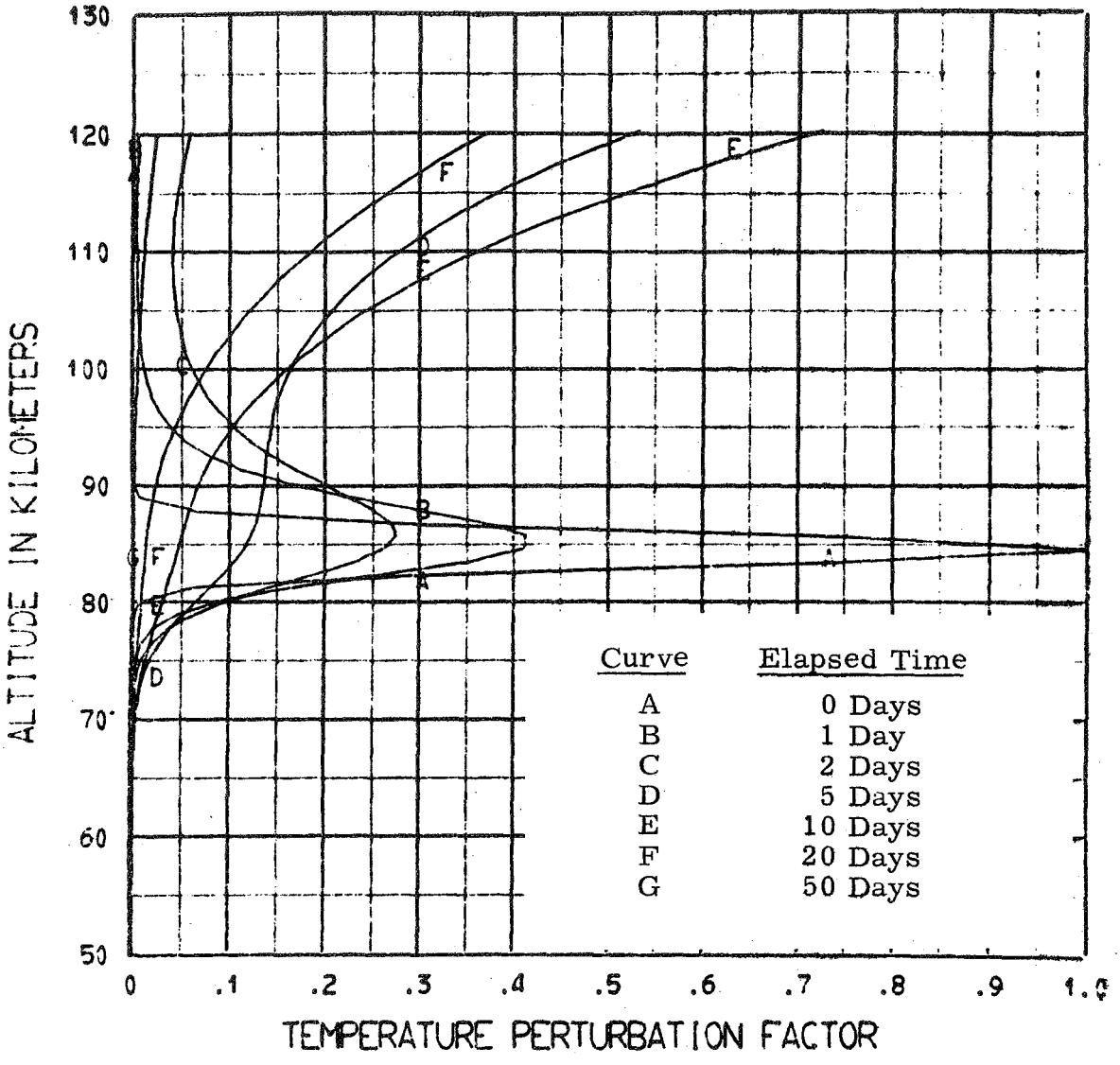

Figure G-2. Response to an instanteous temperature perturbation at 85 Km. ; $\Delta_{max} = 10^{o}K$

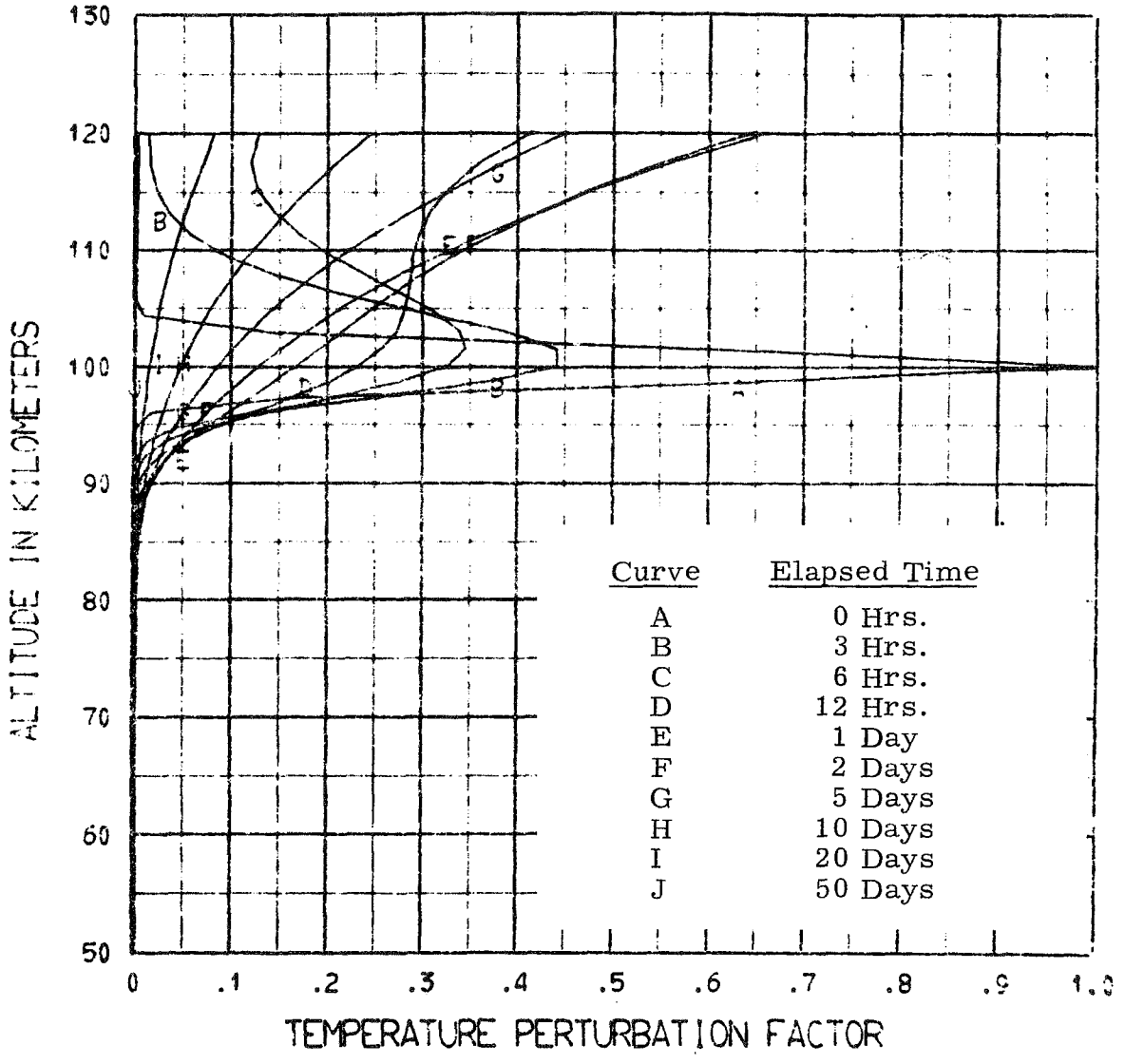

Figure G-3. Response to an instantaneous temperature perturbation at 100 Km; $\Delta_{max}=10^{0}K$

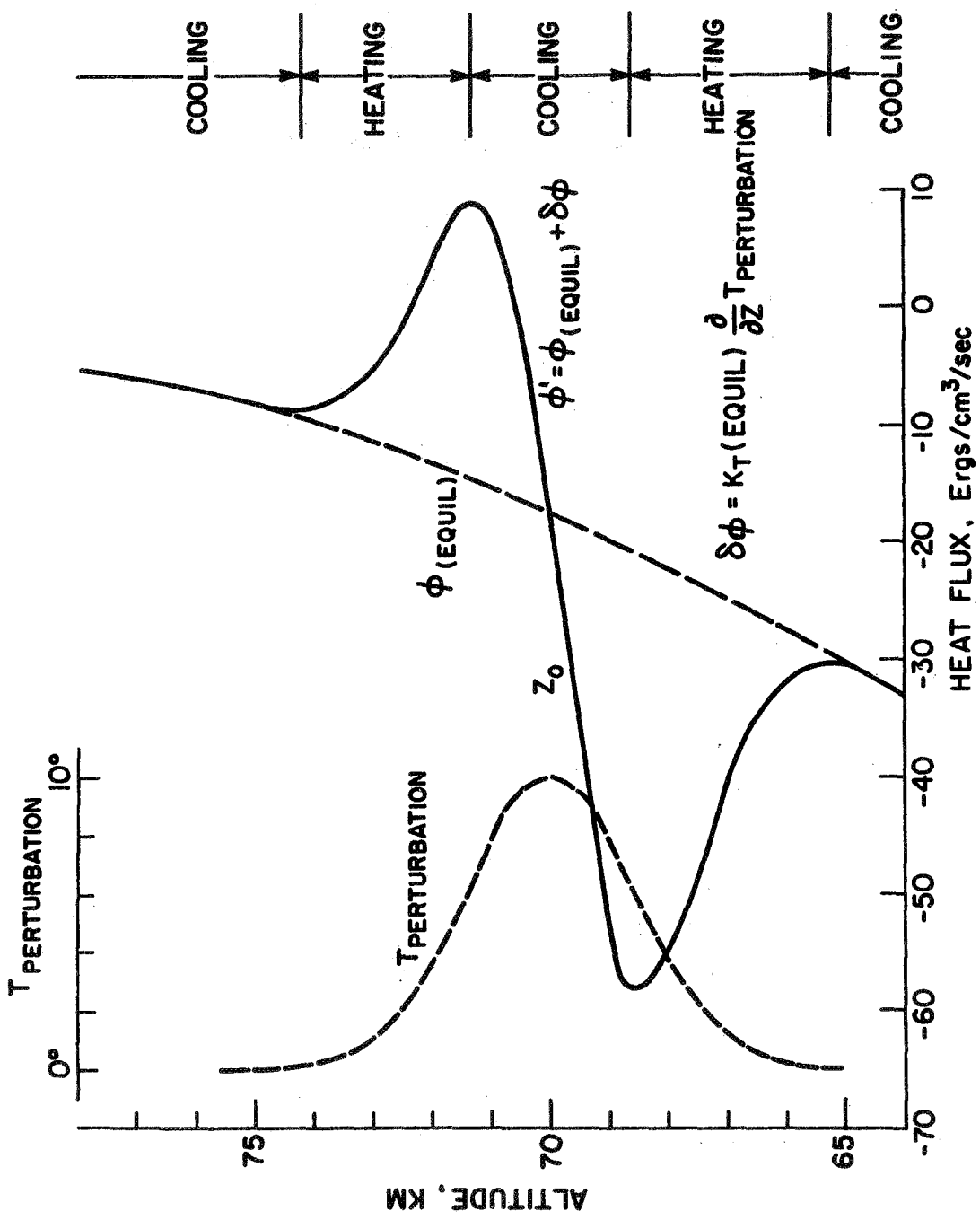

Figure G-4. Typical temperature perturbation used, corresponding perturbation in the heat flux, and resulting regions of heating and cooling

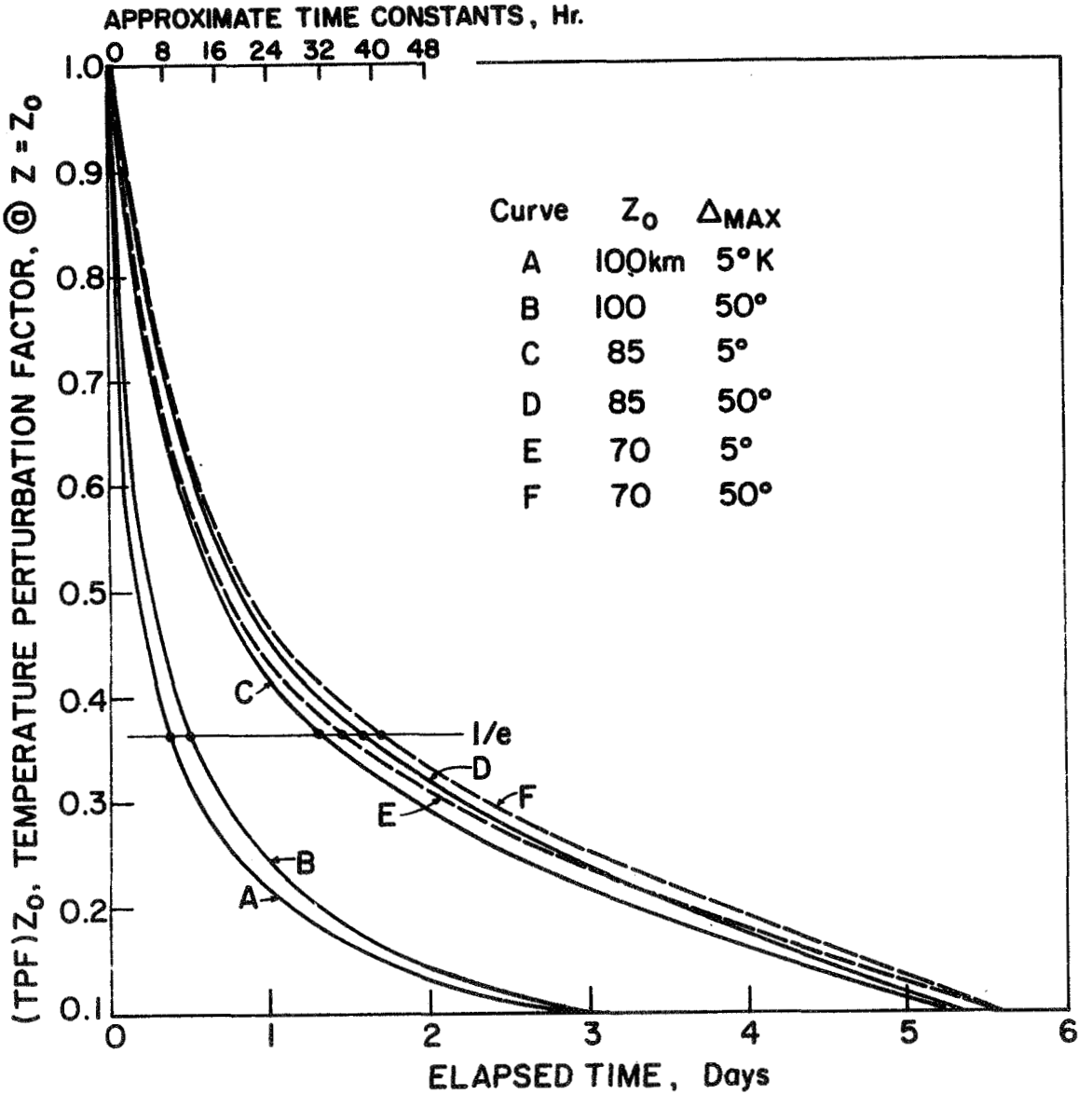

Figure G-5. Rate of decay of temperature perturbations at the initial maxima points and approximate time constants

to a maximum of just over 40 hours for Δ_{max} =50°K at z_o=70 Km. Again one observes that the lower thermosphere is far more flux dominated, hence more responsive, than the mesosphere.

G. 3 HEATING PERTURBATION

Perhaps the most intuitively obvious perturbation is an isolated heat source considered constant in time. Heat sources were modeled by the same Gaussian function as described above; thus the total heating rate became:

$$Q_{TOTAL} = Q_{TOTAL}(equil) + \Delta_{max} \exp\left\{-\left(\frac{z-z_o}{z}\right)^2\right\} \qquad \text{(G. 3)}$$

Typical results are shown in Figures G-6, G-7, and G-8 for z_o= 70 Km, 85 Km, and 100 Km, respectively, with (TPF) as given in Equation (G. 2) and Δ_{max}= 10°K/day. The following are some general observations: as the temperature rises locally the height levels increase, notice for example that pressure height level z_o rises a few kilometers in the span of 100 days; the very large temperature increase in the lower thermosphere reflects both the upward heat flux (or reduced downward heat flux) from the perturbation source and the decrease of the heat capacity of the atmosphere with altitude; and that on the order of 50 to 100 days are required to reach a new equilibrium state. The model response to the heating perturbation is roughly linear as shown in Figure G-9. In this figure are plotted the equilibrium values of (TPF) for each of the z_o's as functions of Δ_{max}.

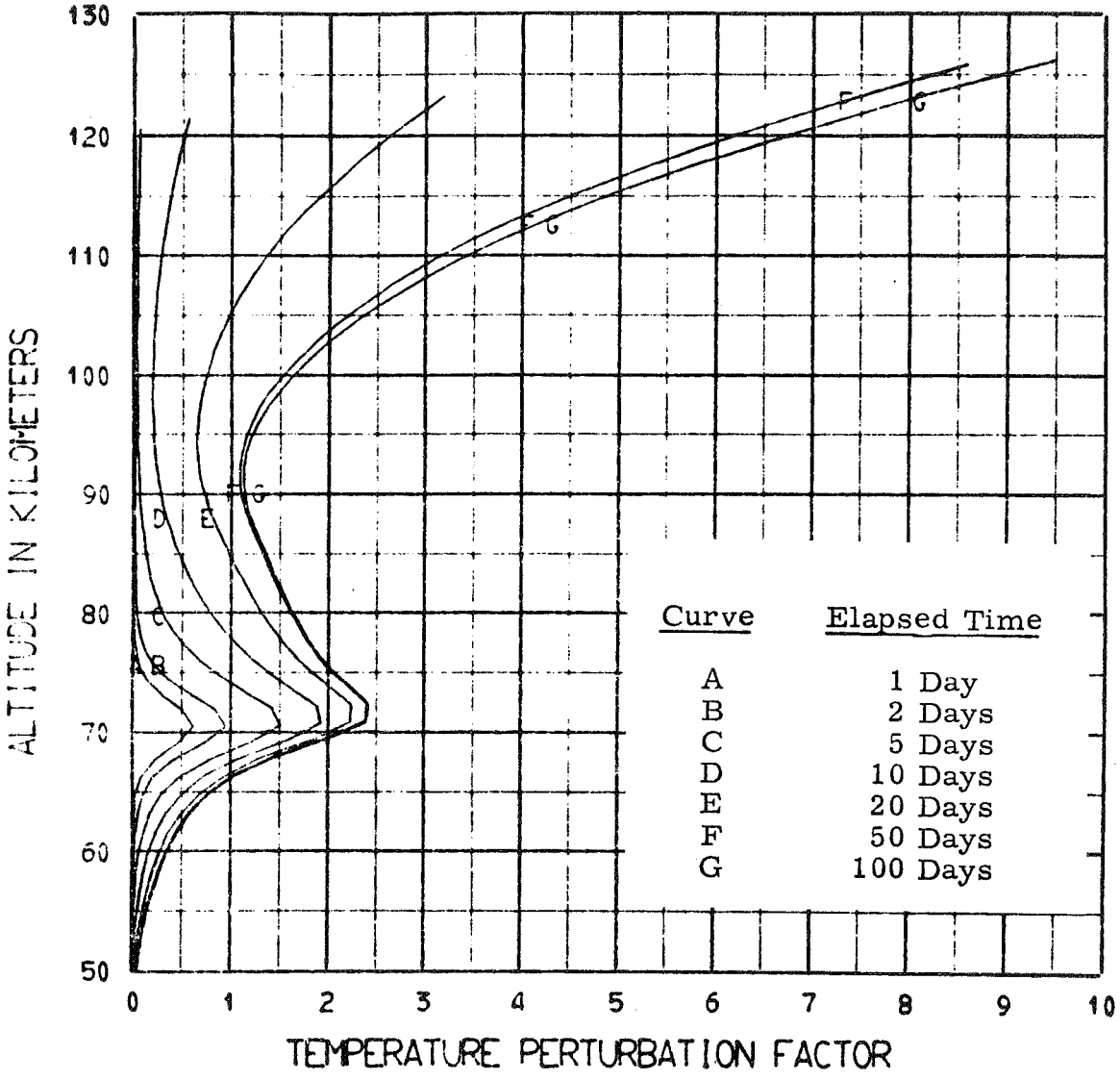

Figure G-6. Approach to new equilibrium temperature profile in response to heating perturbation at 70 Km; Δ_{max}= 10°K/day

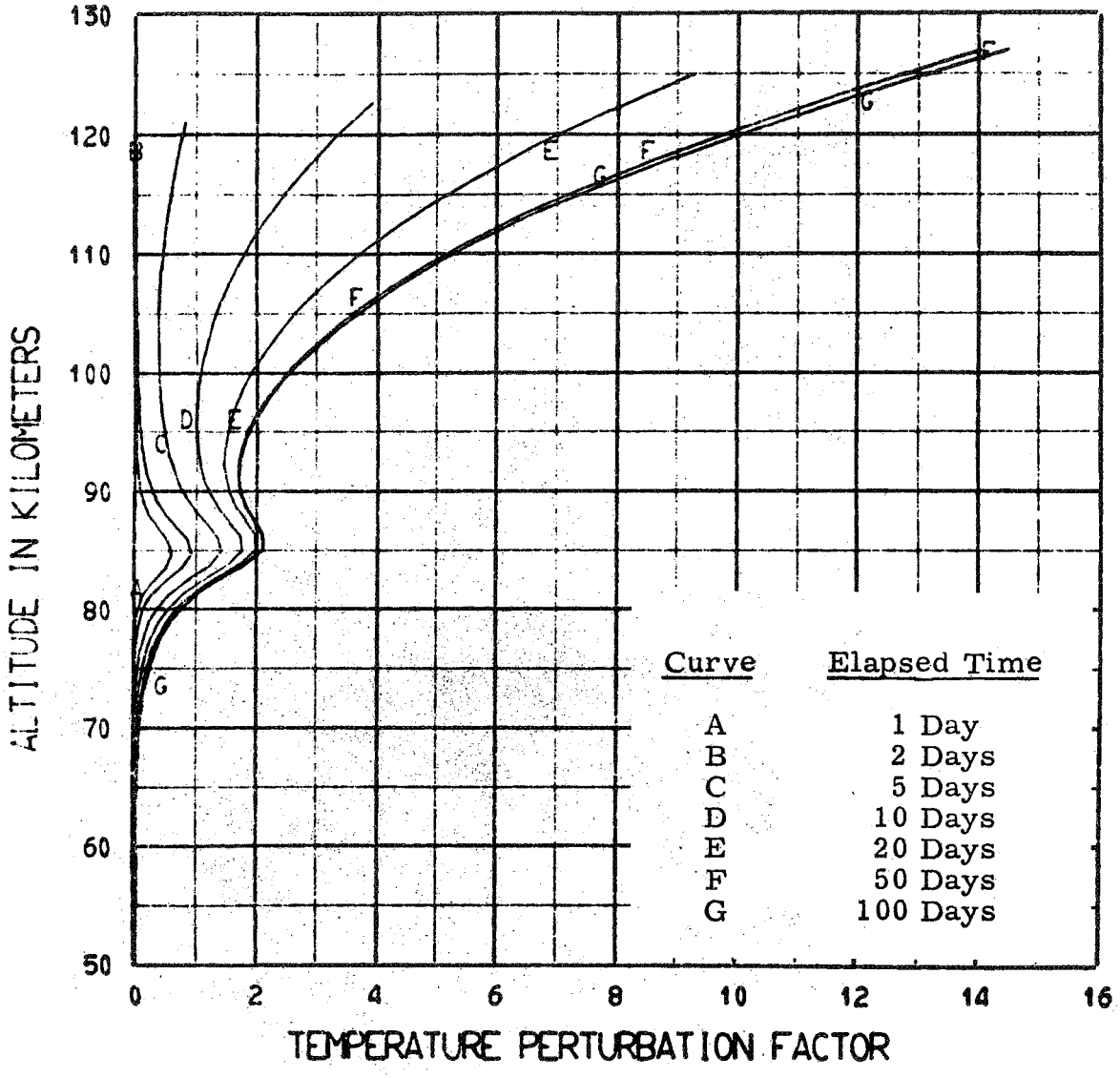

Figure G-7. Approach to new equilibrium temperature profile in response to heating perturbation at 85 Km; Δ_{max} = 10°K/day

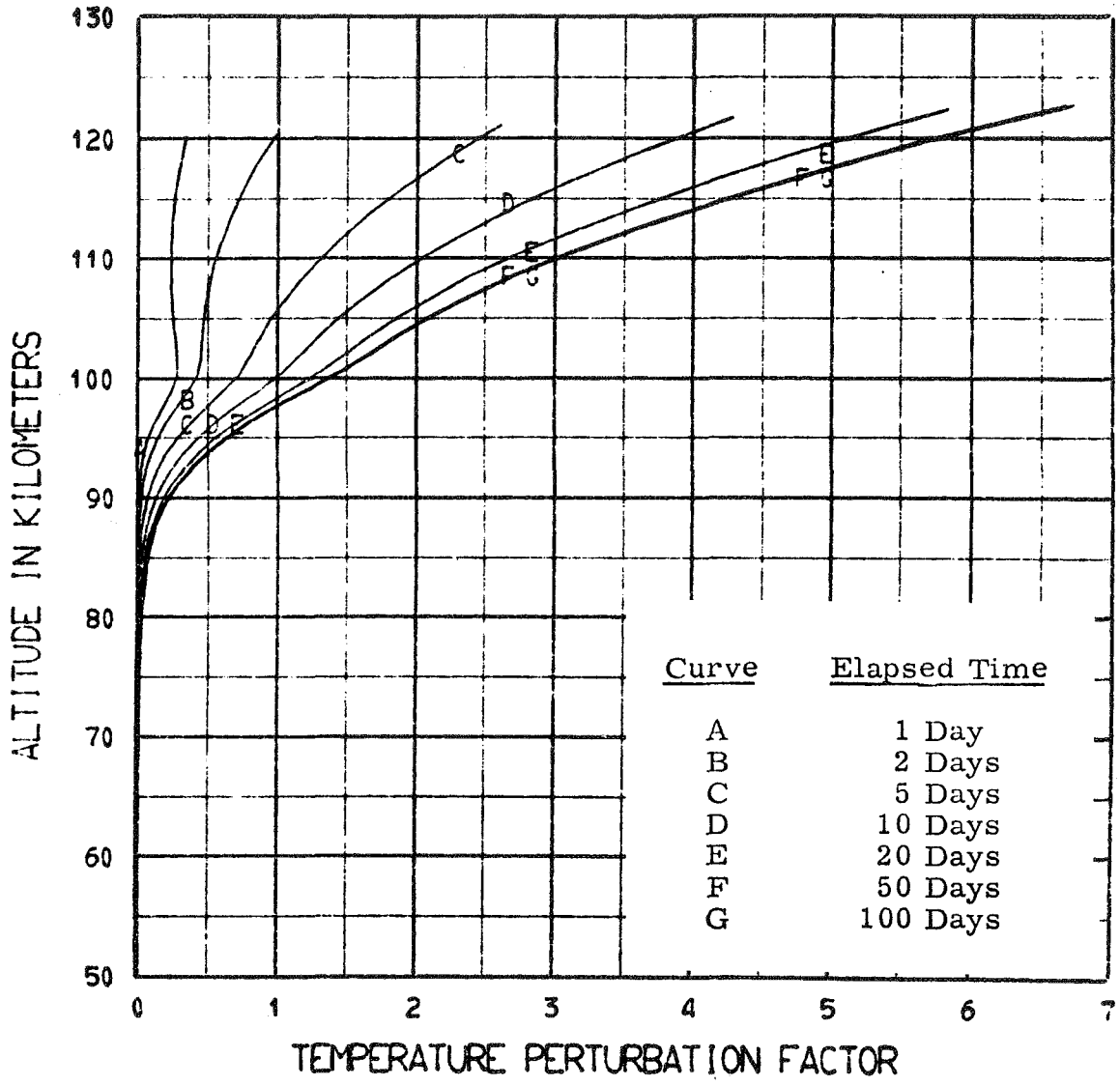

Figure G-8. Approach to new equilibrium temperature profile in response to heating perturbation at 100 km; $\Delta_{max.}=10^{o}K/day$

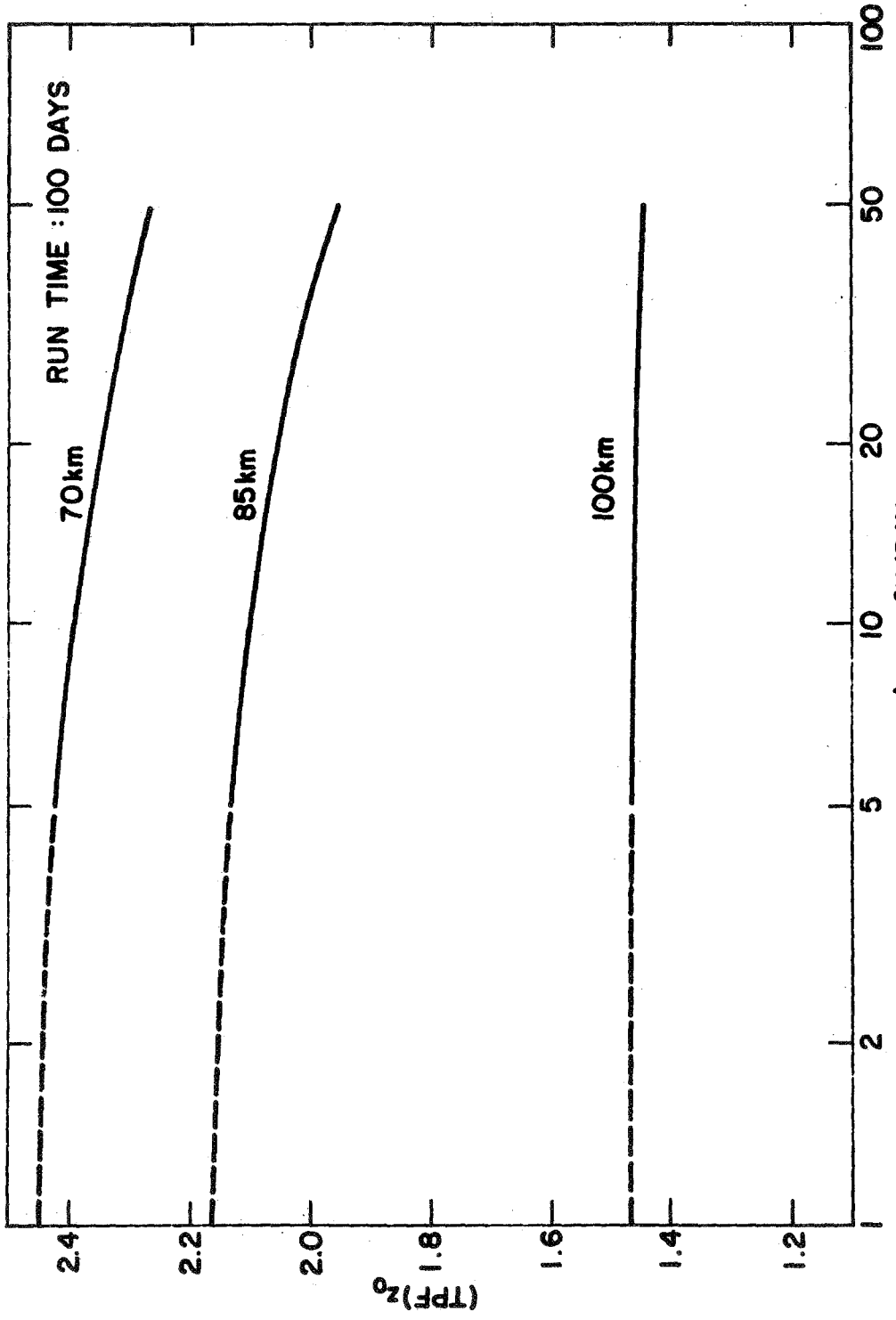

Figure G-9. Comparison of (TPF) at z_o after 100 days of heating perturbation for the values of z_o and Δ_{max} considered

G.4 STABLE LAYER-EDDY TRANSPORT DECREASE

Consider the consequence of a diminished eddy transport caused, for example, by a specific damping process or cessation of generation of the small scale random motions in a particular region. Such a process acts like a valve for the heat flux, which approximates a heat source above in conjunction with a heat sink below. The perturbed eddy thermal conductivity profile used was the following:

$$\tilde{K}_T = \tilde{K}_T(equil) \left\{ \frac{1}{1 + C_{max} \exp\left[-\left(\frac{z - z_o}{2} \right)^2 \right]} \right\} \qquad (G.4)$$

Here C_{max} was taken to be $(\Delta_{max} - 1)$ with $\Delta_{max} = 2,\ 5,\ 10,$ and 20. The expression in the denominator is just one plus the Gaussian considered above.

The results for $\Delta_{max} = 5$ are shown in Figures G-10, G-11, and G-12 for $z_o = 70,\ 85,$ and 100 Km respectively. As anticipated the response and new equilibrium states are similar to the superposition of a heat source just above and a heat sink just below the eddy transport minimum, by comparison with the results of the previous section. The results for the different values of Δ_{max} used will be discussed in the next section.

G.5 STRONG MIXING LAYER-EDDY TRANSPORT INCREASE

If a condition were to exist in which energy were to cascade downward from larger scale ordered motion to smaller scale random motion, as might arise from a specific dissipation mechanism, for example, an increase in the local eddy transport would result. The

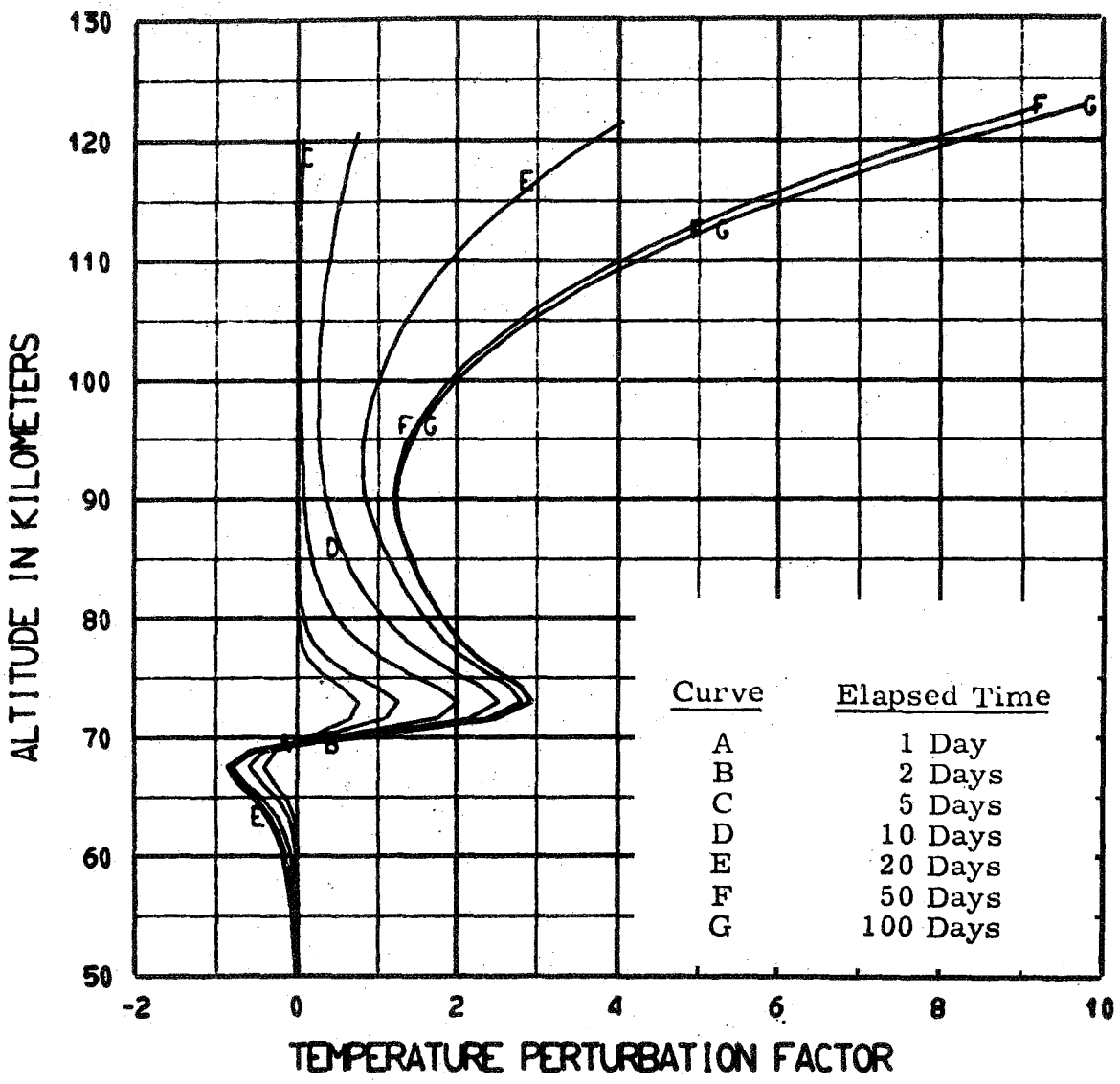

Figure G-10. Approach to new equilibrium temperature profile in response to eddy transport decrease (perturbation) at 70 Km; Δ_{max} =5

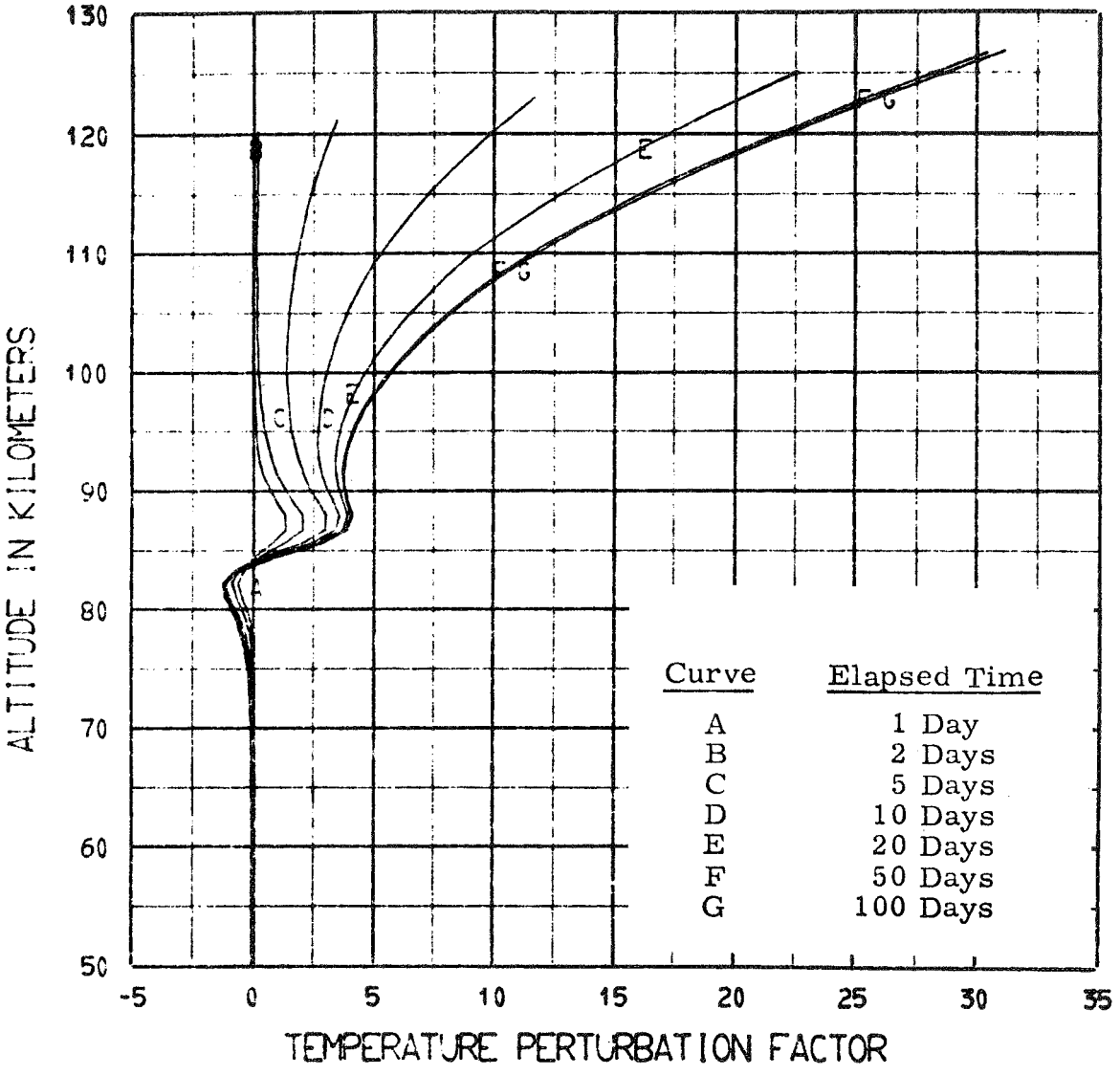

Figure G-11. Approach to new equilibrium temperature profile in response to eddy transport decrease (perturbation) at 85 Km; $\Delta_{max} = 5$

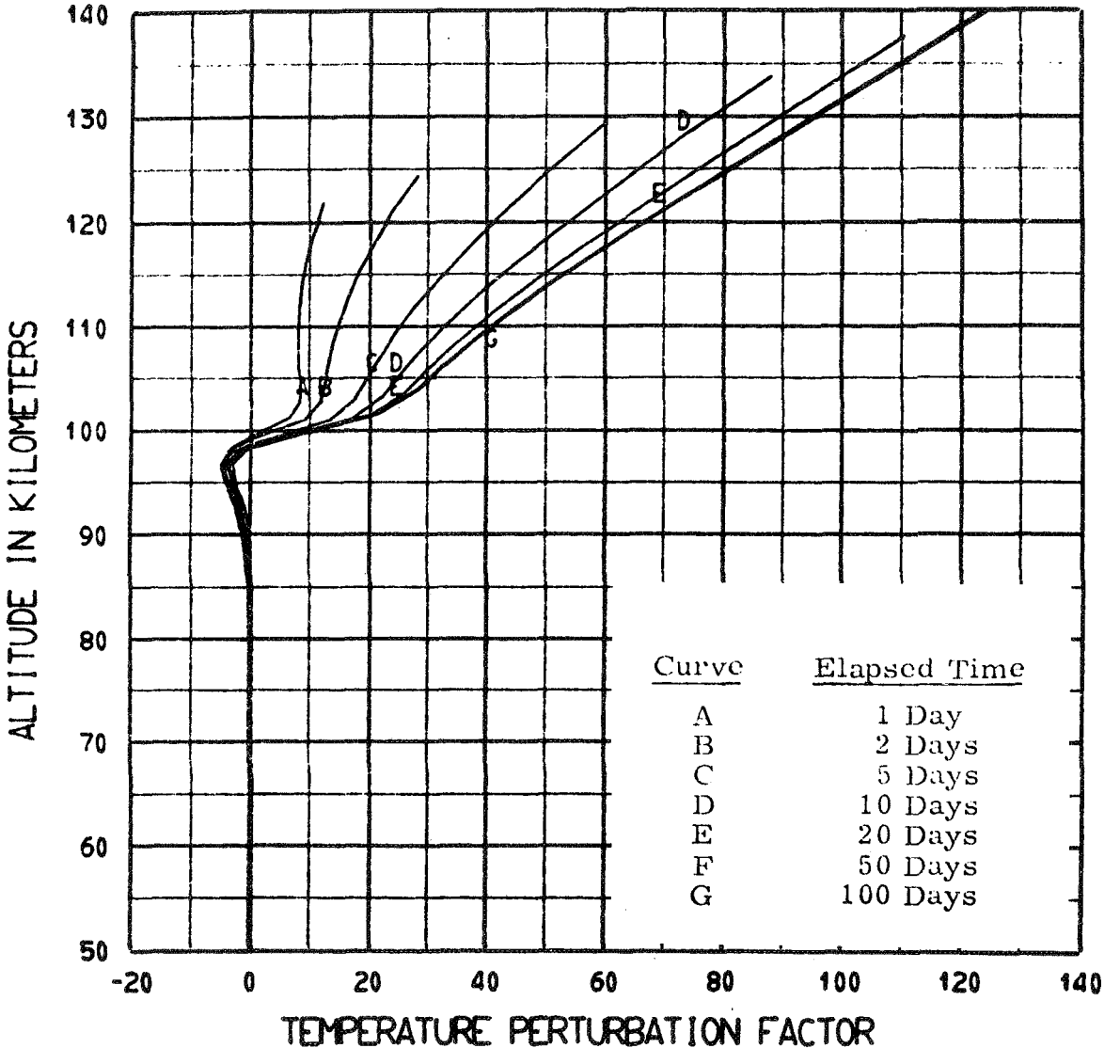

Figure G-12. Approach to new equilibrium temperature profile in response to eddy transport decrease (perturbation) at 100 Km; $\Delta_{max} = 5$

following expression was used to model such an increase in the eddy thermal conductivity:

$$\tilde{K}_T = \tilde{K}_T(equil) + \tilde{K}_T(z_o)\ \frac{\Delta_{max}}{10}\ exp\left[-\left(\frac{z-z_o}{2}\right)^2\right] \qquad (G.5)$$

where $\tilde{K}_T(z_o)$ is the value of $\tilde{K}_T$(equil) at one of the three reference levels, z_o, and Δ_{max}= 5, 10, 20, and 50.

In Figures G-13, G-14, and G-15 the results for z_o= 70, 85, and 100 Km respectively are given for Δ_{max}= 10. These results are qualitatively the mirror image of those discussed above for decreased eddy transport, reflecting again the basic linearity of the model. An overall comparison of both eddy transport perturbations is given in Figure G-16 where (TPF) at the upper boundary (initially 120 Km) is plotted against Δ_{max} for an elapsed time of 100 days. At both 70 Km and 85 Km the relative response is approximately twice as great for the positive perturbation as for the negative. The opposite results occur, however, at 100 Km, undoubtedly the results of the model's greater sensitivity to transport above the mesopause.

G. 6 HEAT FLUX VARIATIONS AT 120 KM

Any changes which might take place in the energy balance of the upper thermosphere ($z > 120$ Km) would appear as variations in the heat flux at 120 Km in the thermal model under consideration. In order to examine the effect of such variations the following expression for the perturbed heat flux was used:

$$\Phi_{TOTAL}^{(120)} = \Phi_{TOTAL}^{(120,\,equil)}\left\{1 + \frac{\Delta_{max}}{100}\right\} \qquad (G.6)$$

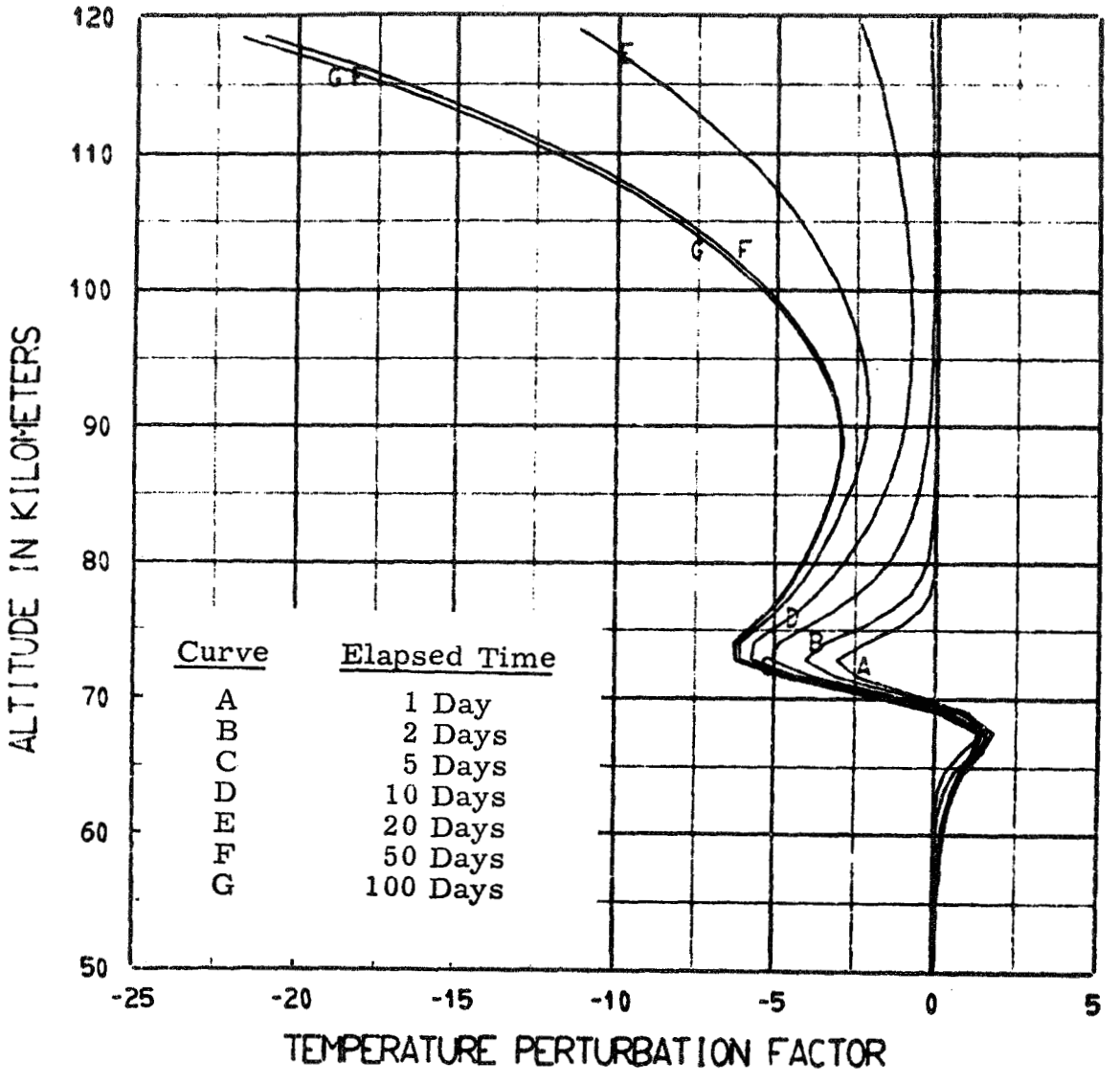

Figure G-13. Approach to new equilibrium temperature profile in response to eddy transport increase (perturbation) at 70 Km; $\Delta_{max}=10$

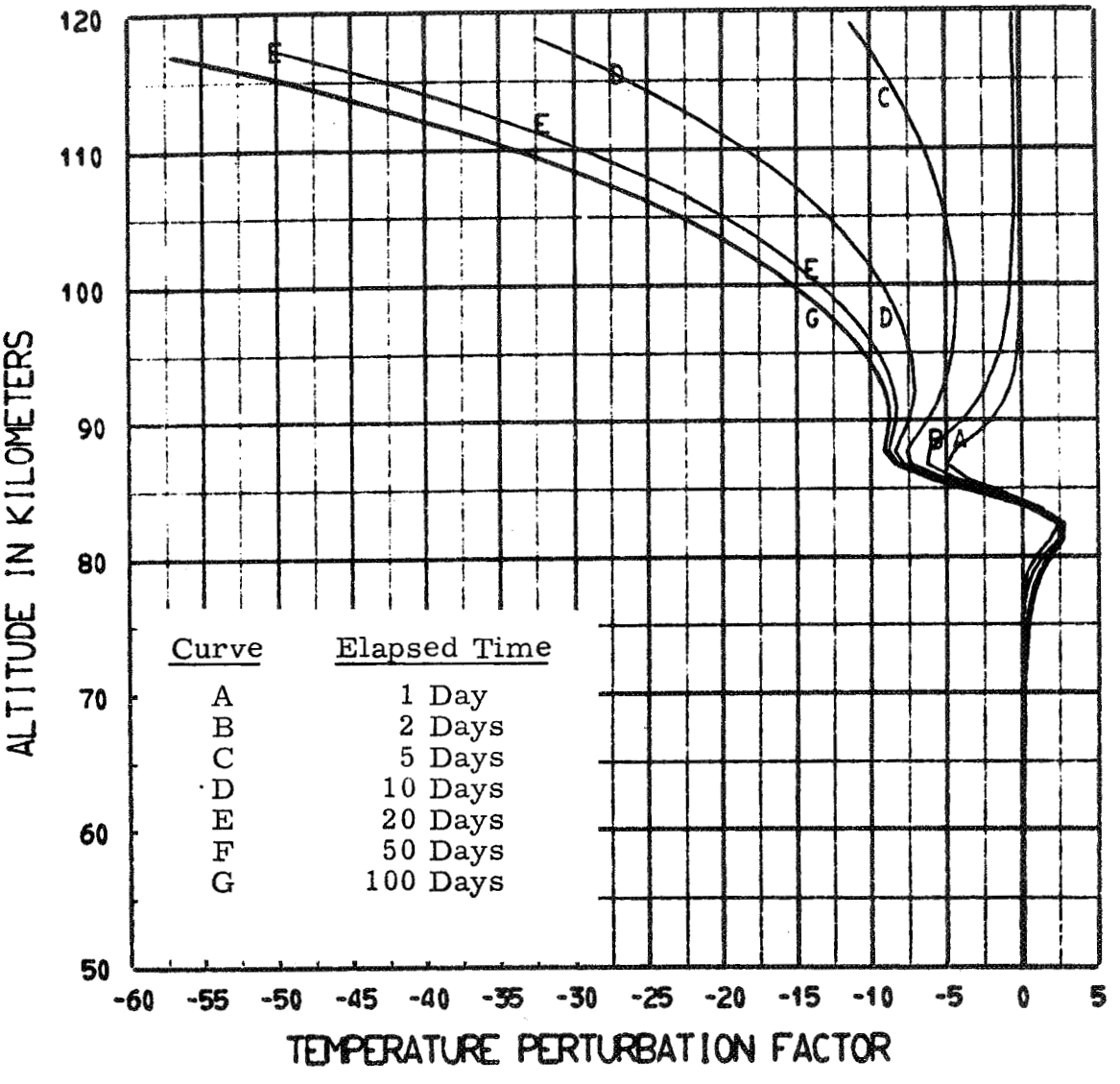

Figure G-14. Approach to new equilibrium temperature profile in response to eddy transport increase (perturbation) at 85 Km; $\Delta_{max}=10$

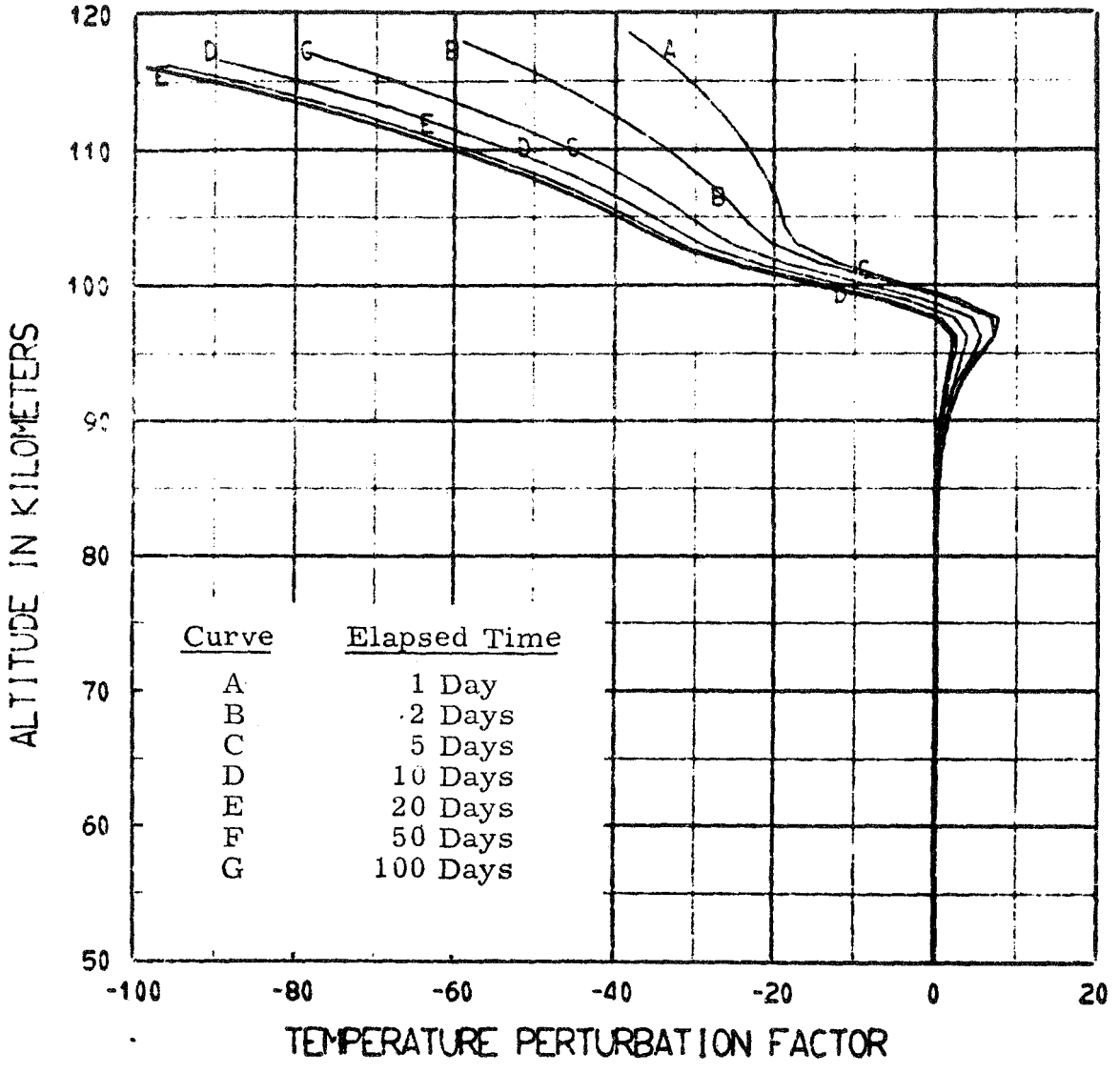

Figure G-15. Approach to new equilibrium temperature profile in response to eddy transport increase (perturbation) at 100 Km; $\Delta_{max} = 10$

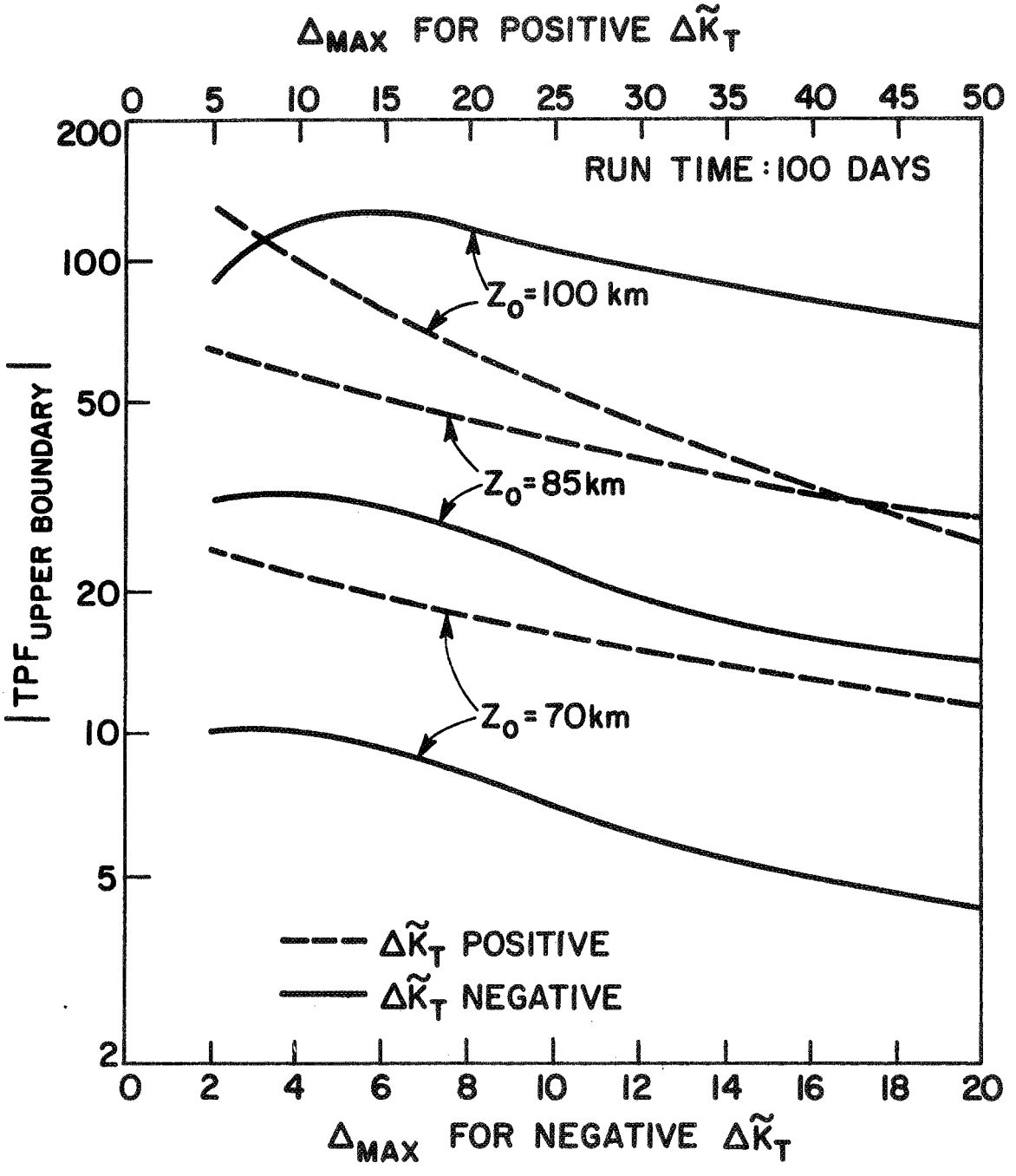

Figure G-16. Comparison of (TPF) at upper boundary after 100 days, for both increase and decrease-type eddy transport perturbations for the values z_o and Δ_{max} considered.

where Δ_{max} = -20, -10, -5, +5, +10, and +20.

The results for Δ_{max} = -20 and Δ_{max} = +20 are shown in Figures G-17 and G-18, respectively and are indicative of those for the other values of Δ_{max} considered. Each of the (TPF) curves show a continuous decrease from the upper boundary (initially at 120 Km) down to about the mesopause with the actual temperature increasing for $\Delta_{max} > 0$ and decreasing for $\Delta_{max} < 0$. The model response is qualitatively similar to that obtained for the heating perturbation at 100 Km (Figure G-8). This tends to substantiate the assertion, made in the discussion on the dissipation of tidal oscillations (Chapter 2). The assertion being that it makes little difference in the adopted mean thermal model whether the dissipation heating which might take place between about 100 and 120 Km is considered an in situ heat source or is lumped into a downward heat flux at 120 Km. The overall results are summarized in Figure G-19 where (TPF) is plotted against Δ_{max} for several pressure height levels, for an elapsed time of 100 days.

G. 7 QUASI-DIURNAL STUDY

It has been widely assumed that the 120 Km level undergoes no diurnal temperature variation, and often such an assumption is used as a boundary condition for modeling the upper thermosphere. Because of this it was decided to examine this assumption through the time dependent thermal model for earth average conditions. The only parameter which was made to undergo a diurnal variation was the solar heating rate. The heat flux at 120 Km was held constant since a rough calculation indicated a period of about a half day was needed to transport heat vertically one scale height at 120 Km, and the major contributor

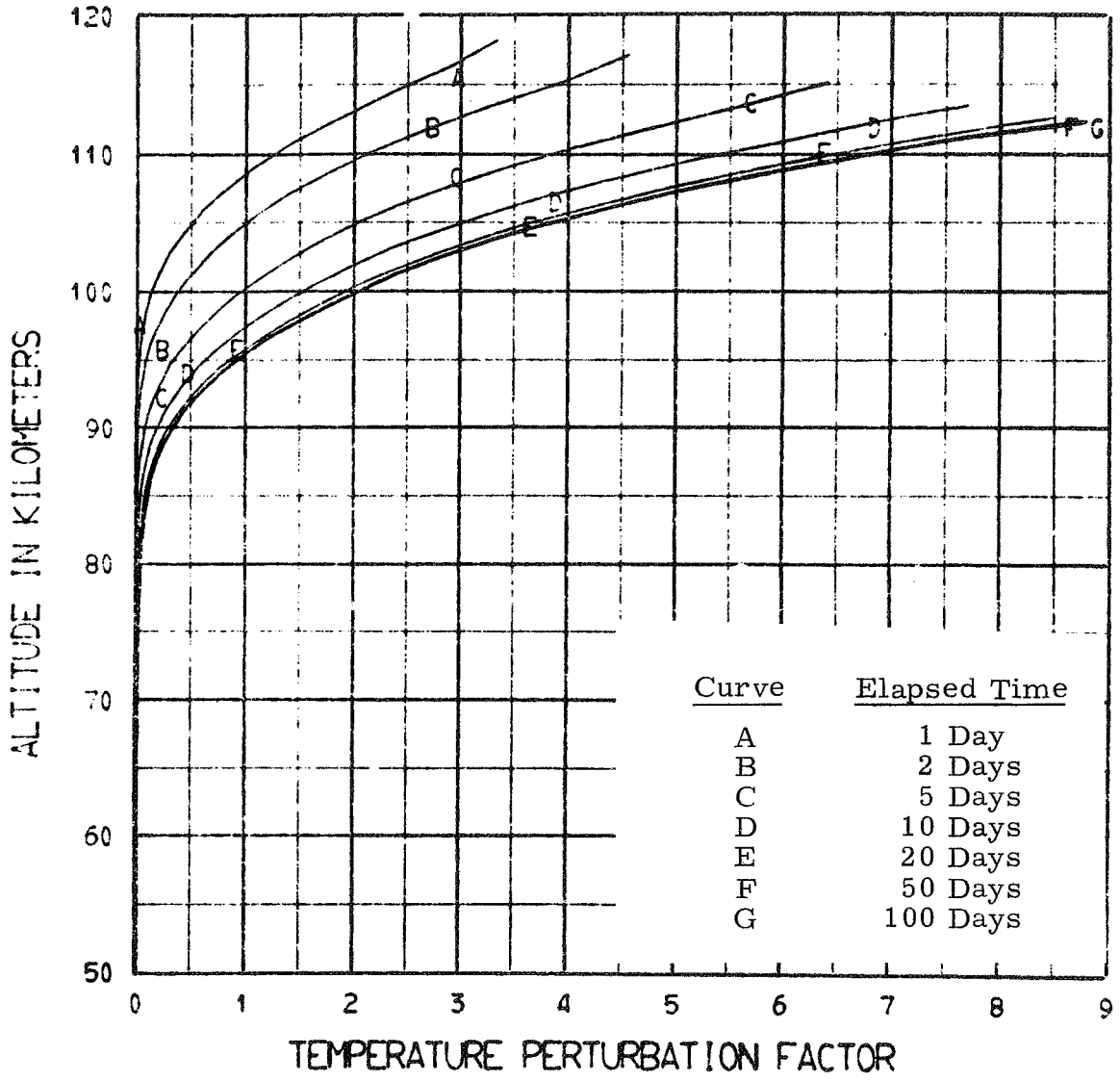

Figure G-17. Approach to new equilibrium temperature profile in response to upper boundary heat flux perturbation; $\Delta_{max} = -20$

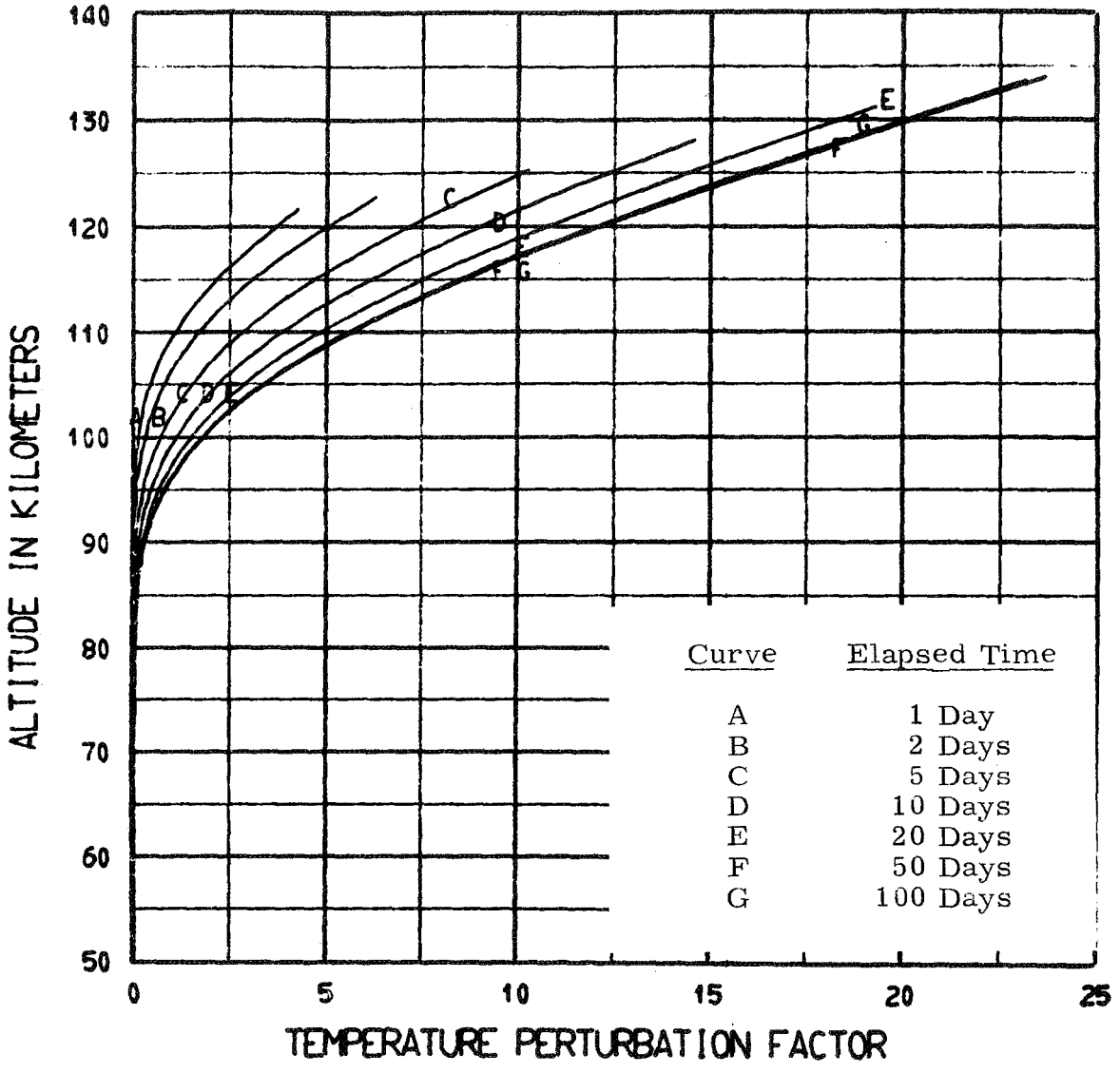

Figure G-18. Approach to new equilibrium temperature profile in response to upper boundary heat flux perturbation; $\Delta_{max} = +20$.

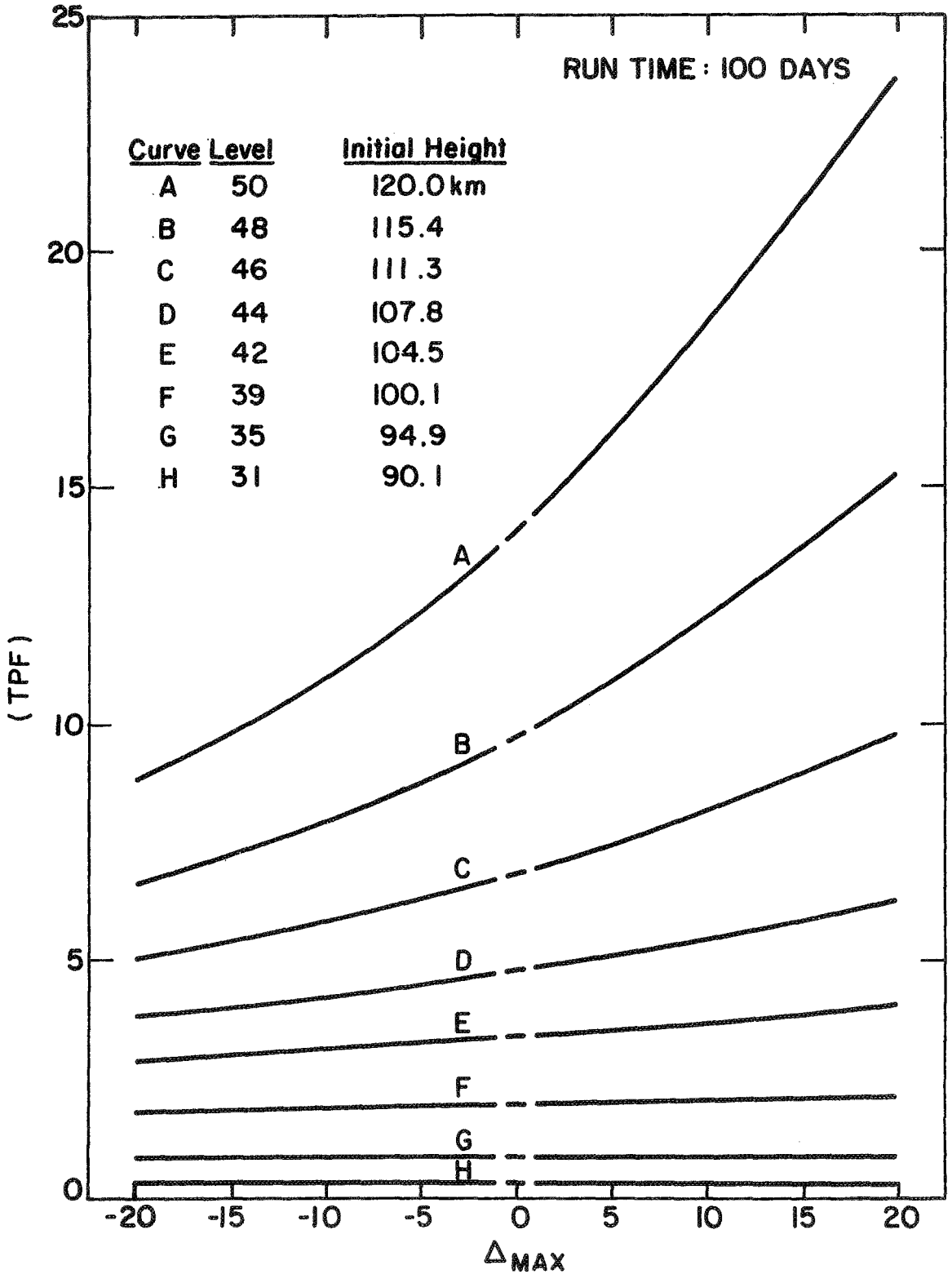

Figure G-19. Comparison of (TPF) at various levels after 100 days for range of upper boundary heat flux perturbations considered

to the heat flux, dissipation of tidal oscillations, was considered time-independent. The diurnal variation of the solar heating rate was approximated by doubling the earth average value for a 12 hour period alternated with zero heating for a 12 hour period. This crude approximation was felt to be quite accurate to within $\pm$ one hour of sunrise/sunset based on detailed calculations of solar heating rates performed in the studies described in Chapter 4. The model was run with one half hour time steps for a total of fifty days although very little change was evident from day to day after the first few days. In Figure G-20 is shown the relative temperature change, given by:

$$\frac{T - T(equil)}{T(equil)} \qquad \text{(G. 7)}$$

for the upper level of the model (initially 120 Km) during the 49th and 50th days. In Figure G-21 is shown the variation in the corresponding height level for the 50th day. The results indicate that the (nominal) 120 Km level does undergo significant diurnal variation of about 15.4^{o}K temperature change and 1 Km height change peak to peak. The effect of variations of this magnitude on the boundary of upper thermospheric models is beyond the scope of this study. Certainly these variations are small compared to the in situ diurnal variations. The results also indicate that the mesopause has the minimum diurnal variation, about 1/2% peak to peak, of the entire model. Thus it would seem ideally suited as a time independent lower boundary for upper thermospheric studies. Mahoney (1966) picked such a lower boundary at 80 Km in modeling the thermal structure of the thermosphere. The diurnal variation in temperature and level height he calculated for his 6th pressure level, at about 118 Km, was a little over 60% of the values calculated at about the same height in the present model.

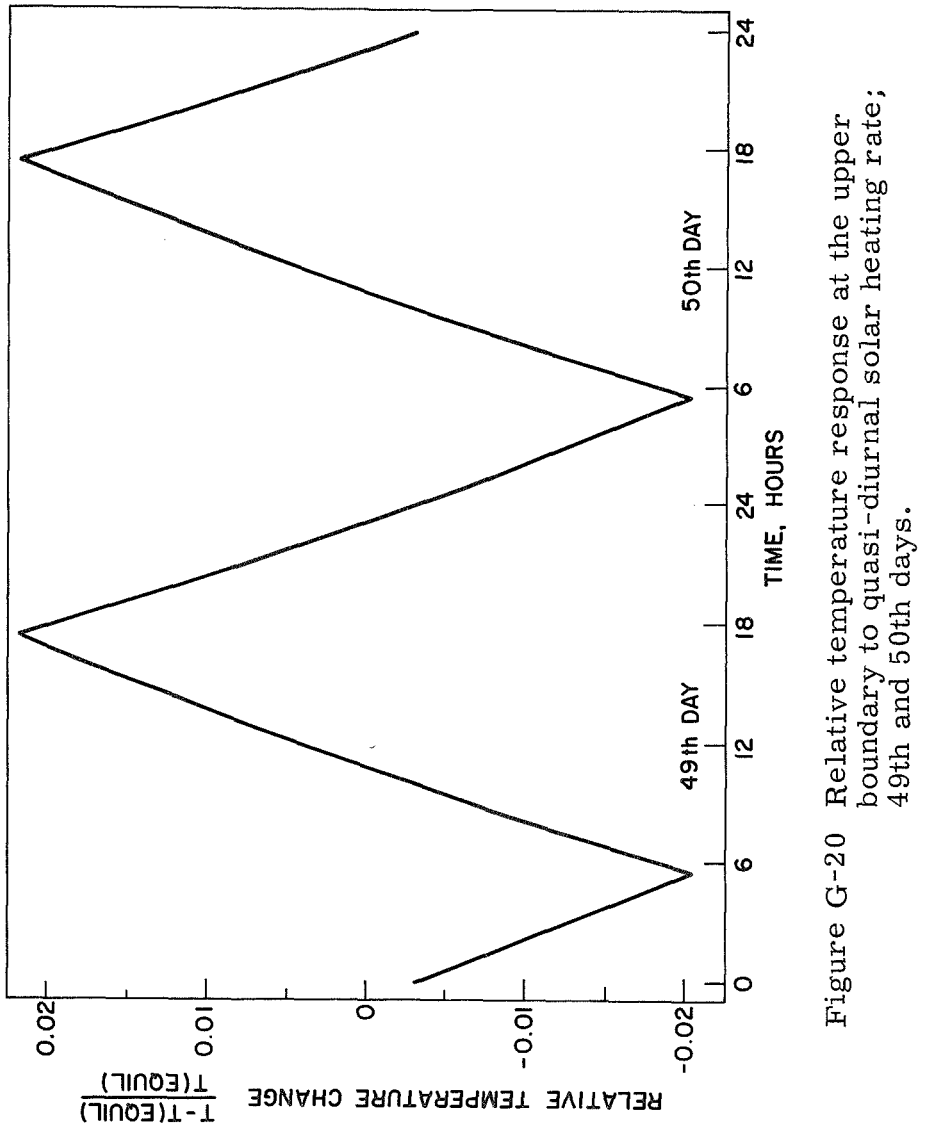

Figure G-20 Relative temperature response at the upper boundary to quasi-diurnal solar heating rate; 49th and 50th days.

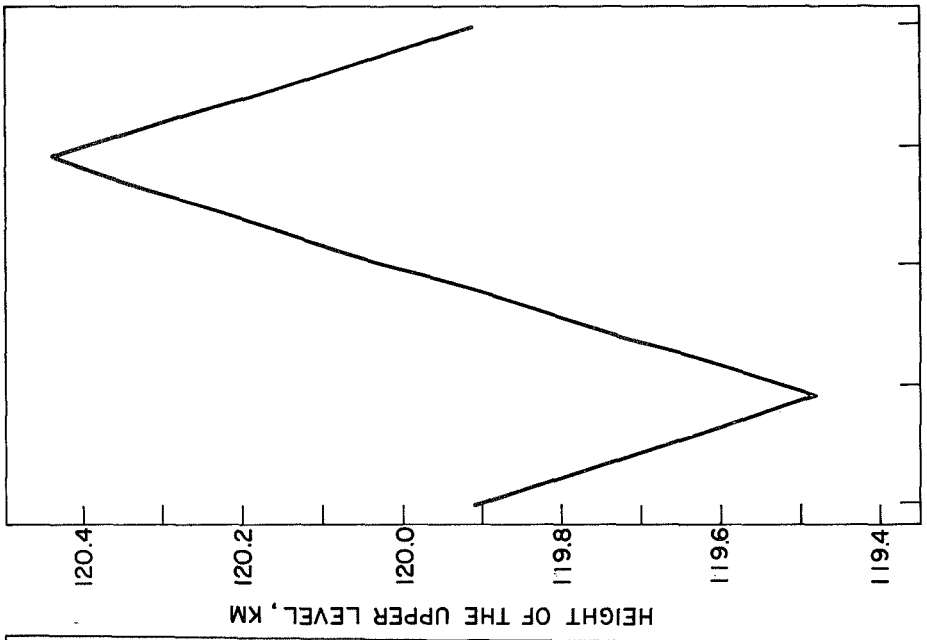

Figure G-21. Height level response at the upper boundary to quasi-diurnal solar heating rate; 50th day

REFERENCES

Anderson, G. P., C. A. Barth, F. Cayla, and J. London. 1969. "Satellite observations of the vertical ozone distribution in the the upper stratosphere." Ann. Geophys., 25, p. 341.

Anderson, J. G. 1970. Rocket Borne Ultraviolet Spectrometer Measurement of OH Resonance Flourescense with a Diffusive Transport Model for Mesospheric Photochemistry. Ph. D. Thesis, Department of Astro-Geophysics, University of Colorado, Boulder, Colorado.

Bates, D. R. 1951. "The temperature of the upper atmosphere." Proc. Phys. Soc., B64, p. 805.

Bates, D. R. 1959. "Some problems concerning the terrestrial atmosphere above about the 100 Km level." Proc. Roy. Soc. London, A253, p. 451.

Blake, A. J., J. H. Carver, and G. N. Haddad. 1966. "Photo-$_o$ absorption cross sections of molecular oxygen between 1250 Å and 2350 Å." J. Quant. Spectrosc. Radiat. Transfer, 6, p. 451.

Blake, D. W., and R. S. Lindzen. 1970. "Effects of dissipation on thermal tides." Paper presented at the Symposium on the Dynamics of the Mesosphere and Lower Thermosphere, Amer. Meteoro. Soc., Boulder, Colorado, June 15-18.

Blamont, J., and C. de Jager. 1961. "Upper atmospheric turbulence near the 100 Km level." Ann. Geophys., 17, p. 134.

Brinkman, R. T., A. E. S. Green, and C. A. Barth. 1966. "A digitalized solar ultraviolet spectrum." Jet Propulsion Lab. Technical Report No. 32-951, NASA CR 77355 (NASA Contract NAS7-100).

Champion, K. S. W. 1968. "Composition of the mesosphere and lower thermosphere." Meteorological Monographs, 8, p. 47.

Chandrasekhar, S. 1960. Radiative Transfer. Dover, N.Y., 393 pp.

Colgrove, F. D., W. B. Hanson, and F. S. Johnson. 1965. "Eddy diffusion and oxygen transport in the lower thermosphere." J. Geophys. Res., 70, p. 4931.

Colgrove, F. D., F. S. Johnson, and W. B. Hanson. 1966. "Atmospheric composition in the lower thermosphere." J. Geophys. Res., 71, p. 2227.

Craig, R. A., and J. C. Gillie. 1969. "Cooling of the thermosphere by atomic oxygen." J. Atmos. Sci., 26, p. 205.

REFERENCES (continued)

Curtis, A. R. 1952. "Discussion of Goody's 'A statistical model for water vapor absorption'." Q. J. R. M. S., 78, p. 638.

Curtis, A. R., and R. M. Goody. 1956. "Thermal radiation in the upper atmosphere." Proc. Roy. Soc. London, A236, p. 193.

Dalgarno. A., and F. J. Smith. 1962. "Thermal conductivity and viscosity of atomic oxygen." Planet. Space Sci., 9, p. 1.

Davidson, N. D. 1962. Statistical Mechanics. McGraw-Hill Book Co., Inc. New York City.

Detwiler, C. R., D. L. Garrett, J. D. Purcell, and R. Tousey. 1961. "The intensity distribution in the ultraviolet solar spectrum." Ann. Geophys., 17, p. 263.

Dingle, A. N., and C. Young. 1965. "Computer applications in the atmospheric sciences." University of Michigan, College of Engineering.

Ditchburn, R., and P. Young. 1962. "The absorption of molecular oxygen between 1850 and 2500 Å." J. Atmos. Terr. Phys., 24, p. 127.

Drayson, S. R. 1967, The Calculation of Long-Wave Radiative Transfer in Planetary Atmospheres. Ph. D. dissertation, Dept. of Meteorology and Oceanography, University of Michigan, Ann Arbor, Michigan.

Drayson, S. R., and E. S. Epstein. 1969. "Consequences of fine structure in the vertical temperature profile on radiative transfer in the mesosphere." Space Research IX., p. 376.

Drayson, S. R. 1970. "Carbon dioxide long-wave radiative transfer for use in models of the middle atmosphere." Paper presented at the Symposium on the Dynamics of the Mesosphere and Lower Thermosphere, Amer. Meteoro. Soc., Boulder Colorado, June 15-18.

Eberstein, I. J. 1969. "Evidence for strongly damped gravity waves in the earth's atmosphere." NASA TM X-63795, Goddard Space Flight Center, Greenbelt, Md.

Evans, W. F. J., D. M. Hunten, E. J. Llewellyn, and A. Vallance Jones. 1968. "Altitude profile of the infrared atmospheric system of oxygen in the dayglow." J. Geophys. Res., 73, p. 2885.

REFERENCES (continued)

Feldman, P. D., and D. P. McNutt. 1969. "Far infrared nightglow emission from atomic oxygen." J. Geophys. Res., 74, p. 4791.

Gillie, J. C. 1970. Private communication.

Glueckauf, E. 1951. The Composition of Atmospheric Air. Compendium of Meteorology, T. F. Malone, Ed., Amer. Met. Soc., p. 3.

Godson, W. L. 1953. "The evaluation of infrared radiative fluxes due to atmospheric water vapor." Q. J. R. M. S., 79, p. 367.

Green, A. E. S. 1966. The Middle Ultraviolet: Its Science and Technology. Ed. by A. E. S. Green, John Wiley & Sons, Inc., New York City.

Greenhow, J. S. 1959. "Eddy diffusion and its effect on meteor trails." J. Geophys. Res., 64, p. 2208.

Groves, G. V. 1969. "Seasonal and latitudinal models of atmospheric structure between 30 and 120 km altitude." Paper presented at Open Meeting of COSPAR W.G. IV, Prague, Tues. 20 May 1969.

Haurwitz, B. 1941. Dynamic Meteorology. McGraw-Hill Book Co., New York City.

Henrici, P. 1962. Discrete Variable Methods in Ordinary Differential Equations. Wiley, New York City.

Hesstvedt, E. 1961. "Note on the nature of noctilucent clouds." J. Geophys. Res., 66, p. 1985.

Hesstvedt, E. 1962. "On the possibility of ice cloud formation at the mesopause." Tellus, 14, p. 290.

Hesstvedt, E. 1968. "On the effect of vertical eddy transport on atmospheric composition in the mesosphere and lower thermosphere." Geofysiske Publikasjoner, XXVII, p. 1.

Hesstvedt, E., and U. B. Jansson. 1969. "On the effect of vertical eddy transport on the distribution of neutral nitrogen components in the D-region." Meteorological and Chemical Factors in D-region Aeronomy-Record of Third Aeronomy Conference, Ed. C. F. Sechrist, Jr., Aeronomy Rept. No. 32, University of Illinois, Urbana, Ill.

REFERENCES (continued)

Hilsenrath, J., et. al. 1955. Tables of Thermal Properties of Gases. National Bureau of Standards, Circular 54.

Hines, C. O. 1960. "Internal gravity waves at ionospheric heights." Can. J. Physics, 38, p. 1441.

Hines, C. O. 1963. "The upper atmosphere in motion." Q. J. R. M. S., 89, No. 379, p. 1.

Hinteregger, H. E. 1962. "Absorption spectrometric analysis of the upper atmosphere in the EUV region." J. Atmos. Sci., 19, p. 351.

Hinteregger, H. E., L. A. Hall, and G. Schmidtke. 1965. Solar XUV Radiation and Neutral Particle Distribution in July 1963 Thermosphere. Space Research V. North-Holland.

Hinteregger, H. E. 1969. "Effects of solar XUV radiation on the earth's atmosphere." Solar-Terrestrial Physics: Terrestrial Aspects (Proceedings of Joint IQSY/COSPAR Symposium, London 1967, Part II.) Annal of the IQSY, Vol. 5, Ed. A. C. Strickland. The M. I. T. Press, Cambridge, Mass.

Hodges, R. R. (Jr.). 1969. "Eddy diffusion coefficients due to instabilities in internal gravity waves." J. Geophys. Res., 74, p. 4087.

Houck, J. R., and M. Harwit. 1969. "For infrared night sky emission above 120 kilometers." Astrophys. J., 157, p. 145.

Houghton, J. T. 1967. "Fluorescence from the ν_3 vibration of carbon dioxide." Proc. Phys. Soc., 91, p. 439.

Hudson, R. D., V. L. Carter, and E. L. Breig. 1969. "Predissociation in the Schumann-Runge band system of O_2: Laboratory measurements and atmospheric effects." J. Geophys. Res., 74, No. 16, p. 4079.

Humphreys, W. J. 1933. "Nacreous and noctilucent clouds." Monthly Weather Review, 61, p. 228.

Hunt, B. G. 1966. "Photochemistry of ozone in a moist atmosphere." J. Geophys. Res., 71, p. 1385.

Hunten, D. M., and M. B. McElroy. 1966. "Quenching of metastable states of atomic and molecular oxygen and nitrogen." Rev. of Geophys., 4, p. 303.

Inn, E. C. Y., and Y. Tanaka. 1959. Ozone Absorption Coefficients. Advances in Chemistry, Series No. 21, 465 pp.

REFERENCES (continued)

Jacchia, L. G. 1964. "Static diffusion models of the upper atmosphere with empirical temperature profiles." Smithsonian Institution Astrophysical Observatory, Special Report No. 170, 15 pp.

Jeans, J. H. 1925. The Dynamical Theory of Gases. Fourth Edition Dover Publications, Inc., New York City.

Johnson, F. S., J. D. Purcell, R. Tousey, and K. Watanabe. 1952. "Direct measurements of the vertical distribution of atmospheric ozone to 70 km altitude." J. Geophys. Res., 57, p. 157.

Johnson, F. S., and E. M. Wilkins. 1965. "Thermal upper limit on eddy diffusion in the mesosphere and lower thermosphere." J. Geophys. Res., 70, p. 1281 and p. 4063.

Johnson, F. S. 1968. "Physical processes influencing the chemistry of planetary atmospheres." Paper presented at the Fourth Western Regional Meeting, American Chemical Society, San Francisco, Calif.

Johnson, F. S., and B. Gottlief. 1969. Composition Changes in the Lower Thermosphere. Space Res. IX. North-Holland.

Justus, C. G., and R. G. Roper. 1968. "Some observations of turbulence in the 80 to 110 km region of the upper atmosphere." Meteorological Monographs, 8, p. 122.

Kellogg, W. W. 1961. "Warming of the polar mesosphere and lower ionosphere in the winter." J. Meteor., 18, p. 373.

Kochanski, A. 1964. "Atmospheric Motions from sodium cloud drifts." J. Geophys. Res., 69, p. 3651.

Kockarts, G., and W. Peetermans. 1970. "Atomic oxygen infrared emission in the earth's upper atmosphere." Planet. Space Sci., 18, p. 271.

Kuhn, W. R. 1966. Infrared Radiative Transfer in the Upper Stratosphere and Mesosphere. Ph. D. dissertation, Dept. of Astro-Geophysics, University of Colorado, Boulder, Colorado.

Kuhn, W. R. 1968. "Radiative transfer in the mesosphere." Univ. of Michigan, Engineering College, Report No. 05863-15-T.

Kuhn, W. R., and J. London. 1969. "Infrared radiative cooling in the middle atmosphere (30-110 km)." J. Atmos. Sci., 26, p. 189.

REFERENCES (continued)

Kuhn, W. R. 1970. "Radiation processes and the distribution of radiative sources and sinks." Paper presented at the Symposium on the Dynamics of the Mesosphere and Lower Thermosphere, American Meteorological Society; Boulder, Colorado, June 15-18.

Lagos, C. P. 1967. "On the dynamics of the thermosphere." M.I.T., Dept. Meteorology, Planetary Circulations Project, Rept. No. 20, M.I.T. -2241-35.

Leovy, C. 1964. "Simple models of thermally driven mesospheric circulation." J. Atmos. Sci., 21, p. 327.

Lettau, H. 1951. Diffusion in the Upper Atmosphere. Compendium of Meteorology, Ed. T. F. Malone, Waverly Press, Inc., Baltimore, p. 320.

Lindemann, F. A., and G. M. B. Dobson. 1923. "A theory of meteors and the density and temperature of the outer atmosphere to which it leads." Proc. Roy. Soc. London, A102, p. 411.

Lindzen, R. S. 1967. "Thermally driven diurnal tide in the atmosphere." Q.J.R.M.S., 93, p. 18.

Lindzen, R. S. 1968. "The application of classical atmospheric tidal theory." Proc. Roy. Soc. London, A303, p. 299.

Lindzen, R. S., and S. Chapman. 1969. "Atmospheric tides." Space Sci. Rev., 10, p. 3.

Mahoney, J. R. 1966. "A study of energy sources for the thermosphere." M.I.T., Dept. Meteorology, Planetary Circulations Project, Rept. No. 17, M.I.T. -2241-16.

Mahoney, J. R. 1968. "A numerical study of the variable structure of the lower thermosphere." Meteorological Monographs, 8, p. 90.

McGrath, W. D., and R. G. W. Norrish. 1957. "The flash photolysis of ozone." Proc. Roy. Soc. London, A242, p. 265.

McGrath, W. D., and J. J. McGarvey. 1967. "The production, deactivation and chemical reactions of $O(^1D)$ atoms." Planet. Space Sci., 15, p. 427.

Merrill, K. M., and R. C. Amme. 1969. "Deactivation of the CO_2 bending mode by collisions with N_2 and O_2." J. Chem. Phys., 51, p. 844.

Miller, D. E., and K. H. Stewart. 1965. "Observations of atmospheric ozone." Proc. Roy. Soc. London, A288, p. 540.

REFERENCES (continued)

Morgan, J. E., and H. I. Schiff. 1963. "Recombination of oxygen atoms in the presence of inert gases." Can. J. Chem., 38, p. 1769.

Murgatroyd, R. J. 1957. "Winds and temperatures between 20 km and 100 km - a review." Q. J. R. M. S., 83, p. 417.

Murgatroyd, R. J., and R. M. Goody. 1958. "Sources and sinks of radiative energy from 30 to 90 km." Q. J. R. M. S., 84, p. 225.

Murgatroyd, R. J., and F. Singleton. 1961. "Possible meridional circulations in the stratosphere and mesosphere." Q. J. R. M. S., 87, p. 125.

Murgatroyd, R. J. 1965. "Winds in the mesosphere and lower thermosphere." Proc. Roy. Soc. London, A288, p. 575.

Murgatroyd, R. J. 1968. "Temperature, density, and pressure variations in the stratosphere and the mesosphere." Meteorological Monographs, 8, p. 57.

Newell, R. E. 1968. "The general circulation of the atmosphere above 60 km." Meteorological Monographs, 8, p. 98.

Noxon, J. F. 1970. "Optical emission from $O(^1D)$ and $O_2(b^1\Sigma_g)$ in ultraviolet photolysis of O_2 and CO_2." J. Chem. Phys., 52, p. 1852.

Peterson, V. L., and T. E. Van Zandt. 1969. "$O(^1D)$ quenching in the ionospheric F-region." Planet. Space Sci., 17, p. 1725.

Plass, G. N. 1956. "The influence of the 9.6 micron ozone band on the atmospheric infrared cooling rate." Q. J. R. M. S., 82, p. 30.

Rawcliffe, R. D., G. E. Meloy, R. M. Friedman, and E. H. Rogers. 1963. "Measurements of vertical ozone from a polar orbiting satellite." J. Geophys. Res., 68, p. 6425.

Read, A. W. 1965. "Vibrational relaxation in gases." Progress in Reaction Kinetics, 3, p. 203.

Reif, F. 1965. Fundamentals of Statistical and Thermal Physics. McGraw Hill, Inc., New York City.

Richtmyer, S. D. 1957. Difference Methods for Initial Value Problems. Interscience, New York City.

Rocket Panel. 1952. "Pressures, densities and temperatures in the upper atmosphere." Phys. Rev., 88, p. 1027.

REFERENCES (continued)

Schiff, H. I. 1968. Neutral Reactions Involving Oxygen and Nitrogen. I.A.G.A. Symposium on Laboratory Measurements of Aeronomic Interest, York University, Sept. 3-4.

Shimazaki, T. 1967. "Dynamic effects on atomic and molecular oxygen density distribution in the upper atmosphere: a numerical solution to equations of motion and continuity." J. Atmos. Terr. Phys., 29, p. 723.

Shimazaki, T. 1968. "Dynamic effects on height distributions of neutral constituents in the earth's upper atmosphere: a calculation of atmospheric model between 70 km and 500 km." J. Atmos. Terr. Phys., 30, p. 1279.

Shimazaki, T., and A. R. Laird. 1970. "A model calculation of the diurnal variation in minor neutral constituents in the mesosphere and lower thermosphere including transport effects." J. Geophy. Res., 75, p. 3221.

Smith, L. G. 1969. "Rocket observations of ozone above 50 km." COSPAR Plenary Meeting, 12th, Prague, Czechoslovakia, May 11-24.

Smith, W. S., L. Katchen, P. Sacher, P. Swartz, and J. Theon. 1964. "Temperature, pressure, density and wind measurements with the rocket grenade experiment 1960-1963." NASA Goddard Space Flight Center, X-651-64-106.

Smith, W. S., J. Theon, L. Katchen, and P. Swartz. 1966. "Temperature, pressure, density, and wind measurements in the upper stratosphere and mesosphere, 1964." NASA TR R-245.

Smith, W. S., J. Theon, P. Swartz, L. Katchen, and J. Horvath. 1967. "Temperature, pressure, density, and wind measurements in the upper stratosphere and mesosphere, 1965." NASA TR R-263.

Smith, W. S., J. Theon, P. Swartz, L. Katchen, and J. Horvath. 1968. "Temperature, pressure, density, and wind measurements in the stratosphere and mesosphere, 1966." NASA TR R-288.

Smith, W. S., J. Theon, P. Swartz, J. Casey, and J. Horvath. 1969. "Temperature, pressure, density, and wind measurements in the stratosphere and mesosphere, 1967." NASA TR R-316

Snelling, D. R., and E. J. Blair. 1967. "Nonadiabatic decomposition of N_2O in the deactivation of $O(^1D)$ by N_2^*." J. Chem. Phys., 47, p. 228.

REFERENCES (continued)

Stein, J. A., and J. C. G. Walker. 1965. "Models of the upper atmosphere for a wide range of boundary conditions." J. Atmos. Sci., 22, p. 11.

Taylor, R. L., and S. Bitterman. 1969. "Survey of relaxation data for processes important in the CO_2-N_2 laser system." Rev. of Modern Phys., 41, p. 26.

Vallance Jones, A., and R. L. Gattinger. 1963. "The seasonal variation and excitation mechanism of the $1.58\mu\ {}^1\Delta_g - {}^3\Sigma_g^-$ twilight airglow band." Planet. Space Sci., 11, p. 961.

Volman, D. H. 1963. "Photochemical gas phase reactions in the hydrogen-oxygen system." Adv. Photochem., 1, p. 43.

Walker, J. C. G. 1965. "Analytic representation of upper atmosphere densities based on Jacchia's static diffusion models." J. Atmos. Sci., 22, p. 462.

Walker, J. C. G., R. S. Stolarski, and A. F. Nagy. 1969. "The vibrational temperature of molecular nitrogen in the thermosphere." Ann. Geophys., 25, p. 831.

Wallace, L., and M. B. McElroy. 1966. "The visual dayglow." Planet. Space Sci., 14, p. 677.

Watanabe, K., and F. F. Marmo. 1956. "Photoionization and total absorption cross section of gases. II. O_2 and N_2 in the region 850 - 1500 Å." J. Chem. Phys., 25, p. 965.

Watanabe, K. 1958. "UV absorption processes in upper atmosphere." Adv. Geophys., 5, p. 181.

Watanabe, K., H. Sakai, J. Mottl, and T. Nakayama. 1958. Hawaii Inst. Geophys., Contr. No. 11.

Webb, W. L. 1969. "The cold earth." ECOM-5272 Atmos. Sci. Lab., U. S. Army Electronics Command, White Sands Missile Range, N. M. Paper presented at the National Meeting of American Astronautical Society, New Mexico State University.

Whipple, F. L. 1952. "Exploration of the upper atmosphere by meteoritic techniques." Ad. Geophys., 1, p. 119.

Wiin-Nielsen, A. 1968. "On the intensity of the general circulation of the atmosphere." Rev. of Geophys., 6, p. 559.

Wiin-Nielsen, A. 1970. Private communication.

REFERENCES (conclusion)

Woolfe, H. M. 1968. "On the computation of solar elevation angles and the determination of sunrise and sunset times." NASA TM X-1646.

Yanowitch, M. 1967. "Effect of viscosity on gravity waves and the upper boundary condition." J. Fluid Mech., 29, Part 2, p. 209.

Young, C., and E. S. Epstein. 1962. "Atomic oxygen in the polar winter mesosphere." J. Atmos. Sci., 19, p. 435.

Young, R. A., and G. Black. 1967. "Deactivation of $O(^1D)$." J. Chem. Phys., 47, 1. 2311.

Young, R. A., G. Black, and T. G. Slanger. 1968. "Reaction and deactivation of $O(^1D)$." J. Chem. Phys., 49, p. 4758.

Zipf, E. C. 1969. "The collisional deactivation of metastable atoms and molecules in the upper atmosphere." Can. J. Chem., 47, p. 1863.